



Durham E-Theses

Thermodynamics of ethylene-vinyl acetate copolymer blends

Clough, Norman E.

How to cite:

Clough, Norman E. (1994) *Thermodynamics of ethylene-vinyl acetate copolymer blends*, Durham theses, Durham University. Available at Durham E-Theses Online: <http://etheses.dur.ac.uk/5489/>

Use policy

The full-text may be used and/or reproduced, and given to third parties in any format or medium, without prior permission or charge, for personal research or study, educational, or not-for-profit purposes provided that:

- a full bibliographic reference is made to the original source
- a [link](#) is made to the metadata record in Durham E-Theses
- the full-text is not changed in any way

The full-text must not be sold in any format or medium without the formal permission of the copyright holders.

Please consult the [full Durham E-Theses policy](#) for further details.

Thermodynamics of Ethylene-Vinyl Acetate Copolymer Blends

September 1994

The copyright of this thesis rests with the author.
No quotation from it should be published without
his prior written consent and information derived
from it should be acknowledged.

Norman E. Clough

University of Durham

Supervisor

Randal W. Richards

University of Durham

A thesis submitted to the University of Durham in partial fulfilment of the
regulations for the Degree of Doctor of Philosophy



12 OCT 1994

Thermodynamics of Ethylene-Vinyl Acetate Copolymer Blends

Norman E. Clough
PhD Thesis September 1994

Abstract

The purpose of this study was to characterise the miscibility of several poly(ethylene-co-vinyl acetate), EVA, based polymer blends. EVA has many industrial applications and is often present as one of several polymeric components. Consequently, there is considerable interest in the thermodynamics of these blend systems.

The thermodynamics of these blends was studied using several techniques: differential scanning calorimetry; phase contrast optical microscopy; small angle neutron scattering and wide angle X-ray scattering. Characterisation was also to include assessing the relative enthalpic and entropic thermodynamic contributions to the Flory-Huggins interaction parameter (χ) of these blends. To determine the enthalpic interaction parameter, a "mixing calorimeter" was designed and constructed to measure accurately the "heat of mixing" values on blending these polymers. Free energy interaction parameters were determined from melting point depression and small angle neutron scattering measurements.

In all the blends studied, the heat of mixing was endothermic and consequently, the enthalpic interaction parameters were positive i.e. unfavourable to miscibility. Miscibility in these blends can therefore only be achieved by a dominant entropic contribution, favourable to miscibility.

Using phase contrast optical microscopy, both miscible and immiscible phase behaviour was observed in this series of blends. This shows good agreement with predictions of miscibility from heat of mixing, melting point and small angle neutron scattering measurements, based on the classical Flory-Huggins lattice theory.

Wide angle X-ray scattering and differential scanning calorimetry results have associated miscible blends with cocrystallisation effects between the blend components.

Small angle neutron scattering has been used to determine the concentration and temperature dependence of interaction parameters in a miscible blend. From these values the upper critical solution temperature (UCST) of the blend was predicted. The enthalpic contributions to these interaction parameters show good agreement with experimental values determined from heat of mixing measurements.

It was concluded that the classical Flory-Huggins lattice theory (despite its many well documented limitations) appears to be particularly suited to the thermodynamic characterisation of miscibility in these polymer blends.

Acknowledgements

The customary thanks to my supervisor, Randal Richards seem inadequate but I dearly thank him for his help, support and relentless encouragement throughout this project. I will remember him for his banter, the "odd" laugh (very odd actually), introducing me to Gin and Tonic and attempting to teach me thermodynamics. I would also like to thank Jim Feast for his many views (some even on chemistry !!), advice and generally laid back approach to life.

As I get even older, I suspect that the thermodynamics will be forgotten and I will be left with the enjoyable memories (or nightmares, as Randal would suggest) of my time at Durham. For these memories, I thank the following special people ;

My fellow Randalites; Donald "nearly got a chapter ready" Davison, Ian "is that a maternity shirt ?" Hopkinson, Cecilia "I can't save my document" Backson and a Feastite, Neil "dendritic" Stainton, all of whom have stayed the course with me.

The "post docs", who were such inspiring examples to me (allegedly); Mark "how many holidays do we get ?" Taylor, Sian "the Swansea Taff" Davies, Lian "Tom Kiff Jnr." Hutchings, Andrew Grainger, Panagiotis "PD" Dounis and Ezat Khosravi.

Gordon Forrest, Dave Parker, Tom Kiff, Stella Gissing and Jean Eccleston for taking the time to gossip with me.

My fellow sporting "nuts" and good friends, Frank Davies and Carole-Anne Smith. Many thanks to Patrique Bayliff for being a lovely friend, proof reading this thesis and even attempting to teach me tennis.

I would like to thank the mechanical (Jim Hodgson, Neil Holmes and Melvin Higham) and electrical (Barry Barker, George Rowe and Kelvin Appleby) workshops for a superb job in constructing the calorimeter. Terry Harrison and Tony Royston (the geriatric computer wizz-kids). Gordon Forrest for SEC measurements, Alan Kenwright and Julia Say for NMR analysis, the glassblowers (Ray Hart and Gordon Haswell), Jimmy Lincoln and Tom Caygill.

I thank EXXON Chemicals for their financial support and to my industrial supervisor, Tuncel Ibrahim for her friendly approach and assistance.

Finally, I would like to give a very big and special thanks to Jayne (who has put up with me for more years than I care to remember) and my offspring, Amy. Without their love, support and patience, this thesis would not have been possible.

To Jayne and Amy

Contents

Abstract		
Acknowledgements		
Contents		
Declaration and Polymer Abbreviations		
1	INTRODUCTION	1
2	THERMODYNAMICS OF POLYMER BLENDS	11
2.1	Introduction	11
2.2	Thermodynamics of Polymer Solutions	12
2.2.1	Entropic contributions to mixing (ΔS_{mix})	12
2.2.2	Enthalpic contributions to mixing (ΔH_{mix})	18
2.2.3	Free Energy of Mixing (ΔG_{mix})	22
2.3	Polymer Blend Miscibility	25
2.4	Limitations of the Flory-Huggins Lattice Theory	26
2.5	Phase Separation	30
2.6	Equation of State Theory	37
2.7	References	40
3.	POLYMER CHARACTERISATION AND SYNTHESIS	42
3.1	Polymers supplied by EXXON Chemical Limited	42
3.2	Polymers Prepared	43
3.3	Characterisation	45
3.3.1	Size Exclusion Chromatography (SEC)	45
3.3.1a	Tetrahydrofuran solution SEC	45
3.3.1b	Aqueous solution SEC	47
3.3.1c	Chloroform solution SEC	47
3.3.2	Density and Coefficient of Thermal Expansion measurements	47
3.3.3	Elemental Analysis	48
3.3.4	Thermogravimetric Analysis	49
3.4	Experimental Details	49
3.4.1	Polymerisation of hydrogenous poly(ethylene glycol) (h-PEG1)	51
3.4.2	Polymerisation of hydrogenous poly(ethylene glycol) (h-PEG2)	53
3.4.3	Polymerisation of deuterated poly(ethylene glycol) (d-PEG)	55
3.4.4	Diesterification of deuterated polyethylene glycol with deuterated docosanoic acid (DPE)	57

3.4.5	Diesterification of poly(ethylene glycol) with docosanoic acid (NECPE)	58
3.4.6	Monoesterification of poly(ethylene glycol) methyl ether with docosanoic acid (NECME)	59
3.5	Analysis (NMR and IR)	59
3.6	Blend Preparation	60
3.7	Discussion	61
3.8	References	62
4	DIFFERENTIAL SCANNING CALORIMETRY	63
4.1	Introduction	63
4.2	Melting point depression theory	65
4.3	Melting point considerations	71
4.4	Experimental	72
4.5	Results	74
4.5.1	EVA blends with semi-crystalline polymers	74
4.5.2	Enthalpies of fusion	76
4.6	Additional DSC results	77
4.6.1	Morphological contributions to melting point depression	77
4.6.2	Effect of melt quenching on melting point and heat of fusion values	79
4.7	Discussion	80
4.8	References	87
5	PHASE CONTRAST OPTICAL MICROSCOPY	88
5.1	Introduction	88
5.2	Apparatus and Sample Preparation	89
5.3	Initial Miscibility Studies	89
5.3.1	EVA:FVA Blends	90
5.3.2	EVA:PE Blends	90
5.3.3	EVA:PI Blends	91
5.3.4	EVA:LMPI Blends	92
5.3.5	EVA:9210 Blends	93
5.3.6	EVA:9233 Blends	93
5.4	Polymer Blend Phase Diagrams	94
5.4.1	Introduction	94
5.4.2	EVA:FVA Blends	95
5.4.2a	15%EVA:85%FVA	96

5.4.2b	25%EVA:75%FVA	96
5.4.2c	46%EVA:54%FVA	97
5.4.2d	60%EVA:40%FVA	97
5.4.2e	83%EVA:17%FVA	98
5.4.2f	EVA:FVA Phase Diagrams	98
5.4.3	EVA:PI Blends	100
5.4.3a	17%EVA:83%PI	100
5.4.3b	39%EVA:61%PI	100
5.4.3c	55%EVA:45%PI	101
5.4.3d	73%EVA:17%PI	101
5.4.3e	EVA:PI Phase Diagram	101
5.5	Discussion	102
5.6	References	105
6	DESIGN AND CONSTRUCTION OF A POLYMER BLEND "HEAT OF MIXING" CALORIMETER	106
6.1	Introduction	106
6.2	Outer Jacket	107
6.3	Inner Jacket	108
6.4	Central Heat Sink	109
6.5	Heat Flow Detecting Units	110
6.6	Calorimeter Cell	111
6.7	Preheating Oven	112
6.8	Temperature Control	112
6.9	Data Measurement, Analysis and Storage	113
6.9.1	Instrument Parameters	113
6.9.2	Measurement	113
6.9.3	Data Analysis	114
6.9.4	Data Storage and Retrieval	114
6.10	Mains Voltage Conditioning	114
6.11	References	114
7	"HEAT OF MIXING" CALORIMETRY	115
7.1	Introduction	115
7.2	Flory-Huggins Theory	118
7.3	Materials	119
7.4	Apparatus and Measurement	119
7.5	Experimental	120

7.6	Electrical Calibration	121
7.7	Calorimeter Testing	123
	7.7.1 Diglyme:Dodecane Blend	124
	7.7.2 Polystyrene:Polybutadiene Blends	125
7.8	Heat of Mixing Results	127
	7.8.1 Blank Heat Effects	127
	7.8.2 EVA Blends with FVA, PI, LMPI and NECPE	129
	7.8.3 Docosane Blends with EVA, FVA, PI, LMPI and NECPE	129
	7.8.4 Solution Blending of Docosane with EVA, FVA, PI, LMPI and NECPE (in toluene solvent)	130
7.9	Discussion	132
7.10	References	137
8	WIDE ANGLE X-RAY SCATTERING	138
8.1	Introduction	138
8.2	Theory	139
8.3	Determining Crystallinity in Polymers	140
	8.3.1 External Comparison	141
	8.3.2 Internal Comparison	142
8.4	Experimental	143
8.5	Determination of Crystallinity in FVA, PE and PI polymers	143
	8.5.1 External Comparison Method	145
	8.5.2 Internal Comparison Method 1	146
	8.5.3 Internal Comparison Method 2 (Profile Fitting)	147
	8.5.4 Crystallinity from Heat of Fusion values	149
8.6	Crystallisation in EVA:FVA, EVA:PE and EVA:PI Blends	151
8.7	Crystallinity in "Amorphous" EVA	153
8.8	Identification of crystalline phases in PE	153
8.9	Discussion	155
8.10	References	159
9	SMALL ANGLE NEUTRON SCATTERING	160
9.1	Introduction	160
9.2	Theory	161
	9.2.1 Thermodynamics	161
	9.2.2 Small Angle Neutron Scattering	164
9.3	Experimental	170
	9.3.1 Blend Preparation	171

9.3.2	Small Angle Neutron Scattering Experiments	171
9.4	Results	172
9.5	Comparison of χ (enthalpic) values from SANS and Heats of Mixing	179
9.6	Determination of Radii of Gyration (and χ_{eff}) values	179
9.7	Discussion	180
9.8	References	185
10	CONCLUSIONS (and suggestions for future work)	187

APPENDICES

APPENDIX A : Melting Point Analysis Results

APPENDIX B : "Heat of Mixing" Calorimetry Results

APPENDIX C : Lectures, Conferences, Courses Attended and Publications.

Declaration

All work contained within this thesis is my own work, unless stated otherwise, and has not previously been submitted for any other qualification.

Polymer Abbreviations

EVA	poly(ethylene-co-vinyl acetate)
FVA	poly(di-n-tetradecyl fumarate-co-vinyl acetate)
PI	poly(di-n-octadecyl itaconate)
LMPI	poly(di-n-octadecyl itaconate) - low molecular weight
PE	n-docosyl diester terminated poly(ethylene glycol)
NECPE	n-docosyl diester terminated poly(ethylene glycol)
DPE	deuterated n-docosyl diester terminated poly(ethylene glycol)
NECME	n-docosyl monoester terminated poly(ethylene glycol)
PEG	poly(ethylene glycol)
9210	hydrogenated poly(5-hexadecyl norbornene)
9233	hydrogenated poly(5-tetradecyl norbornene)

CHAPTER 1

INTRODUCTION

During the early development stages of polymer science, research into new polymer materials concentrated on developing new homopolymers and understanding their basic properties. Variations in the properties of homopolymers can generally only be achieved by changes in the chemical structure i.e. developing new polymers, which has become increasingly expensive. Unique property diversification has therefore generally been achieved by the use of random, block and graft copolymers, polymer blends and polymer composites.

Polymer blends can achieve a range of property compromises, depending on the individual properties of each blend component and the final blend composition, at a fraction of the cost of developing a new polymer. Thus, a range of price/performance options are available leading to a large number of potentially useful and different products. Therefore, polymer blends, especially those which are miscible, are very versatile and can be uniquely "tailored" to provide specific property effects which consequently results in significant commercial importance. Several good reviews on polymer blends are available¹⁻³.

When polymers are blended, they are likely to exhibit a two-phase (immiscible) morphology. This phase separation can be explained in terms of simple thermodynamic theory. A negative change in the free energy of mixing (ΔG_{mix}) is a necessary (but not an exclusive) criteria for miscibility to occur. This is given by:

$$\Delta G_{\text{mix}} = \Delta H_{\text{mix}} - T\Delta S_{\text{mix}}$$

where, ΔH_{mix} is the enthalpy of mixing, ΔS_{mix} is the entropy of mixing and T is the absolute temperature. Generally, polymer blends consist of high molecular weight components and consequently the entropic contribution is considered negligible. Miscibility in these blends can therefore only be achieved by a negative (exothermic)

heat of mixing due to specific enthalpic intermolecular interactions e.g. hydrogen bonding⁴, dipole-dipole coupling⁵ etc. Several authors have reported^{6,7} that certain copolymers are likely to be miscible with other polymers due to intramolecular interactions which result in a net exothermic "heat of mixing" value. In the absence of these enthalpic interactions between the polymers, the ΔH_{mix} is positive (endothermic) and the blend is subsequently immiscible. However, in blends containing low molecular weight polymers, the favourable entropic contribution may be significant and dominate any unfavourable endothermic enthalpy of mixing, resulting in a negative free energy change and consequently, probable blend miscibility⁸.

Immiscible polymer blends generally show large scale phase separation⁹ due to poor adhesion between the polymer components. The phase separation can be sufficiently large, especially in blends containing engineering polymers, to produce voids within the blend which result in extremely poor mechanical properties e.g. impact strength. Improving the adhesion between these polymer phases could therefore, dramatically improve these mechanical properties. The desire for improved adhesion and the commercial implications of polymer blends with improved properties has recently led to the emergence of a new area of polymer science called "compatibilisation", in which "compatibilisers" are added to polymer blends to improve adhesion between the separate polymer phases. The ideal "compatibiliser" is believed to be a block copolymer composed of polymeric segments of both polymer blend components. Consequently, these segments have the characteristics of either polymer, possibly showing multiple glass transition temperatures (T_g) which represent the different polymeric segments in the copolymer. During the processing (or preparation) stage of the blend, the compatibiliser additive is believed to migrate to the interface between the blend components, acting as an emulsifier-type agent with each blend component having a soluble (or miscible) affinity for its analogue segment on the compatibiliser chain. This use of a "solubility link" between immiscible polymers, subsequently results in greater adhesion, reduced phase separation and ultimately, improved mechanical properties¹⁰.

To avoid confusion, the term "miscibility", used to describe single phase polymer-polymer blends should be clarified before proceeding further. Originally, the term "compatible" was used to describe single phase behaviour but this has become very ambiguous as researchers have used this term to describe several "blending effects": good adhesion between the blend components, an averaging of mechanical properties from blending and even to describe immiscible blends which can be processed to produce useful materials. Another alternative term, "solubility" could be used as a more exact description than "compatibility" to describe molecular mixing in polymer blends. For solvent-based mixtures (solvent-solvent, solvent-polymer), "solubility" is the widely accepted term. For polymer-polymer blends, ideal or random molecular mixing i.e. true "solubility" may not accurately describe the true nature of the type of molecular blending. Therefore, researchers have tended to use the term "miscibility" to describe polymer-polymer blends in the "single phase". It should be remembered that "miscibility" does not imply ideal molecular mixing but indicates that the molecular mixing is sufficient to result in **macroscopic** properties which are typical of a single phase material. A popular experimental method of classifying a miscible blend on a macroscopic scale has been the identification of a single T_g value^{3,11}, which lies between the T_g values of the pure blend components. In this instance, miscibility indicates blend homogeneity on a size scale similar to that responsible for the T_g values of the polymer components. Defining miscibility can become confusing when macroscopic and microscopic experimental evidence conflicts i.e. in some polymer blends, heterogeneous (immiscible) structure has been observed at high levels of magnification even though macroscopic properties e.g. a single T_g , imply single phase behaviour. To confuse the interpretation of miscibility further, heterogeneous structures (or domains) have been noted in amorphous homopolymers i.e. atactic polystyrene³.

A further complication in understanding miscibility behaviour is that blends can exhibit both miscibility and immiscibility depending on temperature and blend composition e.g. a polystyrene and poly(vinyl methyl ether) blend forms a clear, one phase mixture at 353K but on heating to 413K, the blend phase separates. Therefore,

miscibility cannot be correctly defined simply by the criteria that the free energy of mixing change (ΔG_{mix}) must be negative. This definition does not distinguish or explain the phase change behaviour of blends from miscible to immiscible states and vice versa, despite maintaining a negative ΔG_{mix} throughout. Thermodynamically, miscibility is therefore dependent on a negative ΔG_{mix} value plus the additional criteria that the composition dependence of ΔG_{mix} i.e. $\partial^2 \Delta G_{\text{mix}} / \partial \phi^2$ is greater than zero for miscibility to occur, where ϕ is the volume fraction.

Polymer blends can be prepared using several methods. Commercial blends are generally produced by mechanically mixing the polymers in the molten, liquid state using an extruder. The molten polymer blend extrudate is then rapidly cooled usually by a water bath to form a solid "lace" which is subsequently granulated. These polymer blend granules are in a convenient form for further processing, storage and transport. Several problems are associated with this blend preparation: high molecular weight polymers have a low diffusion rate and subsequently, the mixing process is very slow, and prolonged mixing in the melt can result in thermal degradation of the polymers. The main advantage of this process is that it can run continuously at low cost. In the laboratory, blends can be conveniently prepared by casting the blend from a common solvent. The advantages of this method are that it requires little material, standard equipment and generally produces homogeneous blend samples. However, phase separation of the blend can still occur if the system becomes thermodynamically unstable on evaporation of the solvent¹² and difficulties may be encountered in removing solvent residues. Another method of producing polymer blends, commercially and in the laboratory, is via "in-situ polymerisation" in which a monomer is polymerised in the presence of the other polymer blend component, usually in solution. This method, which does not guarantee producing a miscible blend, has been used commercially in the production of two-phase rubber toughened plastics¹³. Miscible blends of poly(vinyl chloride) and butadiene-acrylonitrile copolymers were commercialised over 40 years ago¹⁴. However, the level of academic and industrial activity commensurate with the potential importance of polymer blends has only been reached within the last 20 years.

giving an indication of blend miscibility (miscible blends are generally associated with negative χ values!). Determining χ values for polymer blends is a fundamental problem but crucial in understanding the miscibility within the system. Consequently, several techniques have been applied or developed to determine these polymer-polymer interaction parameters, none of which is particularly straightforward and each has their own particular limitations.

A simple technique for determining χ values which has been applied to polymer systems is solvent vapour sorption, in which solvent molecules can be sorbed into a blend to probe the interaction between the two polymers¹, providing absolute thermodynamic information. This method of analysis has been used in inverse gas phase chromatography^{24,25}, which involves eluting a volatile solvent of known physical characteristics over a polymeric stationary phase i.e. the inverse situation to conventional gas chromatography. A major drawback to this method has been the clear dependence of the interaction parameters on the nature of the solvent probe and the long times to attain equilibrium, which are impractical. Light scattering from dilute polymer solution has also been used to determine interaction parameters²⁶. Similarly, small angle neutron scattering (SANS) has also been widely used with great success on a variety of polymer blends²⁷⁻²⁹ and is proving to be a very powerful tool in studies on polymer-polymer interactions. SANS is also absolute, provides the free energy χ value and can be utilised to determine the temperature dependence of χ which is needed to predict the location of phase boundaries and to estimate the relative χ (enthalpy) and χ (excess entropy) contributions to the χ (free energy) value. The main disadvantages of this method are the difficulty in obtaining access to a neutron scattering facility and the need to have one component deuterated which can be prohibitively expensive. For the situation in which one of the components of a polymer blend is semi-crystalline while the other is amorphous, analysis of the melting point depression of the crystalline component is the most suitable and widely used method for determining interaction parameters^{19,30} and has been applied to many blend systems^{17,31}. However, in this approach the determined χ values are only applicable in the observed melting range and

do not give an indication of the dependence of χ on concentration or temperature. The χ values determined from this method are free energy terms consisting of both enthalpic and entropic contributions.

The enthalpic interaction between two fluids can be determined directly by their "heat of mixing" which is related to both the Flory-Huggins and equation of state terms, χ (enthalpic) and X respectively. In polymer blends heat of mixing values are difficult to measure due to their physical state. Low molecular weight analogues are therefore usually selected to represent the polymers of interest and their heat of mixing correlated with the polymer-polymer miscibility^{32,33}, albeit with limited success. It is also possible to measure the heat of dilution of a mixture of polymers by a solvent and by applying Hess's law to infer the heat of mixing between the polymers¹. This technique requires great accuracy as the heat of mixing of the polymer blend is calculated from small differences between very large values.

The purpose of this study was to characterise the miscibility of several poly(ethylene-co-vinyl acetate) - EVA based polymer blends. EVA has many industrial applications and is often present as one of several polymeric components. Consequently, there is considerable interest in the thermodynamics of these blend systems, in order to understand and ultimately control their miscibility. This characterisation was to include assessing the relative enthalpic and entropic thermodynamic contributions to the interaction parameter of these blends.

To determine the enthalpic interaction parameter, a specialised "mixing calorimeter" was to be designed and constructed to measure the heat of mixing on blending these polymers. Free energy interaction parameters were to be determined using one of several possible techniques e.g. melting point depression. It is also intended that phase contrast optical microscopy will be used to identify possible phase boundaries in these blends and that wide angle X-ray scattering will monitor changes in the crystalline phases due to blending.

Comparison of these various χ values, together with optical microscopy and X-ray scattering results will provide a complete "miscibility picture" for each blend system studied.

References

1. D.R.Paul and S.Newman, Eds., Polymer Blends Vol. 1 and 2, Academic Press, New York (1978).
2. K.Solc, Ed., "Polymer Compatibility and Incompatibility - Principles and Practices", Harwood Academic, New York (1982).
3. O.Olabisi, L.M.Robeson and M.T.Shaw, "Polymer-Polymer Miscibility", Academic Press, New York (1979).
4. C.J.T.Landry and D.M.Teegarden, *Macromolecules*, 24, 4310 (1991).
5. Y.Jinghua, G.C.Alfonso, A.Turturro and E.Pedemonte, *Polymer*, 34, 1465 (1993).
6. D.R.Paul and J.W.Barlow, *Polymer*, 25, 487 (1984).
7. G. ten Brinke, F.E.Karasz and W.J.MacKnight, *Macromolecules*, 16, 1827 (1983).
8. J.K.H.Al-Kafaji, Z.Arrifin, J.Cope and C.Booth, *J. Chem. Soc., Faraday Trans. 1*, 81, 223 (1985).
9. A.E.Woodward, "Atlas of Polymer Morphology". Oxford University Press (1988).
10. Bayer Patent Application No. 87109362.1.
11. G.Allen and J.C.Bevington, Vol 2, "Comprehensive Polymer Science", Pergamon Press, (1989).
12. T.Nishi and T.K.Kwei, *Polymer*, 16, 285 (1975).
13. C.B.Bucknall, "Toughened Plastics", Applied Science, London (1977).
14. M.C.Reed, *Mod. Plast.*, 27, 117 (1949).
15. E.P.Cuzek, U.S. Patent 3,383,435 (1968).
16. R.L. Imken, D.R. Paul and J.W. Barlow, *Polym. Eng. Sci.*, 16, 593 (1976).
17. S.A.Liberman and A.S.Gomes, *J. Polym. Sci. Polym. Chem.*, 22, 2809 (1984).
18. J.J.Ziska, J.W.Barlow and D.R.Paul, *Polymer*, 22, 918 (1981).
19. P.J.Flory, "Principles of Polymer Chemistry", Cornell University Press (1953).
20. M.L.Huggins, *J. Am. Chem. Soc.*, 64, 1712 (1942).
21. P.J.Flory, *J. Chem. Phys.*, 10, 51 (1942).
22. G.Allen, Z.Chai, C.L.Chong, J.S.Higgins and J.Tripathi, *Polymer*, 25, 239 (1984).

23. P.J.Flory, R.A.Orwoll and A.Vrij, *J. Am. Chem. Soc.*, 86, 3507 (1964).
24. O.Olabisi, *Macromolecules*, 8, 316 (1975).
25. M.J.El-Hibri, W.Cheng and P.Munk, *ACS Polymer Mater. Sci. Eng.*, 58, 741 (1988).
26. T.Fukada, M.Nagata and H.Inagaki, *Macromolecules*, 17, 548 (1984).
27. C.CHan, B.J.Baurer, J.C.Clark, Y.Muroga, Y.Matsushita, M.Okada, Q.Tran-Cong, T. Chang and I.C. Sanchez, *Polymer*, 29, 2002 (1988).
28. F.S.Bates, S.B.Dierber and G.D.Wignall, *Macromolecules*, 19, 1938 (1986).
29. H.Hasegawa, S.Sakurai, M.Takenaka and T.Hashimoto, *Macromolecules*, 24, 1813 (1991).
30. T.Nishi and T.T.Wang, *Macromolecules*, 8, 909 (1975).
31. J.E.Harris, S.H.Goh, D.R.Paul and J.W.Barlow, *J. Polym. Sci.*, 27, 83 (1982).
32. Z.Chai, S.Roura, D.J.Walsh and J.S.Higgins, *Polymer*, 24, 263 (1983).
33. S.Rostami and D.J.Walsh, *Macromolecules*, 17, 315 (1984).

CHAPTER 2
THERMODYNAMICS OF POLYMER BLENDS

2.1 Introduction

The thermodynamics of polymer blends, first expressed by Scott¹ and Tompa² are essentially based on polymer solution theories^{3,4} which are themselves derived from liquid lattice theories, based on solutions of simple small molecules. This chapter will initially review these fundamental polymer solution thermodynamics and their relationship to polymer-polymer blend systems.

This study into the thermodynamics of several industrial polymer blends was essentially based on the classical Flory⁵-Huggins⁶ lattice theory which has been related to many polymer blends. This theory, from a suggestion by Meyer⁷, was based on the statistical thermodynamics of a hypothetical, rigid "lattice" model and has several limitations due to assumptions and approximations in the original model which will be discussed. Despite these well-documented limitations, the lattice theory continues to be used comprehensively in characterising the thermodynamics of many polymer blends and their phase equilibria.

An "equation of state" approach subsequently developed by Flory and his co-workers^{8,9,10} based on the earlier work of Prigogine¹¹ is generally regarded as a more accurate representation of polymer blend thermodynamics than the original "lattice" theory. In this approach the state parameters (temperature, volume and pressure) of a polymer or polymer blend, which represent their physical characteristics, were linked by a single partition function. From this function, thermodynamic information such as the volume change on mixing plus the heat and entropy of mixing could be evaluated. The thermodynamic expressions for the various quantities in this approach are quite complex and require the input of considerable thermodynamic information which has restricted the widespread use of this approach. The Prigogine-Flory approach has not been applied to this thermodynamic study and therefore only a very brief discussion of the major concepts will be given in order to give a basic understanding of the procedure.

2.2 Thermodynamics of Polymer Solutions

The general thermodynamic relationship which is used to describe polymers in solution systems relates the change in the Gibbs free energy of mixing function (ΔG_{mix}) to enthalpy (ΔH_{mix}) and entropy (ΔS_{mix}) changes, as follows:

$$\Delta G_{\text{mix}} = \Delta H_{\text{mix}} - T\Delta S_{\text{mix}} \quad (2.1)$$

A necessary (but not sufficient) criteria for homogenous polymer solutions to be formed is when the change in the free energy of mixing (ΔG_{mix}) is negative i.e. the free energy of the solution, G_{AB} is lower than the individual free energy components of the mixture, G_{A} and G_{B} :

$$\Delta G_{\text{mix}} = G_{\text{AB}} - (G_{\text{A}} + G_{\text{B}}) \quad (2.2)$$

In order to understand the behaviour of polymers in solution, the relative enthalpic and entropic components to the ΔG_{mix} value must be fully appreciated. To give a fundamental understanding of these components, a mixture of small molecules will be considered first, in order to define ideal and non-ideal behaviour which will then be subsequently related to polymers in solution.

2.2.1 Entropic contributions to mixing (ΔS_{mix})

Raoult's law defines an ideal solution as one in which the activity of each component in a mixture is equal to its mole fraction. This is valid only for components of comparable size and where intermolecular forces between like and unlike molecules are equal i.e. the total energy change of the system is unchanged on mixing ($\Delta H_{\text{mix}}=0$). Therefore, an ideal solution is formed when two components mix to give a free energy change which is completely determined by the entropy gain of each component from the extra degrees of freedom created by the solution process as shown in eqn. 2.3. The entropy gain (ΔS_{mix}) is called the combinatorial (or configurational) entropy and in ideal systems is assumed to be the only entropy contribution.

$$\Delta G_{\text{mix}} = -T\Delta S_{\text{mix}} \text{ (for ideal solutions)} \quad (2.3)$$

The greater entropy of a solution of small molecules when compared with the pure components is related to the number of distinguishable arrangements that the components can adopt in the solution. This can be calculated from the Boltzmann law for the entropy of mixing:

$$\Delta S_{\text{mix}} = k\text{Ln}(W) \quad (2.4)$$

where W is the number of possible molecular arrangements within the mixture and k is the Boltzmann Constant ($1.380662 \times 10^{-23} \text{ J K}^{-1}$).

The molecules of the pure components and their solutions are considered to be arranged with sufficient regularity that justifies representation by a lattice as shown in Figure 2.1.

Consider the mixing of N_1 molecules of component (1) with N_2 molecules of component (2) which is assumed to take place on this hypothetical lattice containing (N_1+N_2) cells. Assuming that mixing is totally random the total number of possible ways that the component molecules can be arranged on the lattice increases during mixing and is equal to $(N_1+N_2)!$. However, as interchanges between molecules of the same species will be indistinguishable i.e. molecules of component (1) with another molecule of (1), the number of distinguishable arrangements will be:

$$W = \frac{(N_1 + N_2)!}{N_1!N_2!} \quad (2.5)$$

Therefore, from the Boltzmann law (eqn. 2.4), the combinatorial entropy, S_C can be derived as :

$$S_C = k\text{Ln} \left[\frac{(N_1 + N_2)!}{N_1!N_2!} \right] \quad (2.6)$$

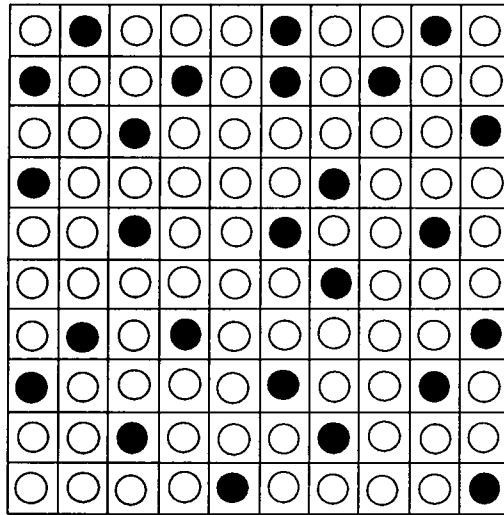


Figure 2.1 : Lattice model representation of a mixture of small molecules

The factorials can be simplified by Stirling's approximation i.e. $\ln(N!) = N \ln(N) - N$, and eqn. 2.6 becomes:

$$S_c = -k \left[N_1 \ln \left(\frac{N_1}{N_1 + N_2} \right) + N_2 \ln \left(\frac{N_2}{N_1 + N_2} \right) \right] \quad (2.7)$$

If x_1 (mole fraction of component 1) is expressed as:

$$x_1 = \left(\frac{N_1}{N_1 + N_2} \right) \quad (2.8)$$

and

$$R = k N_{AV} \quad (2.9)$$

where R is the Gas Constant ($8.314 \text{ J K}^{-1} \text{ mol}^{-1}$) and N_{AV} is the Avogadro Number ($6.022045 \times 10^{23} \text{ mol}^{-1}$).

then

$$S_c = -R(n_1 \ln(x_1) + n_2 \ln(x_2)) \quad (2.10)$$

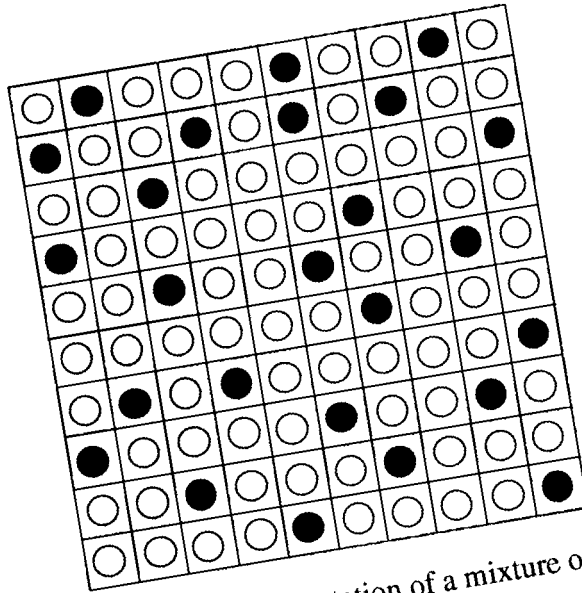


Figure 2.1 : Lattice model representation of a mixture of small molecules

The factorials can be simplified by Stirling's approximation i.e. $\ln(N!) = N \ln(N) - N$, and eqn. 2.6 becomes:

$$S_c = -k \left[N_1 \ln \left(\frac{N_1}{N_1 + N_2} \right) + N_2 \ln \left(\frac{N_2}{N_1 + N_2} \right) \right] \quad (2.7)$$

If x_1 (mole fraction of component 1) is expressed as:

$$x_1 = \left(\frac{N_1}{N_1 + N_2} \right) \quad (2.8)$$

$$R = k N_{AV} \quad (2.9)$$

and

where R is the Gas Constant ($8.314 \text{ J K}^{-1} \text{ mol}^{-1}$) and N_{AV} is the Avogadro Number ($6.022045 \times 10^{23} \text{ mol}^{-1}$).

then

$$S_c = -R (n_1 \ln(x_1) + n_2 \ln(x_2)) \quad (2.10)$$

where n_1 and n_2 are the number of moles of solvent and polymer respectively. As it is assumed that S_C is the only contribution to entropy changes during mixing:

$$\Delta S_{\text{mix}} = -R(n_1 \ln(x_1) + n_2 \ln(x_2)) \quad (2.11)$$

This expression represents the entropic contribution to the free energy of mixing in ideal solutions of small molecules and assumes that combinatorial entropy is the only entropy contribution. Eqn. 2.11 is derived assuming : **(a)** there is no volume change on mixing, **(b)** the molecules are of equal size, **(c)** all interchanges between the component molecules have the same energy ($\Delta H_{\text{mix}} = 0$) and **(d)** the motion of the components about their equilibrium positions remains unchanged on mixing.

By combining eqns. 2.3 and 2.11, an expression for the free energy change in an ideal system i.e. the mixing of small molecules, is obtained:

$$\Delta G_{\text{mix}} = -T\Delta S_{\text{mix}} = RT(n_1 \ln(x_1) + n_2 \ln(x_2)) \quad (2.12)$$

In practice, few liquid mixtures obey Raoult's Law and at least one of the four previous requirements **(a,b,c,d)** for ideal solution behaviour is not obeyed. These mixtures are therefore classed as non-ideal solutions.

Polymer solutions invariably exhibit large deviations from ideality and are classed as non-ideal except at extreme dilutions. The ideal law i.e. eqn. 2.12, is therefore of little value in predicting the thermodynamic properties of these polymer solutions and needs to be modified to represent the mixing of polymer-solvent systems. Non-ideal solutions are generally classed as regular or irregular solutions in which the heat of mixing (ΔH_{mix}) is finite in both cases whilst the entropy of mixing (ΔS_{mix}) can be ideal (regular solutions) or deviate from ideality (irregular solutions). The reasons for the non-ideal behaviour in polymer solutions is due not only to the existence of a finite heat of mixing but the large difference in molecular size between the polymer and solvent molecules.

Consequently the majority of polymer solutions are regarded as irregular, non-ideal solutions.

This can again be represented in terms of a two-dimensional lattice model. As previously shown in Figure 2.1, a non-polymer solution of two types of small molecules can be arranged on a hypothetical lattice in a large but calculable number of ways, W . However, the polymer solution is represented on the lattice as shown in Figure 2.2, with the polymer chain regarded as a series of small segments covalently bonded together. It is this effect of bond connectivity which leads to a deviation from the ideal entropy expression (eqn. 2.11). In the polymer-solvent system there are fewer possible arrangements in which the same number of lattice sites can be occupied by polymer segments as fixing one segment at a lattice point severely limits the number of possible sites for the adjacent segment. Due to this reduction in possible arrangements in the polymer-solvent system, the combinatorial entropy of mixing is small compared to that with normal mixtures of small molecules and differs considerably from that calculated for the ideal system.

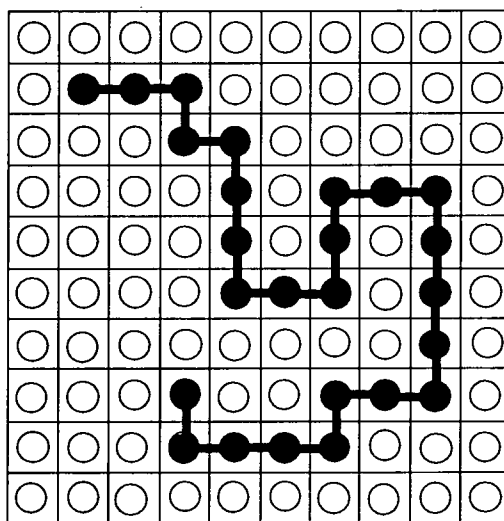


Figure 2.2 : Lattice model representation of a polymer chain molecule in a solvent

Therefore, eqn. 2.12 is unable to approximate the combinatorial entropy contribution in polymer-solvent systems. This led to Flory⁵ and Huggins⁶ separately proposing (but differing only in minor detail) an expression for the combinatorial entropy contribution in

polymer-solvent systems. This polymer solution theory was again based on a lattice model which contained both solvent and polymer molecules and to calculate the number of possible arrangements in which the chain could be accommodated on the lattice, the theory encompassed several restrictions. The polymer chain was sub-divided into m covalently bonded segments each of which had the same volume as the solvent molecules i.e. $m = V_2/V_1$ where V_2 and V_1 refer to the molar volumes of the polymer and solvent respectively. The number of sites available on the lattice was N_1 and mN_2 containing N_1 and N_2 molecules of solvent and polymer respectively. The polymer segments must also occupy m contiguous sites due to their connectivity.

The calculation of possible arrangements on the lattice was considerably more complex than for the non-polymeric solvent systems. This again involved the use of probabilities which finally resulted in the classical Flory-Huggins expression for the entropy of mixing of polymer with solvent.

$$\Delta S_{\text{mix}} = -R(n_1 \text{Ln}(\phi_1) + n_2 \text{Ln}(\phi_2)) \quad (2.13)$$

where ϕ_1 and ϕ_2 are the volume fractions of solvent and polymer respectively and are defined as:

$$\phi_1 = \frac{m_1 n_1}{m_1 n_1 + m_2 n_2} \quad (2.14a)$$

$$\phi_2 = \frac{m_2 n_2}{m_1 n_1 + m_2 n_2} \quad (2.14b)$$

where m is the number average degree of polymerisation. For the solvent, m_1 is generally taken as 1 and the term $m_1 n_1$ simplifies to n_1 .

In eqn. 2.13, the volume fraction has replaced the mole fractions in the natural log terms of the ideal entropy of mixing expressed in eqn. 2.11. This change is due to the

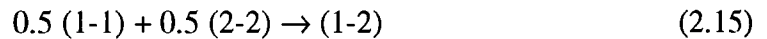
large differences in the size of the solvent and polymer components which would normally result in mole fractions close to unity for the solvent.

Eqn. 2.13 can be applied to polymer-polymer blends in which ϕ_1 and ϕ_2 refer to the separate polymer components. For polymer-polymer systems, eqns. 2.14a and 2.14b continue to be used i.e. when $m_1 \neq 1$.

It should also be remembered that eqn. 2.13 represents only the "combinatorial entropy" which has been calculated based on the external arrangement of the molecules and their segments, rather than their internal configurations.

2.2.2 Enthalpic contributions to mixing (ΔH_{mix})

In both regular and irregular solutions, an energy or heat change generally occurs on mixing i.e. $\Delta H_{\text{mix}} \neq 0$. The free energy of mixing (ΔG_{mix}) in polymer solutions is therefore the entropic component ($-T\Delta S_{\text{mix}}$) as determined by the Flory-Huggins lattice theory plus an enthalpic term (ΔH_{mix}). This enthalpy or heat of mixing change is assumed to arise from a difference in the contact energy between like and unlike molecules i.e. the formation of solvent-polymer (1-2) contacts on mixing requires the breaking of some of the solvent-solvent (1-1) and polymer-polymer (2-2) contacts and this can be represented as^{12,13}:



This can be expressed as an interchange energy per (1-2) contact (ΔE_{12}), as shown:

$$\Delta E_{12} = E_{12} - 0.5 (E_{11} + E_{22}) \quad (2.16)$$

where E_{11} , E_{22} and E_{12} are the contact energies for each "pair contact" or bond.

For a single arrangement of molecules on a lattice containing N_C unlike contacts, the heat of mixing (ΔH_{mix}) for this single configuration from the pure components is:

$$\Delta H_{\text{mix}} = N_C \Delta E_{12} \quad (2.17)$$

The average number of unlike contacts (N_C) during random mixing of the polymer and solvent molecules can be estimated based on the number of contact sites available on the lattice and the probability that neighbouring molecules are different.

In a lattice of co-ordination number z , the total number of contact sites between a polymer molecule and its neighbouring molecules will be $(z-2)$ per polymer repeat unit plus two additional contacts for the terminal units. This gives the total number of contacts to be $(z-2)m_2+2$ where m_2 is the number of repeat units in the polymer. This term can be approximated to zm_2 .

If mixing on the lattice is completely random, the probability that one of these contacts is a solvent molecule adjacent to the polymer molecule is equal to the volume fraction of the solvent component, ϕ_1 . Therefore, for N_2 polymer molecules :

$$N_C = zm_2\phi_1N_2 \quad (2.18)$$

Since,

$$N_2 = N_{\text{AV}}n_2 \quad (2.19)$$

where N_{AV} is the Avogadro number and n_2 the number of moles of polymer (2).

Therefore :

$$N_C = zm_2n_2\phi_1N_{\text{AV}} \quad (2.20)$$

From the definitions of ϕ_1 and ϕ_2 (eqns. 2.14a and 2.14b) :

$$m_2n_2\phi_1 = m_1n_1\phi_2 \quad (2.21)$$

Consequently, if the reverse situation is considered i.e. a solvent molecule surrounded by a polymer molecule, then for n_1 moles of solvent :

$$N_C = zm_1n_1\phi_2N_{\text{AV}} \quad (2.22)$$

Combining eqns. 2.17 and 2.22:

$$\Delta H_{\text{mix}} = z m_1 n_1 \phi_2 \Delta E_{12} N_{\text{AV}} \quad (2.23)$$

This is the well known van Laar expression for the heat of mixing in a two component system. To simplify this expression, a dimensionless "interaction parameter", χ_{12} (Chi), is introduced and is defined by:

$$\chi_{12} = \frac{z \Delta E_{12} N_{\text{AV}}}{RT} \quad (2.24)$$

It can also be expressed in the alternative form:

$$RT\chi_{12} = B V_1 \quad (2.25)$$

where B is the interaction energy density and V_1 is the molar volume of the solvent. The interaction parameter is a very important feature in understanding the miscibility of polymer-solvent and polymer-polymer systems and is essentially the difference in energy that a molecule possesses when surrounded by molecules of another species compared to the pure state. χ_{12} can be positive or negative and from eqn. 2.24, is theoretically inversely proportional to temperature.

From eqns. 2.23 and 2.24, the final expression is:

$$\Delta H_{\text{mix}} = RT m_1 n_1 \phi_2 \chi_{12} \quad (2.26)$$

Generally, solvent molecules are assumed to have m_1 values of 1 and eqn. 2.26 simplifies to :

$$\Delta H_{\text{mix}} = RT n_1 \phi_2 \chi_{12} \quad (2.27)$$

From eqn. 2.1, it is clear that a negative i.e. exothermic ΔH_{mix} value and consequently (from eqn. 2.26) a negative χ_{12} value, is favourable to miscibility (in polymer blends) and dissolution (in polymer solutions). However, for non-polar mixtures, ΔH_{mix} values are generally positive, endothermic quantities resulting in positive χ_{12} values which are unfavourable to miscibility or dissolution.

Several authors^{14,15} have reported that in blends containing random copolymer-type components, a mechanism other than specific interactions can lead to miscibility. Copolymers containing very different covalently bonded monomers i.e. polar and non-polar segments, may have a natural "repulsion" effect. These copolymers are therefore likely to be miscible with other polymers when miscibility can reduce the number of these "unfavourable" interactions between the segments of the same polymer. In these blends, the driving force for blend miscibility i.e. a net exothermic "heat of mixing" (in the absence of entropic contributions) may therefore be realised by *intramolecular* rather than *intermolecular* interactions. The contribution of intramolecular interactions to blend miscibility can clearly be shown by the numerous cases of miscibility involving copolymers when their corresponding homopolymers are immiscible. A classic example of this effect is illustrated by poly(ethylene-co-vinyl acetate) copolymers which are miscible with poly(vinyl chloride) whereas both polyethylene and poly(vinyl acetate) homopolymers are immiscible with poly(vinyl chloride)¹⁶.

χ_{12} values determined from ΔH_{mix} measurements represent the enthalpic interaction between the polymer components. However, as discussed in subsequent sections, χ_{12} is assumed to have the character of a free energy i.e. with entropic contributions. The sign and magnitude of these free energy χ_{12} values enables the free energy interaction between the polymers to be characterised with negative χ_{12} values indicating miscibility/dissolution.

χ_{12} also incorporates all the original parameters of the hypothetical lattice theory. Both the heat of mixing expressions (2.26) and the entropy of mixing expressions (2.13) retain no parameters of the hypothetical lattice theory.

2.2.3 Free Energy of Mixing (ΔG_{mix})

As the separate enthalpic and entropic contributions in polymer solutions have been derived (eqns. 2.27 and 2.13 respectively) and assuming that the combinatorial entropy represents the total entropy change (ΔS_{mix}), these can now be combined in order to give the expression for the free energy of mixing in polymer solutions i.e. $\Delta G_{\text{mix}} = \Delta H_{\text{mix}} - T\Delta S_{\text{mix}}$, as:

$$\Delta G_{\text{mix}} = RTn_1\phi_2\chi_{12} - \left(-RT[n_1\text{Ln}(\phi_1) + n_2\text{Ln}(\phi_2)]\right) \quad (2.28)$$

which rearranges to:

$$\Delta G_{\text{mix}} = RT(n_1\text{Ln}(\phi_1) + n_2\text{Ln}(\phi_2) + n_1\phi_2\chi_{12}) \quad (2.29)$$

This is the classical Flory-Huggins expression for the free energy change on mixing polymer and solvent components³ and is a major "foundation stone" in polymer solution thermodynamics. Eqn. 2.29 has subsequently been applied to polymer-polymer systems, in which subscripts 1 and 2 refer to the separate polymer components, using a slightly modified expression (obtained by combining eqns. 2.26 and 2.13) in which $m_1 \neq 1$:

$$\Delta G_{\text{mix}} = RT(n_1\text{Ln}(\phi_1) + n_2\text{Ln}(\phi_2) + m_1n_1\phi_2\chi_{12}) \quad (2.30)$$

which from eqn. 2.21 can also be expressed as :

$$\Delta G_{\text{mix}} = RT(n_1\text{Ln}(\phi_1) + n_2\text{Ln}(\phi_2) + m_2n_2\phi_1\chi_{12}) \quad (2.31)$$

If the heat of mixing value (ΔH_{mix}) of a polymer blend can be measured at various compositions, then the composition dependence of both the enthalpic interaction parameter (χ_{12}) and the free energy of mixing (ΔG_{mix}) can be measured from eqns. 2.26

and 2.30 respectively (see Chapter 7). By comparing both these thermodynamic quantities, the miscibility (or immiscibility) of the blend can be understood in terms of the separate enthalpic and entropic contributions.

In a blend of polymer (1) and polymer (2), eqn. 2.31 can also be expressed in terms of the chemical potential of polymer (2) in the polymer mixture (μ_2) relative to the chemical potential of the pure component (μ_2^0). Therefore, by partial differentiation of the expression with respect to n_2 i.e. moles of polymer (2), the chemical potential per mole of polymer (2), or relative partial molar free energy is obtained :

$$\mu_2^1 - \mu_2^0 = RT \left[\text{Ln}(\phi_2) + \phi_1 \left(1 - \frac{m_2}{m_1} \right) + \chi m_2 \phi_1^2 \right] \quad (2.32)$$

In the polymer-solvent system, m_1 (solvent repeat unit) = 1 and eqn. 2.32 becomes :

$$\mu_2^1 - \mu_2^0 = RT \left[\text{Ln}(\phi_2) + \phi_1 (1 - m_2) + \chi m_2 \phi_1^2 \right] \quad (2.33)$$

Dividing eqn. 2.32 by the number of repeat units per molecule of polymer (2) which is $m_2 V_{1U}/V_{2U}$ where V_{1U} and V_{2U} are the molar volumes of the repeat units in polymers (1) and (2) respectively, the following expression is obtained :

$$\mu_{2U}^1 - \mu_{2U}^0 = \frac{RTV_{2U}}{V_{1U}} \left[\frac{\text{Ln}(\phi_2)}{m_2} + \phi_1 \left(\frac{1}{m_2} - \frac{1}{m_1} \right) + \chi \phi_1^2 \right] \quad (2.34)$$

This represents the chemical potential difference per repeat unit of polymer (2) in a mixture of polymers (1) and (2). Eqn. 2.34 was derived by Scott¹ and was the first treatment which related the thermodynamic mixing in polymer blends. This equation has subsequently been developed further by Nishi and Wang¹⁷ to determine the χ interaction

parameter from the melting point depression of a semi-crystalline polymer on blending with an amorphous polymer (see Chapter 4).

The original Flory-Huggins expression for a polymer blend (eqn. 2.30) can be modified to represent the free energy of mixing **per lattice segment** in a binary polymer blend, as discussed below.

The volume fraction (ϕ_i) of each polymer component can be expressed in terms of the number of moles (n_i) and the molar volume (V_i) of each component.

$$\phi_i = \frac{n_i V_i}{V} \quad (2.35)$$

where V is the total volume (V_1+V_2). V_i is essentially the volume occupied by all the repeat units (m_i) in the polymer chain which is a function of the lattice segment volume (V_o):

$$V_i = m_i V_o \quad (2.36)$$

From eqns. 2.35 and 2.36 :

$$n_i = \frac{V\phi_i}{m_i V_o} \quad (2.37)$$

Substituting eqn. 2.37 for each polymer component into eqns. 2.13 and 2.26 :

$$\Delta S_{\text{mix}} = -\frac{RV}{V_o} \left(\frac{\phi_1}{m_1} \text{Ln}(\phi_1) + \frac{\phi_2}{m_2} \text{Ln}(\phi_2) \right) \quad (2.38)$$

$$\Delta H_{\text{mix}} = \frac{RTV\phi_1\phi_2\chi_{12}}{V_o} \quad (2.39)$$

The entropy and enthalpy of mixing changes per lattice segment can be obtained by dividing eqns. 2.38 and 2.39 by V/V_0 i.e. the number of segments on the lattice. Combining these contributions according to eqn. 2.1 results in an expression for the free energy of mixing per lattice segment of a binary polymer blend :

$$\frac{\Delta G_{\text{mix}}}{RT} = \frac{\phi_1}{m_1} \text{Ln}(\phi_1) + \frac{\phi_2}{m_2} \text{Ln}(\phi_2) + \phi_1\phi_2\chi_{12} \quad (2.40)$$

This well known expression which assumes that the blend components have equal segment volumes, has been used extensively in studying polymer blends (see Chapter 9 - small angle neutron scattering).

2.3 Polymer Blend Miscibility

From eqn. 2.28, the combinatorial entropy contribution always favours miscibility i.e. a negative ΔG_{mix} value and the degree of this entropy change is highly dependent on the molecular weight of the polymer components. As the molecular weight of the polymer increases, the number of moles (n_i) decreases for a specific weight and the favourable entropy change (ΔS_{mix}) is reduced. In commercial polymer blends, the molecular weight of the polymer components are generally high and consequently the combinatorial entropic contribution is very small and virtually zero.

Furthermore, unless specific interactions occur between the polymer components e.g. hydrogen bonding or polar interactions, the enthalpy or heat change on mixing (ΔH_{mix}) is generally endothermic i.e. a positive ΔH_{mix} which is unfavourable to mixing.

In view of these considerations, it is not surprising that few polymer blends are miscible but several "scenarios" may exist which could result in polymer miscibility:

2.3a. If the polymer components in the blend are relatively low molecular weight, the favourable combinatorial entropy contribution may dominate any unfavourable enthalpy effect (positive ΔH_{mix} value) to result in a negative and favourable free energy of mixing value.

2.3b If the polymer components on mixing have specific intermolecular interactions, the enthalpy of mixing will be exothermic resulting in a negative ΔG_{mix} value which is favourable to miscibility irrespective of the configurational entropy contribution. Therefore, identification of an exothermic heat of mixing value is generally taken to indicate blend miscibility.

2.4 Limitations of the Flory-Huggins Lattice theory

The previously derived expressions for the entropy of mixing in polymer-solvent and polymer-polymer systems are very attractive by virtue of their simplicity. However, the lattice theory treatment encompasses various major assumptions and approximations which must be examined in order to appreciate the limitations of the theory.

2.4a The use of a single lattice model to represent either the pure polymer or solvent components is not an unjustified idealisation. However, the use of the **same** lattice model to represent all intermediate compositions is a major approximation which is not justified by the spacial differences between the components and would only truly be viable if the geometry of the two molecular species were essentially identical. Therefore, improvement of the lattice theory has been essentially directed at refining the original mathematical model to provide a more accurate configurational entropy value. This resulted in considerably more complicated expressions derived by Huggins¹⁸, Miller¹⁹ and Guggenheim¹³ which appear to give no significant improvement in their agreement with experimental data²⁰.

2.4b The lattice theory assumes that configurational entropy ($\Delta S_{\text{mix}}^{\text{con}}$) is the only contribution to the total entropy of mixing. However, any change in the volume of the blend, the vibration frequencies of the components or the assumption that the mixture is random would give a contribution to the entropy of mixing (ΔS_{mix}) in the form of a non-combinatorial "excess entropy" term ($\Delta S_{\text{mix}}^{\text{exc}}$). Therefore, strictly the change in the free energy of mixing is composed of the following parts:

$$\Delta G_{\text{mix}} = \Delta H_{\text{mix}} - T\Delta S_{\text{mix}}^{\text{con}} - T\Delta S_{\text{mix}}^{\text{exc}} \quad (2.41)$$

For regular polymer solutions the excess entropy is zero as defined by Hilderbrand²¹ and the non-ideal behaviour is due entirely to a finite ΔH_{mix} value.

If preferential attractions (or repulsions) occur between the components i.e. ΔH_{mix} is exothermic or endothermic respectively, the molecules will have a tendency to cluster²² and the probability of finding a polymer molecule adjacent to a solvent molecule on the lattice will change. This quasi-chemical interaction²³ contradicts the random mixing approximation which assumes maximum disorder and consequently contributes a negative $\Delta S_{\text{mix}}^{\text{exc}}$ value due to the resulting increase in order within the mixture. Orr¹² and Guggenheim¹³ derived entropy of mixing expressions which considered these interactions and concluded that modifications in calculating the combinatorial entropy, accounting for excess entropy contributions due to non-randomness were negligible compared to the other approximations.

2.4c The main contributors to a significant excess entropy change on mixing were therefore believed to be due to changes in the volume of the solution (or blend) and the vibration frequencies of the components. In the original lattice treatment of polymer solutions, the flexibility of the polymer chain was assumed to be unchanged from the solid to the solution state neglecting possible entropic contributions due to specific interactions between neighbouring polymer-solvent molecules. However, on mixing polymers (1) and (2), new (1-2) intermolecular contacts are formed which change the

internal motion i.e. vibration frequencies of both components and consequently result in non-combinatorial excess entropy changes, in addition to the combinatorial entropy change.

In the above expressions, the interactions which result in the formation of new (1-2) contacts, have been accounted for only in the enthalpic heat of mixing expressions. Therefore, the formation of unlike (1-2) contacts, represented in eqn. 2.16 should also be characterised by an entropy change as well as a heat or energy change. This entropy change (as for the heat change) must be proportional to the number of unlike (1-2) contacts on mixing. Therefore, ΔE_{12} should strictly be interpreted as a free energy change²⁴ consisting of two contributions; the heat or enthalpy change (ΔE_H) plus the product of the absolute temperature and non-combinatorial excess entropy change ($-T\Delta E_S$), as shown:

$$\Delta E_{12} = \Delta E_H - T\Delta E_S \quad (2.42)$$

Flory related the free energy character of ΔE_{12} to the separate enthalpy and excess entropy contributions in polymer solutions³. Consequently, the interaction parameter, χ_{12} , in a blend of polymers (1) and (2) defined by eqn. 2.24 was considered to be a free energy term containing both enthalpic (χ_H) and non-combinatorial (excess) entropic contributions (χ_S) i.e. :

$$\chi_{12} = \chi_H + \chi_S \quad (2.43)$$

From eqns. 2.24 and 2.42 :

$$\chi_H = \frac{z\Delta E_H N_{AV}}{RT} \quad (2.44)$$

$$\chi_S = -\frac{z\Delta E_S N_{AV}}{R} \quad (2.45)$$

These contributions were defined by Flory³ as :

$$\chi_H = -T(\partial\chi_1/\partial T) \quad (2.46)$$

$$\chi_S = \partial(T\chi_1)/\partial T \quad (2.47)$$

To represent the excess entropic contributions on mixing polymer blends, eqn. 2.30 becomes:

$$\Delta G_{\text{mix}} = RT(n_1 \text{Ln}(\phi_1) + n_2 \text{Ln}(\phi_2) + m_1 n_1 \phi_2 \chi_H + m_1 n_1 \phi_2 \chi_S) \quad (2.48)$$

Intuitively, on polymer blending, the excess entropy change due to the formation of new (1-2) contacts would be expected to be positive i.e. an increase in disorder. This results in a positive ΔE_S change and consequently (from eqn. 2.45), a negative χ_S value which favours miscibility.

If ΔE_{12} is independent of temperature, the non-combinatorial entropy contribution ($-T\Delta E_S$) in eqn. 2.42 is zero and χ_{12} (like χ_H) is inversely proportional to temperature, as shown in eqn. 2.24 and has the general form :

$$\chi_{12} = \frac{a}{T} + b \quad (2.49)$$

Therefore, χ_{12} decreases monotonically as a function of temperature (T) until at a critical χ_{12} value the blend becomes immiscible (see section 2.5 - Phase Separation).

2.4d The lattice theory assumes that both components in a mixture or solution have the same segmental volume and thereby on mixing, no volume change occurs. However, the entropy of a system depends on its volume and systems which dilate or contract on mixing have a significant excess entropy contribution to the free energy of mixing. This excess entropy can be sufficiently large as to dominate the thermodynamics of the blend

or solution and can ultimately determine the miscibility of the system. The inability of the lattice theory to account for excess entropy contributions is a major limitation in the approach and this will be discussed further in the context of phase separation (section 2.5).

2.4e The molecules of each polymer component are assumed to be distributed randomly throughout the lattice. However, this assumption is only relevant at relatively high polymer concentrations.

2.4f Using the treatment, the blend interaction parameter (χ) value is independent of composition. However, χ has been shown many times to be dependent on composition which has subsequently been described in terms of the surface area difference between the component segments²⁵ and the effect of non-random mixing^{14,23}.

Despite these limitations, the Flory-Huggins lattice theory continues to find widespread use in miscibility studies on polymer blends which is due to its relative simplicity compared to the "equation of state" approach.

2.5 Phase Separation

By examining the temperature and composition dependence of the free energy change on mixing polymer components, as previously derived by the Flory-Huggins lattice theory, predictions can be made regarding the phase equilibria within these systems.

The necessary thermodynamic conditions for a polymer blend to be miscible at a specific composition and temperature are that the free energy change on mixing (ΔG_{mix}) must be less than the free energies of the individual polymer components (eqn. 2.50) and the second derivative of the free energy with respect to composition is always positive (eqn. 2.51).

Criteria for Miscibility :

$$(i) \quad \Delta G_{\text{mix}} < 0 \quad (2.50)$$

$$(ii) \quad \frac{\partial^2 \Delta G_{\text{mix}}}{\partial \phi_2^2} > 0 \quad (2.51)$$

In the absence of specific intermolecular interactions (hydrogen bonding, dipole-dipole etc.), polymer blends generally have endothermic i.e. positive ΔH_{mix} values. From eqn. 2.1, this indicates that enthalpically, the blend favours immiscibility i.e. miscibility criteria (i) is not met. If the combinatorial entropy contribution (which always favours mixing) is small i.e. in high molecular weight polymers, the enthalpic component will dominate and consequently the free energy change on mixing will be positive and the blend immiscible.

However, enthalpy of mixing values are generally regarded as independent of temperature (eqn. 2.23) and constant for a specific polymer pair composition. In contrast, the entropic component and consequently the free energy change are directly dependent on the absolute temperature and both become increasingly negative and favourable to miscibility as temperature increases. This temperature dependence results in the phase behaviour noted in Figure 2.3 (bottom), in which an unstable, immiscible polymer blend eventually forms a stable miscible phase as the temperature is increased, i.e. the criteria for miscibility (eqns. 2.50 and 2.51) are met.

This miscibility curve can be understood in terms of the free energy-composition profiles at certain temperatures (T_1, T_2, T_3, T_C, T_4) as shown in Figure 2.3 (top). For a polymer blend at temperature T_4 , the free energy-composition profile is concave, satisfies both criteria for miscibility and is therefore miscible at all compositions.

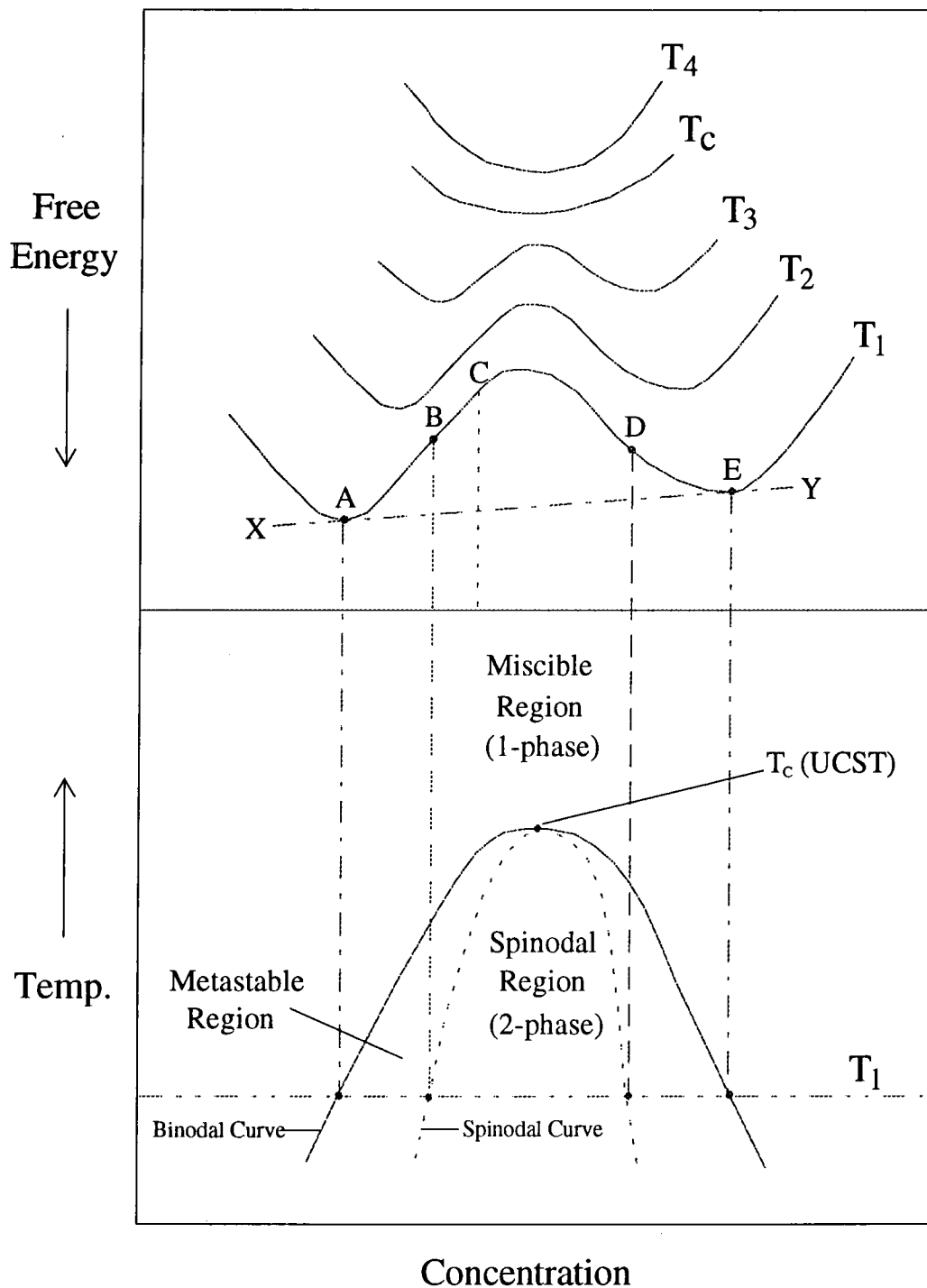


Figure 2.3 : Phase Separation in Polymer Blends

However, if the free energy profile displays convexity, as noted at temperature T_1 , a polymer blend of composition C will phase separate into two phases of composition A and E which are measured from the double tangent XY . Between compositions B and D (which encompasses composition C), $\partial^2 \Delta G_{\text{mix}} / \partial \phi_2^2$ is negative and therefore any small fluctuations in composition will result in a lower free energy value than the original

system. Consequently, spontaneous phase separation occurs into phases of composition A and E i.e. the lowest free energy states. Compositions at B and D mark a change in the curvature of the free energy curve i.e. $\partial^2 \Delta G_{\text{mix}} / \partial \phi_2^2 = 0$ and therefore, these form the compositional boundary of the spontaneous separation. This boundary is defined as the spinodal and the spontaneous phase separation is known as spinodal decomposition.

In the composition ranges A to B and D to E, $\partial^2 \Delta G_{\text{mix}} / \partial \phi_2^2$ is positive and any small fluctuations will result in an increase in free energy which subsequently prevents phase separation. Relatively large concentration fluctuations are therefore required to result in the free energy reduction which is necessary for phase separation to occur. These composition ranges are therefore regarded as metastable phases and the limit of metastability is again the lowest free energy compositions at tangent points A and E. Phase separation in the metastable region occurs via a "nucleation and growth" process in which the large concentration fluctuations necessary to induce phase separation are termed nuclei.

As the temperature is increased i.e. T_2 and T_3 , the contact points of the tangent XY on the free energy profiles begin to coincide and the locus of these points at various temperatures forms the binodal or "cloud point curve", which separates the stable (miscible) region from the metastable phase. The locus of the points at $\partial^2 \Delta G_{\text{mix}} / \partial \phi_2^2 = 0$ forms the spinodal which separates the metastable phase from the unstable (immiscible) spinodal region.

As the temperature continues to increase, a critical state is finally achieved at which the spinodal meets the binodal to form an homogenous one phase mixture at T_C , which in this type of phase diagram is referred to as the upper critical solution temperature (UCST). At this critical temperature:

$$\frac{\partial^2 \Delta G_{\text{mix}}}{\partial \phi^2} = \frac{\partial^3 \Delta G_{\text{mix}}}{\partial \phi^3} = 0 \quad (2.52)$$

Therefore, the critical conditions for miscibility in polymer blends are obtained when the second and third derivatives of the free energy change, as expressed in eqns. 2.30 and 2.31, with respect to concentration are zero. From these differential equations, the polymer mixture at the critical temperature (T_c) have critical χ and ϕ_1 values expressed as :

$$\chi_c = \frac{1}{2} \left[\frac{1}{m_1^{1/2}} + \frac{1}{m_2^{1/2}} \right]^2 \quad (2.53)$$

$$(\phi_1)_c = \frac{m_2^{1/2}}{m_1^{1/2} + m_2^{1/2}} \quad (2.54)$$

where m_1 and m_2 are the degrees of polymerisation i.e. the number of repeat units in both polymers. χ_c is the minimum value of χ on the spinodal curve at which the blend spontaneously phase separates and is obtained at a volume fraction $(\phi_1)_c$. The value of χ_c is always positive and for high molecular weight polymer blends with large m values, is very small and regarded as zero. Miscibility in these systems is therefore generally associated with a negative χ value. For polymer solutions (and low molecular weight polymer blends), χ_c can be close to the maximum of 0.5 and miscibility can theoretically be achieved at small positive χ values.

The original Flory-Huggins lattice theory predicts that χ_{12} decreases monotonically with temperature rise (eqn. 2.24) which implies that the "miscibility" of a polymer blend system or, in the case of a polymer solution, the solvating power of the solvent continuously improves as the temperature is raised. Consequently, the lattice theory can only predict UCST behaviour. However, experimental evidence clearly indicates that this is not the only type of phase separation with Freeman and Rowlinson²⁶ first showing that polymer solutions can separate into two phases on raising as well as lowering the temperature. Prior to these results this new critical temperature had not been observed as the boiling point of the solvent was usually at a lower temperature. As the upper

critical solution temperature (UCST) was at the top of a two-phase region, the new critical temperature was called a lower critical solution temperature (LCST) as it lay at the bottom of a two phase region as shown in Figure 2.4.

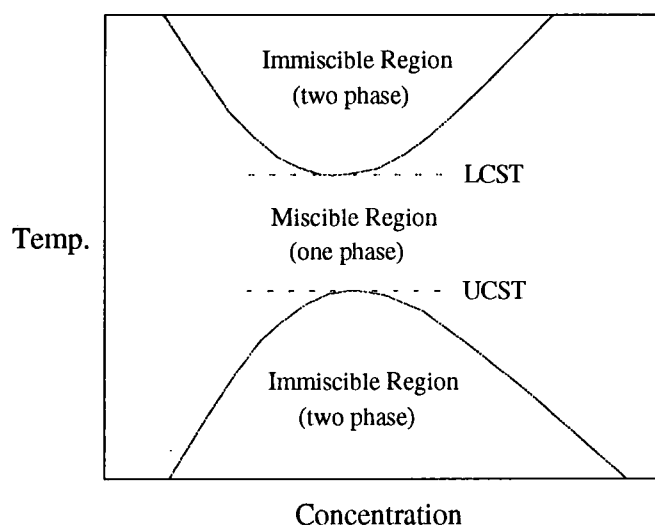


Figure 2.4 : Phase separation boundaries in polymer mixtures

To account for both UCST and LCST behaviour as the temperature is increased, the χ_{12} value must first decrease to a critical value (χ_c) at which miscibility occurs (UCST) before passing through a minimum and then increasing to a critical value at which phase separation occurs (LCST).

Generally, UCST behaviour occurs in blends of low molecular weight components which have a positive ΔH_{mix} i.e. a positive χ_H value and a number of examples have been reported^{27,28}. In these systems, miscibility at the UCST represents the point at which the large, favourable configurational entropy begins to dominate the unfavourable enthalpic component finally resulting in miscibility. In these low molecular weight blends, LCST behaviour is extremely rare.

In contrast, for blends containing high molecular weight homopolymers, LCST behaviour is generally exhibited where intermolecular interactions result in negative ΔH_{mix} (and χ_H) values e.g. chlorinated polyethylene with poly(methylmethacrylate)²⁹ and poly(ethylene oxide) with poly(vinyl acetate)³⁰. For phase separation to occur in these

blends, the entropy of mixing value must be negative i.e. unfavourable to miscibility which finally results in phase separation at the LCST. In these high molecular weight blends, UCST behaviour is seldom observed.

It therefore appears that LCST behaviour indicates a fundamental difference between high molecular weight and low-molecular weight polymer blends. A UCST is due to a positive or endothermic ΔH_{mix} in low molecular weight mixtures whereas the LCST arises from a negative contribution to the entropy of mixing in high molecular weight mixtures.

A negative entropy of mixing is difficult to explain within the confines of the original lattice assumptions. Generally the disorder of a system i.e. the combinatorial and non-combinatorial (excess) entropy contributions, would be expected to increase i.e. be positive on mixing. As the combinatorial contribution can only be positive and favourable, the negative entropy change which results in positive χ_S values and LCST behaviour must be due to the excess entropy term ($\Delta S_{\text{mix}}^{\text{exc}}$).

The inability of the Flory-Huggins lattice theory to predict the negative excess entropy term which is instrumental in LCST behaviour, was due to the initial assumption that the volume of the lattice remained constant on mixing. If this restriction is removed then a contraction in volume on mixing would result in an intuitively, more ordered system and consequently a negative excess entropy contribution. These negative entropy contributions, due to volume changes, become increasingly unfavourable to miscibility as the temperature increases until phase separation eventually occurs at the LCST. The existence of an LCST has also been attributed to other causes i.e. specific intermolecular interactions (hydrogen bonding, dipole-dipole etc.) result in exothermic (negative) heat of mixing values which generally indicate miscibility of the polymer components. However, these interactions and consequently, the heat of mixing values, may be strongly dependent on temperature and this can ultimately effect miscibility. In addition, these interactions may also result in some degree of order within the solution or blend resulting in a decrease in the excess entropy contribution which is unfavourable to mixing.

The Flory-Huggins lattice theory is based on a rigid lattice model which is strictly valid only at absolute zero i.e. the temperature at which the molecules are expected to be motionless. The lattice theory cannot quantify the negative excess entropy contributions due to volume changes and therefore fails to predict LCST behaviour. This limitation led to the development of an elaborate "equation of state" approach based on a flexible lattice model which incorporated the effects of volume, temperature and pressure.

2.6 Equation of State Theory

As previously discussed, the Flory-Huggins lattice theory does not account for the volume changes on mixing which can result in excess entropy contributions. This led to Flory and co-workers^{8,9,10} continuing the earlier work of Prigogine¹¹ and developing a new expression for ΔG_{mix} based on the "equation of state" properties of the pure components which was subsequently applied to polymer-polymer blends by MacMaster³¹. This approach considered a flexible lattice, whose volume could change with temperature, pressure and composition of the solutions.

"Equation of state" theories are more ambitious than the Flory-Huggins lattice theory and consequently the various thermodynamic expressions in this approach are complex. Comprehensive details on the derivation of these expressions are documented elsewhere^{4,22,32} and will not be reproduced here. This section will serve to give only a very brief discussion of this elaborate approach.

As the temperature of a mixture is increased, the separate components (polymer-polymer, polymer-solvent) expand at different rates which create free volume differences between the components. The free volume of the components increasingly diverge as the temperature is increased which corresponds to a loss in entropy and when this negative entropy is sufficiently large, phase separation occurs at the LCST.

The term "free volume" refers to the unoccupied space in the component due to the inefficient packing of the polymer chains in the amorphous region of the sample. Consequently the free volume of a component is a measure of the volume available for

the component to undergo rotational and translational motion and this will increase with temperature as the molecular motion increases.

The equation of state theories modify the temperature dependence of the binary interaction parameter (χ_{12}) to take into account the negative entropic contributions due to dissimilarities in the free volume between the components, as shown :

$$\chi_{12} = \frac{X_{12}}{T} + B(T) \quad (2.55)$$

X_{12} is the enthalpic component of the interaction parameter, T is the absolute temperature and $B(T)$ is a term representing the "free volume" dissimilarities between the components which is positive with an exponential dependence on temperature. The first term in eqn. 2.55 essentially obeys the Flory-Huggins lattice theory in which χ_{12} decreases with a corresponding increase in temperature until at a critical χ_{12} value, miscibility occurs (UCST). However, the second term in this expression, $B(T)$ which represents the free volume dissimilarities between the components, gains in importance as the temperature increases and subsequently modifies the nature of χ_{12} , resulting in increasingly positive values which at a critical value (χ_c) result in phase separation at the LCST.

It is therefore clear from eqn. 2.55 that the appearance of LCST behaviour is due to entropic components from free volume differences. Cowie³³ gave a good, simplistic illustration of the LCST in terms of the flexible lattice theory for polymer solutions which is equally applicable to polymer blends. As the polymer and solvent lattices expand at different rates on increasing temperature, the highly expanded solvent lattice must be distorted in order to accommodate the less expanded polymer lattice and this distortion results in an entropy loss. Eventually, a temperature is reached in which the distortion becomes so large that the entropy loss results in phase separation (LCST).

The "equation of state" approach has been applied to various polymer blends^{34,35} to compare predicted and experimentally determined LCST spinodal curves and clearly

shows several improvements over the original Flory-Huggins rigid lattice theory. However, the popularity of the approach in the thermodynamic studies of polymer blends continues to be limited due to the large amount of thermodynamic data input which is required to provide an accurate model.

2.7 References

1. R.L.Scott, J. Chem. Phys., 17, 279 (1949).
2. H. Tompa, Trans. Faraday Soc., 45, 1142 (1949).
3. P.J.Flory, "Principles of Polymer Chemistry", Cornell University Press (1953).
4. O.Olabisi, L.M.Robeson and M.T.Shaw, "Polymer-Polymer Miscibility", Academic Press, New York (1979).
5. P.J.Flory, J. Chem. Phys., 9, 660 (1941).
6. M.L.Huggins, J. Chem. Phys., 9, 440 (1941).
7. K.H.Meyer, Helv. Chem. Acta, 23, 1063 (1940).
8. P.J.Flory, R.A.Orwoll and A.Vrij, J. Am. Chem. Soc., 86, 3515 (1964).
9. P.J.Flory, J. Am. Chem. Soc., 87, 1833 (1965).
10. B.E.Eichinger and P.J.Flory, Trans. Faraday Soc., 64, 2035 (1968).
11. I.Prigogine, "The Molecular Theory of Solutions", North-Holland, Amsterdam (1957).
12. W.J.C.Orr, Trans. Faraday Soc., 40, 320 (1944).
13. E.A.Guggenheim, Proc. Roy. Soc. (London), A183, 213 (1944).
14. D.R.Paul and J.W.Barlow, Polymer, 25, 487 (1984).
15. G. ten Brinke, F.E. Karasz and W.J. Macknight, Macromolecules, 16, 1827 (1983).
16. C.F.Hammer, Macromolecules, 4, 69 (1971).
17. T.Nishi and T.T.Wang, Macromolecules, 8, 909 (1975).
18. M.L.Huggins, J. Phys. Chem. 46, 151 (1942).
19. A.R.Miller, Proc. Cambridge Phil. Soc., 39, 54 (1943).
20. P.J.Flory and W.R.Krigbaum, Annual Review of Physical Chemistry, 2, 383 (1951).
21. J.H.Hildebrand and R.L.Scott, "Regular Solutions", Prentice-Hall, Englewood Cliffs, N.J. (1962).
22. D.Patterson, Rubber Chem. and Tech., 40, 1 (1967).
23. J.K.H.Al-Kafaji and C.Booth, J. Chem. Soc. Faraday Trans. 1, 79, 2695 (1983).

24. E.A.Guggenheim, *Trans. Faraday Soc.*, 44, 1007 (1948).
25. A.J.Staverman, *Recl. Trav. Chim. Pays-Bas*, 56, 885 (1937).
26. P.I.Freeman and J.S.Rowlinson, *Polymer*, 1, 20 (1959).
27. R.Koningsveld, L.A.Kleintjens and H.M.Schoffeleers, *Pure Appl. Chem.*, 39, 1 (1974).
28. G.Allen, Z.Chai, C.L.Chong, J.S.Higgins and J.Tripathi, *Polymer*, 25, 239 (1984).
29. C.Zhikuan, S.Ruona, D.J.Walsh and J.S.Higgins, *Polymer*, 24, 263 (1983).
30. Y.Jinghua, G.C.Alfonso, A.Turturro and E.Pedemonte, *Polymer*, 34, 1465 (1993).
31. L.P.MacMaster, *Macromolecules*, 6, 760 (1973).
32. K.Solc, Ed., " *Polymer Compatibility and Incompatibility - Principles and Practices*", Harwood Academic, New York (1982).
33. J.M.G.Cowie, " *Polymers : Chemistry and Physics of Modern Materials*", Chapman and Hall, NY.
34. S.Rostami and D.J.Walsh, *Macromolecules*, 17, 315 (1984).
35. S.Cimmino, E.Martuscelli, M.Saviano and C.Silvestre, *Polymer*, 32, 1461 (1991).

CHAPTER 3

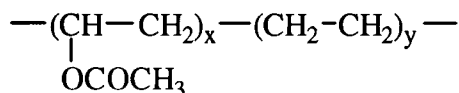
POLYMER CHARACTERISATION AND SYNTHESIS

The following chapter describes the initial characterisation of materials supplied by EXXON Chemical Limited, in order to determine their purity, molecular weight and thermal stability. Several analogues of these industrial samples have also been prepared and their synthesis and subsequent characterisation is described.

Blends of these polymers have been prepared and subsequent chapters will discuss their characterisation using techniques such as differential scanning calorimetry (Chapter 4), optical microscopy (Chapter 5), wide angle X-ray scattering (Chapter 8), heats of mixing (Chapter 7) and small angle neutron scattering (Chapter 9).

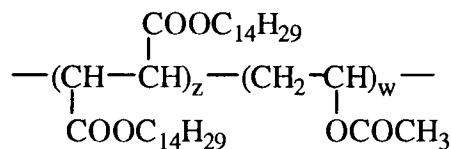
3.1 Polymers supplied by EXXON Chemical Limited

3.1a Random copolymer of ethylene and vinyl acetate (EVA) :



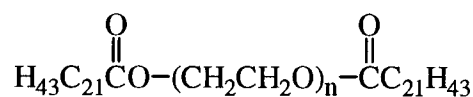
(EVA)

3.1b Alternating copolymer of tetradecyl diester of fumaric acid and vinyl acetate (FVA) :



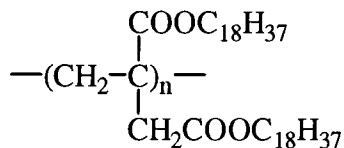
(FVA)

3.1c Docosyl diester of poly(ethylene glycol) (PE). The poly(ethylene glycol) segment in this ester was an equimolar mixture of molecular weights (M_p) 200, 400 and 600 :



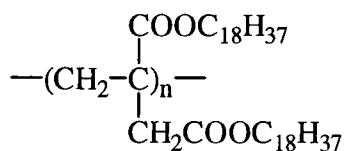
(PE)

3.1d Poly(di-n-octadecyl itaconate) (PI) :



(PI)

3.1e Low molecular weight poly(di-n-octadecyl itaconate) (LMPI) :



(LMPI)

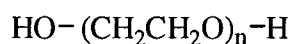
Each of the industrial samples was heated separately at 373K, under vacuum for 24 hours to remove residual solvent and then stored in a sealed desiccator.

At room temperature, EVA was a very viscous, opaque liquid which on heating to 373K became transparent, FVA was a viscous but mobile, clear liquid and the remaining samples, PE, PI and LMPI were brittle, crystalline solids.

3.2 Polymers Prepared

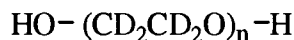
3.2a Hydrogenous poly(ethylene glycol) of target molecular weight M_p 400 (h-PEG).

See experimental 3.4.1 and 3.4.2 :



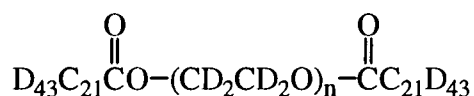
(h-PEG)

3.2b Deuterated poly(ethylene glycol) of target molecular weight M_p 400 (d-PEG). See experimental 3.4.3 :



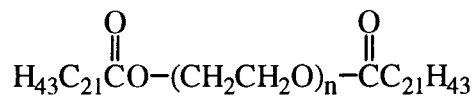
(d-PEG)

3.2c Deuterated docosyl diester of poly(ethylene glycol) (DPE). The poly(ethylene glycol) segment in this ester was approximately M_p 400. See experimental 3.4.4 :



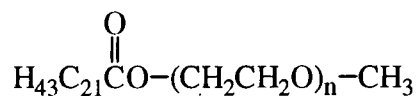
(DPE)

3.2d Hydrogenous docosyl diester of poly(ethylene glycol) (NECPE). The poly(ethylene glycol) segment in this ester was approximately M_p 400. See experimental 3.4.5 :



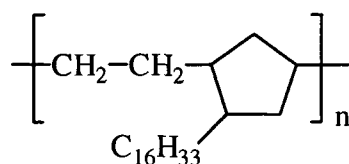
(NECPE)

3.2e Hydrogenous docosyl monoester of poly(ethylene glycol) methyl ether (NECME). The poly(ethylene glycol) segment in this ester was approximately M_p 350. See experimental 3.4.6 :



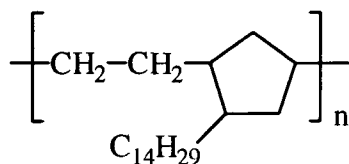
(NECME)

3.2f Hydrogenated poly(5-hexadecyl norbornene) (9210). Prepared by C.A.Smith¹ :



(9210)

3.2g Hydrogenated poly(5-tetradecyl norbornene) (9233). Prepared by C.A.Smith¹ :



(9233)

3.3 Characterisation

3.3.1 Size Exclusion Chromatography (SEC)

Three SEC methods were available for molecular weight determinations, based on different solvents: water, chloroform and tetrahydrofuran with the ideal solvent system dependent on polymer type.

For the poly(ethylene glycol) oligomer samples (h-PEG, d-PEG), the tetrahydrofuran (THF) system was found to be unsuitable giving very low M_n and M_w values. This was possibly due to the polarity of the polymers and their solubility in THF. Water and chloroform solvent SEC methods were therefore used for these samples.

3.3.1a Tetrahydrofuran solution SEC

For all polymers with the exception of the poly(ethylene glycol) oligomers, SEC measurements were carried out in THF using a Viscotek Differential Refractometer/Viscometer dual detector (Model 200). This system is generally regarded as the most reliable and accurate technique for determining molecular weight values due to the use of dual detectors (providing the polymer is soluble in THF!).

The samples were prepared by dissolving in filtered/degassed Analar grade THF solvent (concentration 0.1%^{w/v}) and filtered through a 0.2 μm polypropylene-backed

PTFE filter. The sample solutions were pumped through styrene/divinylbenzene gel columns (Polymer Labs, 10 μ m mixed) at temperature 308K, using a Knauer HPLC Pump 64 (flow rate 1cm³/min) to the detector. All samples apart from 9210 and 9233 were analysed in duplicate. The instrument was calibrated using various molecular weight polystyrene standards. Results are shown in Table 3.1.

Sample	M _n	M _w	M _w /M _n
EVA1	2670	6290	2.36
EVA2	3369	7825	2.32
PI1	10730	12190	1.14
PI2	9067	10290	1.13
LMPI1	6794	7684	1.13
LMPI2	6408	7203	1.12
FVA1	15200	59600	3.92
FVA2	16770	65600	3.91
PE1	1240	1350	1.09
PE2	1159	1279	1.10
NECPE1	1449	1442	1.00
NECPE2	1317	1311	1.00
NECME1	836	874	1.05
NECME2	771	805	1.05
DPE1	1146	1239	1.08
DPE2	1149	1258	1.10
9210 ^a	44000	79200	1.8
9233 ^a	68000	163200	2.4

Table 3.1 : SEC measurements in tetrahydrofuran

a. Values taken from reference (1).

3.3.1b Aqueous solution SEC

For the aqueous solvent system, SEC measurements were carried out using a Knauer differential refractometer single detector. The samples were prepared by dissolving in filtered and degassed 1M aqueous sodium nitrate solution (buffered at pH 7.0), at a concentration of 0.1%^{w/v}. The sample solutions (containing an ethanol flow marker) were filtered through a 0.2 μ m cellulose nitrate filter and pumped to the detector through a Polymer Laboratories PL aquagel OH 50 column (8 μ m bead size) at room temperature using a Knauer HPLC Pump 64 (flow rate 1cm³/min). The instrument was calibrated using poly(ethylene glycol) standards of molecular weight (M_p) 106, 194, 440, 600, 960 and 1470.

3.3.1c Chloroform solution SEC

For the chloroform system, the samples were dissolved in filtered and degassed chloroform (distilled laboratory grade) at a concentration of 0.1%^{w/v}. The sample solutions (containing a toluene flow marker) were filtered through a 0.2 μ m polypropylene backed-PTFE filter and pumped to a Waters Differential Refractometer R401 single detector through three Polymer Laboratories PL gel (5 μ m bead size) columns of pore sizes 10²Å, 10³Å and 10⁵Å respectively, using a Waters model 590 pump. Again, calibration was carried out using poly(ethylene glycol) standards.

3.3.2 Density and Coefficient of Thermal Expansion measurements

These measurements were carried out by EXXON Chemicals Limited (Table 3.2).

Measurement	EVA	FVA	PE	PI	LMPI
Density at 288K (g/cm ³)	0.955	0.960	1.029	0.895	0.921
Coefficient of Thermal Expansion, v/v x10 ⁻⁴	–	7.0	7.0	6.8	–

Table 3.2

3.3.3 Elemental Analysis (C,H,N)

Duplicate samples were analysed for carbon, hydrogen and nitrogen using a Carlo Erba Strumentazione Elemental Analyser - MOD 1106 using a combustion technique.

The instrument was calibrated by combustion of standard compounds. In all samples supplied, no nitrogen was detected and oxygen content was estimated by % difference.

Samples were analysed in duplicate and the results are shown in Table 3.3.

Sample	% Carbon	% Hydrogen	% Oxygen
EVA1	75.7	12.3	12.0
EVA2	76.1	12.4	11.5
Theoretical	(76.5)	(12.1)	(11.3)
PI1	78.5	13.0	8.5
PI2	78.3	12.8	8.9
Theoretical	(77.5)	(12.4)	(10.1)
LMPI1	78.3	13.0	8.7
LMPI2	77.9	12.8	9.3
Theoretical	(77.5)	(12.4)	(10.1)
FVA1	76.1	11.9	12.0
FVA2	75.4	12.1	12.6
Theoretical	(72.7)	(11.2)	(16.1)
PE1	70.0	11.9	18.2
PE2	69.9	11.7	18.5
Theoretical ^a	(70.3)	(11.6)	(18.1)
NECPE1	70.7	12.0	17.3
NECPE2	70.6	12.0	17.4
Theoretical ^a	(70.3)	(11.6)	(18.1)
NECME1	66.6	11.3	22.1
NECME2	66.5	11.3	22.2
Theoretical ^b	(67.0)	(11.3)	(21.7)
DPE1 ^c	62.08	20.50 (² H)	17.42
DPE2 ^c	61.85	20.42 (² H)	17.73
Theoretical ^d	62.98	20.78 (² H)	16.24

Table 3.3 : Elemental Analysis

- a. Based on an average of 9 poly(ethylene glycol) repeat units i.e. M_p 400.
- b. Based on an average of 8 poly(ethylene glycol) repeat units i.e. M_p 350.
- c. Results obtained by comparison with high purity deuterated docosanoic acid.
- d. Based on an average of 9 deuterated poly(ethylene glycol) repeat units i.e. M_p 440.

Apart from FVA, the analysis closely agrees with the theoretical values. The discrepancy in the FVA analysis maybe due to residual solvent and/or a slight stoichiometric misbalance between the fumarate and vinyl acetate. Elemental analysis results on samples 9210 and 9233 were not available.

3.3.4 Thermogravimetric Analysis (TGA)

TGA was carried out using a Stanton Redcroft - Thermal Sciences TG 760 thermobalance. The instrument was calibrated daily using 5-10mg standards and the furnace temperature checked regularly. All samples were solvent cast from chloroform and dried in a vacuum oven at 303K for 24 hours. For each sample, 5mg was heated in a nitrogen atmosphere (flow rate 30cm³/min) at a rate of 10K/min until the sample residue was <10% of the initial sample weight.

Weight % residue vs. temperature plots for each polymer are shown in Figure 3.1.

3.4 Experimental Details

As the industrial ester sample (PE) contained high levels of docosanoic acid impurity (see Analysis section 3.5), a pure diester sample was prepared (NECPE) which was subsequently used in differential scanning calorimetry (DSC) and "heat of mixing" experiments. The poly(ethylene glycol) block in NECPE was supplied by Aldrich as PEG 400 and had a quoted molecular weight of approximately M_p 400 which is the average M_p molecular weight of this segment in the industrial (PE) sample. The docosyl monoester of a poly(ethylene glycol) methyl ether (NECME) M_p 350 was also prepared for DSC studies to determine possible effects of esterification type i.e. mono or di, on blend interactions.

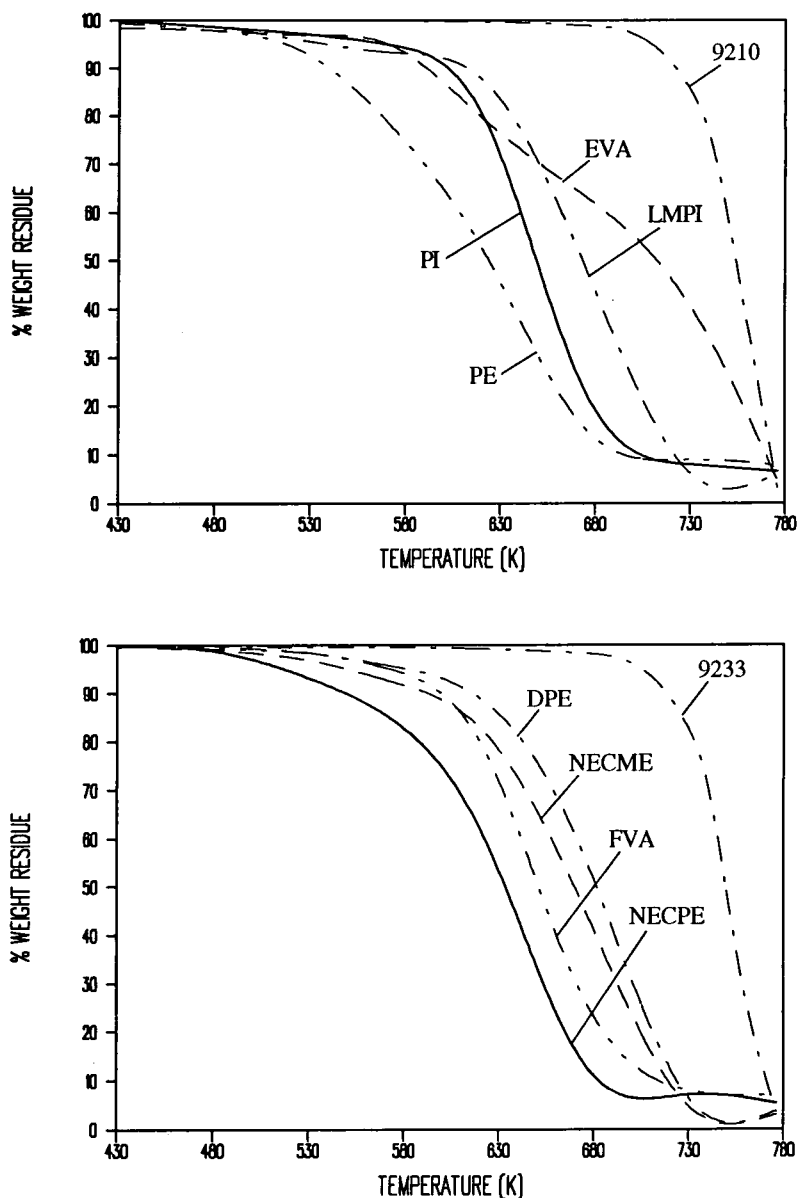


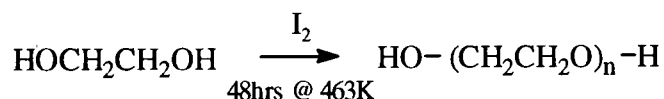
Figure 3.1 : Thermal Gravimetric Analysis

Also, in this project, small angle neutron scattering (SANS) studies were to be carried out on blends of poly(ethylene-co-vinyl acetate) and the docosyl diester of poly(ethylene glycol). For these SANS studies, a fully deuterated docosyl diester was prepared (DPE) containing a deuterated poly(ethylene glycol) segment of molecular weight (M_p) and polydispersity values similar to PEG 400 (supplied by Aldrich), in order to represent the hydrogenous ester samples used in other characterisation studies. The synthetic route to the deuterated diester consisted initially of polymerising deuterated poly(ethylene glycol) to the required molecular weight i.e. M_p 400. Several

methods have been reported^{2,3,4} for preparing poly(ethylene glycols) oligomers of a specific molecular weight. Unfortunately, these methods suffer from several problems; low yields, multi-stage synthesis routes and starting materials of deuterated di or triethylene glycol which are prohibitively expensive. The experimental procedure to polymerise the poly(ethylene glycol) was therefore based on a method recently reported by Schnabel⁵ which outlined the polymerisation of deuterated ethylene glycol (a relatively cheap deuterated component) to poly(ethylene glycol) oligomers. The disadvantage of this method was that the main deuterated products were di, tri and tetra ethylene glycols with the higher oligomers having yields of only a few weight percent. As the deuterated poly(ethylene glycol) was to have a molecular weight of approximately M_p 400 i.e. an average of nine ethylene glycol repeat units, this method had to be modified and optimised considerably. The polymerisation of hydrogenous ethylene glycol (h-PEG) was therefore used to establish an experimental procedure i.e. reaction time, temperature, nitrogen flow and catalyst levels required to achieve this molecular weight target. From this optimised experimental procedure, the deuterated sample was polymerised to the correct molecular weight (d-PEG) and subsequently esterified with deuterated docosanoic acid to produce the deuterated diester (DPE).

Experimental details of these polymerisations and esterifications are given in the following sections.

3.4.1 Polymerisation of hydrogenous poly(ethylene glycol) (h-PEG1)



Analar ethylene glycol (30.06g) containing approximately 1% iodine (0.30g) formed a deep brown solution which was stirred under a nitrogen purge in an oil bath at 463K. After 24 hours, a sample was taken from the solution, 1% iodine was again added

(0.28g) and the reaction continued for a further 24 hours. Throughout the reaction, a slow evolution of water vapour was noted, together with rapid iodine sublimation. Due to sublimation, brown iodine crystals were formed on the attached condenser and eventually the solution became clear with no evidence of the iodine catalyst. Presumably, this gradual loss of catalyst is the reason for further iodine additions.

After a total reaction time of 48 hours, the very pale brown solution was removed from the oil bath and allowed to cool. An aliquot from this solution was then distilled using a Kugelrohr "bulb to bulb" distillation apparatus, at a reduced pressure of 0.025-0.03 mbar and a temperature range of 318K to 393K, to produce three fractions (A,B,C) including the boiler residues. The relative weight percentage of each fraction in the reaction mixture is shown in Table 3.4.

Fraction	% w/w
A (low boiling)	73.1
B	10.6
C (high boiling)	16.3

Table 3.4

During the fractional distillation, residual iodine sublimed from the reaction mixture and was only present as a pale brown coloration in fraction A which contained the low boiling, low molecular weight poly(ethylene glycols). The molecular weight of fractions A, B and C plus samples taken at 24 and 48 hours were determined using aqueous solution SEC and compared to values obtained for poly(ethylene glycol) (PEG) samples of average molecular weight (M_p), 200, 400 and 600 (supplied by Aldrich) - see Table 3.5.

Sample	M_p	M_n	M_w	Polydispersity (M_w/M_n)
Fraction A	112	53	114	2.15
Fraction B	196	43	165	3.82
Fraction C	238	170	214	1.26
Reaction at 24 hours	112	39	112	2.88
Reaction at 48 hours	114	9	118	12.34
PEG 200 (Aldrich)	192	6	165	26.40
PEG 400 (Aldrich)	309	288	361	1.25
PEG 600 (Aldrich)	595	442	534	1.21

Table 3.5 : Aqueous SEC analysis

From the SEC analysis, the molecular weight (M_p) value of PEG 400 was lower than expected whereas the PEG 200 and 600 samples closely agreed with the quoted values. Fraction C (reaction mixture residues) has the largest molecular weight of the reaction samples with an M_p value between that of PEG 200 and 400 and a polydispersity value very similar to PEG 400. As the yield of Fraction C is only 16%^{w/w} of the reaction mixture, further development of the method was required to prepare poly(ethylene glycols) of the required molecular weight, at an acceptable yield.

3.4.2 Polymerisation of hydrogenous poly(ethylene glycol) (h-PEG2)

The experimental procedure was essentially as detailed previously in 3.4.1. In an attempt to increase both molecular weight and yield values, this experiment was carried out with no nitrogen sparge in order to reduce the sublimation rate of the iodine catalyst, thereby increasing the long-term concentration of catalyst in the ethylene glycol starting material. Additionally, the reaction time was extended from 48 to 72 hours.

After 24 hours at 463K, the solution remained a pale brown colour due to the reduced iodine sublimation (in the previous experiment, the solution was virtually colourless at this stage). A further 1% iodine was added to the solution and again at 54 hours. The reaction was allowed to continue for a total of 72 hours. Again a sample of the final reaction mixture was distilled using Kugelrohr distillation apparatus at a reduced pressure of 0.02-0.03 mbar and a temperature range of 393K to 423K to produce 3 fractions (D,E,F) and the weight percentage of each fraction in the reaction mixture is shown in Table 3.6.

Fraction	% w/w
D (low boiling)	34.1
E	3.7
F (high boiling)	62.2

Table 3.6

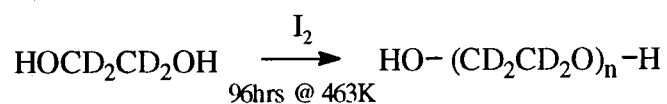
The main fractions, D and F, plus samples taken at 48 and 72 hours were analysed by aqueous solution SEC for molecular weight determination and compared to PEG 400 and 600 values (Table 3.7). The PEG 400 and 600 values closely agree with the previous SEC analysis results in section 3.4.1. Again, the reaction mixture residue i.e. fraction F, had the highest molecular weight of the fractions but this is slightly lower than the PEG 400 value. However, due to the reduced sublimation of the iodine catalyst and longer reaction times, the yield of this fraction was increased dramatically to over 60% w/w, which was regarded as acceptable.

Sample	M _p	M _n	M _w	Polydispersity (M _w /M _n)
Fraction D	131	7	133	16.88
Fraction F	260	217	360	1.65
Reaction at 48 hours	124	10	145	14.06
Reaction at 72 hours	210	52	279	5.28
PEG 400 (Aldrich)	308	242	371	1.53
PEG 600 (Aldrich)	620	465	564	1.21

Table 3.7 : Aqueous SEC analysis

This modified experimental procedure to prepare poly(ethylene glycols) of a target molecular weight of M_p 400 at reasonable yield values, was subsequently used in the polymerisation of deuterated ethylene glycol (see section 3.4.3). However, in the deuterated polymerisation, a very low nitrogen flow was used, sufficient only to maintain an inert atmosphere over the reaction mixture without encouraging catalyst sublimation and the reaction time was increased from 72 to 96 hours to allow for a further increase in molecular weight.

3.4.3 Polymerisation of deuterated poly(ethylene glycol) (d-PEG)



5g of deuterated ethylene glycol (supplied by MSD Isotopes of quoted purity >99%) containing 1%^{w/w} iodine was stirred under a very low nitrogen purge in an oil bath at 463K. The polymerisation was allowed to continue for a total of 96 hours with further 1% iodine aliquots added at 24 hour intervals. Throughout the reaction, iodine slowly

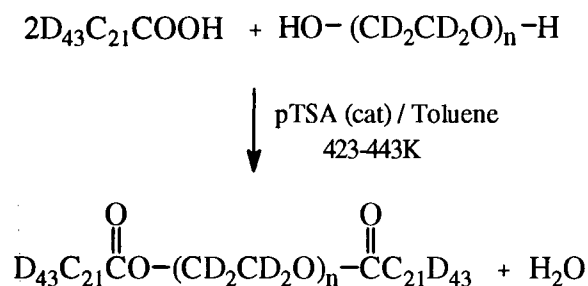
sublimed out of solution (hence the need for further additions), accompanied by the slow evolution of water. The resulting solution was then fractionated at 423K/0.025 mBar for 60 minutes using Kugelrohr distillation apparatus to remove low molecular weight poly(ethylene glycol) fractions and the final product was obtained in 42%^{w/w} yield. Samples of the deuterated product (d-PEG) and PEG 400 (supplied by Aldrich) were analysed in duplicate for molecular weight using chloroform solution SEC (see Table 3.8).

Sample	M_p	M_n	M_w	Polydispersity (M_w/M_n)
d-PEG -1	447	432	476	1.10
d-PEG -2	457	439	476	1.09
PEG 400 -1 (Aldrich)	448	422	438	1.04
PEG 400 -2 (Aldrich)	445	423	436	1.03

Table 3.8 : Chloroform SEC analysis

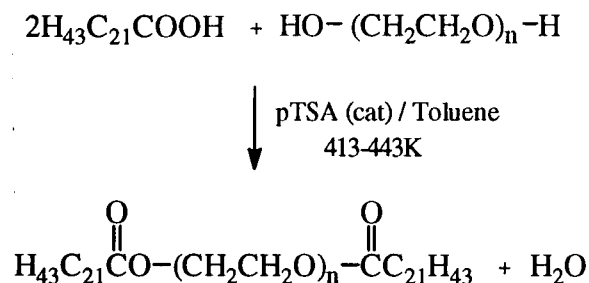
Although previous hydrogenous poly(ethylene glycol) samples were analysed using aqueous SEC, this resulted in PEG 400 values which were consistently lower than expected. However, chloroform SEC appears to give a value closer to that quoted i.e. M_p 400, although it should be noted that M_p values quoted for these Aldrich PEG samples are merely an average and not intended as absolute standards. From the SEC measurements it is clear that the deuterated poly(ethylene glycol) and PEG 400 samples are very similar in terms of molecular weight and polydispersity.

3.4.4 Diesterification of deuterated polyethylene glycol with deuterated docosanoic acid (DPE)



Deuterated docosanoic acid (0.98968g, 2.578 mmoles) and deuterated poly(ethylene glycol), M_p 452 (0.58350g, 1.291 mmoles) were esterified in Analar toluene (40cm³) using a para-toluenesulphonic acid catalyst (0.01655g, 1.0%^{w/w}). The docosanoic acid (supplied by MSD Isotopes of quoted purity >99%) was recrystallised twice from Analar toluene prior to use and the poly(ethylene glycol) (d-PEG) was as prepared previously in section 3.4.3. The catalyst addition level was high to ensure that the esterification reaction went to completion and was later removed by aqueous washing. The esterification was carried out under nitrogen using a Dean and Stark condenser to collect the toluene and water (from esterification) azeotrope. The solution was held at an oil bath temperature of 423K (2.5 hours), 433K (2 hours) and finally, 443K (1 hour). Throughout, toluene was slowly withdrawn from the Dean and Stark. On cooling, the solution crystallised into a waxy solid which was crushed to a fine powder with a pestle and mortar. To remove catalyst and possible unreacted poly(ethylene glycol) residues, the ester was stirred for 1 hour in two separate 50cm³ aliquots of deuterium oxide (D₂O). The resulting fine, white powder was filtered and dried in a vacuum oven at 353K for 48 hours. The product yield after esterification was 96%^{w/w}.

3.4.5 Diesterification of poly(ethylene glycol) with docosanoic acid (NECPE)

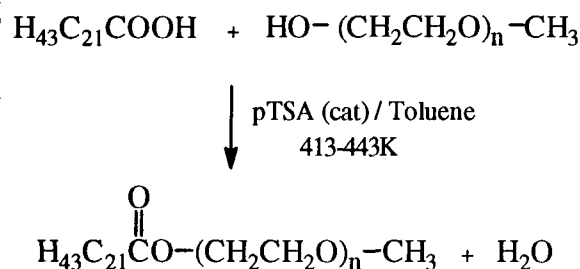


Docosanoic acid (3.99366g, 11.73 mmoles) and poly(ethylene glycol) M_p 400 (PEG 400 ex. Aldrich) (2.34520g, 5.86 mmoles) were esterified in toluene (60cm³) using a para-toluenesulphonic acid catalyst (0.056g, 0.8% w/w). All reagents were Analar grade. The esterification was carried out under nitrogen in an oil bath using a Dean and Stark condenser to collect the toluene and water azeotrope.

The reaction mixture was initially held at an oil bath temperature of 413K for 2 hours with toluene gently refluxing. Over a 3 hour period, 35cm³ of toluene was removed from the Dean and Stark condenser and the oil bath temperature gradually increased to 443K. Finally, the solution was held at 443K for 30 minutes to remove the remaining toluene fraction.

On cooling, the solution crystallised into a waxy solid which was crushed to a fine white powder using a pestle and mortar and then stirred in 500cm³ of 1M NaOH for 30 minutes to neutralise and consequently solubilise possible acidic residues. The suspension was then filtered and the resulting powder stirred for 2 x 30 minute periods in 500cm³ aliquots of distilled water to remove unreacted poly(ethylene glycol) and catalyst residues. After filtering, the product was dried in a vacuum oven at 373K for 24 hours. The yield after esterification and washing was 83% w/w.

3.4.6 Monoesterification of poly(ethylene glycol) methyl ether with docosanoic acid (NECME)



Docosanoic acid (4.00251g, 11.75 mmoles) and poly(ethylene glycol) methyl ether, M_p 350 (4.11324g, 11.75 mmoles) were esterified in toluene (60cm³) using a para-toluenesulphonic acid catalyst (0.0736g, 0.9%w/w). All reagents were Analar grade supplied by Aldrich. The reaction profile was carried out as per section 3.4.5 (esterification of poly (ethylene glycol) - NECPE).

The product was finally dried in a vacuum oven at 373K for 24 hours and a waxy-solid was formed on cooling.

3.5 Analysis (NMR and IR)

¹³C, ¹H NMR (in deuterated chloroform solvent supplied by Aldrich) and IR analysis on the industrial samples (apart from PE) was consistent with the structures outlined in section 3.1. From ¹H NMR, the statistical average composition of EVA was determined at 7 moles of ethylene per mole of vinyl acetate. The ¹³C spectra on the PE sample indicated significant impurities including free, unesterified docosanoic acid at a concentration of approximately 5-10%.

The ¹³C spectra for both PE and NECPE samples (Figure 3.2) clearly show the much higher levels of impurity in the industrial material. In subsequent characterisation chapters, comparison of experimental results from both these samples may indicate any contribution from the docosanoic acid impurity. The prepared docosyl monoester of a

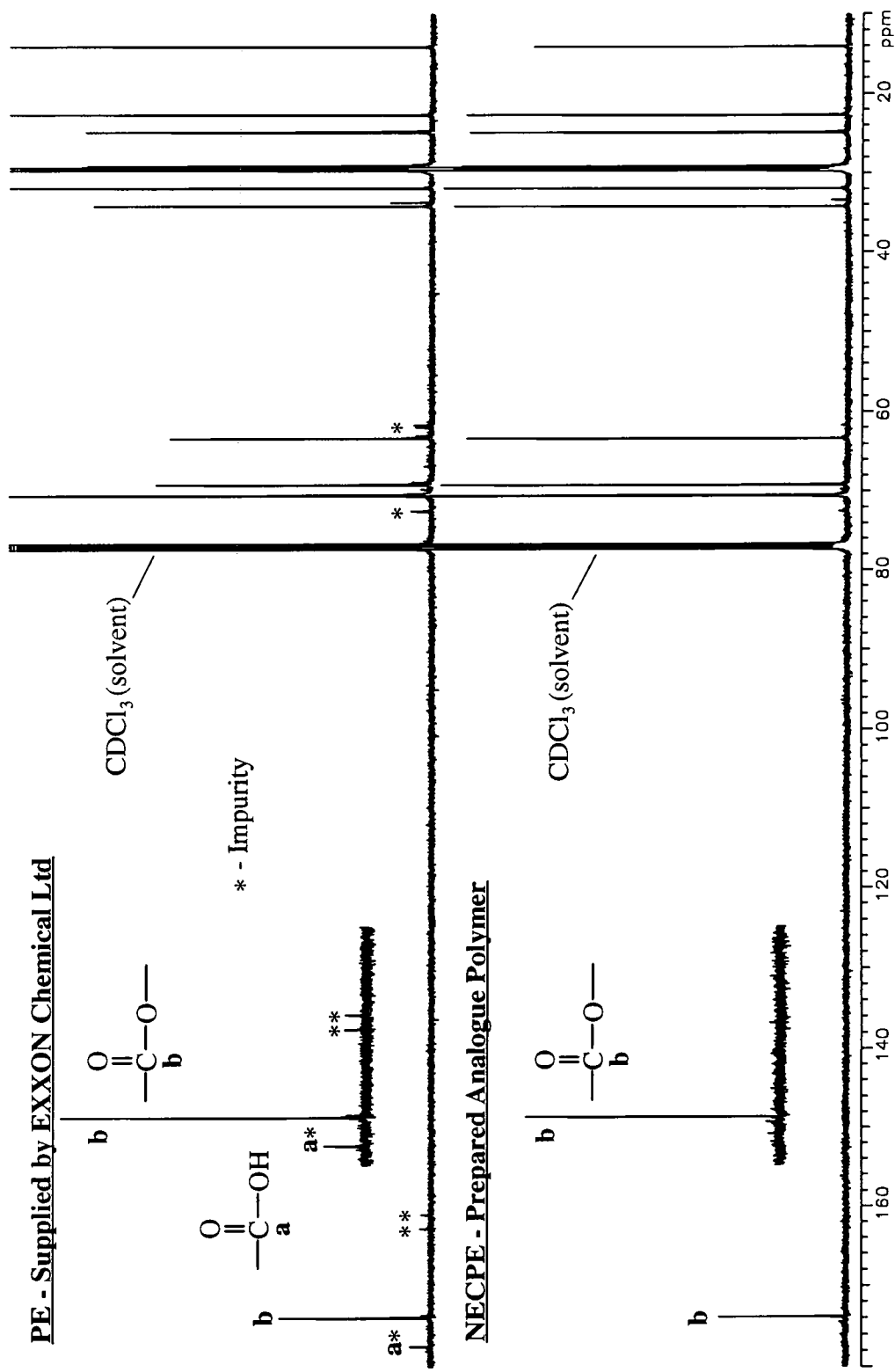


Figure 3.2 : ¹³C nmr analysis on docosyl diesters of poly(ethylene glycol)

poly(ethylene glycol) methyl ether (NECME) was also free from impurities (including docosanoic acid) and unambiguously assigned from ^{13}C nmr analysis (Figure 3.3).

The ^{13}C nmr spectra for DPE is shown in Figure 3.4. As deuterium decoupling was not available, all peaks (apart from the ester) show a low intensity, broad splitting pattern. The ester peak is noted at 174ppm with no evidence of free, unesterified docosanoic acid present. Peak positions at approximately 28 and 70ppm represent carbon atoms within the docosyl and poly(ethylene glycol) environments, respectively. The peak at 28ppm suggests that the deuterated docosyl segment may contain a very small amount of hydrogenous material which due to the effect of proton decoupling, appears as a single sharp peak (labelled "H"). As the intensity of the hydrogenous and not the deuterated signal is enhanced by the decoupling effect, the relative peak areas (or heights) do not give a true indication of the impurity concentration. In such cases, the hydrogenous signal is exaggerated and the amount of hydrogenous material is therefore considered to be negligible in comparison to the deuterated component. The low intensity signals represent the various carbon environments within the ester and have positions corresponding to the ^{13}C spectra on the hydrogenous material (NECPE), shown in Figure 3.2.

Analysis on 9210 and 9233 samples has previously been reported¹.

3.6 Blend Preparation

Blends of EVA with various polymers (PI, LMPI, FVA, PE, NECPE, NECME, DPE, 9210 and 9233) were prepared by solvent casting from chloroform solutions with a total polymer concentration of 10%^{w/v}. The solvent was allowed to evaporate at room temperature for up to 1 week and the resulting films were dried at 323K under vacuum for 24 hours. The dried blends were stored in a sealed desiccator. Characterisation details of these polymer blends are described in subsequent chapters.

NECME - Prepared Analogue Polymer

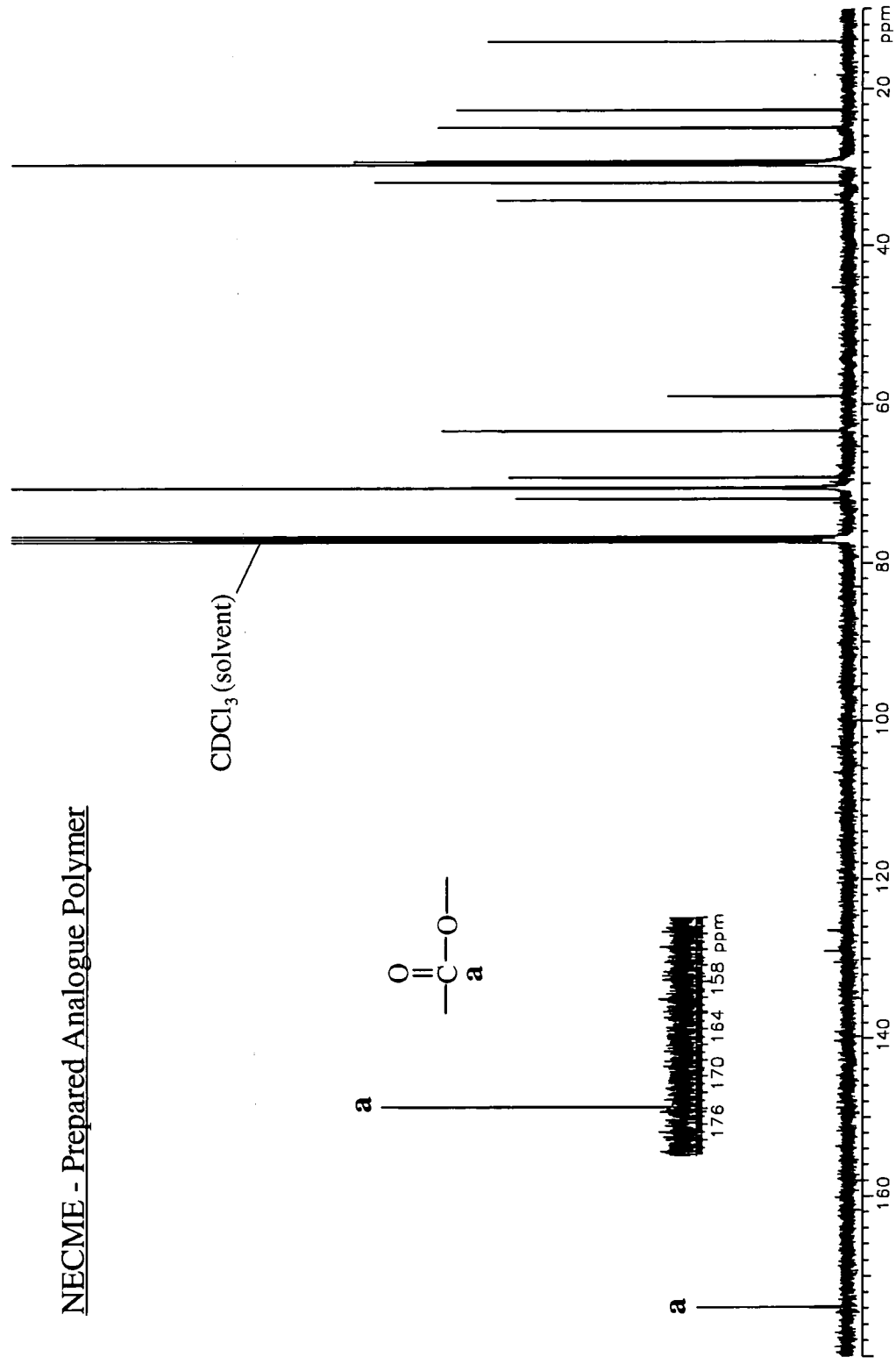


Figure 3.3 : ¹³C nmr analysis on the docosyl monoester of poly(ethylene glycol) - NECME

DPE - Prepared Analogue Polymer

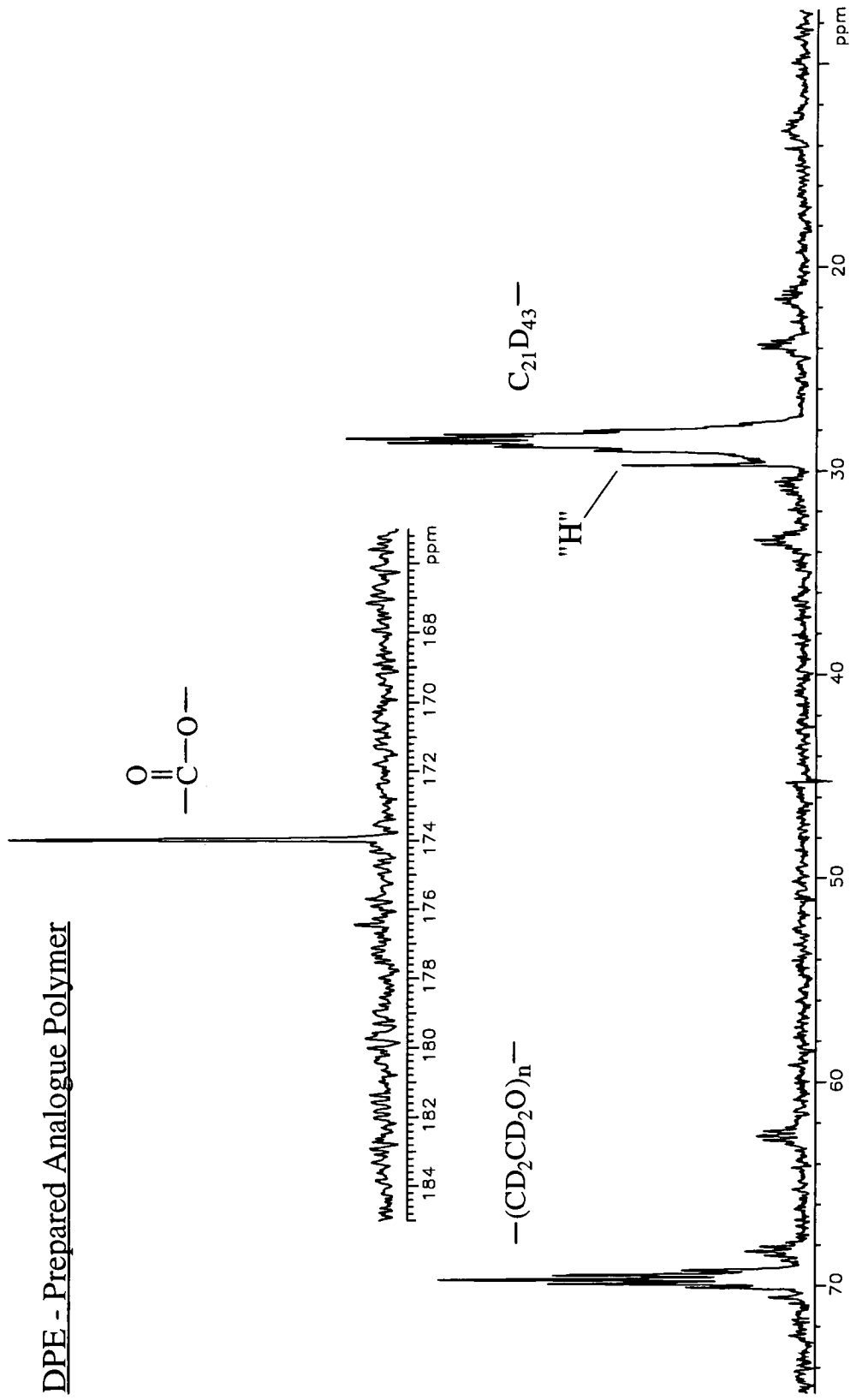


Figure 3.4 : ^{13}C nmr analysis on deuterated docosyl diester of poly(ethylene glycol) - DPE

3.7 Discussion

From SEC measurements, it is clear that the hydrogenated poly(n-alkyl norbornene) samples (9210, 9233) are very high molecular weight polymers with a polydispersity of approximately 2. The EVA and FVA copolymers also have high polydispersity values.

The remaining polymers have relatively low molecular weight values (especially the poly(ethylene glycol) esters), with polydispersities close to unity and this may contribute significantly to their miscibility with other polymers, as discussed in subsequent chapters.

NMR and IR analysis on the samples is consistent with their predicted structures although the actual structure of the EVA and FVA copolymers is likely to be highly complex due to tacticity, conformations (head-head, head-tail etc.) and molar compositions. The industrial sample of the poly(ethylene glycol) diester (PE) clearly contained a significant amount of unreacted docosanoic acid, either due to incomplete esterification or a stoichiometric excess of the acid. This high impurity level was the reason for the preparation of a pure diester (NECPE).

At the onset of this project, EVA blends with the poly(ethylene glycol) diester were believed to be particularly interesting and characterisation was to include small angle neutron scattering studies (Chapter 9). A fully deuterated poly(ethylene glycol) diester was therefore prepared (DPE) with a deuterated poly(ethylene glycol) segment of near identical molecular weight to that used in the pure hydrogenous diester (NECPE). A docosyl monoester of poly(ethylene glycol) was also prepared (NECME) to determine possible effects of esterification type (mono or di) on the interaction with EVA.

The TGA analysis indicates that the 9210 and 9233 samples have very good thermal stability up to 700K. In contrast, the hydrogenous diester samples (PE and NECPE) have the lowest thermal stability and this may hinder high temperature studies on blends containing these polymers i.e. Optical Microscopy (Chapter 5).

References

1. C.A.Smith, PhD Thesis, Durham University (1993).
2. A.Marshall, R.H.Mobbs and C.Booth, European Polymer Journal, 16, 881 (1980).
3. H.H.Teo, R.H.Mobbs and C.Booth, European Polymer Journal, 18, 541 (1982).
4. G.Coudert, M.Mpassi, G.Guillaumet and C.Selve, Synthetic Communications, 16(1), 19 (1986)
5. R.Schnabel, Journal of Labelled Compounds and Radiopharmaceuticals, 31(2), 91 (1992).

CHAPTER 4

DIFFERENTIAL SCANNING CALORIMETRY

4.1 Introduction

When a substance undergoes a physical or chemical change, a corresponding change in enthalpy occurs and a heat change into or out of the system is observed. This is the basis of thermal analysis techniques which essentially consist of Differential Thermal Analysis (DTA) and Differential Scanning Calorimetry (DSC).

In DTA, the sample and an inert reference (typically an empty sample pan) are heated at a uniform rate from a single heat source (Figure 4.1). Thermocouples in both sample and reference cells detect heat changes by measuring the temperature difference (ΔT) between the sample (T_S) and the reference (T_R). The temperature difference ($\Delta T = T_S - T_R$) will remain constant until the sample undergoes a heat change e.g. during melting of a crystalline sample, the heat change will be endothermic and T_S will temporarily lag behind T_R , but if the sample crystallises the heat change is exothermic and T_S will exceed T_R , again temporarily. After melting or crystallisation is complete, the sample returns to a "steady state" and the temperature changes are recorded as peaks in the DTA curve. Due to differences in the heat capacity of the sample and reference, the temperature difference is never zero and the profile of the DTA curve essentially represents the heat capacity change of the sample with temperature.

The major drawback of DTA measurements is that the ΔT value is dependent on the thermal conductivity and bulk density of the sample. Therefore, this technique at best, can only give semi-quantitative information. However, since the development of DSC, quantitative thermal analysis measurements have become possible. In this technique, the sample and reference cells are again heated at a constant rate but from individual heaters (Figure 4.1) and instead of measuring the temperature difference between the sample and reference, the heaters increase the energy input to either sample or reference cell to maintain both at the same programmed temperature.

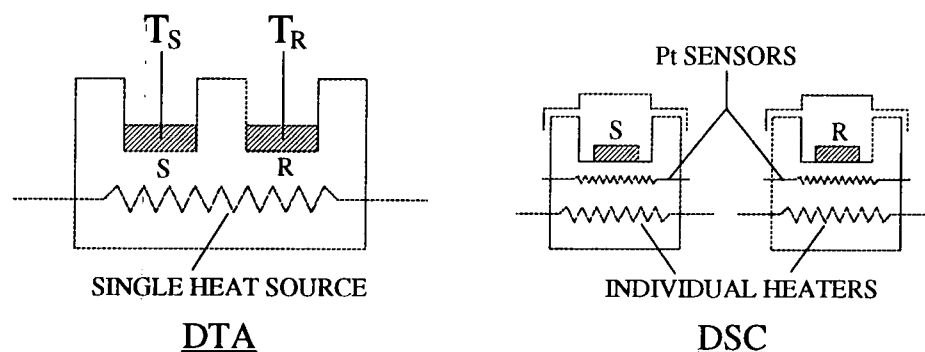


Figure 4.1 : Thermal Analysis Techniques

This technique is particularly useful for polymers because polymerisation or structural changes e.g. crystallisation, melting and glass transition (T_g) temperatures all show characteristic DSC curves. DSC thermograms showing these heat changes (Figure 4.2) are similar to DTA curves but actually represent the amount of electrical energy supplied to the system, not ΔT and so the areas under these peaks will be proportional to the heat change which occurred.

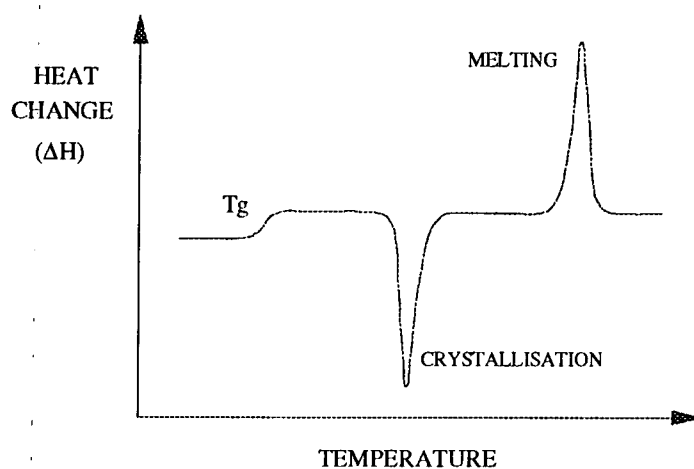


Figure 4.2 : DSC Thermogram

In polymer blends, DSC has been used extensively to determine miscibility limits^{1,2} and, as in this study, can be used to determine Flory - Huggins interaction parameters, χ^{3-6} , when one of the blend components is semi-crystalline. This is a particularly straightforward method of determining χ from the melting point depression of the crystalline phase when blended with the other (amorphous) component. Although the

composition and temperature dependence of χ are not obtained by this method, it provides a relatively quick and reliable indication of the blend miscibility.

4.2 Melting point depression theory

At the equilibrium melting point (T_m^0) of a semi-crystalline polymer, the amorphous and crystalline phases are in equilibrium i.e. the chemical potential (μ) of both phases are equal ($\mu_A = \mu_C$). If a low molecular weight diluent is added to the amorphous phase, the chemical potential of this phase, μ_A is reduced. In this case, to re-establish the equilibrium position ($\mu_A = \mu_C$), the crystalline phase melts at a lower temperature. Consequently, the "diluent effect" depresses the melting point of the crystalline phase.

The thermodynamic considerations of mixing in polymer-diluent systems⁷ have been successfully extended to crystalline polymer-amorphous polymer systems by Nishi and Wang⁸. Amorphous polymers which are miscible with the amorphous phase of semi-crystalline polymers can act as diluents, depressing the melting point of the crystalline phase, as discussed above. The thermodynamic mixing of two polymers was first treated by Scott⁹, using the Flory-Huggins approximation^{7,10}. Scott expressed the chemical potential, μ_{2U}^1 of the crystallisable polymer units in the amorphous phase of the polymer blend relative to its chemical potential in the amorphous phase of the pure semi-crystalline polymer, μ_{2U}^0 , as:

$$\mu_{2U}^1 - \mu_{2U}^0 = \frac{RTV_{2U}}{V_{1U}} \left[\frac{\ln(1-\phi_1)}{m_2} + \phi_1 \left(\frac{1}{m_2} - \frac{1}{m_1} \right) + \chi\phi_1^2 \right] \quad (4.1)$$

Chapter 2 outlines how this expression is obtained. Subscripts 1 and 2 refer to the amorphous and semi-crystalline polymer components respectively, V_U is the molar volume of the repeating units, ϕ is the volume fraction and m is the degree of polymerisation. χ is the polymer-polymer interaction parameter, R is the gas constant and T is the absolute temperature.

$\mu_{2U}^1 - \mu_{2U}^0$ represents the lowering of the chemical potential of the crystallisable unit in the amorphous phase of the blend due to the presence of the amorphous polymer diluent.

The difference in chemical potential of the crystalline polymer unit, μ_{2U}^C and the same unit in the standard state i.e. the pure amorphous phase, μ_{2U}^0 is equal to the negative term of the free energy of fusion per repeat unit (ΔG_{2U}) and therefore, can be expressed as:

$$\mu_{2U}^C - \mu_{2U}^0 = -\Delta G_{2U} = -(\Delta H_{2U} - T\Delta S_{2U}) \quad (4.2)$$

where ΔH_{2U} and ΔS_{2U} are the enthalpy and entropy of fusion per repeat unit for the 100% crystalline component, respectively. The $\Delta H_{2U}/\Delta S_{2U}$ ratio is assumed to be independent of temperature and equal to the equilibrium melting point, T_m^0 , since $\mu_{2U}^C - \mu_{2U}^0 = 0$ when $T = T_m^0$. Therefore:

$$\mu_{2U}^C - \mu_{2U}^0 = -\Delta H_{2U} \left(1 - \left(\frac{T}{T_m^0} \right) \right) \quad (4.3)$$

At the melting point of the polymer blend, the chemical potentials of the semi-crystalline polymer in both the crystalline and amorphous phases should be equal and this condition occurs when :

$$\mu_{2U}^C - \mu_{2U}^0 = \mu_{2U}^1 - \mu_{2U}^0 \quad (4.4)$$

Therefore, substituting equations 4.1 and 4.3 into equation 4.4 and replacing T by T_{mb}^0 , the equilibrium melting point of the blend, we obtain the following :

$$\left[\frac{1}{T_{mb}^{\circ}} - \frac{1}{T_m^{\circ}} \right] = - \frac{RV_{2U}}{\Delta H_{2U} V_{1U}} \left[\frac{\text{Ln}(1-\phi_1)}{m_2} + \phi_1 \left(\frac{1}{m_2} - \frac{1}{m_1} \right) + \chi \phi_1^2 \right] \quad (4.5)$$

(1) (2) (3)

which relates T_{mb}° to the volume fraction of the diluent, ϕ_1 . Terms (1) and (2) account for configurational (or combinatorial) entropy contributions to the melting point depression and consequently, the free energy of mixing. It should be noted that the Flory-Huggins lattice theory (see Chapter 2) from which equation 4.5 is derived, assumes that configurational entropy is the only entropic contribution. These entropic contributions decrease as the molecular weight of the polymer (which is assumed to be linear) increases. Term (3) is the enthalpic contribution and is determined by the interaction parameter, χ .

In Scott's original study, degree of polymerisation values, m_1 and m_2 , were related to the ratio of the polymer molar volumes, V_1 and V_2 and a molar volume V_o of one sub-molecule i.e. a repeat unit, as shown:

$$m_1 = \frac{V_1}{V_o} \quad (4.6)$$

In the absence of molar volumes, m values have generally been derived from the ratio of the number average molecular weight of the polymer (M_n) to the molecular weight of the repeat unit.

For high molecular weight polymers, both m_1 and m_2 are large and terms (1) and (2) become negligible. Consequently, equation 4.5 simplifies to:

$$\left[\frac{1}{T_{mb}^{\circ}} - \frac{1}{T_m^{\circ}} \right] = - \frac{RV_{2U}}{\Delta H_{2U} V_{1U}} (\chi \phi_1^2) \quad (4.7)$$

which is the well known Nishi-Wang expression⁸, relating the equilibrium melting point depression to the thermodynamic mixing i.e. miscibility, of crystalline and amorphous polymers. Equation 4.7 has been used many times to evaluate χ values³⁻⁶ in polymer blends, by conventionally plotting $(1/T_{mb}^{\circ} - 1/T_m^{\circ})$ against ϕ_1^2 and deriving χ from the slope. The use of eqn. 4.7 in this way has recently been critically reviewed¹¹. Equation 4.7 clearly shows the decisive role of the interaction parameter, χ on the melting behaviour of the crystalline polymer - amorphous polymer blend. In this case, a depression in melting point can only be achieved if χ is negative which agrees with Scott's condition for miscibility to occur between the two polymers⁹;

$$\chi \leq \chi_{\text{CRIT}}$$

where,

$$\chi_{\text{CRIT}} = \frac{1}{2} \left[\frac{1}{m_1^{1/2}} + \frac{1}{m_2^{1/2}} \right]^2 \quad (4.8)$$

The χ_{CRIT} value which is always positive, corresponds to the minimum value of χ , at which the blend spontaneously phase separates i.e. on the spinodal curve. In polymer blends, the χ_{CRIT} value is very small and in high molecular weight polymer mixtures is regarded essentially as zero. Therefore, as a general rule, miscibility can only occur when χ is negative, as shown by a melting point depression.

A free energy density parameter, B is characteristic of the polymer pair and related to the interaction parameter, χ by the following:

$$\chi = \frac{BV_{1U}}{RT_{mb}^{\circ}} \quad (4.9)$$

By substituting equation 4.9 into equation 4.5, the following expression which again encompasses configurational entropy contributions, is obtained :

$$\left[\frac{1}{T_{mb}^{\circ}} - \frac{1}{T_m^{\circ}} \right] = -\frac{RV_{2U}}{\Delta H_{2U}} \left[\phi_1^2 \left(\frac{B}{RT_{mb}^{\circ}} \right) + \frac{\text{Ln}(1-\phi_1)}{m_2} + \phi_1 \left(\frac{1}{m_2} - \frac{1}{m_1} \right) \right] \quad (4.10)$$

which may be rearranged to :

$$Y = \left[\frac{1}{T_{mb}^{\circ}} - \frac{1}{T_m^{\circ}} \right] \frac{\Delta H_{2U}}{RV_{2U}} + \frac{\text{Ln}(1-\phi_1)}{m_2} + \phi_1 \left(\frac{1}{m_2} - \frac{1}{m_1} \right) = -\frac{B}{R} \frac{\phi_1^2}{T_{mb}^{\circ}} \quad (4.11)$$

(1) (2)

As in eqn. 4.5, the combined values of (1) and (2) in eqn. 4.11 represent the fraction of the total melting point depression which is due to configurational entropy contributions. In theory, the resulting B value from the slope of Y versus ϕ_1^2/T_{mb}° and the subsequently derived χ values (over the observed melting range) are representative of the enthalpic contribution (χ_H) which can be related to χ_H values from "heat of mixing" experiments (see Chapter 7). This is based on the assumption that configurational entropy is the only entropic component, ignoring non-configurational "excess entropy" contributions. At large values of m, (1) and (2) contributions are again considered to be negligible and are omitted resulting in eqn. 4.12 which is essentially a rearrangement of the original Nishi-Wang expression (eqn. 4.7).

$$X = \left[\frac{1}{T_{mb}^{\circ}} - \frac{1}{T_m^{\circ}} \right] \frac{\Delta H_{2U}}{RV_{2U}} = -\frac{B}{R} \frac{\phi_1^2}{T_{mb}^{\circ}} \quad (4.12)$$

From eqn. 4.12, χ values derived from the slope of X versus ϕ_1^2/T_{mb}° are essentially free energy values consisting of both enthalpic (χ_H) and entropic (χ_S) components. Typical ($\chi_H+\chi_S$) values for well-characterised miscible blends from melting point depression data are -0.157 at 333K for poly(ethylene oxide)-poly(methyl methacrylate)⁴ and -0.295 at 433K for poly(vinylidene fluoride)-poly(methyl methacrylate)⁸ mixtures.

Paul et al. have used molar volumes (V) of the polymers in place of m values^{3,12} to determine the entropic terms (1) and (2). Subsequently, these entropic components were regarded as negligible contributions to the melting point depression and the condensed Nishi-Wang expression (eqn. 4.12) has been used to determine interaction parameters. As molar volumes could be in the order of 10^3 to 10^6 for polymers having much smaller m values, it is not surprising that the use of molar volumes in place of m values results in negligible entropic contributions i.e. terms (1) and (2) in eqn. 4.11. Although the use of molar volumes would appear to be incorrect, the assumption that the configurational entropy contributions to melting point depression are negligible in these blends is probably still correct as the polymers are relatively high molecular weight and thereby have large m values, justifying the use of eqn. 4.12. For blends in which the entropic components are believed to contribute significantly to the melting point depression, number average degree of polymerisation (m) values are predominantly used^{5,13,14} in eqn. 4.11.

Eqn. 4.11 (using either degree of polymerisation or molar volume values) has seldom been used to determine specific χ_H interaction parameters with the vast majority of crystalline-amorphous polymer blends analysed using eqn. 4.12 to give $(\chi_H + \chi_S)$ values. Many authors have often justified the use of this shortened expression by simply (and even routinely) assuming that the entropy contributions are negligible even in relatively low molecular weight polymers⁴ and this arouses some scepticism in the ability of the full expression (eqn 4.11) to account fully for the configurational entropy⁵.

Eqns. 4.11 and 4.12 based on the concept of the Flory-Huggins lattice theory and derived from the original Nishi-Wang (eqn. 4.7) and Scott (eqn. 4.1) expressions have been used in this study to determine Flory-Huggins interaction parameters which are attributed to enthalpic (χ_H) and free energy ($\chi_H + \chi_S$) contributions between crystalline and amorphous polymers at the melting point. The majority of polymers in this study are of low molecular weight (with potentially large configurational entropy contributions) and are highly branched. Due to the density of the branching, it is believed that these polymer blends will have unique entropic contributions (see Discussion) which cannot

be fully accounted for in the full Nishi-Wang expression (eqn. 4.11), based on linear chains. The use of eqn. 4.11 is therefore likely to produce inaccurate values of χ_H but will serve in this study as an "indication" of the purely enthalpic contribution to miscibility in these blends and for comparison with "heat of mixing" measurements.

The dependence of χ on composition and temperature cannot be established by melting point depression analysis and although the Nishi-Wang expressions are based on assumptions that χ is independent of composition, it has been shown that χ is indeed compositional dependent¹⁵. However, this technique serves as a relatively quick and reliable method of determining an average free energy polymer-polymer interaction parameter value which indicates the miscibility of an amorphous-crystalline polymer blend at the melting point. The use of melting point depression data to determine the purely enthalpic interaction is much more subjective due to the assumption that all entropy contributions are configurational which are subsequently calculated based only on a linear polymer model.

4.3 Melting point considerations

The use of melting point values of various blend compositions to determine χ values is based on the view that the depression in the melting point of a semi-crystalline polymer is primarily the result of thermodynamic interactions between the crystalline phase and a miscible amorphous phase (consisting of a mixture of the two polymers) with which it is in equilibrium. The melting points determined should therefore strictly be equilibrium values (T_m°) i.e. the "true" melting temperature of the crystalline phase at infinite lamellar thickness without morphological changes such as imperfections and thickness variations within the crystalline regions which can also be responsible for melting point variations¹⁶. The T_m° value of a completely crystalline polymer is never actually achieved and is usually determined by DSC using an indirect method: plotting melting temperature (T_m) against crystallisation temperature (T_c) and extrapolating to $T_m=T_c$ to give the T_m° value.

Nishi and Wang studied the isothermal crystallisation of poly(vinylidene fluoride) (PVF₂) and poly(methyl methacrylate) (PMMA) mixtures⁸. As the melting point depression noted in this blend system was unaffected by a change in T_c or the rate of heating (from the T_c to the melting point of the crystalline phase) it was concluded that morphological changes such as crystal imperfections and reduction in lamellar thickness were not major factors in the lowering of the melting point in these mixtures. The use of experimental rather than equilibrium melting points could be justified as the T_m versus T_c plots of the various blend compositions all had very similar gradients.

However, morphological contributions may be significant in other blends i.e. mixtures of poly(2,6-dimethyl-1,4-phenylene oxide) and isotactic polystyrene¹⁷, and the Nishi-Wang treatment has been extended further to take morphological effects into account for these blends^{13,18}.

The use of melting point data to extract polymer-polymer interaction parameters (χ) has recently been critically reviewed by Runt and Gallagher¹¹ which highlighted the "problem" in determining accurate experimental melting points (T_m) of crystals formed at various T_c values. Due to crystal reorganisation during the actual thermal analysis experiment i.e. heating from T_c to T_m , the resulting T_m values do not truly represent crystallisation solely at the T_c . Therefore the use of these "inaccurate" experimental values to determine subsequent equilibrium melting points from plots of T_m versus T_c , which tend to be extrapolated over large temperature ranges and can also show curvature⁵, could result in considerable errors due to these morphological changes and the resulting χ values must be viewed with caution.

4.4 Experimental

Blends of EVA with various semi-crystalline polymers (see Table 4.1) were prepared by solvent casting from chloroform solutions with a total polymer concentration of 10% w/v. The solvent was allowed to evaporate at room temperature for up to 1 week and the resulting films were dried at 323K under vacuum for 24 hours. The dried blends were stored in a sealed desiccator.

MELTING POINT DEPRESSION ANALYSIS

Semi-crystalline polymers (blended with amorphous poly(ethylene-co-vinyl acetate) - EVA)

Crystalline Polymer	Origin	Abbreviation
poly(di-n-tetradecyl fumarate-co-vinyl acetate)	EXXON Chemical Ltd.	FVA
poly(di-n-octadecyl itaconate)	EXXON Chemical Ltd.	PI
poly(di-n-octadecyl itaconate) - low molecular weight	EXXON Chemical Ltd.	LMPI
n-docosyl diester terminated poly(ethylene glycol)	EXXON Chemical Ltd.	PE
n-docosyl diester terminated poly(ethylene glycol)	Synthesised	NECPE
deuterated n-docosyl diester terminated poly(ethylene glycol)	Synthesised	DPE
n-docosyl monoester terminated poly(ethylene glycol)	Synthesised	NECME
hydrogenated poly(5-hexadecyl norbornene)	Synthesised*	9210
hydrogenated poly(5-tetradecyl norbornene)	Synthesised*	9233

* C.A. Smith, PhD Thesis, Durham University (1993).

Table 4.1

Due to significant impurities in the industrial poly(ethylene glycol) diester sample (PE), a pure diester sample (NECPE) and a monoester variant (NECME) were prepared and investigated to determine the effect of mono and di esterification on any interaction with EVA. A fully deuterated diester sample (DPE) used in small angle neutron scattering studies (see Chapter 9) has also been examined for possible differences in the interaction of EVA with deuterated and hydrogenous samples. Structure, synthesis and characterisation details of these polymers are given in Chapter 3.

DSC thermograms were obtained using a Perkin-Elmer DSC-7, calibrated using Indium and Zinc standards. All samples and standards were analysed in a nitrogen atmosphere. The procedure for all samples was an initial scan to determine the melting temperature. A new sample was then heated from ambient temperature to a temperature 20K above the initial melting temperature at a rate of 200K/min and held at this higher temperature for 2 minutes to remove any crystalline artefacts of previous thermal treatments. The samples were then cooled at 10K/min to a starting temperature and held for two minutes to equilibrate. Melting points and enthalpies of fusion were then obtained by heating each sample at 10K/min to 20K above the maximum temperature of the melting endotherm. Melting points quoted are the onset values of the endotherm (unless stated otherwise).

Standard deviations of the melting points in EVA:FVA and EVA:PE blends have been calculated based on 8 DSC measurements on the pure FVA and PE semi-crystalline polymers. The standard deviation of the melting points in the remaining blends was determined separately for each blend from multiple analysis. Error bars on the plots of melting point depression versus composition are \pm one standard deviation (based on a small sample population).

Figures 4.3, 4.4 and 4.5 are typical examples of DSC thermograms for the PI, FVA and NECPE semi-crystalline polymers. The thermogram of PE is typical of all the poly(ethylene glycol) esters showing two melting endotherms with a slight shoulder on the lower melting phase. These phases are known to be due to separate poly(ethylene glycol) and docosyl crystallisation phases¹⁹ (see wide angle X-ray scattering - Chapter

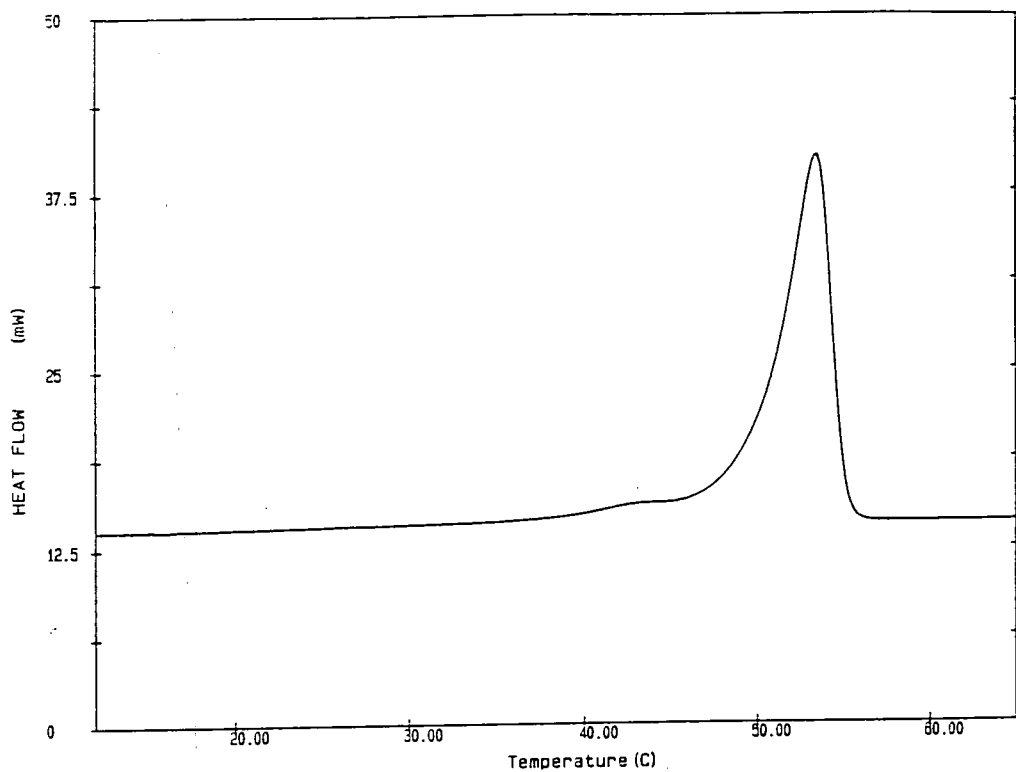


Figure 4.3 : DSC thermogram of poly(di-n-octadecyl itaconate) - PI

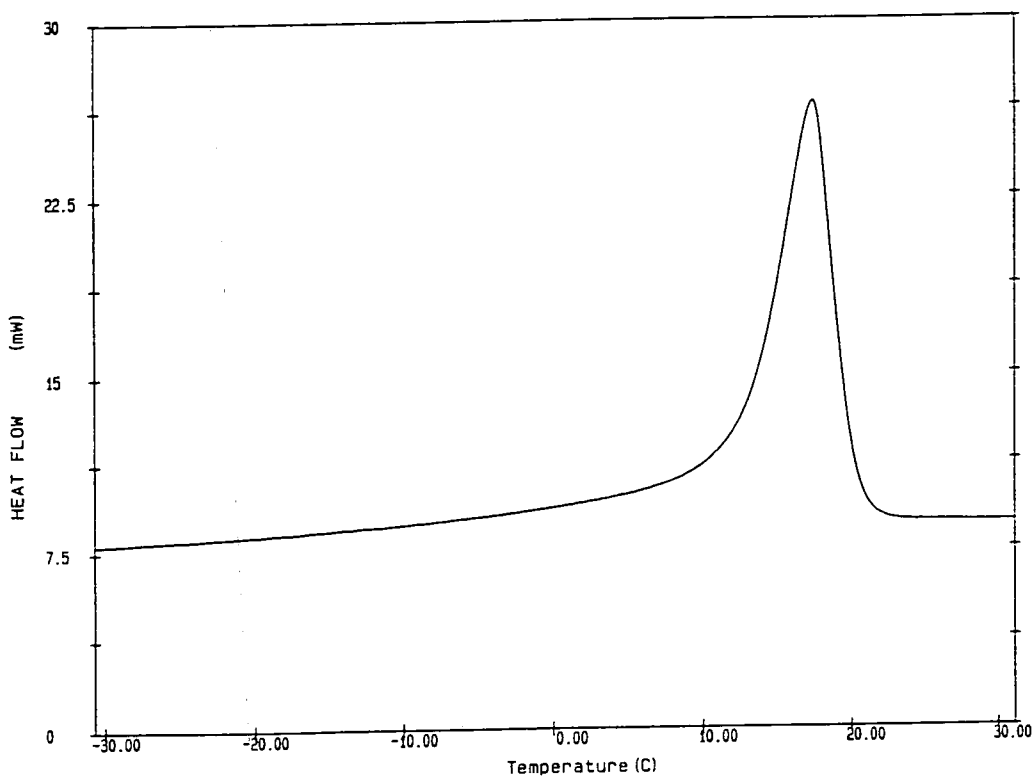


Figure 4.4 : DSC thermogram of poly(di-n-tetradecyl fumarate-co-vinyl acetate) - FVA

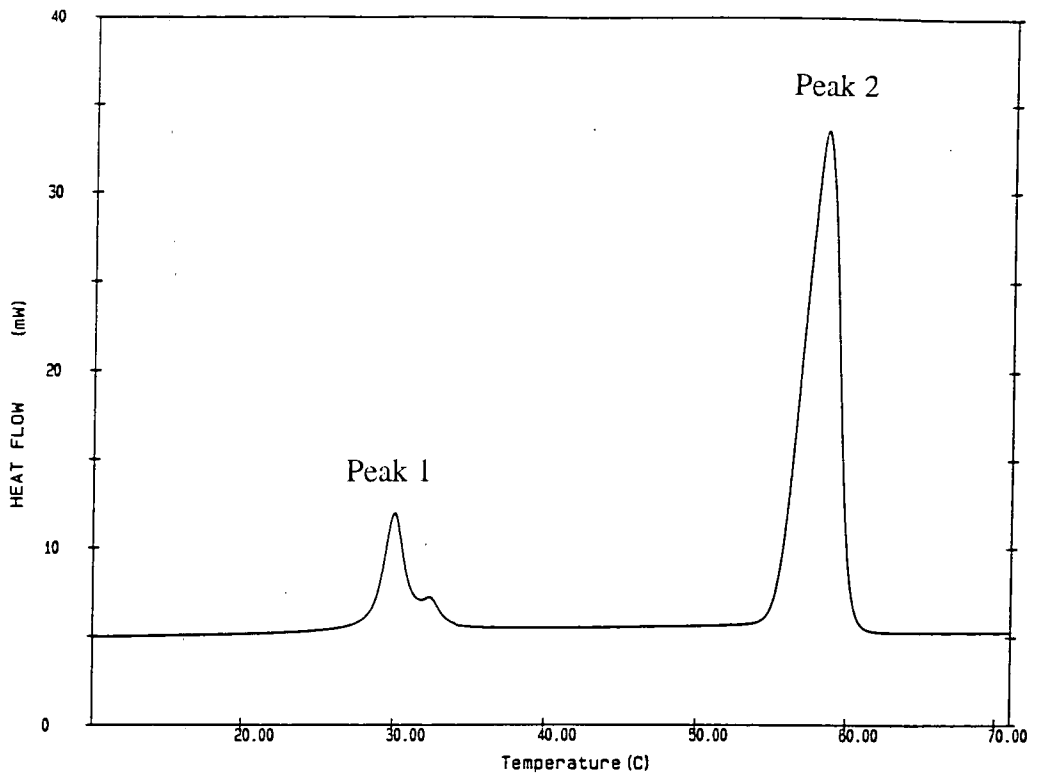


Figure 4.5 : DSC thermogram of n-docosyl terminated poly(ethylene glycol) - NECPE

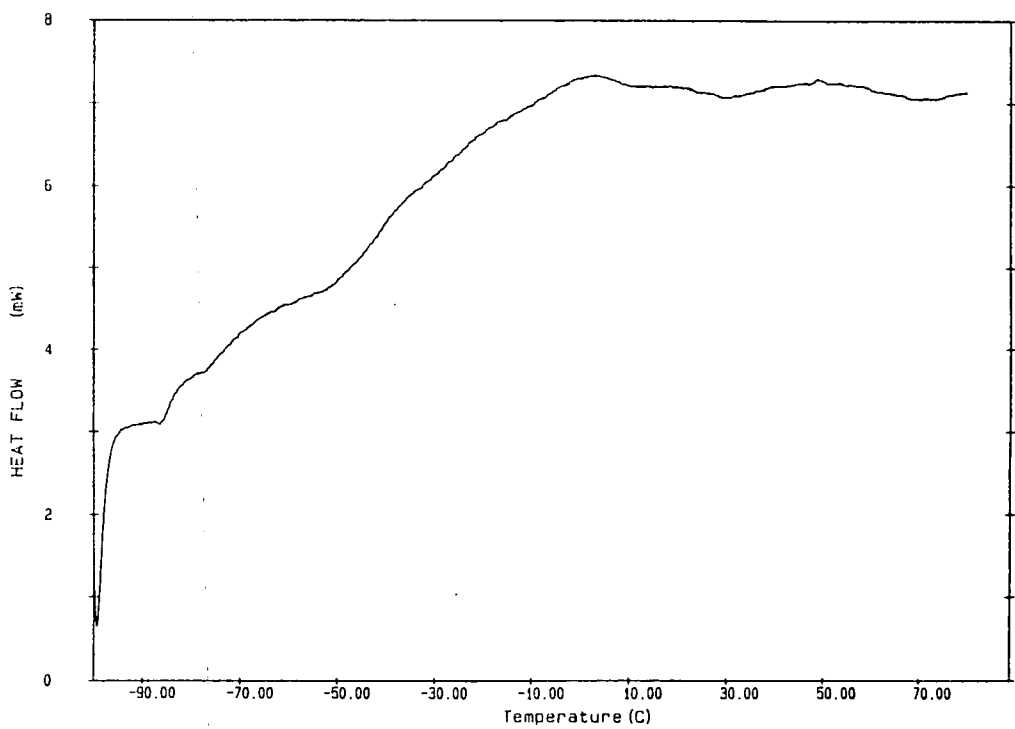


Figure 4.6 : DSC thermogram of poly(ethylene-co-vinyl acetate) - EVA

8). In the following results and discussion sections, the lower melting (poly(ethylene glycol)) endotherm is referred to as Peak 1 with the higher melting (docosyl) endotherm named as Peak 2.

4.5 Results

The glass transition temperature (T_g) of these polymers and their blends has not been identified clearly in this work. In these blends, this is due to the effect of the EVA phase which clearly shows no crystalline melting endotherm, but has a mountainous-type DSC profile (Figure 4.6) which contributes many confusing, possible "transitions" to the thermogram of the blend.

The various thermodynamic parameters in the full Nishi-Wang expression (eqn. 4.11) are shown for each polymer in Appendix A.1. Volume fractions and degrees of polymerisation have been determined from density and number average molecular weight (M_n) values respectively (see Chapter 3). The molar volume of each repeat unit has been determined by the ratio of the molecular weight of the repeat unit to the density of the polymer. Predicted "enthalpies of fusion" for each fully crystalline polymer (ΔH_{2U}) have been determined from the observed DSC "enthalpy of fusion" values and fractional crystallinities obtained either from powder diffraction profiles or comparison methods (see wide angle X-ray scattering - Chapter 8).

4.5.1 EVA blends with semi-crystalline polymers

Melting point results including the parameters use in the subsequent data analysis are shown in detail for each of these blends in Appendix A. as Tables: A.2,A.3 (EVA:PI); A.4,A.5 (EVA:LMPI); A.6,A.7 (EVA:FVA); A.8,A.9 (EVA:PE); A.10,A.11 (EVA:NECPE); A.12,A.13 (EVA:NECME); A.14,A.15 (EVA:DPE); A.16 (EVA:9210) and A.17 (EVA:9233).

Figures 4.7 to 4.9 show the variation in the observed melting point values of these blends with EVA composition. The melting point depressions range from approximately 2K-17K depending on the blend system.

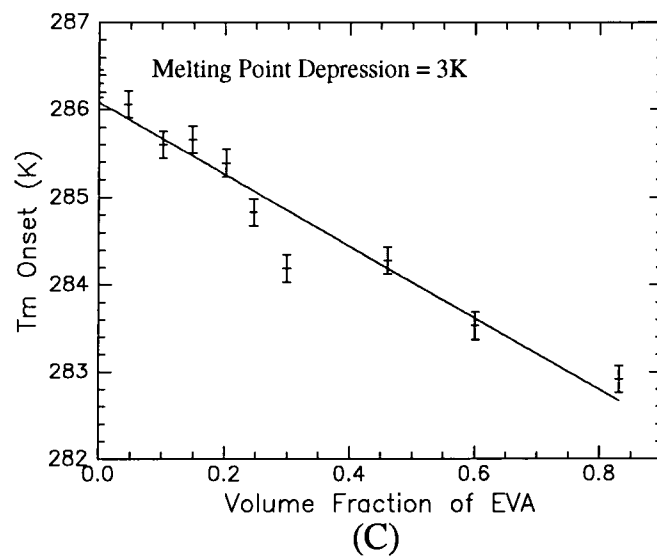
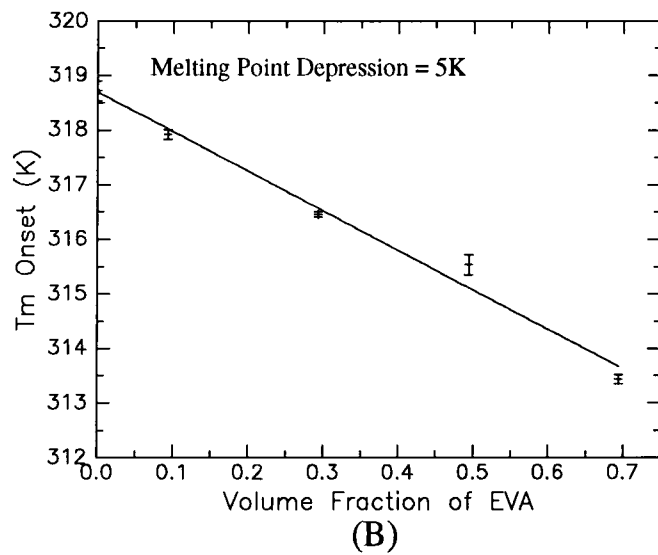
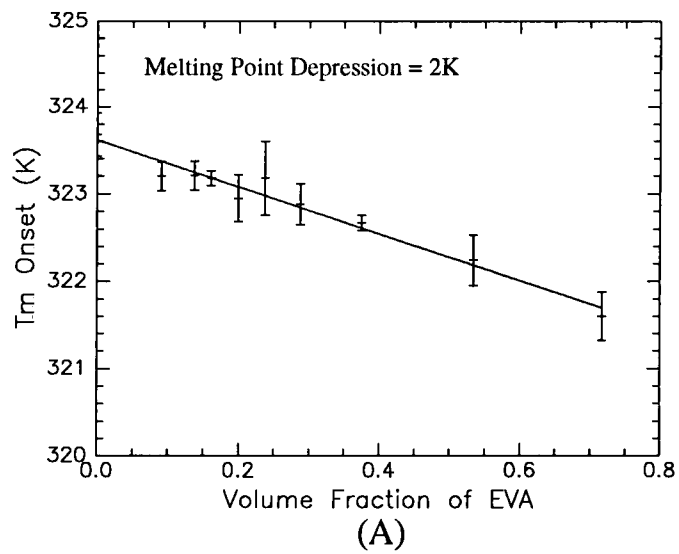


Figure 4.7 : Melting Point Depressions in EVA blends with :
PI (A); LMPI (B); FVA (C).

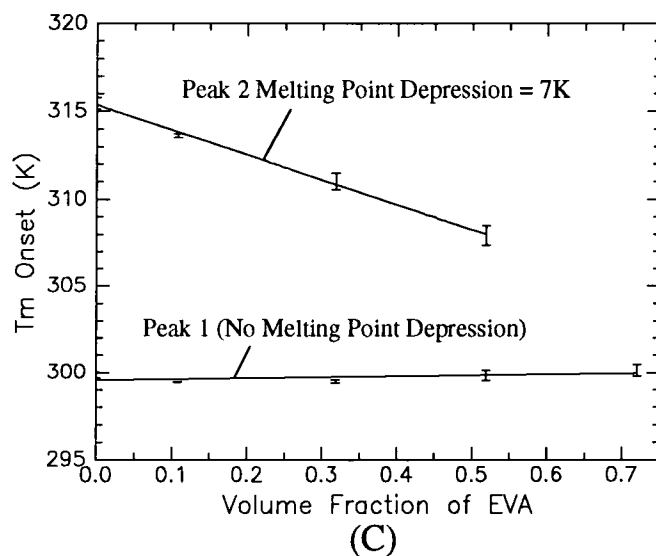
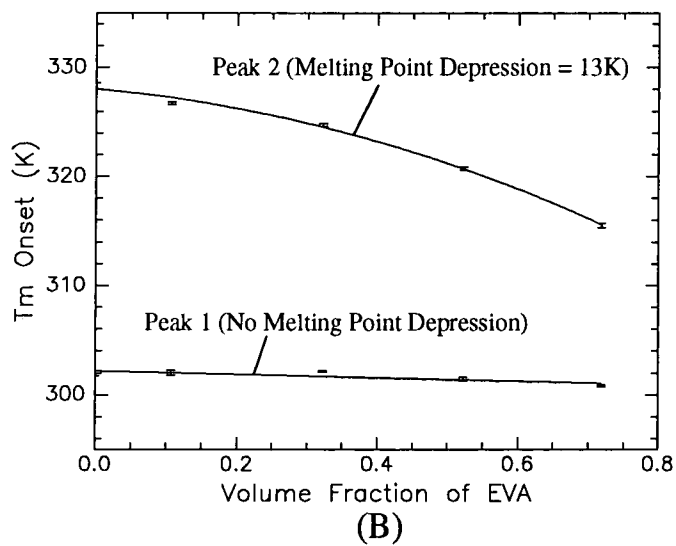
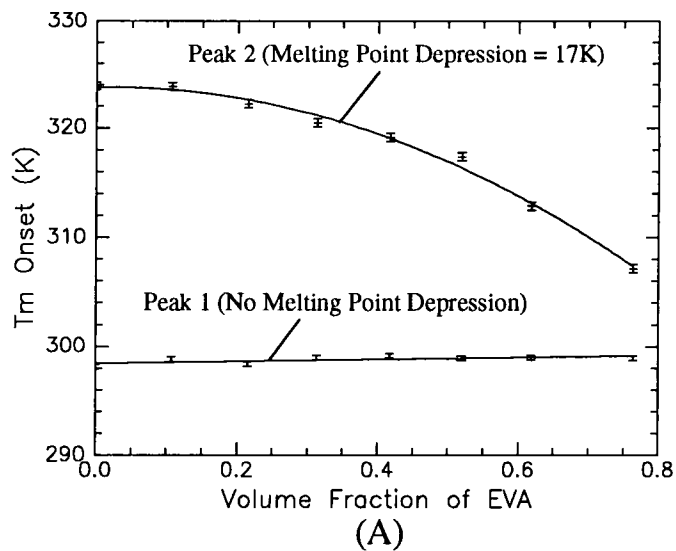


Figure 4.8 : Melting Point Depressions in EVA blends with :
PE (A); NECPE (B); NECME (C).

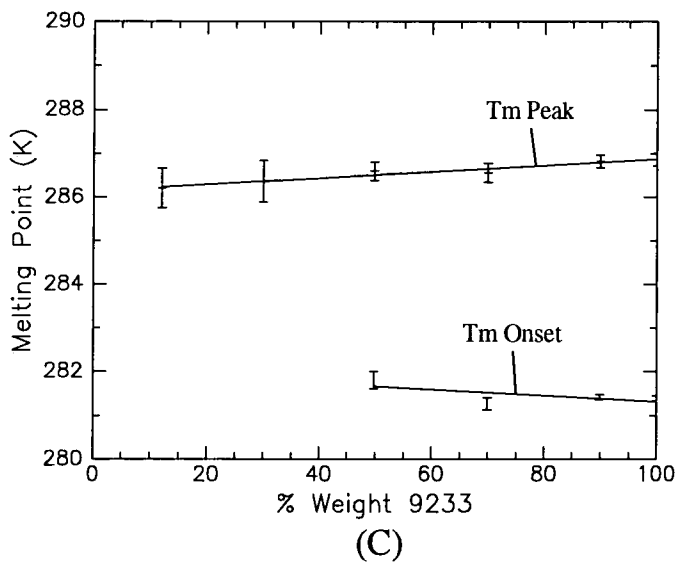
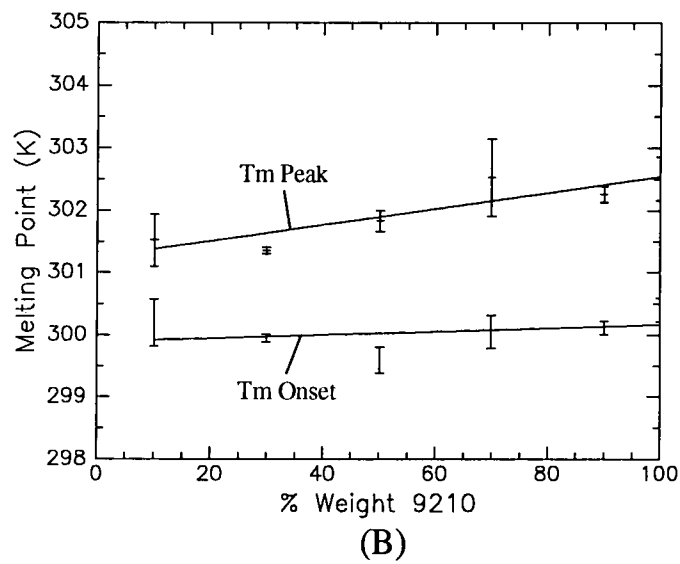
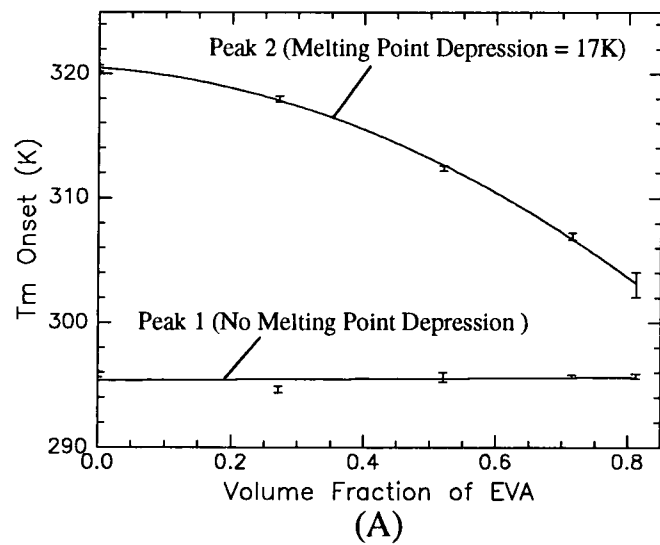


Figure 4.9 : Melting Point Depressions in EVA blends with :
DPE (A); 9210 (B); 9233 (C).

Considering the precision of the DSC instrument, the melting point analysis in both EVA:9210 and EVA:9233 blends appears to indicate that there is no significant depression i.e. $\leq 1\text{K}$ in the melting point of 9210 or 9233, on blending with EVA. Consequently, χ interaction parameters could not be determined for these blends. Also, due to the very broad melting endotherm in 9233 and its low crystallinity/heat of fusion value, reliable T_m (onset) values could not be determined at high EVA volume fractions. In these blends, T_m (peak) values have also been quoted.

In EVA blends with the poly(ethylene glycol) esters i.e. PE, NECPE, NECME and DPE, as the EVA composition increased there was no apparent change in the melting point of the lower melting phase (Peak 1) whereas the melting point of Peak 2 was depressed dramatically by up to 17K, as shown for example in Figure 4.10. Melting point depression analysis to determine χ values was therefore based on the higher melting phase (Peak 2).

Using the full Nishi-Wang expression (eqn. 4.11) which accounts for the entropic contributions due to the molecular length of the polymers, the plots of Y versus ϕ_1^2/T_{mb}° are shown for each blend in Figures 4.11, 4.12 and 4.13. In these blends this relationship is assumed to be linear with a negative slope, representative of the enthalpic blend interaction at the melting point. From this slope, the enthalpic B_H and χ_H values were determined for each blend system over the observed melting range (Tables 4.2 and 4.3).

In the shortened Nishi-Wang expression (eqn. 4.12), the entropic contributions are not accounted for and the melting point depressions represented as X are due to **both** enthalpic and entropic components. The plots of X (the value of which is much smaller than Y in eqn. 4.11) versus ϕ_1^2/T_{mb}° are essentially linear with a positive slope and frequently a slight positive intercept (Figures 4.14, 4.15 and 4.16). From the slope, the free energy density parameter (enthalpic and entropic), B_{H+S} and $(\chi_H+\chi_S)$ were determined over the observed melting range (Tables 4.2 and 4.3)

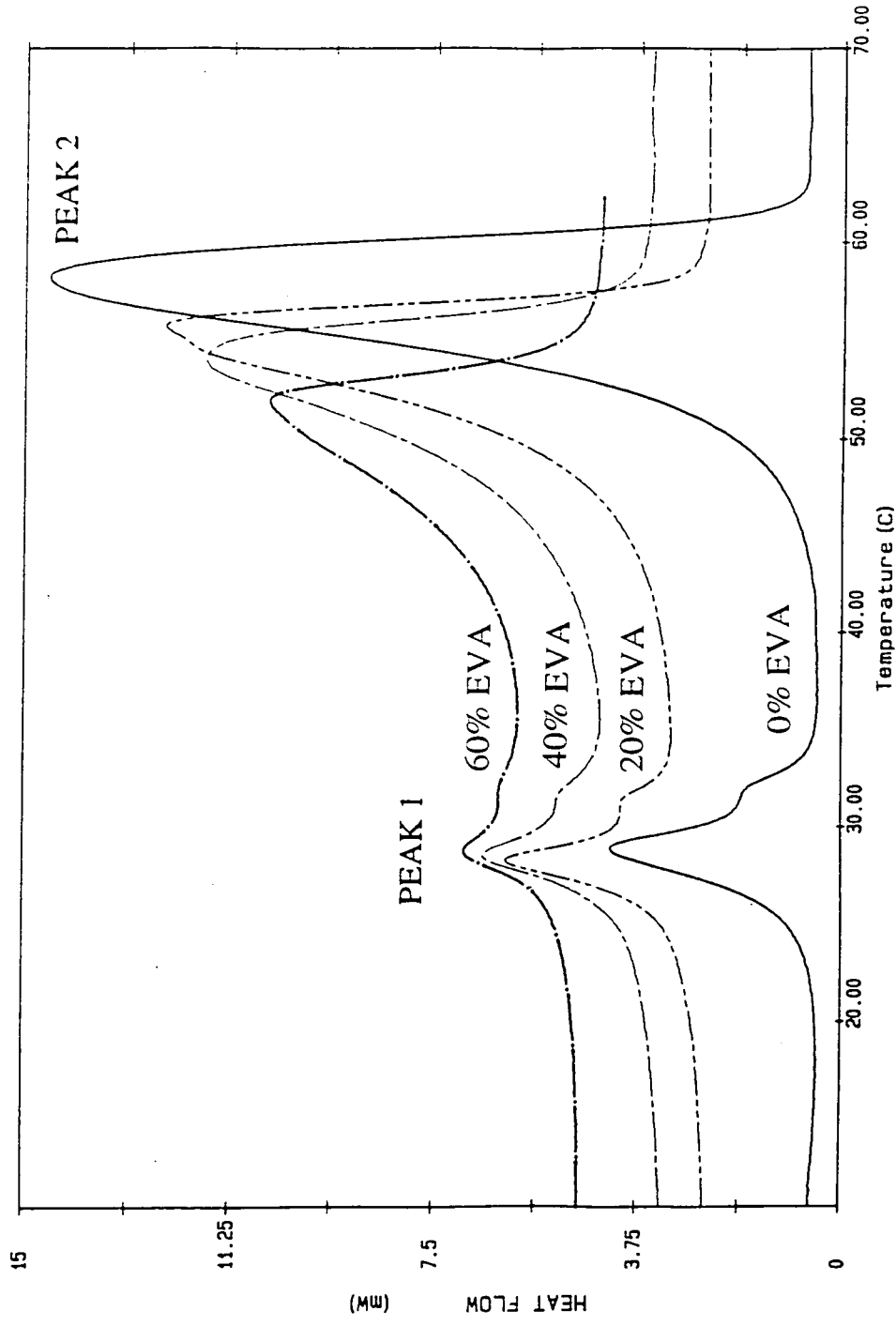


Figure 4.10 : Melting Point Depression in EVA:PE blends

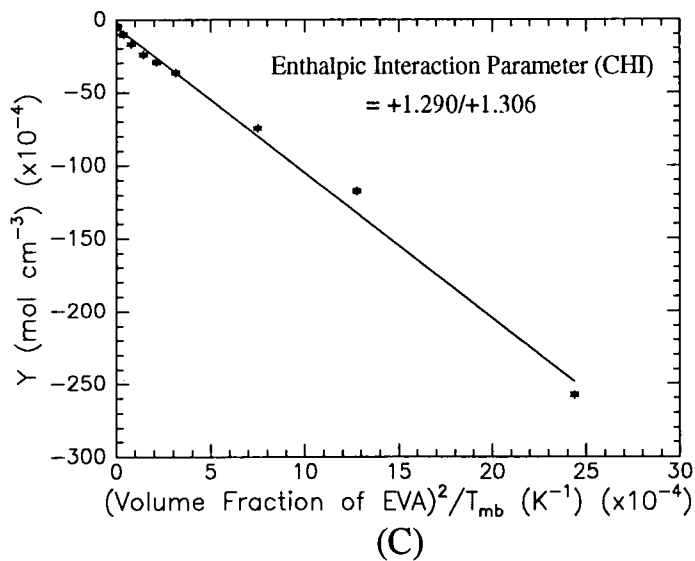
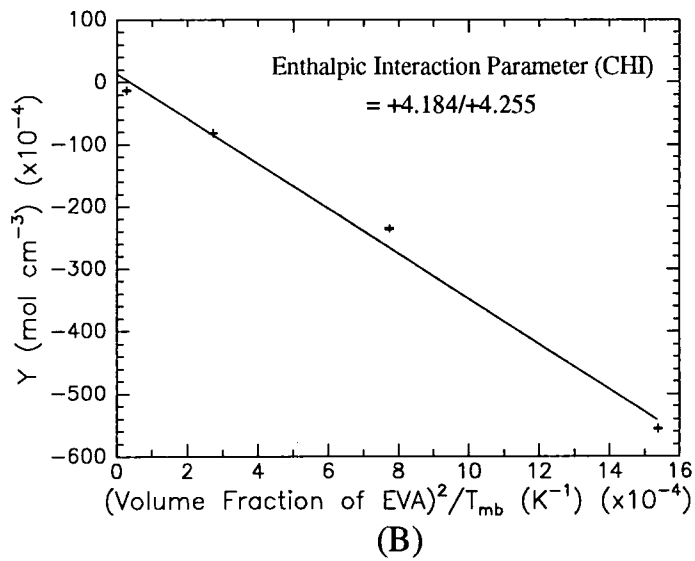
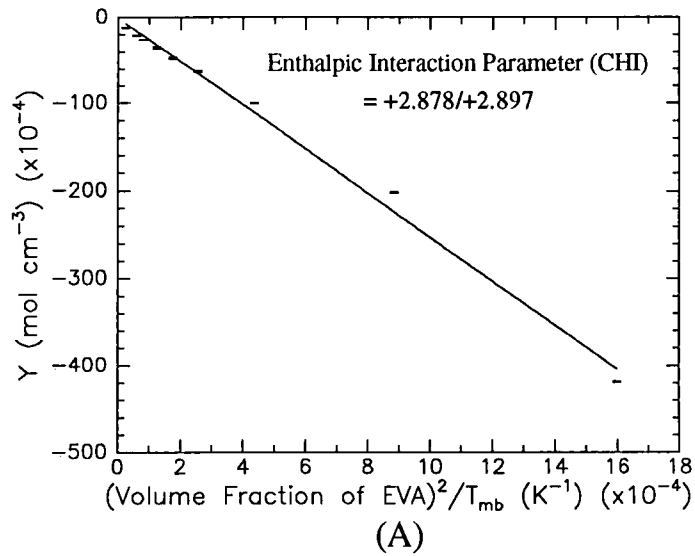


Figure 4.11 : Enthalpic Interaction Parameters in EVA blends with :
PI (A); LMPI (B); FVA (C).

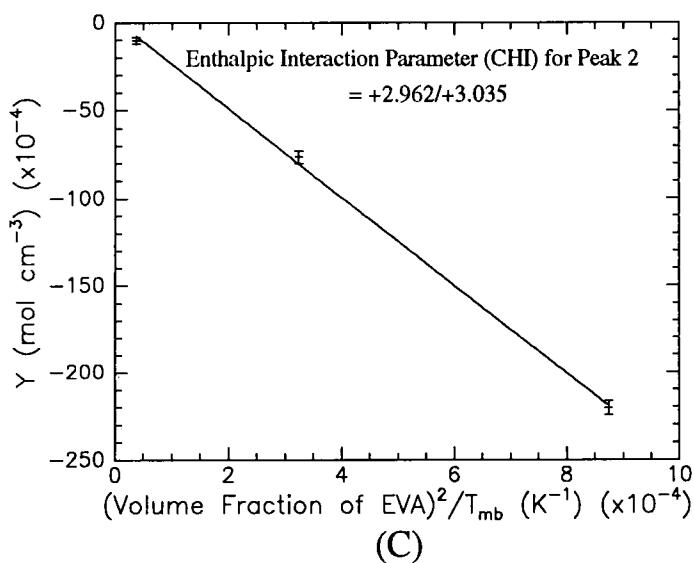
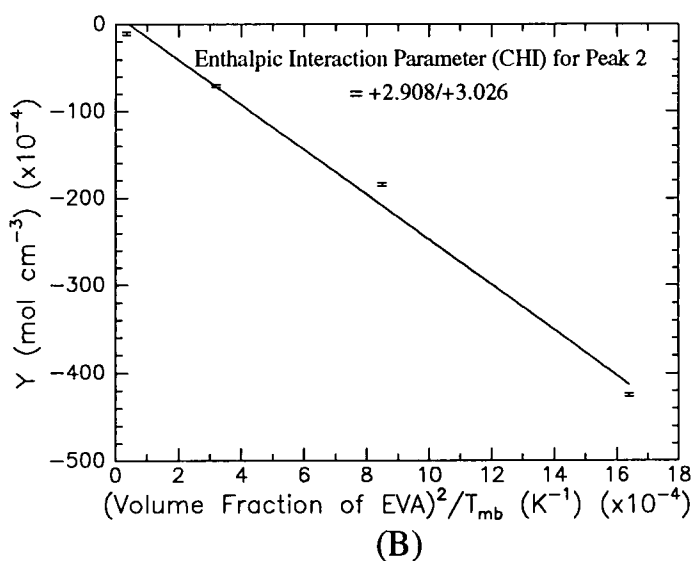
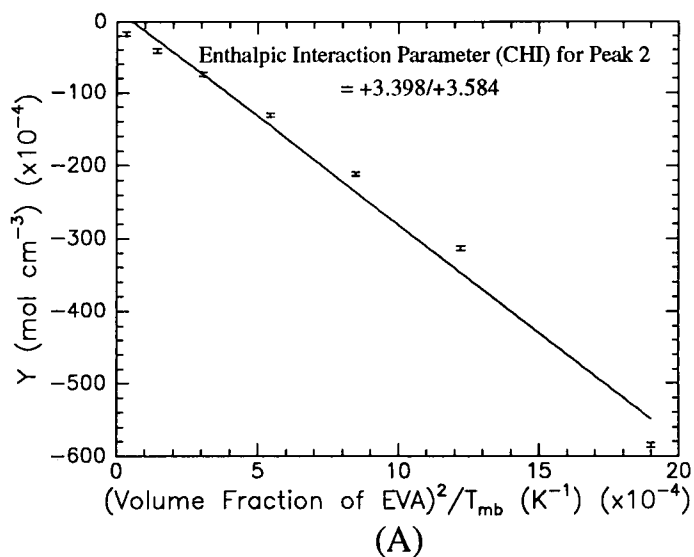


Figure 4.12 : Enthalpic Interaction Parameters in EVA blends with :
PE (A); NECPE (B); NECME (C).

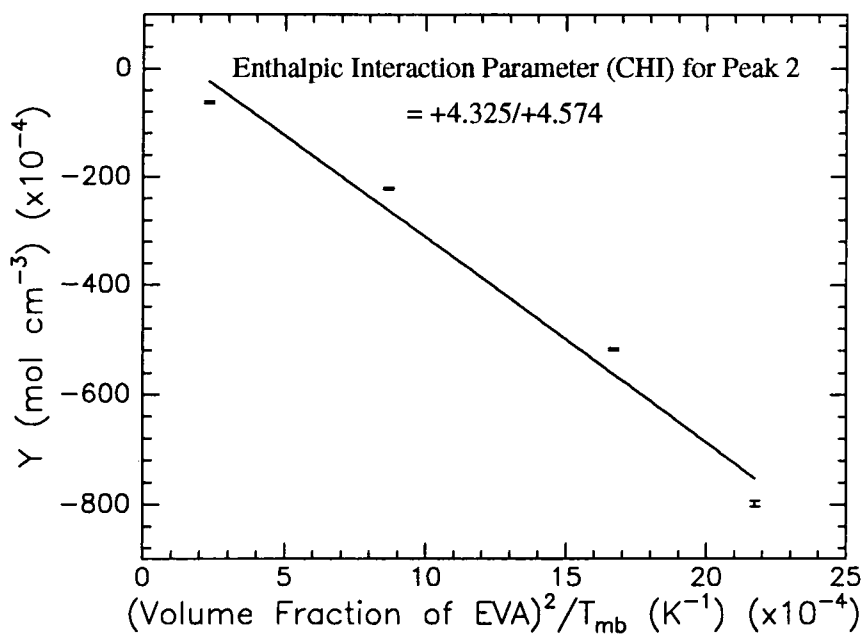


Figure 4.13 : Enthalpic Interaction Parameters in EVA:DPE blends

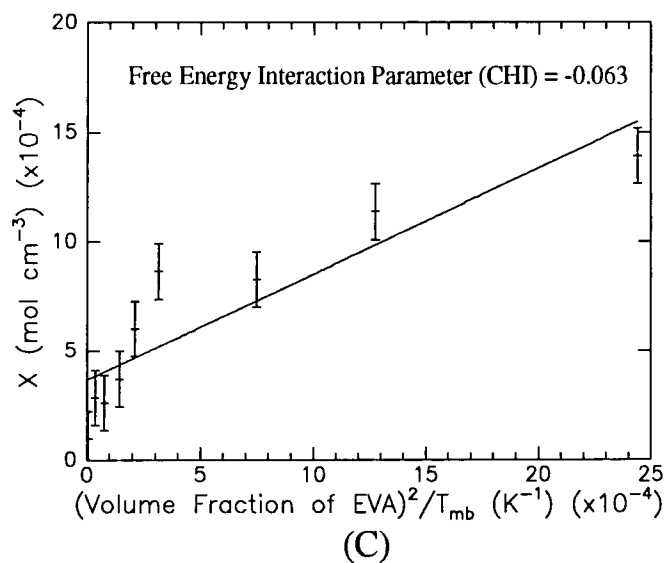
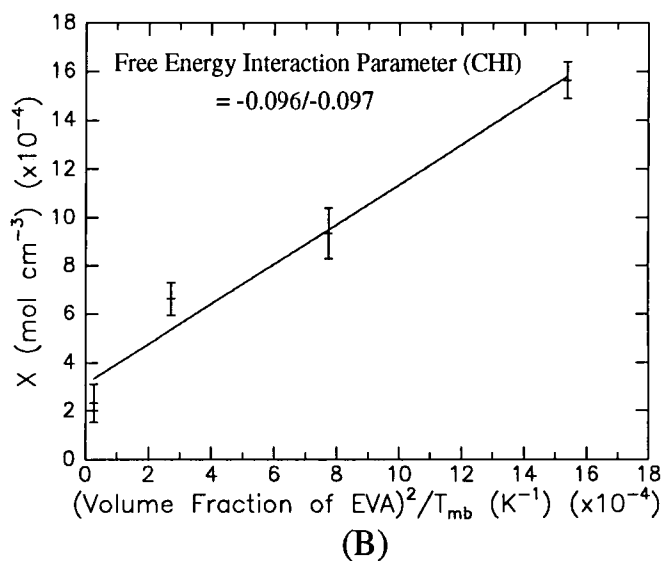
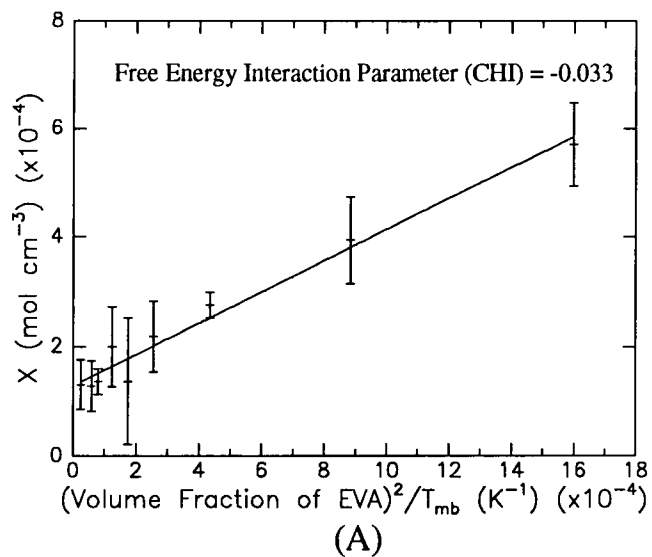


Figure 4.14 : Free Energy Interaction Parameters in EVA blends with :
PI (A); LMPI (B); FVA (C).

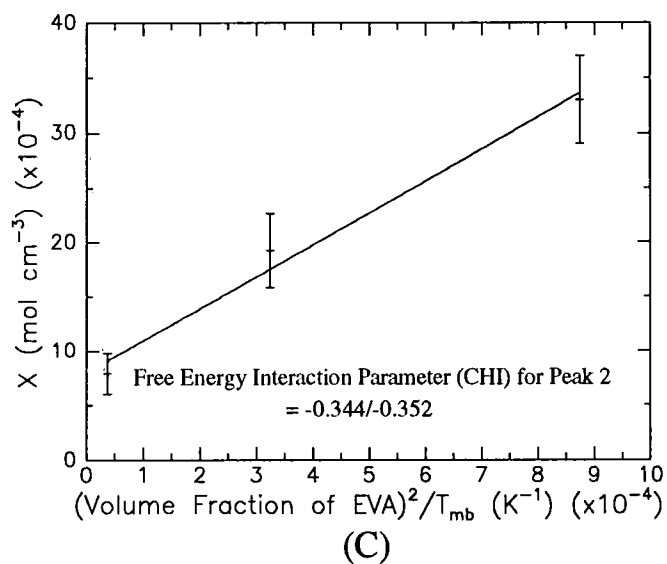
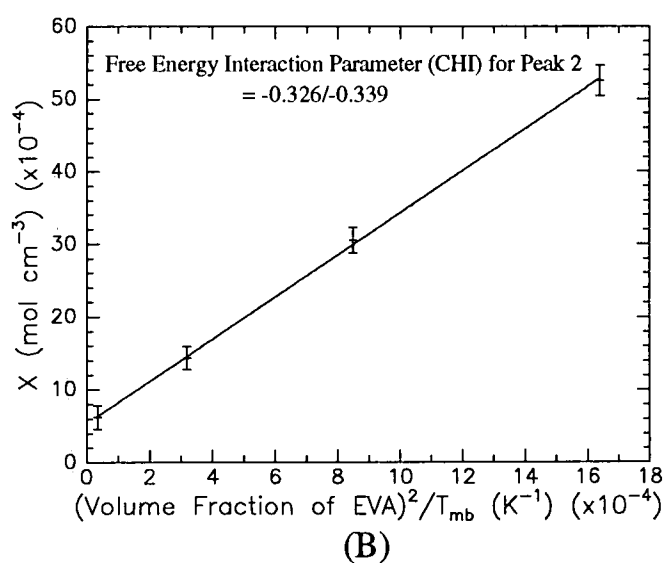
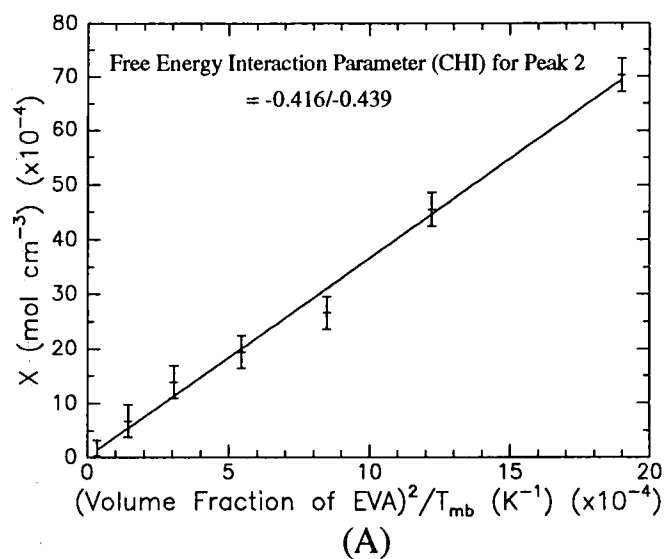


Figure 4.15 : Free Energy Interaction Parameters in EVA blends with :
PE (A); NECPE (B); NECME (C).

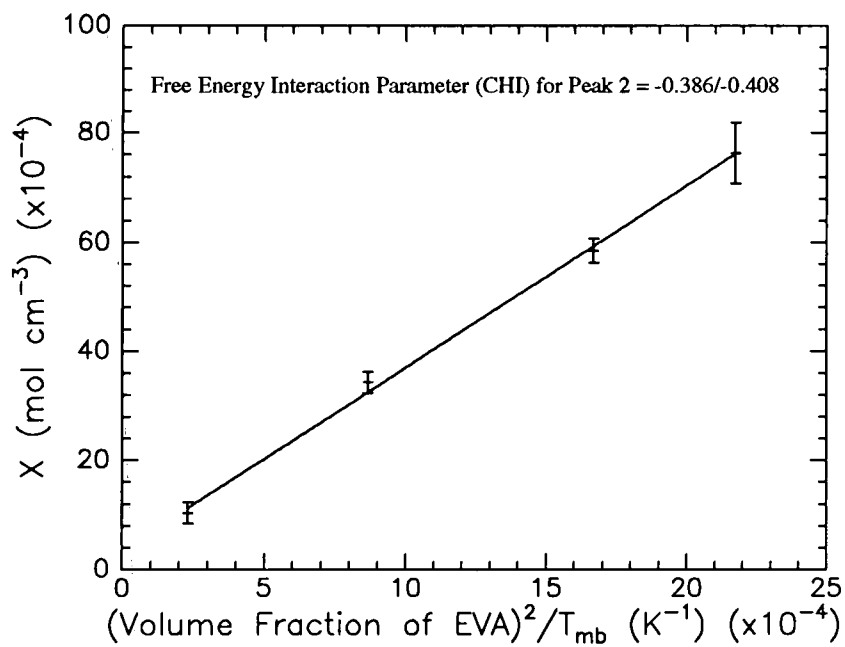


Figure 4.16 : Free Energy Interaction Parameters in EVA:DPE blends.

Polymer Blend	Melting Point Depression (K)	Melting Point Range (K)	Slope (Enthalpic) Eqn. 4.11 $\frac{Y}{\phi_1^2/T_{mb}^{\circ}}$ (mol cm ⁻³ K)	Slope (Enthalpic+Entropic) Eqn. 4.12 $\frac{X}{\phi_1^2/T_{mb}^{\circ}}$ (mol cm ⁻³ K)
EVA:PI (Tables A.2, A.3)	2.1 @ 0.717 ϕ_1 (Figure 4.7)	323.7/321.6	-25.196 (Figure 4.11)	0.285 (Figure 4.14)
EVA:LMPI (Tables A.4, A.5)	5.3 @ 0.694 ϕ_1 (Figure 4.7)	318.7/313.4	-36.069 (Figure 4.11)	0.824 (Figure 4.14)
EVA:FVA (Tables A.6, A.7)	3.4 @ 0.831 ϕ_1 (Figure 4.7)	286.3/282.9	-9.992 (Figure 4.11)	0.485 (Figure 4.14)
EVA:PE (Tables A.8, A.9)	16.8 @ 0.764 ϕ_1^* (Figure 4.8)	323.9/307.1	-29.773 (Figure 4.12)	3.644 (Figure 4.15)
EVA:NECPE (Tables A.10, A.11)	12.8 @ 0.719 ϕ_1^* (Figure 4.8)	328.3/315.5	-25.822 (Figure 4.12)	2.895 (Figure 4.15)
EVA:NECME (Tables A.12, A.13)	7.5 @ 0.519 ϕ_1^* (Figure 4.8)	315.4/307.9	-25.275 (Figure 4.12)	2.933 (Figure 4.15)
EVA:DPE (Tables A.14, A.15)	17.4 @ 0.812 ϕ_1^* (Figure 4.9)	320.5/303.1	-37.489 (Figure 4.13)	3.346 (Figure 4.16)

* refers to the higher melting endotherm (Peak 2). In all EVA blends with PE, NECPE, NECME and DPE, the melting point of Peak 1 is unaffected by EVA content. No significant melting point variation was noted in the EVA:9210 and EVA:9233 blends (Figure 4.9).

Table 4.2 : Melting Point Depressions in EVA-based Polymer Blends

Polymer Blend	χ_{CRIT} Eqn. 4.8	B_{H} (J/cm ³) (Enthalpic) Eqn. 4.11 (Y vs. $\phi_1^2/T_{\text{mb}}^\circ$)	χ_{H} (Enthalpic) Eqn. 4.11 (Y vs. $\phi_1^2/T_{\text{mb}}^\circ$)	$B_{\text{H+S}}$ (J/cm ³) (Enthalpic + Entropic) Eqn. 4.12 (X vs. $\phi_1^2/T_{\text{mb}}^\circ$)	$\chi_{\text{H+S}}$ (Enthalpic + Entropic) Eqn. 4.12 (X vs. $\phi_1^2/T_{\text{mb}}^\circ$)
EVA:PI	+0.064	209.490	+2.878/+2.897	-2.370	-0.033
EVA:LMPI	+0.090	299.892	+4.184/+4.255	-6.851	-0.096/-0.097
EVA:FVA	+0.030	83.078	+1.290/+1.306	-4.032	-0.063
EVA:PE (Peak 2)	+0.079	247.545	+3.398/+3.584	-30.298	-0.416/-0.439
EVA:NECPE (Peak 2)	+0.070	214.695	+2.908/+3.026	-24.070	-0.326/-0.339
EVA:NECME (Peak 2)	+0.084	210.147	+2.962/+3.035	-24.386	-0.344/-0.352
EVA:DPE (Peak 2)	+0.084	311.699	+4.325/+4.574	-27.820	-0.386/-0.408

Table 4.3 : Blend Interaction Parameters (χ) in EVA-based Polymer Blends

4.5.2 Enthalpies of fusion

Enthalpies of fusion (ΔH_f) were determined from the area under the melting endotherm and the values for the pure semi-crystalline polymers are shown in Table 4.4, with T_m onset values for each of the semi-crystalline polymers.

From the "enthalpy of fusion" values and assuming that a melting point transition has a free energy of fusion change (ΔG_f) of 0, the "entropy of fusion" (ΔS_f) values have been determined, using the relationship, $\Delta G_f = \Delta H_f - T\Delta S_f$.

Entropy of fusion values at the melting point of each semi-crystalline polymer are shown in Table 4.4.

Polymer	T_m (Onset) (K)	Enthalpy of Fusion (J/g)	Entropy of Fusion (J/gK)
PI	323.68 (0.25)	94.63 (0.6)	0.292
LMPI	318.72 (0.18)	95.17 (0.1)	0.299
FVA	286.30 (0.16)	44.87 (0.4)	0.157
PE (Peak 1)	298.12 (0.21)	16.84 (0.5)	0.056
PE (Peak 2)	323.90 (0.37)	104.56 (1.3)	0.323
NECPE (Peak 1)	301.95 (0.23)	18.89 (0.5)	0.063
NECPE (Peak 2)	328.31 (0.28)	106.57 (1.3)	0.325
NECME (Peak 1)	299.87 (0.16)	15.73 (0.6)	0.052
NECME (Peak 2)	315.46 (0.32)	88.99 (1.8)	0.282
DPE (Peak 1)	295.81 (0.23)	15.19 (0.48)	0.051
DPE (Peak 2)	320.47 (0.24)	83.67 (1.37)	0.261
9210	302.51 (0.19)	45.85 (0.36)	0.153
9233	281.39 (0.06)	33.60 (0.29)	0.119

Table 4.4

Higher melting endotherm (Peak 2)

Lower melting endotherm (Peak 1)

In Figures 4.17, 4.18 and 4.19, the enthalpies of fusion are plotted as a function of the crystalline polymer weight fraction for EVA blends with PI, LMPI, FVA, PE, NECPE, NECME, DPE, 9210 and 9233 respectively.

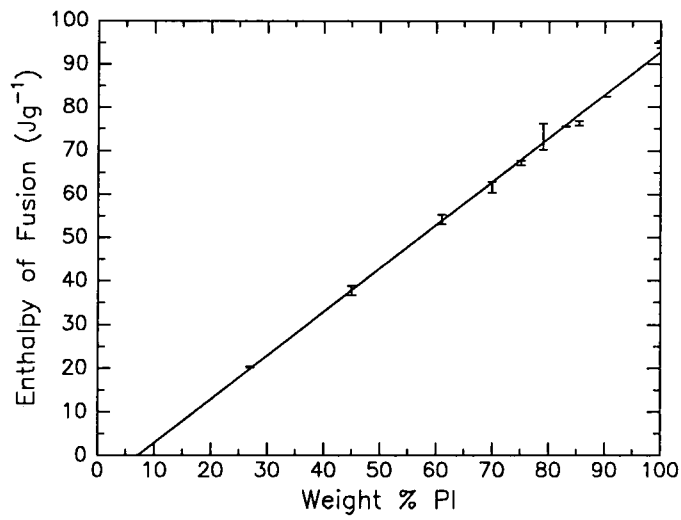
In the EVA blends with the poly(ethylene glycol) esters, the enthalpies of fusion for Peak 2 are always greater than the predicted value, based on the enthalpy of fusion of the pure semi-crystalline polymer and its weight fraction in the blend. This trend has also been noted in the EVA:LMPI blends and suggests that there maybe some incorporation of EVA molecules into these crystalline regions, thereby increasing the degree of crystallisation. In contrast, enthalpies of fusion for Peak 1 in the ester blends are always slightly less than predicted and consequently, may indicate that crystallisation of the lower melting phase is hindered by the EVA phase. Overall, the increase in crystallisation appears to dominate in these blends as shown by the total combined enthalpies of fusion (Peaks 1 and 2).

Enthalpies of fusion for the EVA:FVA and EVA:PI blends are slightly lower than the predicted values which again suggests that crystallisation in these blends is hindered by the EVA phase. Enthalpy of fusion values for EVA:9210 and EVA:9233 blends appear relatively scattered but also imply that crystallisation in these blends is frustrated by the EVA amorphous phase.

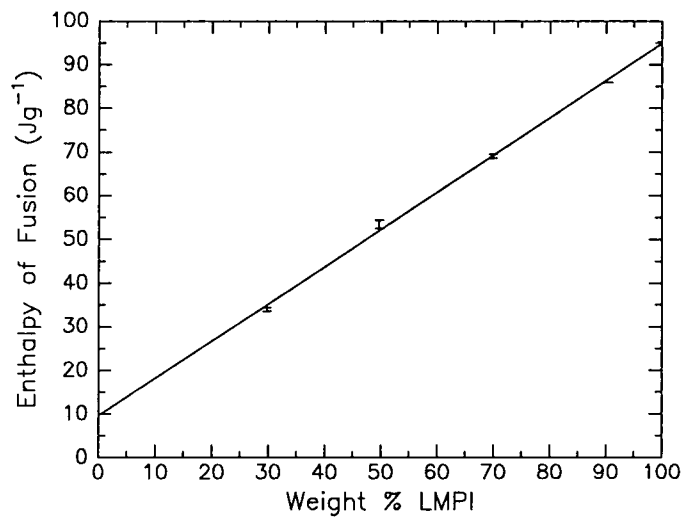
4.6 Additional DSC results

4.6.1 Morphological contributions to melting point depression

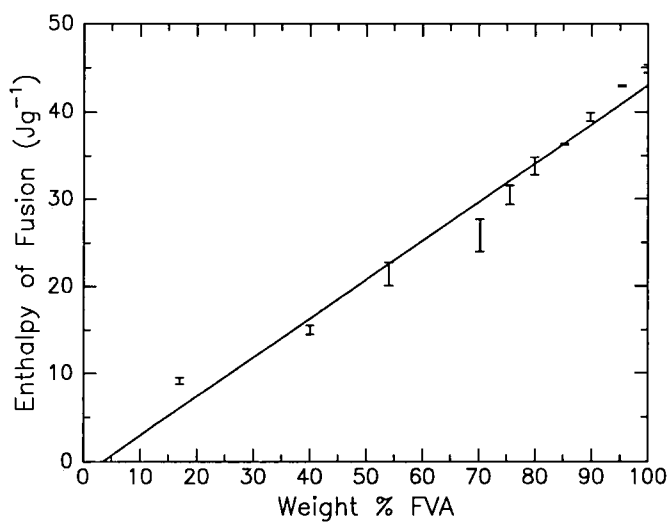
Further DSC experiments were carried out to investigate the melting point depression effects of possible morphological changes due to different starting temperatures. The standard starting temperatures of the DSC thermograms for EVA:PI, EVA:FVA and EVA:PE blends are 273K, 253K and 263K respectively. Tables 4.5, 4.6 and 4.7 show results on **single** DSC measurements for EVA:PI, EVA:FVA and EVA:PE (Peak 2) blends at starting temperatures of 203K, 223K and 193K respectively with the standard deviation errors based on multiple measurements on the pure semi-crystalline polymers.



(A)



(B)



(C)

Figure 4.17 : Enthalpies of Fusion in EVA blends with :
PI (A); LMPI (B); FVA (C).

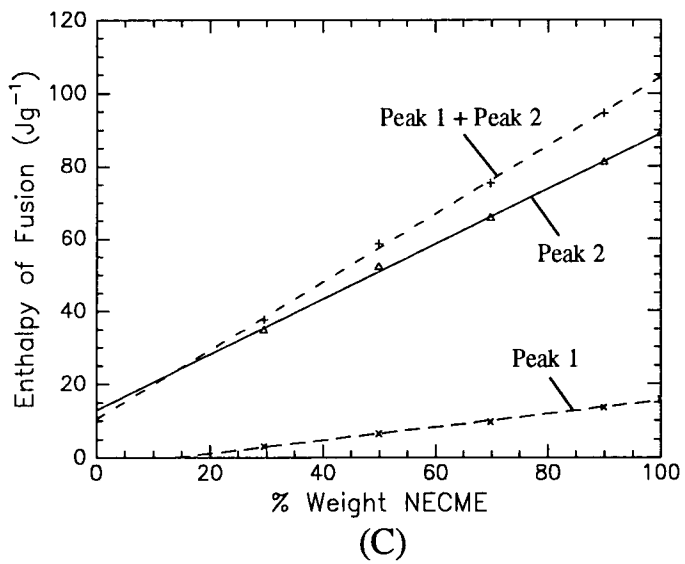
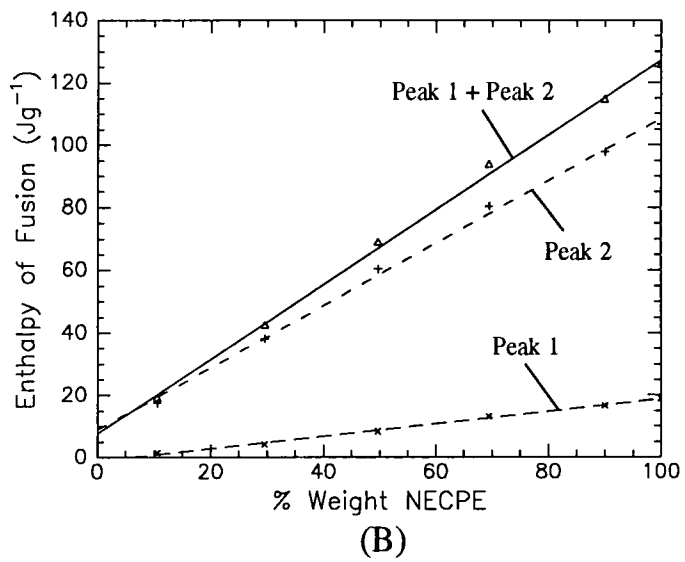
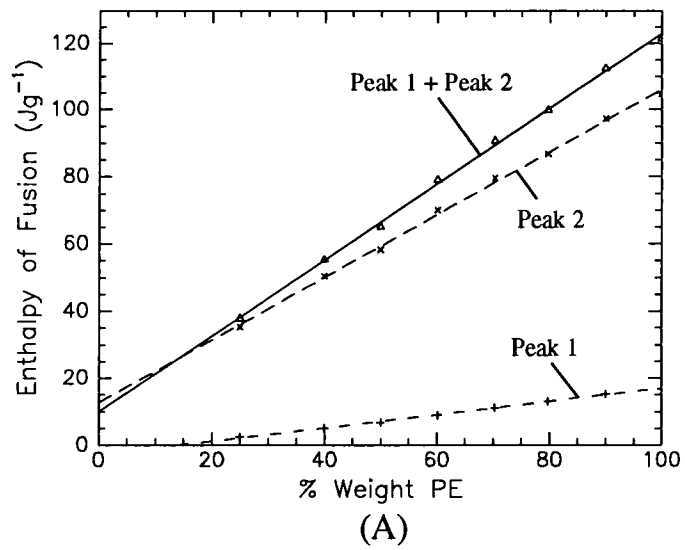


Figure 4.18 : Enthalpies of Fusion in EVA blends with :
PE (A); NECPE (B); NECME (C).

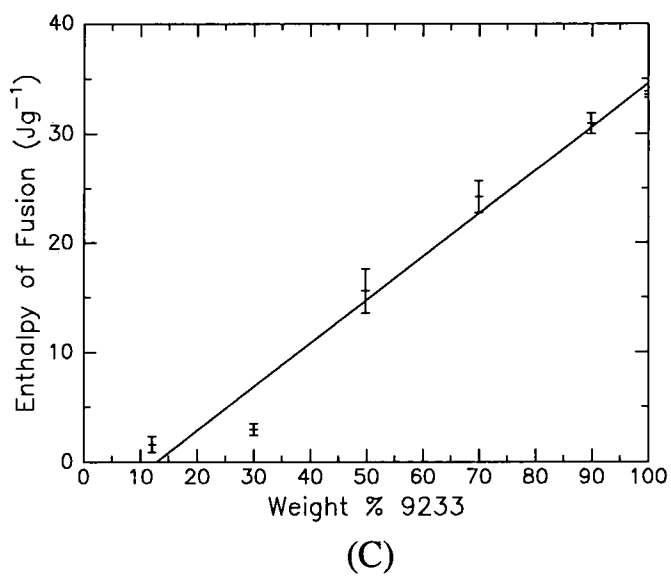
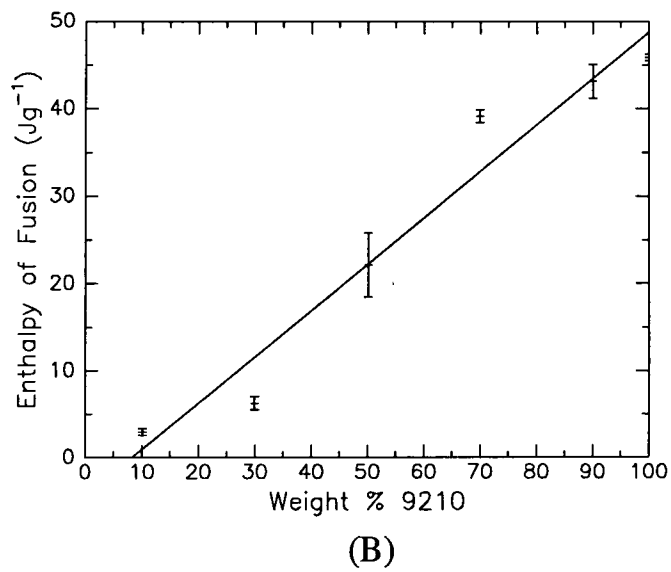
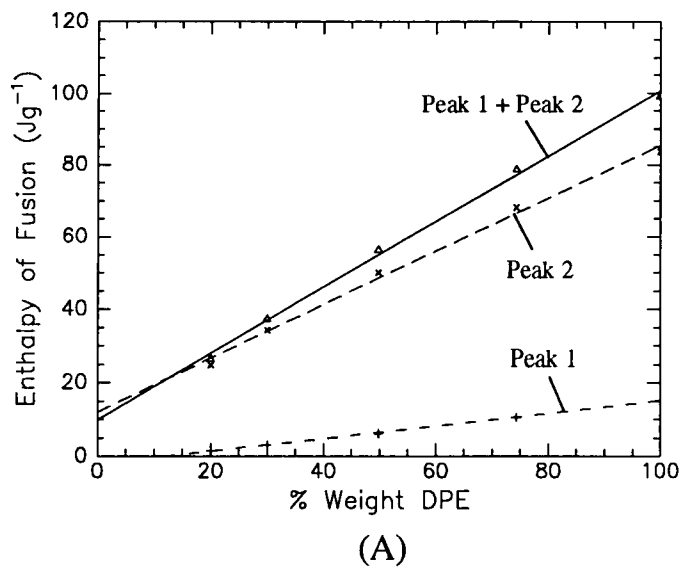


Figure 4.19 : Enthalpies of Fusion in EVA blends with :
DPE (A); 9210 (B); 9233 (C).

The resulting melting points have been compared with the melting point depression at the standard starting temperatures (Figure 4.20). The lower starting temperature in the EVA:PI and EVA:FVA blends appears to have reduced the melting point of the pure crystalline polymer by approximately 1K. However, the melting point depression value of each blend appears to be reasonably independent of the initial starting temperature.

Polymer Blend (w/w)	EVA Volume Fraction	Melting Point Onset (K)
PI 100%	0	323.02 ± 0.318
PI 83%:EVA 17%	0.161	321.73 ± 0.318
PI 61%:EVA 39%	0.375	321.10 ± 0.318
PI 45%:EVA 55%	0.534	320.41 ± 0.318
PI 27%:EVA 73%	0.717	320.11 ± 0.318

Table 4.5 : DSC measurements on EVA:PI blends (Starting Temperature 203K)

Polymer Blend (w/w)	EVA Volume Fraction	Melting Point (Onset) (K)
FVA 100%	0	284.65 ± 0.155
FVA 95.4%:EVA 4.6%	0.046	284.48 ± 0.155
FVA 89.82%:EVA 10.18%	0.102	284.39 ± 0.155
FVA 85.18%:EVA 14.82%	0.149	283.86 ± 0.155
FVA 79.87%:EVA 20.13%	0.202	283.01 ± 0.155
FVA 75.51%:EVA 24.49%	0.246	282.96 ± 0.155
FVA 70.18%:EVA 29.82%	0.299	282.18 ± 0.155

Table 4.6 : DSC measurements on EVA:FVA blends (Starting Temperature 223K)

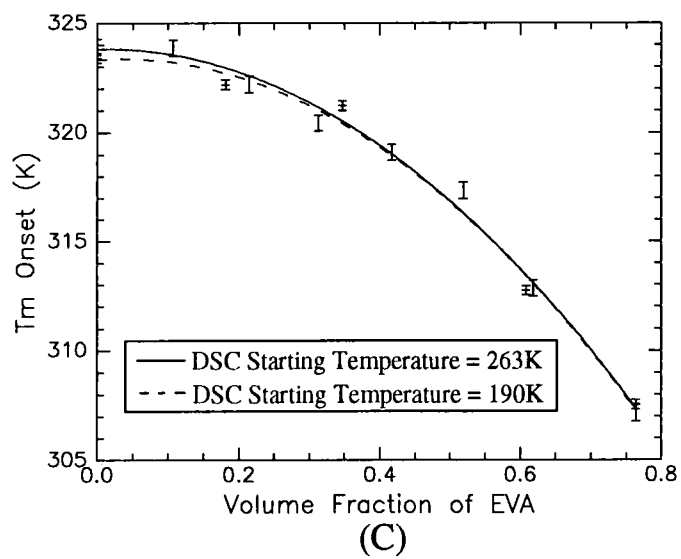
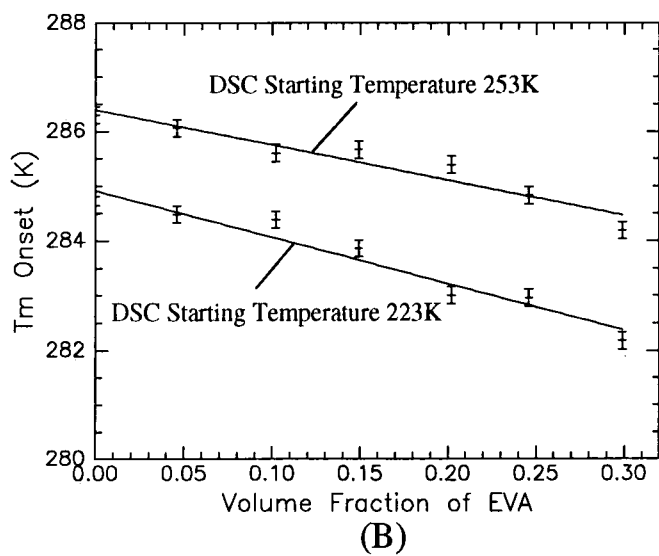
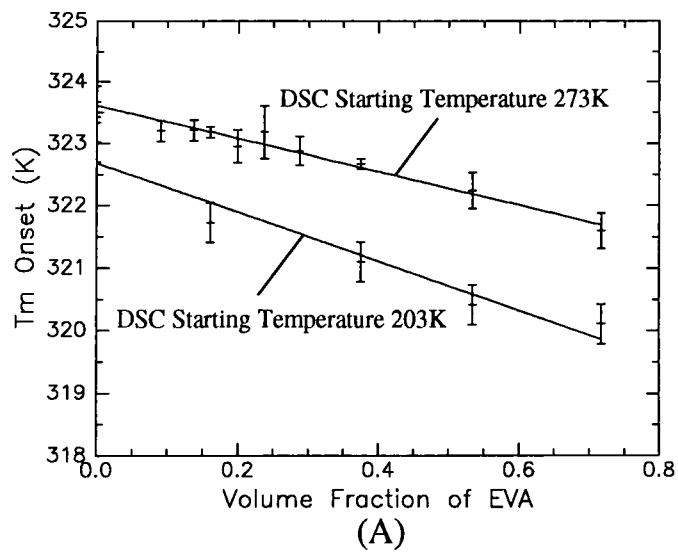


Figure 4.20 : Morphological Contributions to Melting Point Depression in EVA blends with : PI (A); FVA (B); PE (C).

Polymer Blend (w/w)	EVA Volume Fraction	Melting Point (Onset) (K)
PE 100%	0	323.40 ± 0.214
PE 83%:EVA 17%	0.181	322.19 ± 0.214
PE 67%:EVA 33%	0.347	321.23 ± 0.214
PE 41%:EVA 59%	0.608	312.75 ± 0.214
PE 25%:EVA 75%	0.764	307.55 ± 0.214

Table 4.7 : DSC measurements on EVA:PE blends (Starting Temperature 193K)

4.6.2 Effect of melt quenching on melting point and heat of fusion values

In all experiments, quenching blends from the melt has negligible effect on the melting point or heat of fusion of the crystalline component. The reproducible heat of fusion indicates the very fast recrystallisation characteristic of the FVA, PI and PE polymers.

4.7 Discussion

In EVA blends with the various semi-crystalline polymers, the melting point depression values, across the composition range vary from 2K (EVA:PI) to 17K (EVA:DPE). These melting point depression values represent the various degrees of miscibility between the amorphous phases of EVA and the semi-crystalline polymers.

From the full and abbreviated Nish-Wang expressions (eqns. 4.11, 4.12), blend interaction parameters (χ) have been determined from these melting point depression values, representing both the purely enthalpic (χ_H) and the free energy ($\chi_H + \chi_S$) interactions. The free energy value represents the "true miscibility" of the blends whereas the enthalpic value (as in "heat of mixing" values) gives the enthalpic contribution to this free energy value.

Clearly EVA blends with the poly(ethylene glycol) esters (PE, NECPE, NECME and DPE) are very miscible in the observed melting range, as shown by very large, negative ($\chi_H + \chi_S$) values, determined from the depression in melting point of the high melting endotherms (Peak 2). However, in contrast, the melting point of the lower melting endotherms (Peak 1) are unaffected by increasing EVA compositions, suggesting that their separate amorphous phases are immiscible. As Peaks 1 and 2 have been assigned as separate poly(ethylene glycol) and docosyl crystallisation phases respectively¹⁹ (see Chapter 8), the results may indicate that in the amorphous region of the polymers, EVA is miscible with the docosyl phase but is immiscible with the poly(ethylene glycol) phase. The immiscibility between EVA of this composition (12.5 mol % vinyl acetate) and poly(ethylene glycol) has also been reported elsewhere^{2,20}.

Impurities in the industrial PE sample appear to result in a slightly larger, negative ($\chi_H + \chi_S$) value and a greater melting point depression than the pure diester sample (NECPE), on blending with EVA. As the main impurity in PE is unesterified docosanoic acid, these differences maybe due to melting point effects from EVA interactions with the crystalline acid. The determined interaction parameters for EVA blends with the pure diester (NECPE) and monoester (NECME) were very similar which indicates that differences in the esterification type (mono or di) have no apparent effect on the large

ester interaction i.e. miscibility, on blending with EVA. Similarly, the determined interaction parameters of the deuterated diester (DPE) and hydrogenous diester (NECPE) samples closely agree which strongly suggests that deuteration does not significantly alter the "thermodynamics of mixing" in these polymer blends. Therefore, small angle neutron scattering studies on EVA:DPE blends (Chapter 9) can be related with reasonable confidence to the characterisation of the hydrogenous blend.

The determined $(\chi_H + \chi_S)$ values for the EVA:PI, EVA:LMPI and EVA:FVA blends (Table 4.3) are negative but close to the χ_{CRIT} value indicating possible, "borderline miscibility". From this series of blends, the EVA:LMPI has the largest melting point depression ($\approx 6\text{K}$) and negative $(\chi_H + \chi_S)$ value. Consequently, this blend would be expected to have greater miscibility than the EVA:PI or EVA:FVA blends. EVA blends with the poly(n-alkyl norbornenes) (9210, 9233), both appear to have little interaction i.e. no significant melting point depression which suggests that these blends are immiscible (cf. Optical Microscopy - Chapter 5).

Generally, the plots of X versus $\phi_1^2/T_{\text{mb}}^\circ$ used in the shortened Nishi-Wang expression, tended to have slight positive intercepts which were larger (in relation to the total melting point depression) for EVA blends containing the highly branched polymers, PI, LMPI and FVA. These positive intercepts have been observed in many other polymer blend systems^{4,6,12} and have been loosely assigned to possible entropic contributions.

The enthalpic interaction parameter (χ_H) is highly positive for all the blends and indicates that enthalpically, the blends are immiscible. The blends would therefore be predicted to have endothermic "heat of mixing" values which also result in positive χ_H values. The prediction of endothermic "heat of mixing" values for EVA blends with PI, LMPI, FVA and NECPE has been shown to be correct by subsequent "heat of mixing" measurements. Therefore, it would appear that miscibility in these blends can only be achieved by a large and favourable entropic contribution in order to counteract and dominate these unfavourable enthalpic interactions, to result in a negative $(\chi_H + \chi_S)$ value. In contrast, applying the full and condensed Nishi-Wang expressions to the original

Nishi-Wang PVF₂:PMMA melting point data, results in ($\chi_H + \chi_S$) and χ_H values which are both negative (see Figure 4.21) indicating an **exothermic** "heat of mixing" which has previously been predicted for this blend system due to a polar interaction between the PVF₂ and the PMMA¹². The negative intercept of the enthalpic Y values for this data may indicate an overestimation of the entropic contribution due to the relatively high polydispersity values of both polymers.

It should be remembered that in the full Nishi-Wang expression, the calculation of the configurational entropy is based on the molecular length of a linear polymer. However, PI, LMPI and FVA are highly branched polymers and entropic contributions from, in effect, "low molecular weight side arms" are not accounted for. EVA also has a degree of branching from pendant acetate groups and possible ethylene fragments such as propyl, butyl branches. It is believed that unique, favourable entropic contributions are associated with the branched nature of polymers during blending due to free volume i.e. "holes" in the blend which reduce packing density. These additional entropic contributions may account for the relatively large positive intercepts noted in the X versus ϕ_1^2/T_{mb}° plots for blends containing these branched polymers. Recent work on linear and branched polyethylene blends has outlined these entropic "free volume" contributions^{5,21}. However, several authors have hypothesised that χ increases (becomes more positive) with branching until at a critical level of branching, immiscibility occurs despite the favourable "branching entropy" contribution²². The inability to account for these "branched entropy contributions" fully, may significantly influence the accuracy of the determined χ_H values for these blend systems. The resulting χ_H values should therefore be regarded, at best, as merely an "indication" of the enthalpic contribution rather than absolute values.

From the Nishi-Wang expression, the favourable entropic contribution to the free energy of mixing increases as molecular weight and therefore, degrees of polymerisation (m) values, decrease. Thus, it would appear that the miscibility of the EVA blends with the poly(ethylene glycol) esters is due to large favourable entropic contributions from the low molecular weight of both the polymers (especially the esters). In the EVA

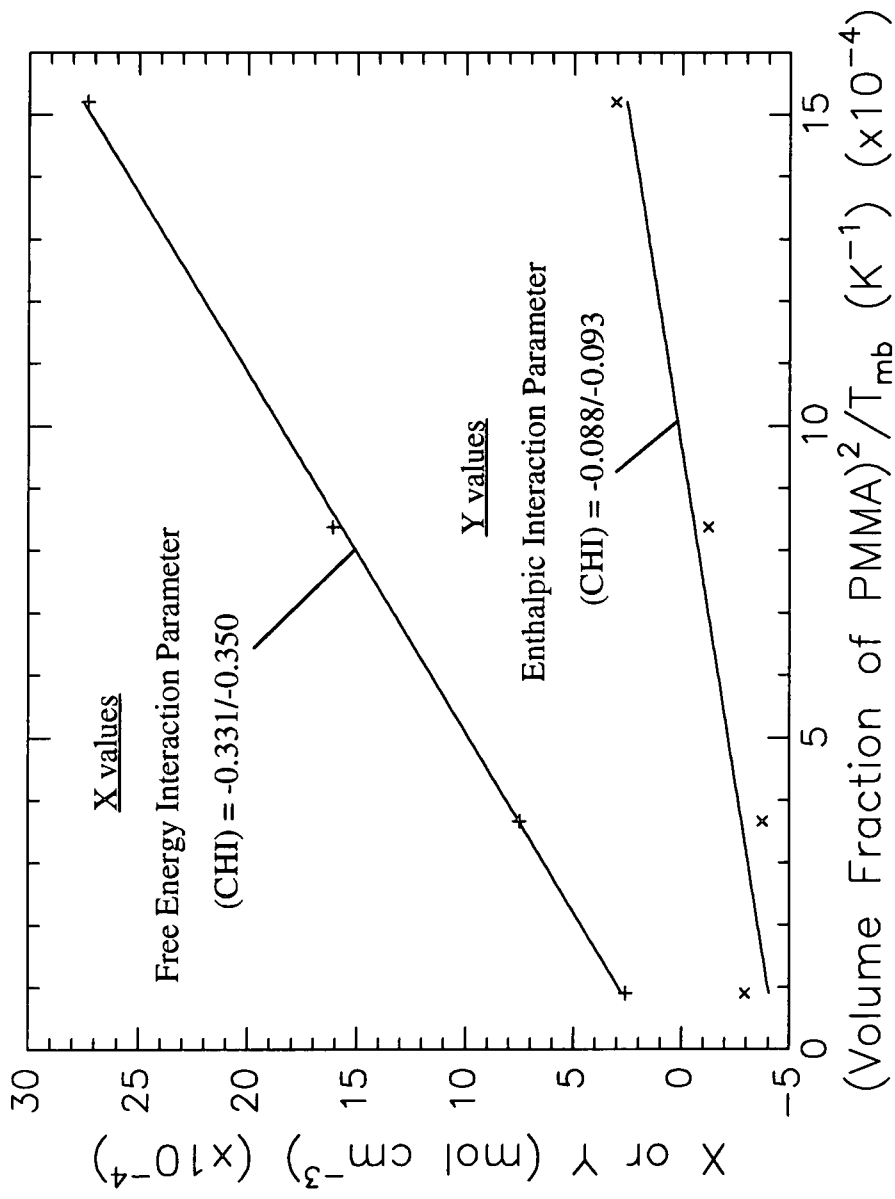


Figure 4.21 : Determination of Interaction Parameters (χ) for PVF₂:PMMA mixtures from original Nishi-Wang Melting Point data.

blends with PI, LMPI and FVA, the molecular weight of the semi-crystalline polymers are greater than the esters but sufficiently small that favourable entropic contributions result in a small melting point depression and possible "borderline miscibility". In contrast, hydrogenated poly(n-alkyl norbornenes) - 9210 and 9233, are of sufficiently high molecular weight and polydispersity that configurational entropy contributions are assumed to be very small when blended with EVA. This may account (in the absence of intermolecular interactions) for the negligible melting point depression values in the EVA:9210 and EVA:9233 blends which suggest blend immiscibility.

As degree of polymerisation (m) values are required in the determination of the configurational entropy contribution, the use of different molecular weight values i.e. number average (M_n) or weight average (M_w), to determine these m values is an important consideration and another possible source of error in determining the entropic contributions in these blend systems. In this study, m values were determined by the ratio of M_n (measured by Size Exclusion Chromatography) to the weight of the polymer repeat unit. This approach is justified when polydispersity (M_w/M_n) values are reasonably small i.e. 1-2. However, in the case of FVA, the M_n and M_w values are very different and the polydispersity is approximately 4 whereas the remaining semi-crystalline polymers have polydispersity values close to unity (EVA has a polydispersity of 2.3). Therefore, the use of M_n values in the EVA:FVA blend (with no allowance for the very high M_w value) may result in artificially high, favourable entropic contributions and consequently this may lead to a false estimation of miscibility.

The EVA:LMPI and EVA:PI blends differ only in the molecular weight of the poly(itaconate) polymer with LMPI (M_n 6601) and PI (M_n 9899). Therefore, the EVA:LMPI blend would be predicted to have a greater, favourable configurational entropic contribution to miscibility than the EVA:PI blend, by virtue of its lower molecular weight. This accounts for the greater melting point depression and the larger, negative ($\chi_H + \chi_S$) value in the EVA:LMPI blend compared to the EVA:PI blend. The slight reduction in the molecular weight of the poly(itaconate) component has resulted in a significant increase in the blend miscibility (see Optical Microscopy - Chapter 5).

Enthalpy of fusion values for the EVA:LMPI blend and the higher melting crystalline phase (Peak 2) in the EVA:poly(ethylene glycol) ester blends are greater than predicted based on the simple dilution of the crystalline component by the presence of the EVA amorphous phase. It therefore appears possible that cocrystallisation is occurring in these blends between the ethylene sequences in EVA and the aliphatic docosyl ends (in the poly(ethylene glycol) esters) or octadecyl branches (in LMPI). However, in the EVA:FVA, EVA:PI blends and the lower melting crystalline phase (Peak 1) in the EVA:poly(ethylene glycol) ester blends, there is a small reduction in the enthalpy of fusion to that predicted by simple dilution, and crystallisation in these blends appears to be hindered by the EVA phase. Enthalpies of fusion for the EVA:9210 and EVA:9233 blends also suggest that crystallisation is being hindered, but due to the relatively large scatter in these results, this is not certain. The influence of a second polymer on the crystallisation of a semi-crystalline component in a polymer blend has been discussed by Starkweather²³, who reported that there was no general rule which predicts the effect of miscibility on crystallinity as the degree of crystallisation may increase or decrease depending on the blend system. For EVA blends with the polyitaconate samples, LMPI and PI, both types of crystallisation behaviour are noted, enhancing and frustrating the crystallisation process respectively. The EVA:LMPI blend has a larger interaction i.e. melting point depression than the EVA:PI blend and the greater miscibility. It therefore appears clear that in this case, an increase in miscibility is associated with a corresponding increase in crystallisation due possibly to miscibility in **both** amorphous and crystalline phases. This may be applicable to EVA blends with the poly(ethylene glycol) esters. In these blends, Peak 2 which has a large melting point depression value and is believed to be miscible with EVA, shows an increase in the degree of crystallisation on blending with EVA. In contrast, Peak 1 which has no observed melting point depression and is regarded as immiscible with EVA, shows a crystallisation decrease.

The melting points of the polymer blends in this study are experimental as opposed to equilibrium values. There is a high degree of confidence in these experimental values

due to repeated runs and samples analysed in duplicate and triplicate. As reviewed by Runt¹¹, the importance of accurately determined experimental melting points in which there are no morphological effects due to reorganisation is accepted. Since the crystallisation conditions are the same for the pure semi-crystalline components as for the blends we could assume that the melting point depression observed is the result of thermodynamic contributions rather than morphological effects. However, there is also some "evidence" to support the view that these blends, as in the PVF₂:PMMA blend originally studied by Nishi and Wang, do not suffer from the morphological changes which can effect the experimental melting point: The three main polymer blends in this study, EVA:FVA, EVA:PI and EVA:PE have melting point depressions and heats of fusion which are essentially unaffected by large changes in the starting temperature of the DSC analysis run (after cooling from the melt) and by quenching experiments. If the melting point depression was due in part to morphological effects, a large change in the initial run temperature would be expected to considerably alter these effects with a corresponding change in the melting point depression value and this is not apparent. The remaining EVA-based blends essentially consist of variants of the semi-crystalline FVA, PI and PE components and are expected to behave similarly. It should be noted that in the blends which have significant morphological changes¹⁷, the melting point and heat of fusion values were very dependent on the thermal treatment during analysis.

The polymers, especially PI and PE are low molecular weight and crystallinity is due essentially to the tetradecyl (C14), octadecyl (C18) side chain crystallisation in FVA, PI respectively and the docosyl (C22) end chain crystallisation in PE¹⁹. Therefore, as the crystalline phase is effectively very low molecular weight polyethylene, it is not surprising that these polymers are very fast to crystallise and quenching has little effect on the melting point or the heat of fusion.

Therefore, it is clear that the melting point and heat of fusion of these polymers are "robust" to potentially large morphological changes from different initial starting temperatures and quenching. Thus, as in the PVF₂:PMMA system, originally studied by Nishi-Wang, the melting point depression in these blends appears to be primarily due to

thermodynamic interactions rather than morphological effects. The melting points obtained during this study were therefore regarded as accurate experimental values and it is believed that the theoretical interpretation in distinguishing between entropic and enthalpic contributions to miscibility is correct. Crystallisation studies have not been used to determine the equilibrium melting point of the blends due to the impractical length of time required and the possible errors previously stated.

4.8 References

1. S.Shen and J.M.Torkelson, *Macromolecules*, 25, 721 (1992).
2. S.Cimmino, E.Martuscelli, M.Saviano and C.Silvestre, *Polymer*, 32, 1461 (1991).
3. J.E.Harris, S.H.Goh, D.R.Paul and J.W.Barlow, *J. Polym. Sci.*, 27, 839 (1982).
4. S.A.Liberman and A.S.Gomes, *J. Polym. Sci. Polym. Chem.*, 22, 2809 (1984).
5. J.Martinez-Salazar and M.Sanchez-Cuesta, *Polymer*, 32, 2984 (1991).
6. J.J.Ziska, J.W.Barlow and D.R.Paul, *Polymer*, 22, 918 (1981).
7. P.J.Flory, *J. Chem. Phys.*, 12, 425 (1944).
8. T.Nishi and T.T.Wang, *Macromolecules*, 8, 909 (1975).
9. R.L.Scott, *J. Chem. Phys.*, 17, 279 (1949).
10. P.J.Flory, "Principles of Polymer Chemistry", Cornell University Press, Ithaca, N.Y., (1953).
11. J.Runt and K.P.Gallagher, *Polymer Communications*, 32, 180 (1991).
12. R.L.Imken, D.R.Paul and J.W.Barlow, *Polym. Eng. Sci.*, 16, 593 (1976).
13. T.K.Kwei and H.L.Frisch, *Am. Chem. Soc.*, 11, 1267 (1978).
14. Won Ho Jo and Ick Hwan Kwon, *Macromolecules*, 24, 3368 (1991).
15. P.J.Flory and H.Hocker, *Trans. Faraday Soc.*, 67, 2258 (1971).
16. J.Hoffmann and J.Weeks, *J. Res. Nat. Bur. Stds.*, 66A, 17 (1962).
17. W.Wenig, F.E.Karasz and W.J.Macknight, *J. Appl. Phys.*, 46, 4194 (1975).
18. M.Bohdanecky, L.Simek and S.Petrik, *Polymer Communications*, 31, 137 (1990).
19. R.D.Tack, Internal EXXON Communication.
20. C.D.Han, H.S.Chung and J.K.Kim, *Polymer*, 33, 546 (1992).
21. J.Plans, M.Sanchez-Cuesta and J.Martinez-Salazar, *Polymer*, 32, 2989 (1991).
22. G.ten Brinken, F.E.Karasz and W.S.Macknight, *Macromolecules*, 16, 1827 (1983).
23. K.Solc, Ed., "Polymer Compatibility and Incompatibility - Principles and Practices", Harwood Academic, New York (1982).

CHAPTER 5
PHASE CONTRAST OPTICAL MICROSCOPY

5.1 Introduction

Optical microscopy is an important characterisation technique in studying the microstructure of polymer blend systems. However, as many polymers have similar refractive indices, the optical contrast between the distinct polymer phases can be very low which generally results in poor imaging of a polymer blend system. Using special condenser and objective lenses, phase contrast optical microscopy is a facility which enhances this contrast by first splitting the transmitted beam into light which is undeviated after passing through the sample from light deflected due to sample interactions e.g. diffraction. These different light paths are then recombined in an interferometer which shears the beams vertically against each other and from this interference, greater image contrast is achieved. However, it should be noted that optical microscopy suffers from relatively poor resolution which is determined by the wavelength of light (typically 200-600 nm) and therefore a micrograph of a polymer blend can be deceptive if a two-phase immiscible blend system has domains smaller than this wavelength.

This optical study into the miscibility of several EVA-based polymer blends essentially consists of two parts :

- a) Initial miscibility studies which are representative of these blends in the melt state i.e. in excess of the melt temperature of the crystalline polymer phase. The observed phase behaviour can then be related to the χ values determined from melting point depression analysis (Chapter 4).

- b) The dependence of temperature on the miscibility of these blends at various compositions which enables a phase diagram for each blend to be constructed.

5.2 Apparatus and Sample Preparation

The study was carried out using an OLYMPUS BH2 microscope fitted with a phase contrast condenser and a CK10/CK20 objective. The temperature of the sample was varied by a LINKAM THM 600 hot stage via a LINKAM TMS 91 controller. The image from the microscope was monitored by a JVC KYF-30 video camera and relayed as a SVHS signal via a LINKAM VTO 232 text overlayer, to a SONY UP-5000P mavigraph printer.

Blends of amorphous (EVA) with various semi-crystalline polymers (FVA, PE, PI, LMPI, 9210 and 9233) were prepared as described in Chapter 3 and stored in a sealed dessicator prior to use. A small amount of each sample (including pure polymer components) was compressed at ambient temperature between two glass cover slips. Liquid nitrogen, controlled by a LINKAM CS 196 cooling system was used to cool (or quench) the samples at a specified rate.

5.3 Initial Miscibility Studies

During these initial miscibility experiments, various compositions of EVA blends with the semi-crystalline polymers were melted at temperatures of between 343K-393K i.e. relatively close to the melting point of the crystalline phase. In all cases, the blends at these temperatures were transparent showing no image contrast, despite the phase contrast facility. The blends were therefore cooled from this melt temperature at a fixed rate of 10K/min to a temperature below the blend crystallisation temperature and the resulting well-defined blend morphology was assumed to be representative of the blend miscibility at the melt temperature.

As in differential scanning calorimetry, the heating and cooling rates in this study were 10K/min in order to compare the resulting blend morphologies with results from melting point depression analysis. Experiments involving rapid cooling (100K/min) of these samples from the melt showed no significant change in the blend morphologies to that obtained using the standard cooling rate of 10K/min.

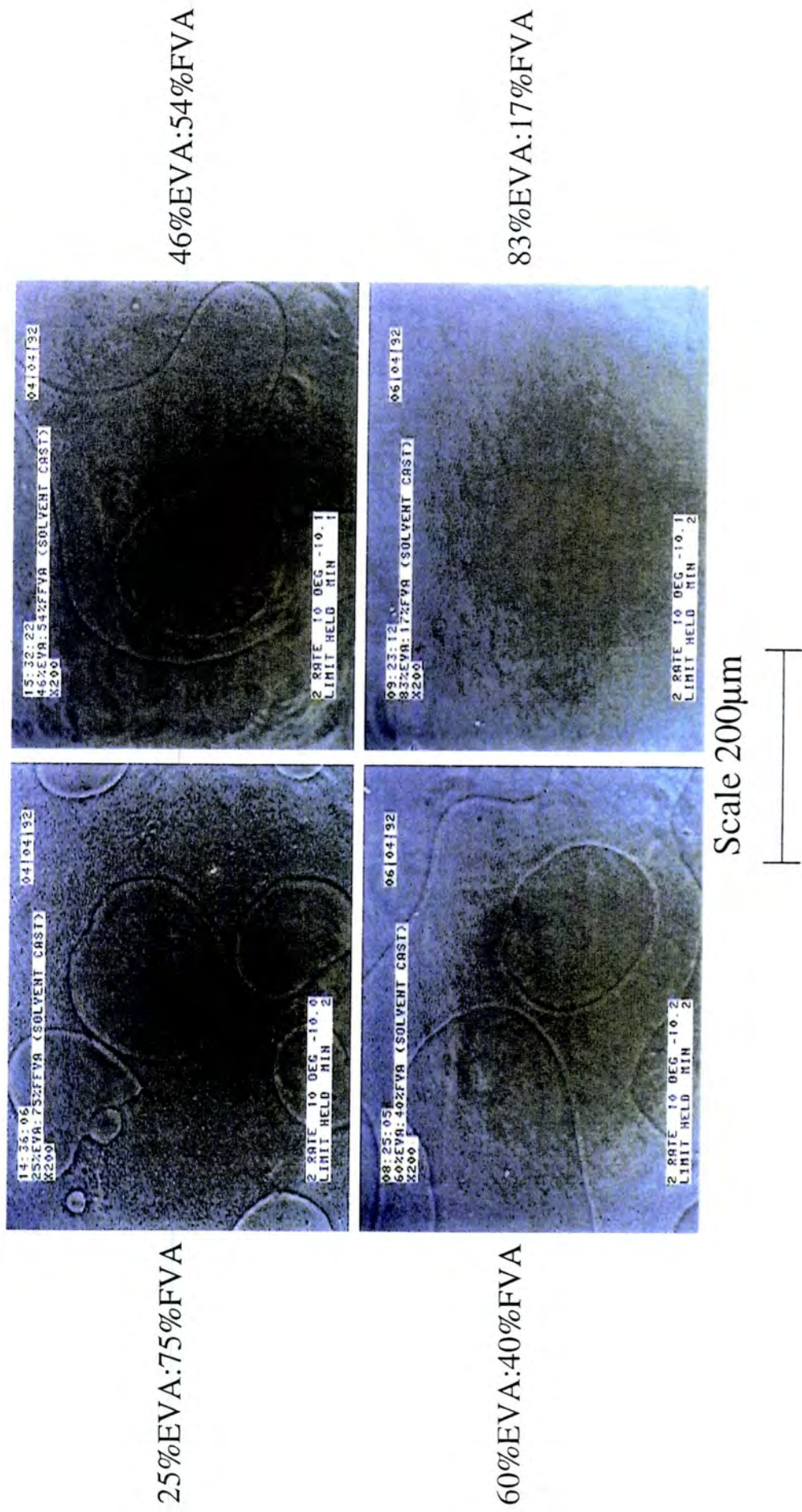


Figure 5.1 : EVA:FVA Blends (Cooled from 373K Melt Temperature)

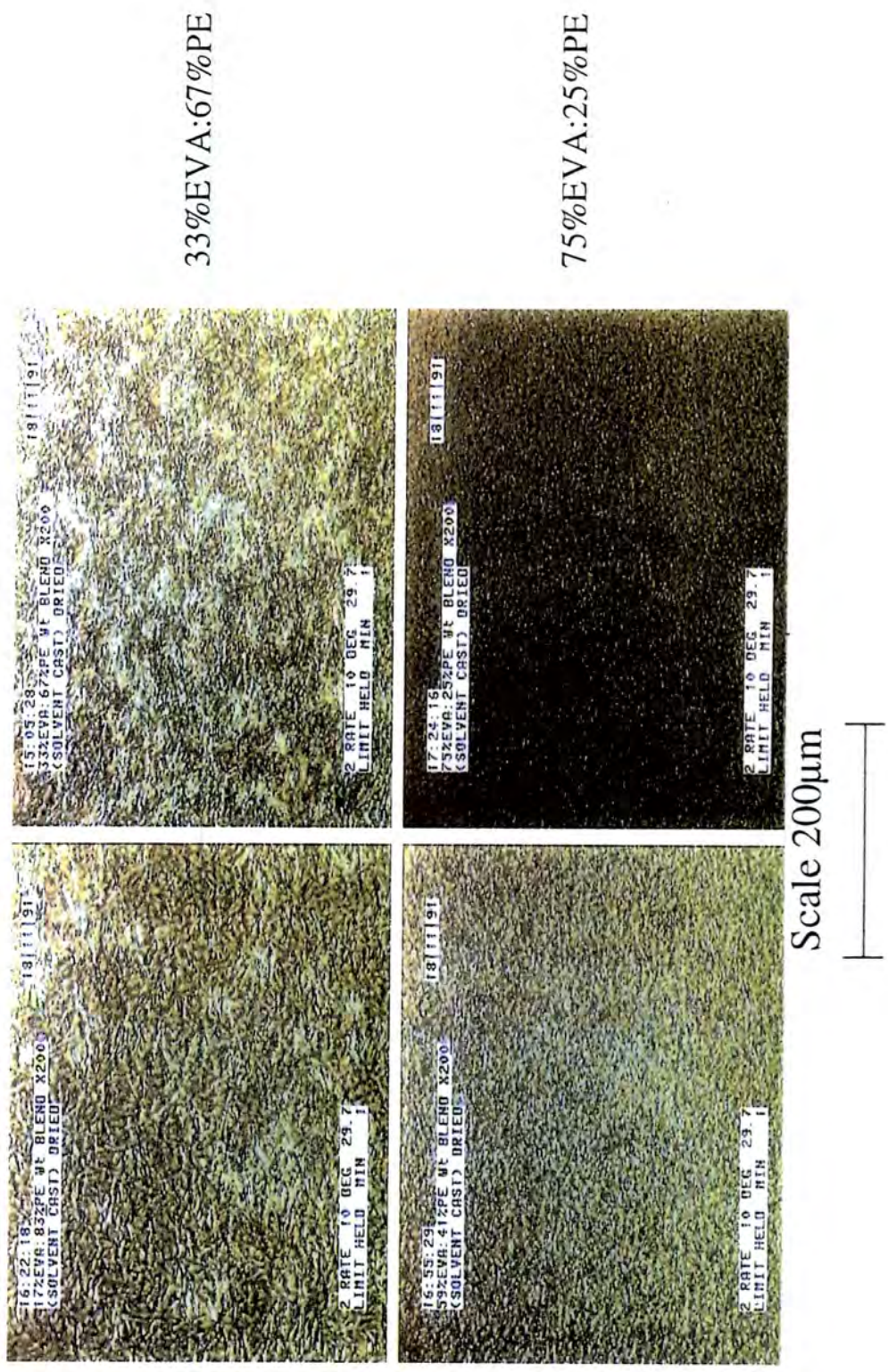
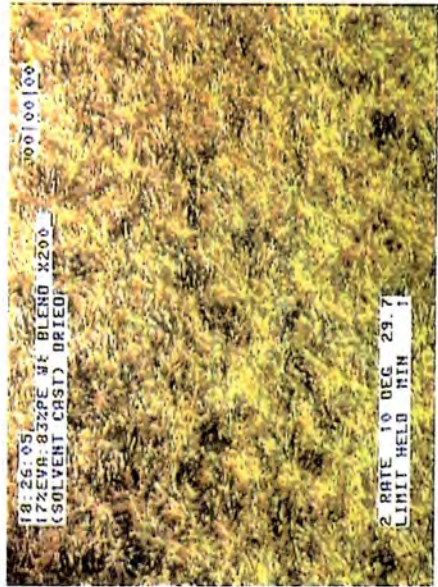


Figure 5.2 : EVA:PE Blends (Cooled from 353K Melt Temperature)



17%EVA:83%PE



33%EVA:67%PE



59%EVA:41%PE



75%EVA:25%PE

Scale 200μm




Figure 5.3 : EVA:PE Blends (Cooled from 393K Melt Temperature)

5.3.1 EVA:FVA Blends (Figure 5.1)

Temperature Profile: 303K → 373K (Rate 10K/min) Initial melting
373K → 263K (Rate 10K/min) Morphology noted
263K → 373K (Rate 10K/min) Reheat
373K → 263K (Rate 10K/min) Morphology noted

Four EVA:FVA blend compositions were studied containing a wt.% EVA fraction of 25, 46, 60 and 83. Each blend was cooled from the melt temperature (373K) to 263K in order to crystallise the FVA component. During the sample reheat, the effect of the amorphous EVA component on the melting point of FVA could not be determined as the blends showed no indication of molten flow or physical change during melting apart from a slow change in the image contrast.

The EVA:FVA blends show large scale phase separation when cooled from the 373K melt to 263K and are clearly immiscible apart from the 83%EVA:17%FVA blend which has a fine homogenous appearance after cooling and appears to be miscible. This "miscibility window" at high EVA concentrations will be studied further (see section 5.4.2e) to establish a possible phase boundary.

On further heating and cooling all blend morphologies were retained and therefore appear stable.

5.3.2 EVA:PE Blends (Figures 5.2, 5.3)

Temperature Profile: 303K → Melt (Rate 10K/min) Initial heating
Melt → 303K (Rate 10K/min) Morphology noted
303K → Melt (Rate 10K/min) Reheat
Melt → 303K (Rate 10K/min) Morphology noted

PE and EVA:PE blends were evaluated at two separate melt temperatures of 353K and 393K. The EVA:PE blend compositions contained a wt.% EVA fraction of 17, 33, 59 and 75. During initial heating from 303K, the pure crystalline PE appears to melt in two phases of similar melting point i.e. at 328K rapid melting occurs leaving large crystalline areas which finally melt at \approx 343K. On cooling to 303K, a fine textured morphology is formed which on reheating, melts in one phase at 329K. The initial morphology obtained after cooling from the melt temperature is stable to further heating and cooling stages.

In the EVA:PE blends, increasing EVA concentrations reduce the onset of melting of the PE crystalline phase by up to \approx 12K. At high PE concentrations (83%, 67%) the morphologies on cooling from the melt are essentially identical to that of the pure PE, with no apparent phase separation. As the PE concentration is reduced (41%, 25%) the morphology appears to be changing towards the mottled-type structure of pure EVA and again no phase separation is noted. On reheating all blends melted in one phase. The blend morphologies, like PE are stable to a further heating and cooling step.

An interesting effect shown in the EVA:PE blends is that during the initial heat-up, the blends (as in PE) appear to melt in two phases of very similar melting point. However, in the EVA:PE blends the size of this second melting phase is reduced dramatically compared to PE alone, even at low EVA "dilution".

The melt temperatures of 353K and 393K show little difference in their effect on the blend morphologies after cooling to 303K.

5.3.3 EVA:PI Blends (Figures 5.4, 5.5)

<u>Temperature Profile:</u>	303K \rightarrow Melt (Rate 10K/min)	Initial heating
	Melt \rightarrow 303K (Rate 10K/min)	Morphology noted
	303K \rightarrow Melt (Rate 10K/min)	Reheat
	Melt \rightarrow 303K (Rate 10K/min)	Morphology noted

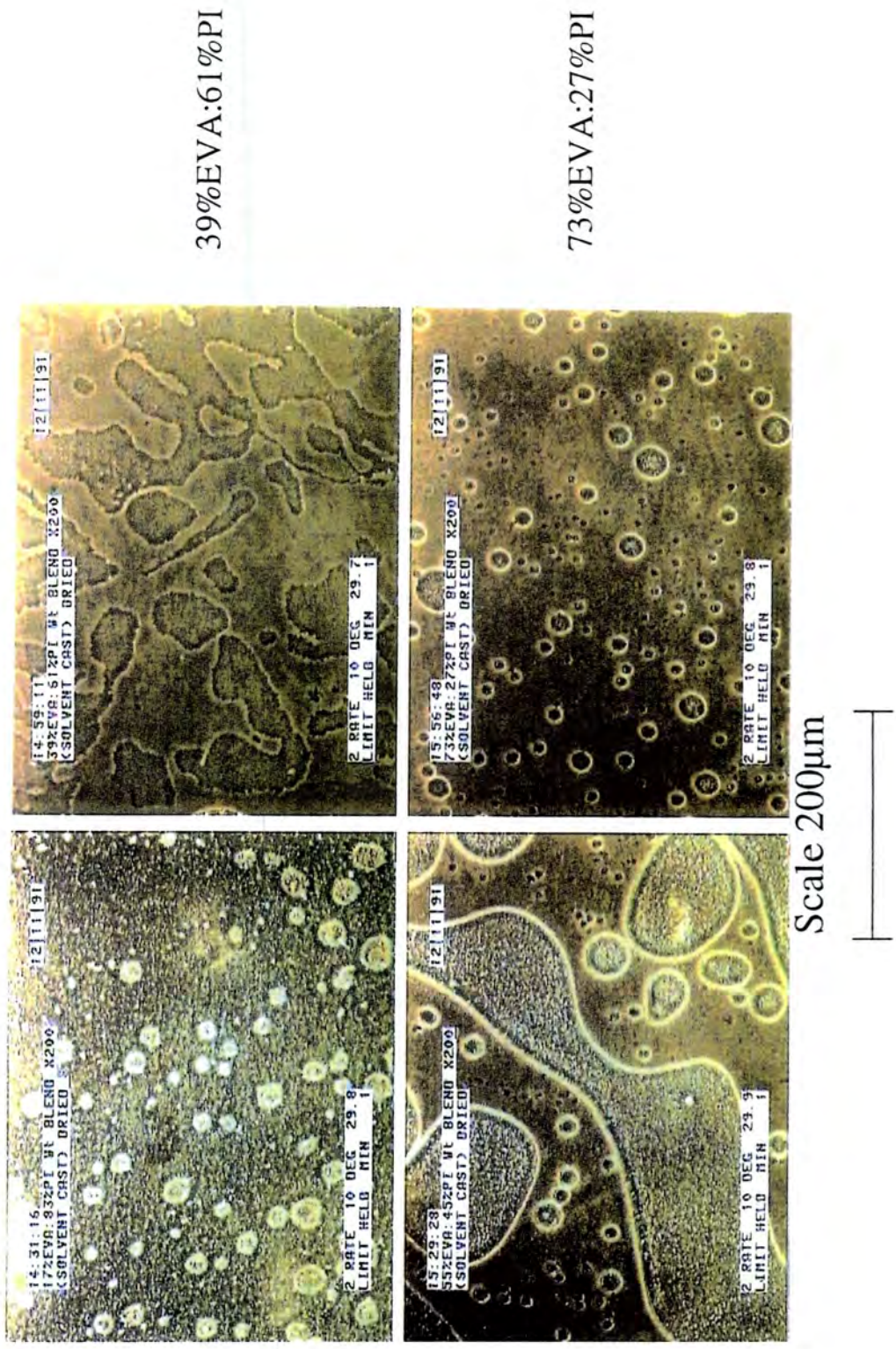


Figure 5.4 : EVA:PI Blends (Cooled from 343K Melt Temperature)



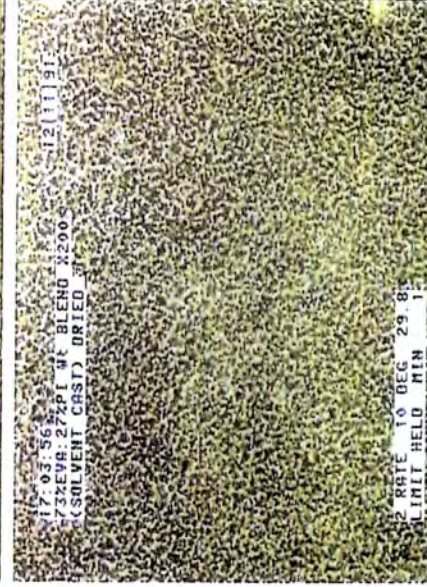
17%EVA:83%PI



39%EVA:61%PI



55%EVA:45%PI



73%EVA:27%PI

Scale 200 μ m



Figure 5.5 : EVA:PI Blends (Cooled from 393K Melt Temperature)

EVA:PI blends were evaluated at melt temperatures of 343K and 393K. The EVA:PI blend compositions contained a wt.% EVA fraction of 17, 39, 55 and 73. During the initial heating of the pure PI component, melting begins to occur at 324K and on cooling from the melt temperature to 303K, a fine homogenous morphology is formed which is stable to further heating and cooling stages. In the EVA:PI blends, increasing EVA concentrations depress the onset of melting of the PI crystalline phase by up to 3K. Blends cooled from 343K all show clear phase separation which ranges from droplet dispersions in blends containing high EVA or PI concentrations (17%EVA:83%PI, 73%EVA:27%PI) to large separate phases in compositions which are more closely matched (39%EVA:61%PI, 55%EVA:45%PI).

Increasing the melt temperature to 393K appears to increase the observed blend miscibility after cooling to 303K. The droplet dispersions become smaller and more dispersed (the 73%EVA:27%PI blend has essentially an homogeneous appearance!). Although large phases can still be clearly seen in the 39%EVA:61%PI and 55%EVA:45%PI blends, "phase inversion" is apparent at this higher melt temperature (small EVA phases dispersed in the PI phase and vice versa) which indicates a degree of miscibility between the components.

Again, as in the pure PI, all blend morphologies are stable to further heating and cooling stages.

5.3.4 EVA:LMPI Blends (Figure 5.6)

Temperature Profile: 303K → 343K (Rate 10K/min) Initial heating (Hold 1 min)
343K → 303K (Rate 10K/min) Morphology noted

The EVA:LMPI blend compositions contained a wt.% EVA fraction of 30, 55, 70 and 88. LMPI and PI are both polyitaconate samples with LMPI having a lower molecular weight (see Chapter 3 - experimental). At these compositions, the blend forms a fine homogenous morphology on cooling from a melt temperature of 343K to

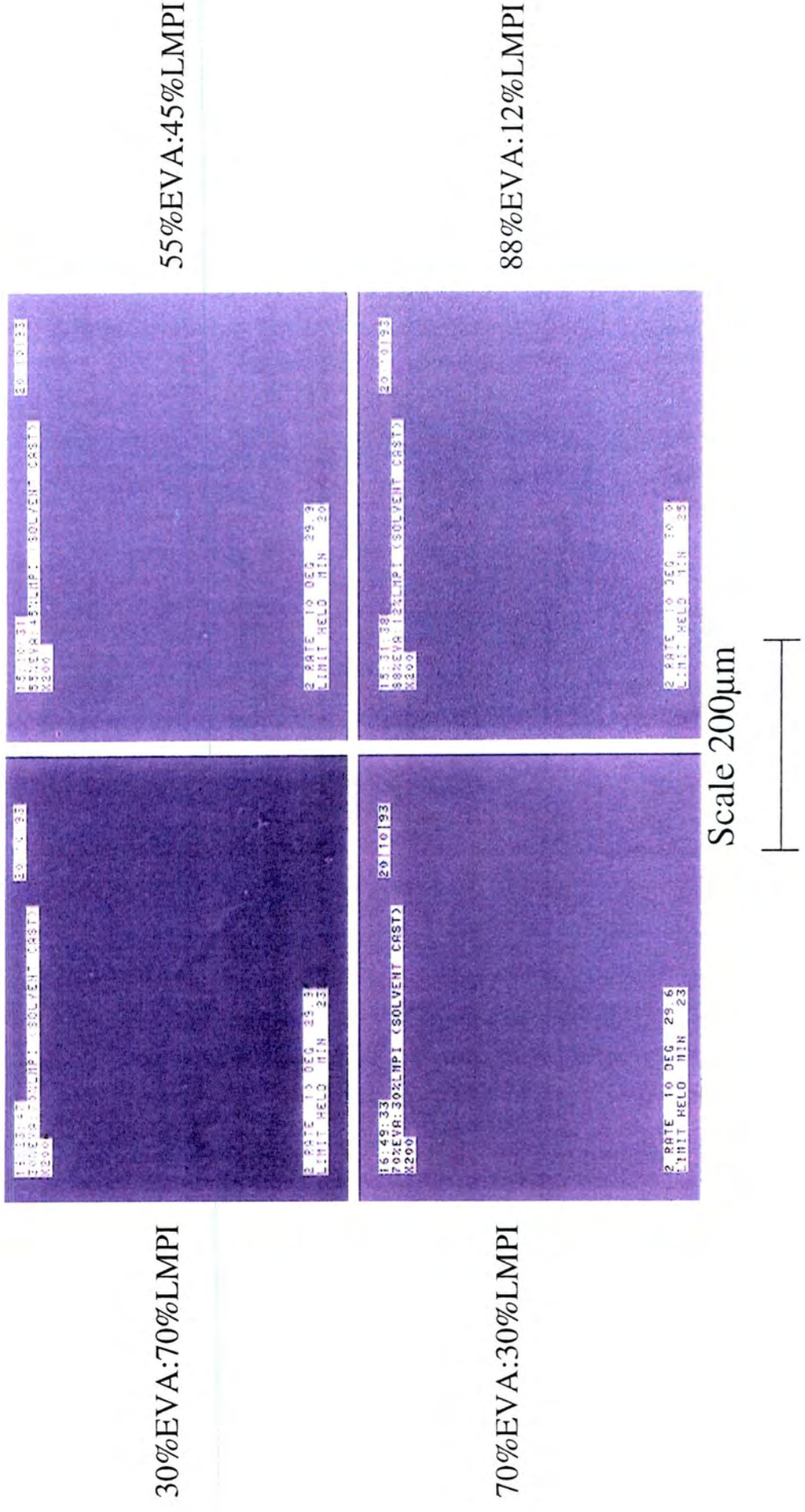


Figure 5.6 : EVA:LMPI Blends (Cooled from 343K Melt Temperature)

303K, in contrast to the phase separation noted under identical heating conditions in the EVA:PI blends.

5.3.5 EVA:9210 Blends (Figure 5.7)

Temperature Profile: 298K → 313K (Rate 10K/min) Initial heating (Hold 2 min)

313K → 253K (Rate 10K/min) Morphology noted (Hold 2 min)

253K → 313K (Rate 10K/min) Reheat (Hold 2 min)

313K → 253K (Rate 10K/min) Morphology noted

The EVA:9210 blend compositions contained wt.% EVA fractions of 10, 30, 50, 70 and 90. After initial melting at 313K, each blend was cooled to 253K in order to crystallise the 9210 component. On cooling, all blends show phase separation in the form of droplet dispersions or larger "island pools" of polymer. These morphologies are stable to further heating and cooling stages. Figure 5.7 shows blend morphologies for wt.% EVA fractions of 30, 50, 70 and 90. The composition of EVA appears to have no observable effect on the melting point of the 9210 component.

5.3.6 EVA:9233 Blends (Figure 5.8)

Temperature Profile: 298K → 253K (Rate 10K/min) Morphology noted (Hold 2 min)

253K → 313K (Rate 10K/min) Initial heating (Hold 2 min)

313K → 253K (Rate 10K/min) Morphology noted

The EVA:9233 blend compositions contained wt.% EVA fractions of 10, 30, 50, 70 and 88. Each blend was cooled from a melt temperature of 313K to 253K in order to crystallise the 9233 component. The resulting blends showed various degrees of phase separation from elongated small droplet dispersions to large polymer phases, apart from the 10%EVA:90%9233 blend which appears to show a relatively homogenous-type

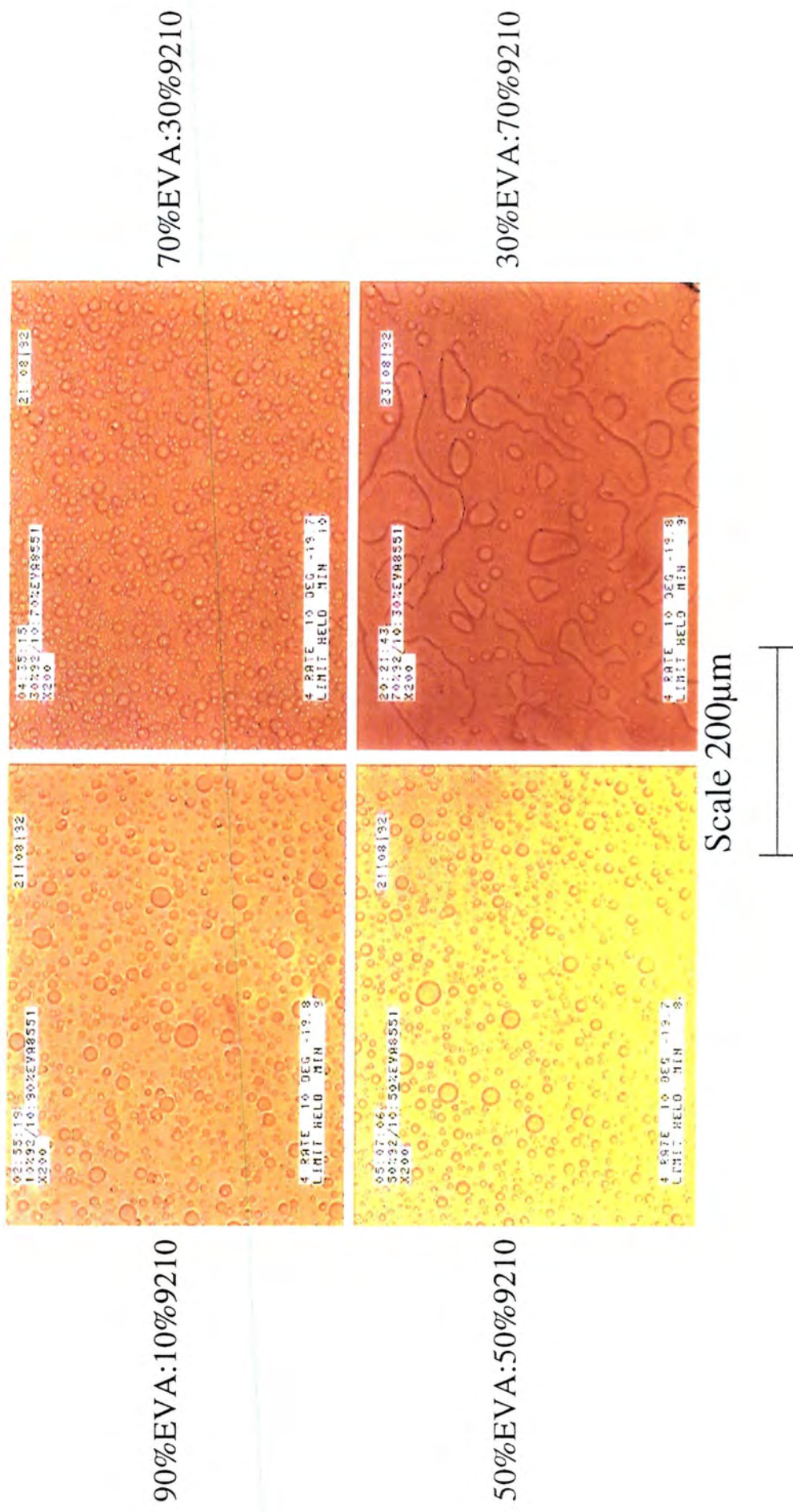


Figure 5.7 : EVA:9210 Blends (Cooled from 313K Melt Temperature)

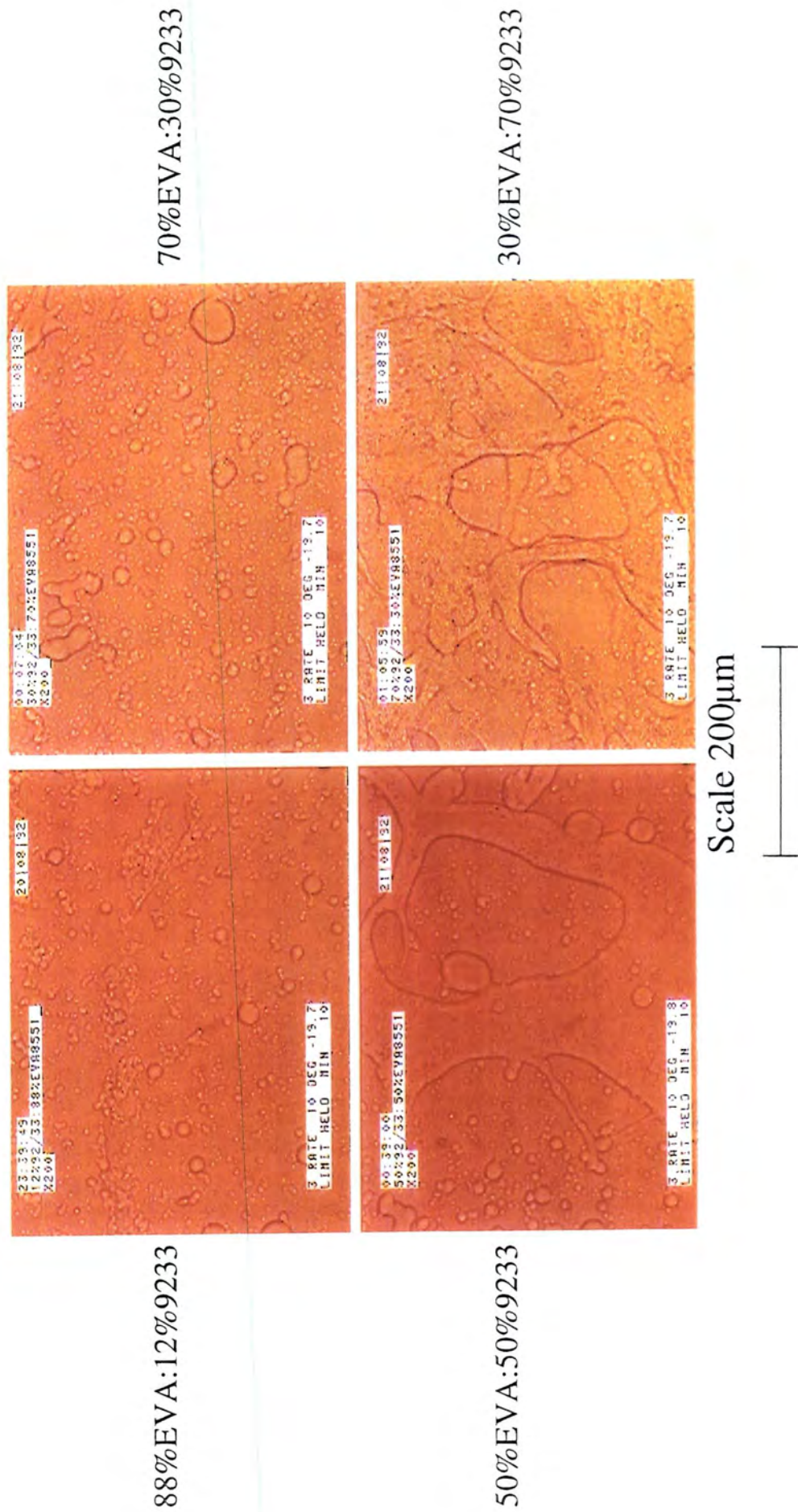


Figure 5.8 : EVA:9233 Blends (Cooled from 313K Melt Temperature)

morphology. Figure 5.8 shows blend morphologies for wt.% EVA fractions of 30, 50, 70 and 88. No melting point change was noted in the 9233 crystalline phase on blending with the EVA component.

5.4 Polymer Blend Phase Diagrams

5.4.1 Introduction

From optical microscopy observations, phase diagrams were initially to be proposed for the three major polymer blends in this study, EVA:FVA, EVA:PE and EVA:PI. The effect of heating and cooling rates on the phase diagram of the EVA:FVA blends was also to be investigated. As melt temperatures of up to 573K were to be used, possible thermal degradation effects were considered. From thermogravimetric analysis (TGA - Chapter 3), the EVA, FVA and PI polymers at 573K have very similar weight loss values i.e. 5.4, 5.0 and 5.2% respectively. However, the PE component has a much larger weight loss of 22.5% at 573K and significant thermal degradation is noted at lower temperatures. As the optical observations were to be obtained after blends were held at melt temperatures for up to 15 minutes, it is likely that the already large thermal stability difference (noted from TGA) between PE and the remaining polymers will be increased further during these studies. Consequently, construction of the EVA:PE phase diagram has not been possible.

The miscibility of the EVA:FVA and EVA:PI blends was followed by observing the blend morphology after cooling from the melt to 263K. The blends were then classified by the following : **I** (Immiscible) if the blend is phase separated, **M** (Miscible) if the blend appears homogeneous (although this may indicate that the phases are so finely dispersed that phase separation cannot be seen !) and **I/M** if phase separation is still present but instead of large polymer phases, the blend is a fine dispersion and/or showing "phase inversion" characteristics, both of which appear to indicate (as in the EVA:PI blend) an increase in miscibility.

Examples of the optical micrographs used to determine the EVA:FVA and EVA:PI phase diagrams are shown in Figures 5.9-5.12 (46%EVA:54%FVA and 83%EVA:17%FVA) and 5.15-5.16 (17%EVA:83%PI and 55%EVA:45%PI).

5.4.2 EVA:FVA Blends

To note the combined effects of temperature and large differences in the cooling and heating rates on the EVA:FVA phase diagram, the following profiles were used :

Temperature Profile 1: 298K → Melt (Rate 10K/min) Hold 2 mins
(slow heating/cooling rate) Melt → 263K (Rate 10K/min) Hold

Temperature Profile 2: 298K → Melt (Rate 100K/min) Hold 15 mins
(fast heating/cooling rate) Melt → 263K (Rate 100K/min) Hold

The melt temperatures chosen were 323, 373, 423, 473, 523, 548 and 573K. The 10K/min rate and the 2 minute temperature hold in profile 1 was carried out to relate possible morphology effects to DSC results which have the same profile. In profile 2, the extended temperature hold (15 mins) was to allow sufficient time for polymer diffusion to occur within the blend which may not be possible with a 2 min hold. The 100K/min rate was used to "quench" the blend from the melt temperature to 263K under temperature control. From this "quench" the resulting morphology at 263K is regarded as representative of the blend at the melt temperature due to the minimal residence time of the blend in other phase areas during cooling. Consequently, profile 2 i.e. the fast heating and cooling rate is regarded as the more accurate method of determining blend morphologies which are representative of the melt temperature. The technique of blend quenching has been used in differential scanning calorimetry to determine phase boundaries by associating blend miscibility with a single glass transition temperature (T_g)¹.

The following results refer to the morphologies obtained at **263K** i.e. after cooling from the various melt temperatures. Identification of the separate EVA and FVA phases

in these blends is possible as the EVA phase has a lighter coloration to that of FVA which is advantageous when both polymer concentrations are similar.

5.4.2a 15%EVA:85%FVA

For this blend, profile 1 was not carried out. Using profile 2, the blend at room temperature showed a cluster appearance rather than smooth polymer islands or droplets. On heating samples to 323, 373, 423 and 473K, then cooling to 263K the morphologies are essentially similar with elongated, smooth pools of EVA in an FVA matrix. However, when cooled from 523K the blend still contained large EVA areas but a dispersion of much smaller droplets was noted (phase inversion ?). This may indicate the initial stages of miscibility at this melt temperature and indeed increasing the melt temperature to 548K and 573K produces a fine, homogeneous morphology on cooling to 263K.

5.4.2b 25%EVA:75%FVA

At room temperature this blend also showed a cluster-type appearance. Using profile 1 and melt temperatures of 323, 373 and 423K, the blend showed large phase separation on cooling to 263K. Cooling from 473K and 523K melts, the blend contained many finely dispersed circular droplets together with larger pools of EVA. These small circular droplets can be assumed to be EVA which due to increased miscibility are finely dispersed in the FVA phase showing "phase inversion" on cooling. Interestingly, there appears to be no phase inversion of FVA into the EVA phases. From the 548K melt, the blend is a fine dispersion and finally, cooling from 573K produces a very fine, homogeneous morphology. Therefore, the miscibility in this blend appears to increase significantly from 473-573K.

These miscibility changes are also noted using profile 2 with the extended 15 minute hold at 523K producing a fine dispersion of polymer droplets (indicating the possible onset of miscibility) and an homogeneous phase when cooled from 548K and 573K melts.

5.4.2c 46%EVA:54%FVA (Figures 5.9, 5.10 - Temperature Profile 1)

At room temperature the blend consists of large phase separated areas which are due to the large concentration of each polymer. Using profile 1 (Figures 5.9 and 5.10) at melt temperatures of 323, 373 and 423K, the blend on cooling to 263K again shows large scale phase separation. From 473-548K melts, these large phase areas appear to breakdown into smaller droplets and the resulting dispersion can be assumed to be phase inversion of EVA droplets into the FVA matrix. The large EVA phases after cooling from melt temperatures of 473-523K, again contain no FVA phase. However from the 548K melt, phase inversion in both phases is noted i.e. large pools of EVA and FVA containing within them a fine dispersion of FVA and EVA phases respectively. Finally, after cooling from the 573K melt to 263K, the blend is homogenous. Thus, as in the 25%EVA:75%FVA blend, the miscibility appears to be increasing from 473-573K with the most notable being the 548-573K change from a clearly phase separated blend to an apparently homogeneous "miscible" system.

Profile 2 also shows similar observations i.e. cooling from a 523K melt results in a small droplet dispersion but from 548K and 573K melts, a fine homogeneous phase is formed.

5.4.2d 60%EVA:40%FVA

At room temperature this blend consisted of separate polymer phases of widely varying size from small droplets to large "islands". Using profile 1, after cooling from 323, 373 and 423K melt temperatures, the blend shows large scale phase separation similar to that noted in the 46%EVA:54%FVA blend. From 473-548K melts, miscibility appears to increase, with phase inversion of EVA droplets into the larger FVA phases clearly noted on cooling to 263K but again, no FVA phase is dispersed in the EVA matrix. This change in miscibility from 473K is also shown using profile 2 although cooling from the 523K melt produces phase inversion in **both** EVA and FVA phases with an homogenous blend formed from 548K and 573K melt temperatures.

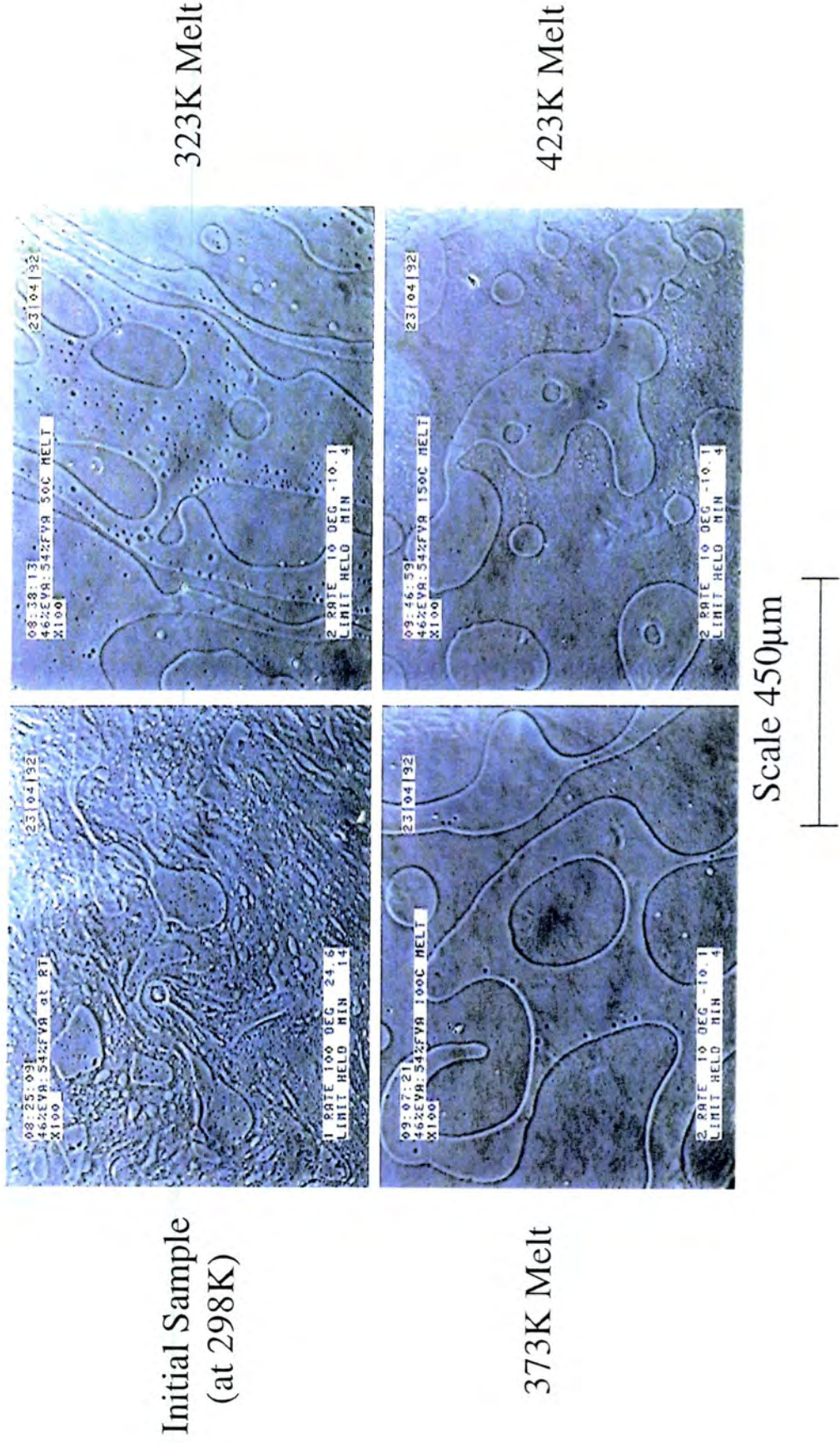
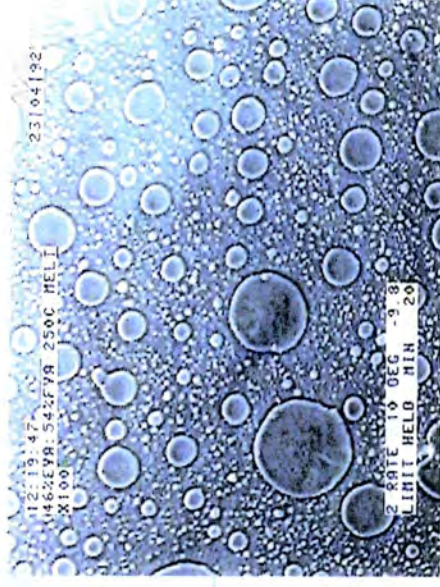


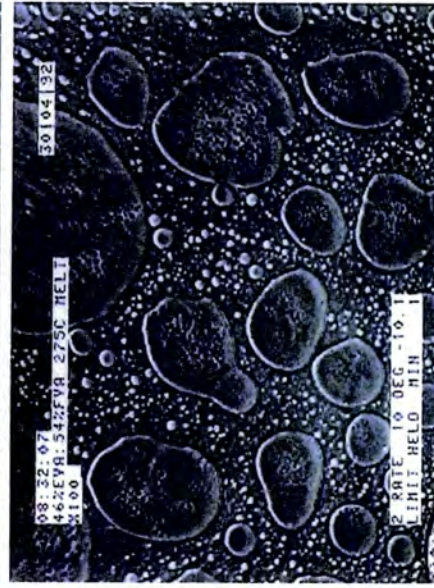
Figure 5.9 : 46%EVA:54%FVA Blend (Cooled from 323K, 373K and 423K Melt Temperatures - Profile 1)



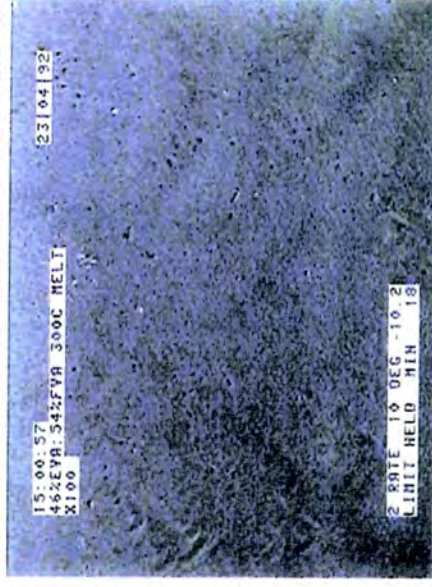
473K Melt



523K Melt



548K Melt



573K Melt

Scale 450 μ m



Figure 5.10 : 46%EVA:54%FVA Blend (Cooled from 473K, 523K, 548K and 573K Melt Temperatures - Profile 1)

5.4.2e 83%EVA:17%FVA (Figures 5.11 and 5.12 - Temperature Profile 1)

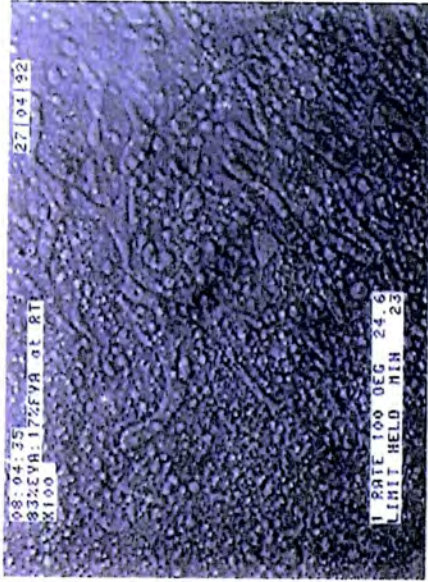
From the initial miscibility studies this blend appears to be miscible after cooling to 263K from a 373K melt temperature (section 5.3.1). At room temperature the FVA forms various domain sizes from small droplets to island pools. Using profile 1 (Figures 5.11 and 5.12), the 323K melt shows small circular droplets but melt temperatures of 373, 423 and 473K form one homogeneous phase on cooling to 263K. From the 523K and 548K melts, phase separation occurs with the 548K melt showing phase inversion in both phases. Cooling from the 573K melt, again produces an homogenous blend.

Using profile 2, the blend morphology after cooling from a 323K melt showed a finer dispersion to that noted from profile 1. This suggests that further miscibility is occurring at 323K due to the extended 15 minute temperature hold in profile 2. After cooling from 373, 423 and 473K melts, an homogenous blend is essentially formed but again at 523K, phase separation occurs. In profile 2, cooling from the 548K melt produces an homogeneous phase whereas using profile 1, a phase separated blend is formed. This may be explained in terms of the slower heating and cooling rates in profile 1 which result in a longer residence time within an immiscible phase region i.e. at 523K before and after reaching the 548K melt. Consequently, phase separation "artefacts" may possibly be noted using profile 1. Also, the extended 15 minute hold in profile 2 allows sufficient diffusion time for any such "spurious" phase separation to regain miscibility. Again, cooling from the 573K melt produces a single homogeneous phase.

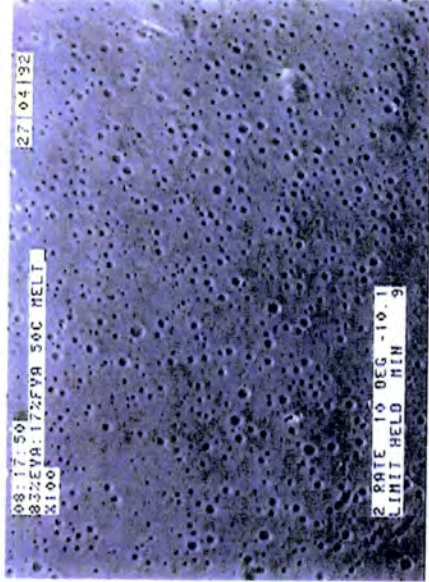
5.4.2f EVA:FVA Phase Diagrams

Using these blend morphologies which are studied after slow and rapid cooling from various melt temperatures (323K-573K) i.e. temperature profiles 1 and 2 respectively, phase diagrams for the EVA:FVA blend system have been proposed using the miscibility classification (**I**, **M**, **I/M**) outlined in the introduction section 5.4.1 (Figures 5.13 and 5.14).

Initial Sample
(at 298K)



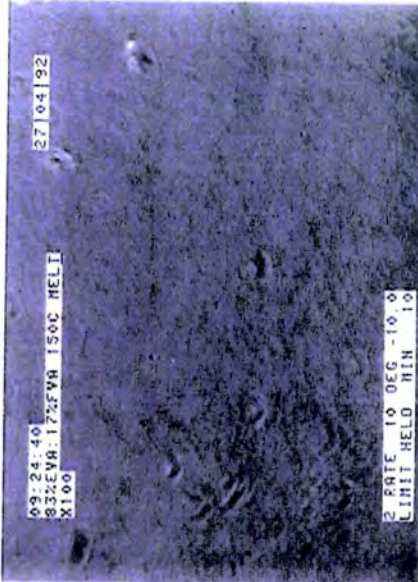
323K Melt



373K Melt



423K Melt

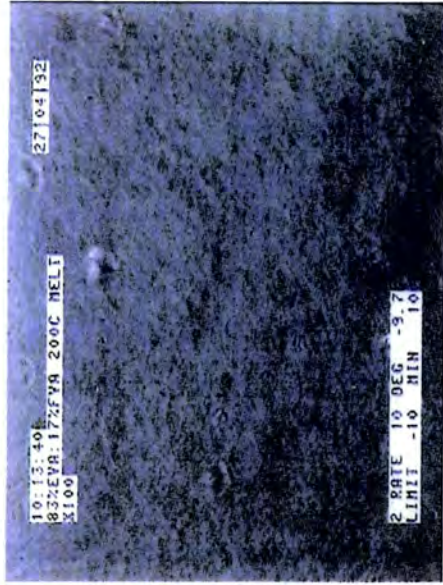


Scale 450μm

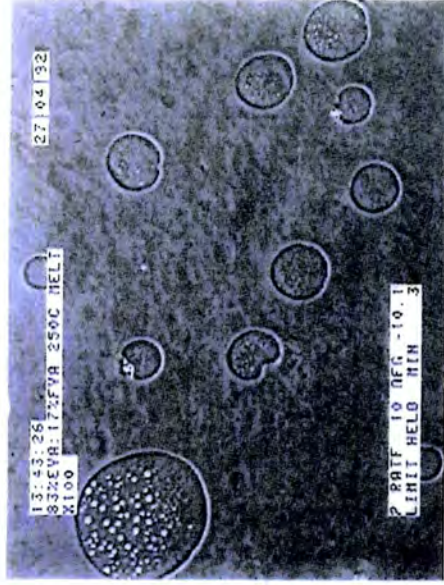


Figure 5.11 : 83%EVA:17%FVA Blend (Cooled from 323K, 373K and 423K Melt Temperatures - Profile 1)

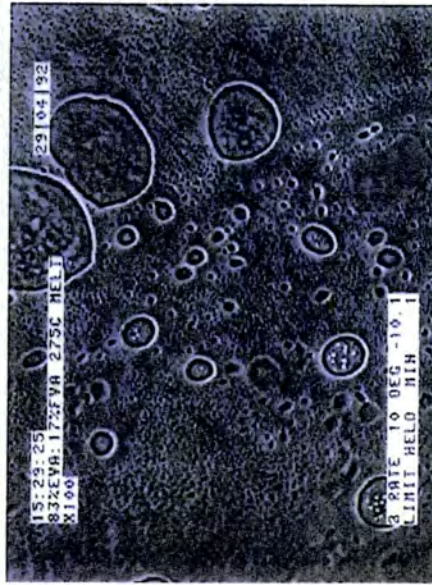
473K Melt



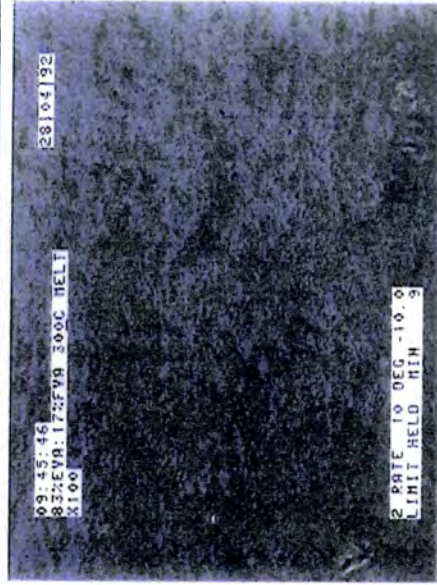
523K Melt



548K Melt



573K Melt



Scale 450µm



Figure 5.12 : 83%EVA:17%FVA Blend (Cooled from 473K, 523K, 548K and 573K Melt Temperatures - Profile 1)

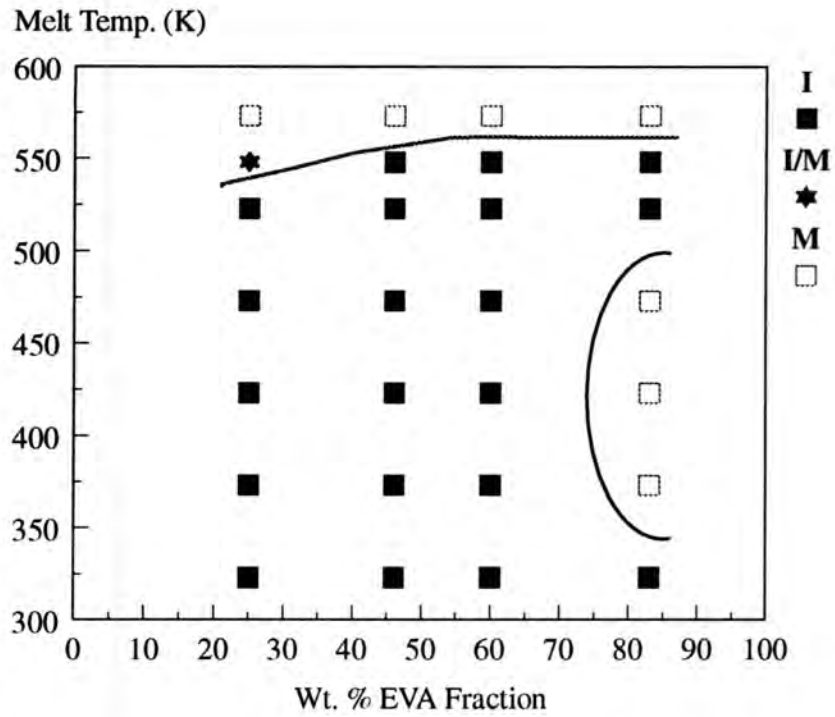


Figure 5.13 : Blend Morphologies in EVA:FVA Blends (Profile 1)

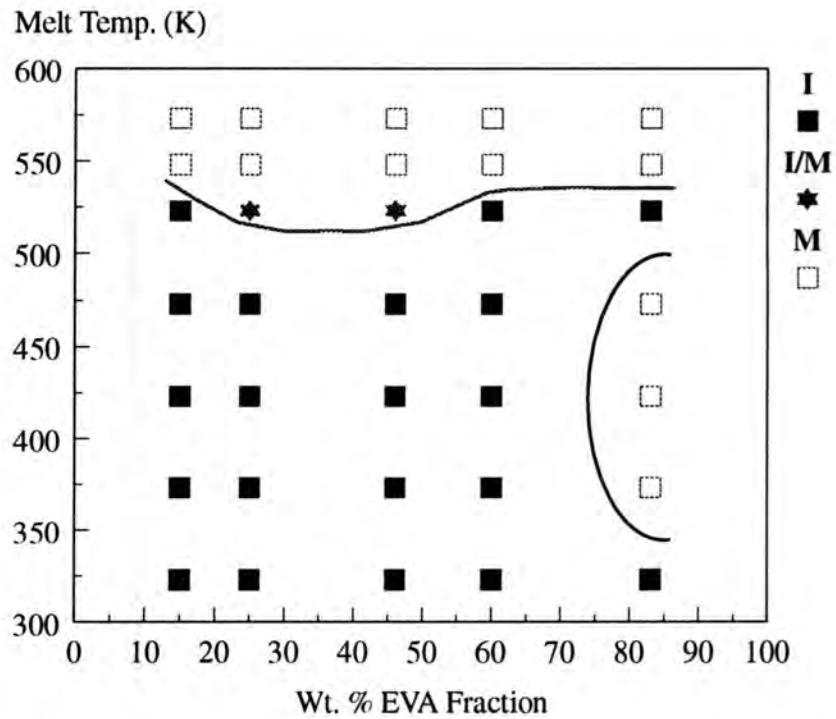


Figure 5.14 : Blend Morphologies in EVA:FVA Blends (Profile 2)

5.4.3 EVA:PI Blends

For all EVA:PI blend compositions, the following temperature profile was used :

Temperature Profile: 298K → Melt (100K/min) Hold 15 min

Melt → 298K (10K/min) Morphology noted

The melt temperatures chosen were 343, 373, 423 and 473K. Due to the possible thermal degradation problems of EVA (see discussion section) and possibly PI, blend morphologies obtained from melt temperature >473K were not considered. In contrast to EVA:FVA, the EVA:PI blends were crystalline at room temperature and prior to the initial melting stage, blend morphologies could not be determined. The following results therefore refer to morphologies obtained at **263K** i.e. after cooling from the various melt temperatures.

5.4.3a 17%EVA:83%PI (Figure 5.15)

On cooling from the 343K melt temperature, pools of EVA were noted dispersed in the PI matrix. As the melt temperature is increased, these EVA phases are reduced in size until at 423K and 473K melt temperatures, an homogenous "miscible" phase appears to be formed on cooling.

5.4.3b 39%EVA:61%PI

On cooling the blend from the 343K melt temperature, large phase separated regions of both EVA and PI phases are noted. As the temperature is increased to 373K and 423K, the EVA phases become smaller and more rounded in appearance with possible signs of "phase inversion" i.e. a fine dispersion of the PI component within the EVA "pools". At the 473K melt, both phases form a small, reasonably homogenous dispersion although larger discrete phases can still be noted.

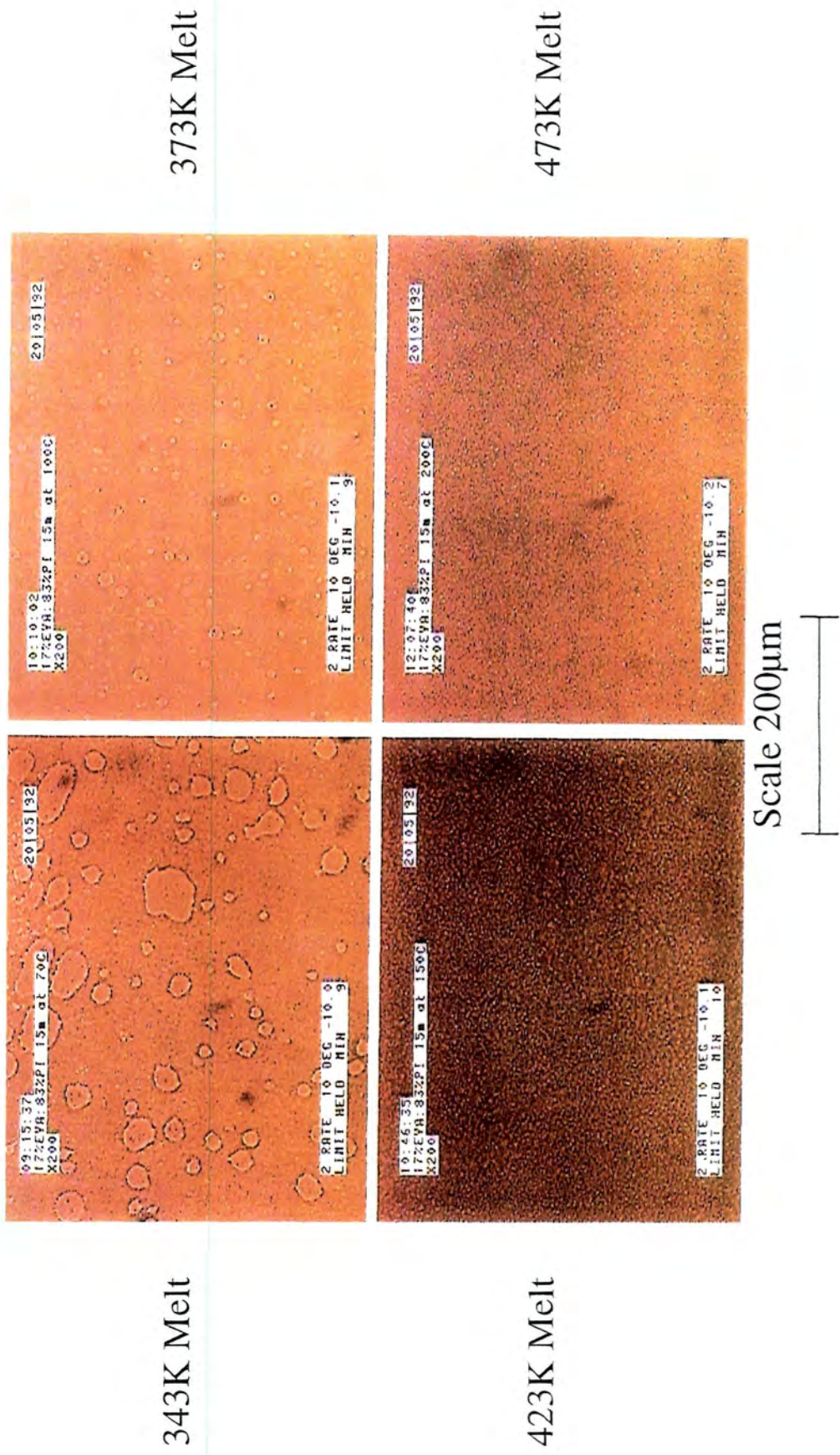
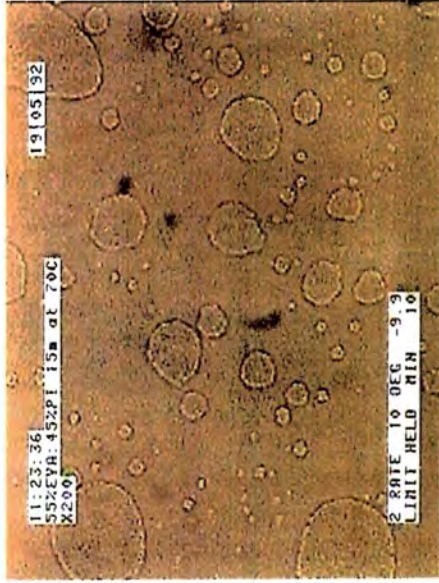


Figure 5.15 : 17%EVA:83%PI Blend (Cooled from 343K, 373K, 423K and 473K Melt Temperatures)

343K Melt



373K Melt



423K Melt



473K Melt



Scale 200µm



Figure 5.16 : 55%EVA:45%PI Blend (Cooled from 343K, 373K, 423K and 473K Melt Temperatures)

5.4.3c 55%EVA:45%PI (Figure 5.16)

At melt temperatures of 343, 373 and 423K, the morphologies of the blend on cooling to 263K are clearly phase separated with "phase inversion" noted from the 373K and 423K melts. In contrast, after cooling from the 473K melt, the blend forms a reasonably homogenous, "speckled" morphology.

5.4.3d 73%EVA:27%PI

The blend morphology on cooling from 343K shows phase separation with various sized PI droplets immersed in the EVA matrix. As the temperature is increased to 373K and 423K, fine dispersions are formed until at 473K, the blend is clearly homogenous with no separate phases noted.

5.4.3e EVA:PI Phase Diagram

Using the nomenclature outlined to describe miscibility (I, M, I/M), a phase diagram for the EVA:PI blend system has been proposed (Figure 5.17).

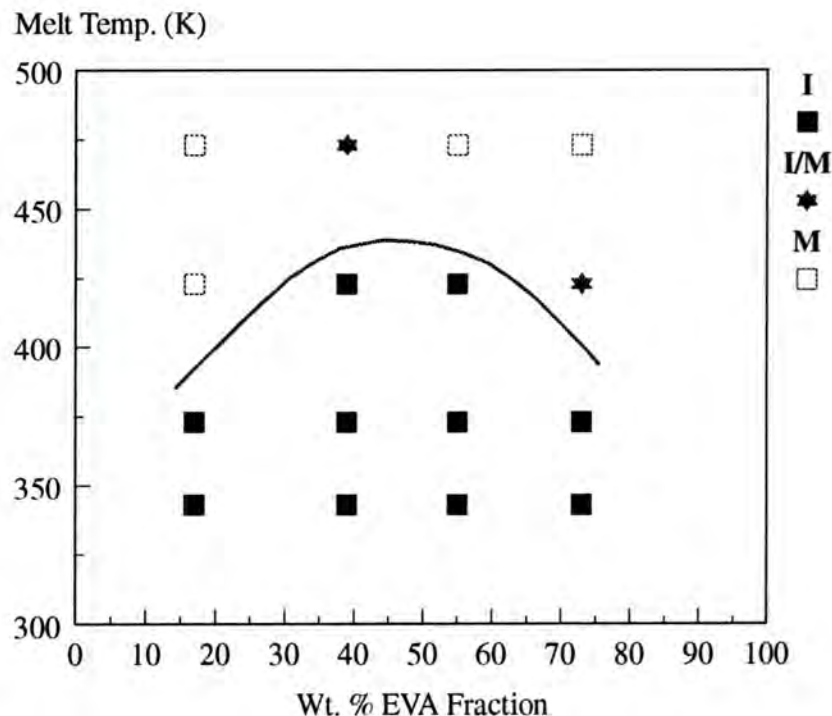


Figure 5.17 : Blend Morphologies in EVA:PI Blends

5.5 Discussion

From the initial miscibility studies, the observed morphologies of these blends agree with predicted miscibilities from melting point depression analysis (Chapter 4) and indeed the observed melting point depression in these blends as determined by DSC and Optical Microscopy techniques closely agree. This suggests that these morphologies which are obtained after cooling from various melt temperatures are representative of the blend miscibility at the melt temperature.

It is clear that both the EVA:LMPI and EVA:PE blends form homogenous morphologies on cooling with no indication of separate polymer phases. This suggests that these blends are miscible at these melt temperatures. The remaining blends show the characteristics of phase separation to varying degrees. However, on cooling from a 373K melt, the EVA:FVA blend shows large scale phase separation apart from the 83%EVA:17%FVA composition which has a fine homogenous appearance suggesting miscibility at the melt temperature. Although the EVA:PI blend after cooling from the melt, is clearly phase separated at all compositions, an increase in the melt temperature from 343K to 393K appears to increase blend miscibility. This increase in miscibility at the higher melt temperature is shown in the form of "phase inversion" i.e. the PI phase immersed in the EVA phase and vice versa and a relatively homogenous morphology formed from the 73%EVA:27%PI blend.

EVA blends with the polyitaconate samples, PI (M_n 9899) and LMPI (M_n 6601) show very different morphologies on cooling, suggesting that the lower molecular weight of the LMPI component is responsible for the observed miscible behaviour of the EVA:LMPI blends. This change in miscibility has also been predicted from melting point depression analysis (Chapter 4) and will be discussed further in Chapter 7 (heats of mixing).

During the initial heat-up of the PE component, rapid melting is noted at 328K which has previously been assigned (from DSC measurements - Chapter 4 and WAXS - Chapter 8) to a docosyl crystalline phase. However, on melting this phase, large crystal phases continue to remain which finally melt at higher temperatures. This suggests

possible impurities in the PE component which has subsequently been confirmed by ^{13}C nmr analysis (Chapter 3) and determined as free, unesterified docosanoic acid. The appearance of this "impure" high melting phase is reduced considerably in the EVA:PE blends. It can be speculated that this is due to the melting point depression effect of the docosanoic acid impurity on blending with the EVA component which consequently results in an "impure" melting phase which is essentially "hidden" within the PE (docosyl) melting phase.

Due to the poor resolution in optical microscopy, the blends which appear homogeneous can in fact consist of microphase separated dispersions. These dispersions can only be clearly identified using high resolution techniques such as scanning electron microscopy or transmission electron microscopy. In this optical study the appearance of such an "homogeneous" morphology is associated with a high degree of miscibility within the blend system. It is believed that in order to achieve this morphology, the degree of miscibility must be significant at the melt temperature prior to cooling.

As shown in Figures 5.13 and 5.14, the EVA:FVA phase diagrams are similar using the two temperature profiles. It is clear that the blend is essentially immiscible apart from at high temperatures ($>548\text{K}$) or high EVA concentrations ($\approx 80\%$). The 15 minute hold in profile 2 allows sufficient time for mixing to occur by diffusion, thereby giving a true estimation of miscibility and reduces the high temperature onset of miscibility by $\approx 25\text{K}$ compared to profile 1. The 83%EVA:17%FVA blend has a large "miscibility window" with an homogeneous phase formed on cooling from $\approx 323\text{-}473\text{K}$ and $>548\text{K}$ melt temperatures. In contrast, high FVA concentration blends are essentially immiscible apart from at high temperatures ($>548\text{K}$). Therefore FVA appears to be miscible in high EVA concentrations but **not** vice versa. This is shown throughout the blends where FVA phases contain small dispersed droplets of EVA, whereas EVA does not appear to contain any dispersed FVA polymer, presumably due to the solubility of FVA in the EVA phase. Although phase inversion is generally only noted in the FVA phase, certain blends show phase inversion in both phases i.e. 46%EVA:54%FVA (Figure 5.10) from 548K melts (profile 1) and 60%EVA:40%FVA from 323K (profile 1) and 523K (profile

2) melt temperatures. These melt temperatures correspond to the two temperature ranges at which the 83%EVA:17%FVA blend is observed to phase separate which may account for the observed phase inversion i.e. FVA dispersed in the EVA phase.

At high melt temperatures (>548K) the EVA:FVA blends appear to volatilise slightly. As reported², ester pyrolysis in EVA readily occurs at these temperatures and the volatilisation may therefore be due to the acetic acid evolved from deacetylation of the ester, resulting in the formation of double bonds in the polymer³. Unsaturation in the polymer can then result in rapid molecular weight increases and eventual gel formation⁴. Similar degradation products from FVA are also possible. It therefore appears likely that at these high melt temperatures, the blends have undergone significant chemical transformation and the subsequent morphologies at temperatures >548K are not representative of the true miscibility in EVA:FVA blends.

The EVA:PI phase diagram (Figure 5.17) appears to show "typical" upper critical solution temperature behaviour with all blend compositions miscible at a critical temperature of $\approx 450\text{K}$. The increase in miscibility of these blends with temperature appears to be a gradual process from the clear phase separation noted at lower temperatures to a gradual decrease in the size of the dispersed polymer phases as the temperature is raised until an essentially homogenous morphology is obtained.

To distinguish the separate binodal and spinodal phase boundaries in these blends, morphologies at specific melt temperatures must be monitored closely with time i.e. in the binodal (or metastable) region, phase separation takes place by the formation of spherical droplets which grow with time whereas in the spinodal (unstable) region segregation take place by spontaneous demixing⁵. Unfortunately, as already explained, phase contrast at melt temperatures of $\approx 343\text{-}523\text{K}$ appears to be ineffective with the blends appearing transparent i.e. with no image contrast. Therefore blend morphologies can only be noted on cooling to temperatures which are sufficient to induce crystallisation of the crystalline polymer phase and consequently, separate binodal and spinodal phase boundaries have not been determined. It should therefore be noted that

the phase boundaries noted in this study merely serve, at best as an indication of a phase change at a particular blend composition.

5.6 References

1. S. Cimmino, E. Martuscelli, M. Saviano and C. Silvestre, *Polymer*, 32, 1461 (1991)
2. B. Sultan and E. Sorvik, *J. Appl. Poly. Sci.*, 43, 1737 (1991).
3. B. Sultan and E. Sorvik, *J. Appl. Poly. Sci.*, 43, 1747 (1991).
4. B. Sultan and E. Sorvik, *J. Appl. Poly. Sci.*, 43, 1761 (1991).
5. I.G. Voight-Martin, K.H. Leister, *J. Poly. Sci. Polym. Phys.*, 24, 723 (1986).

CHAPTER 6
DESIGN AND CONSTRUCTION OF A POLYMER BLEND
"HEAT OF MIXING" CALORIMETER

6.1 Introduction

The overall design of the calorimeter was based on a model first constructed in the early 1970's by Chong¹ at Imperial College and still in use today. This design was itself based on a National Bureau of Standards model used for solution calorimetry².

The calorimeter is a batch-type heat conduction calorimeter which depends on the ability to control precisely and accurately at melt temperatures of up to 393K whilst measuring very small "heat of mixing" values (exothermic and endothermic) due to polymer mixing.

The calorimeter consists of a cell which contains the polymer components in separate compartments prior to mixing. This cell is tightly sandwiched between two highly sensitive heat flow devices (thermopiles) which ultimately measure the heat flow into or out of the cell i.e. the endothermic or exothermic "heat of mixing". The cell and thermopiles are encased in an aluminium heat sink which is controlled at a precise temperature ($\pm 0.001\text{K}$) by two heater jackets. After the temperature of the calorimeter and cell has stabilised, the cell is inverted and the polymer components pour out of their separate compartments and begin to mix. In this position, the heat sink is "rocked" gently from side to side to encourage homogeneous blending.

During the initial design stage of the calorimeter, the following major factors concerning the "heat of mixing" in polymer blends were taken into consideration when deciding on the instrument specifications:

6.1a. The operating temperature range of the calorimeter must be sufficient to ensure that all the polymers are in the melt phase i.e. above the crystalline melting point of the semi-crystalline polymers and are mobile at these melt temperatures.

- 6.1b.** The viscosity of the polymers in this study are relatively low due to their low molecular weight but require slow agitation during mixing in order that the polymers mix and form homogeneous blends (and reproducible "heat of mixing" values) within a reasonable time period.
- 6.1c.** Polymers generally have low thermal conductivity values and therefore, the time period necessary to monitor the heat change to completion is expected to be considerable. The calorimeter must therefore be capable of long term stability during the "heat of mixing" experimental measurement, to ensure that the total heat change is detected.
- 6.1d.** The "heat of mixing" in polymer blends can be very small ($<0.01\text{J/g}$ of mixture) and again the long term stability of the calorimeter and the sensitivity of the thermopile detectors must be sufficient to enable this heat change to be detected and accurately measured.

The design of the calorimeter is shown in Figures 6.1 and 6.2 which show side and front cross-sectional views respectively. The detailed specifications of each major component are outlined below.

6.2 Outer Jacket

The outer heat jacket is made of an aluminium cylinder, 33cm long, 30cm outer diameter with a 12mm wall thickness. The end plates of the cylinder are of 6mm thickness with a 30cm diameter. The end plates are secured to the main cylinder body by 12 evenly spaced 5mm socket-cap allen screws. The tufnell axle of the central heat sink passes through the end plates via appropriately sized holes of 25mm diameter surrounded by a 50mm diameter PTFE washer fixed into each end plate. A 35mm x 70mm rectangular cut-out at the midpoint of the cylinder length facilitates the side loading of the calorimeter cell into and out of the heat sink.

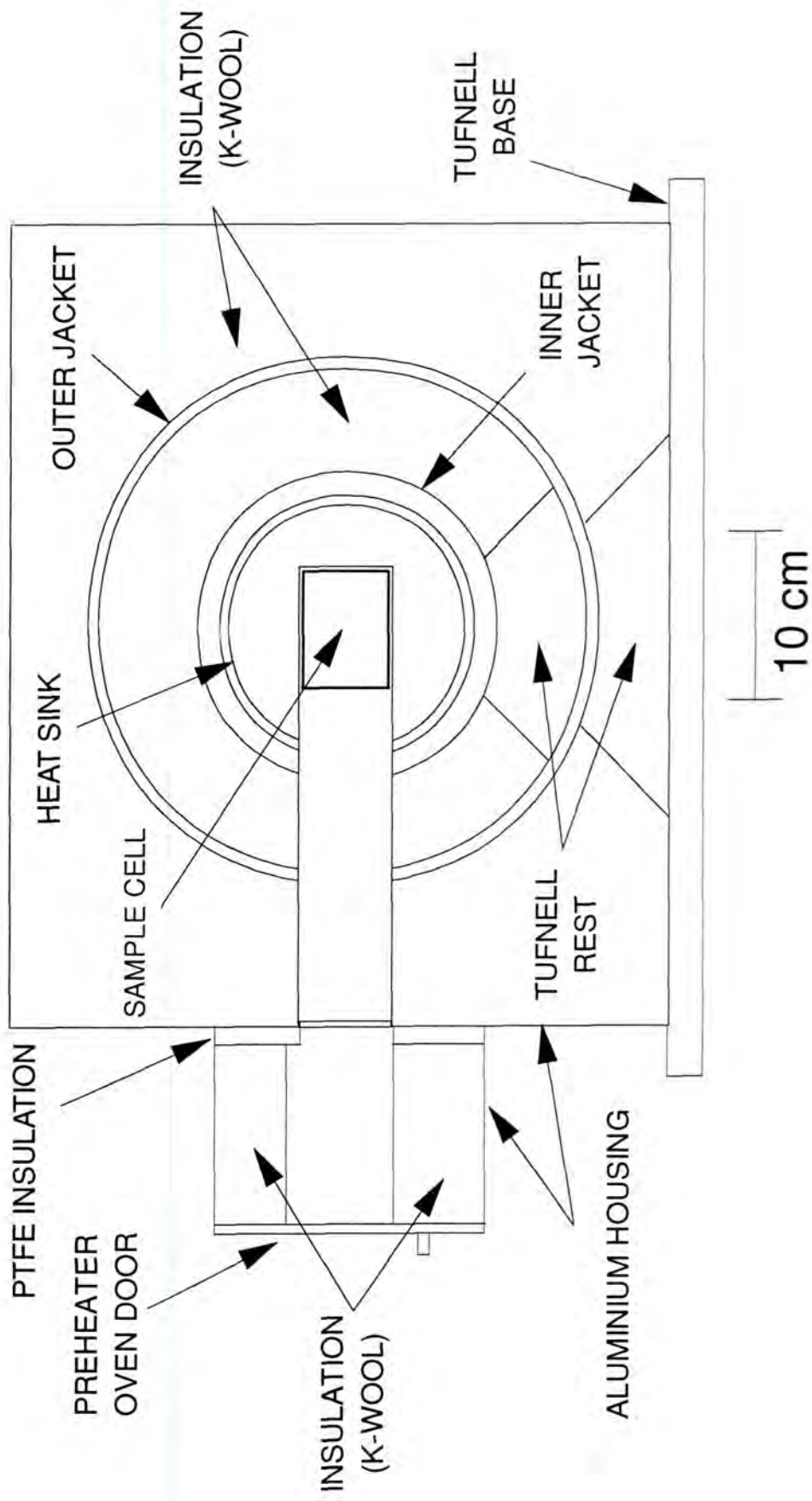


Figure 6.1 : Polymer Blend Calorimeter - Side View

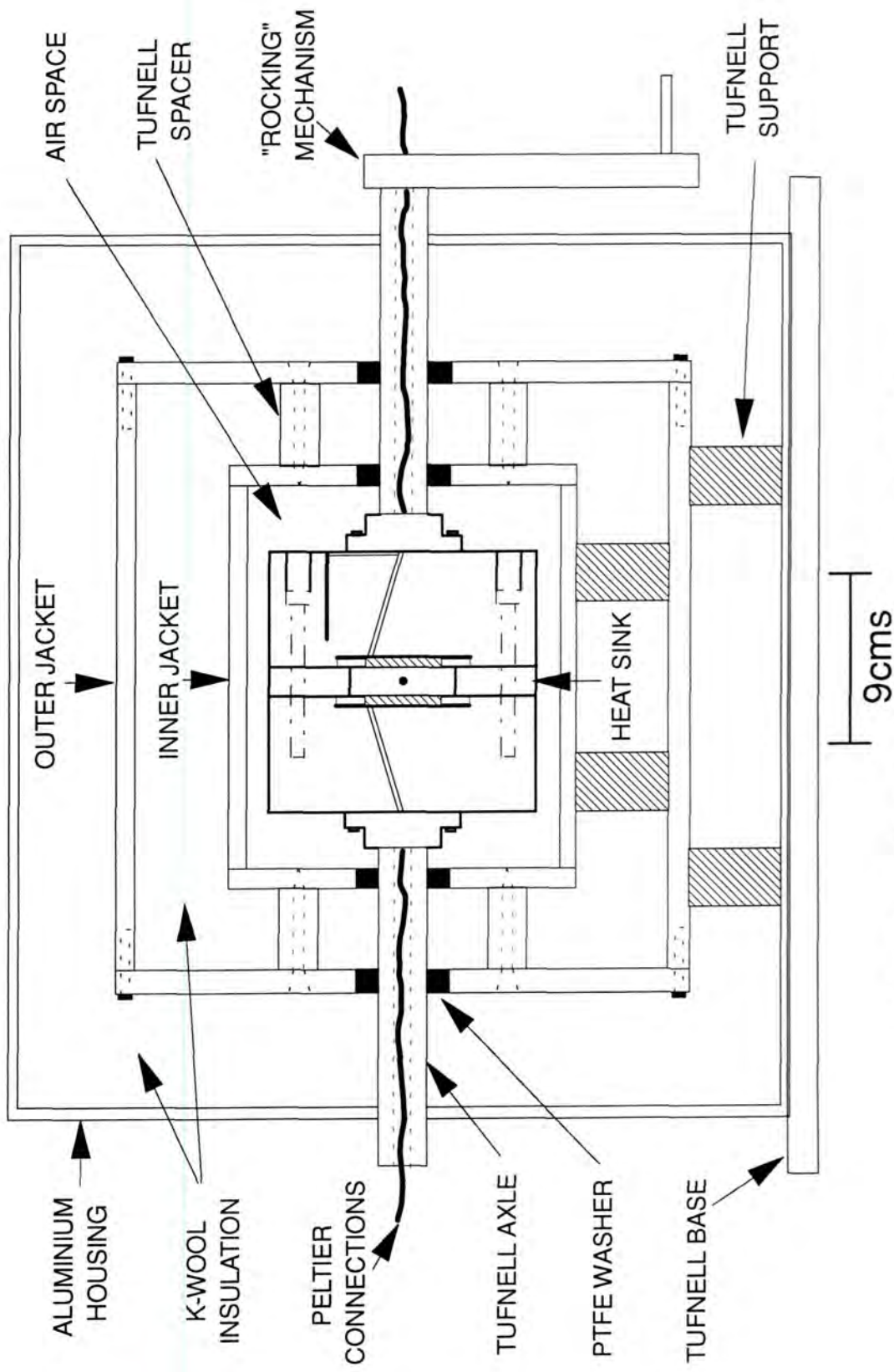


Figure 6.2 : Polymer Blend Calorimeter - Front View

The outer heat jacket is heated by flat nichrome resistance wires, bifilar wound around the cylinder using a special tool to ensure a constant distance between them. The wires are wound as a pair and firmly held in place and insulated using layers of polyamide and polyester tape. Bifilar winding i.e. two wires in close contact carrying equal and opposite currents, is necessary in order to produce a net magnetic field which cancels out, preventing stray electromotive force (EMF) being generated when the heat sink is rotated. The nichrome tape was secured with fibre glass based tape and the terminals were attached to a ceramic junction block which was fixed to the cylinder. The cylinder was grounded to earth and insulation tested several times. The outer jacket was fixed to two tufnell rests by screw fittings and secured to the tufnell baseboard.

6.3 Inner Jacket

The inner heat jacket is made of an aluminium cylinder 22cm long, 18cm outer diameter with a 13mm wall thickness. The cylinder end plates are 13mm thick, 18cm diameter with 25mm holes through which the central heat sink axle passes. A 50mm diameter PTFE insert is again present to reduce friction as the heat sink is "rocked". The end plates are secured to the cylinder by 6 evenly spaced 5mm socket-cap allen screws. The end plates of both the inner and outer heat jackets are joined at each end by 6 x 25mm diameter tufnell rods of length 44mm attached to each end plate by 6 x 2BA countersunk screws.

A vertical rectangular cut-out is machined at the mid-point of the cylinder in line with the cut-out on the outer jacket. A tufnell tunnel guide is placed through both these cut-outs and the calorimeter cell is guided through this tunnel to the central heat sink. The guide is sealed (to avoid heat loss) by a removable tufnell plug. As in the outer heat jacket, the inner jacket is heated by means of nichrome resistance tape with similar insulating, securing tapes used and again is grounded to earth. The inner jacket is secured to two tufnell rests by screw fittings which are then attached to the outer jacket. The space between the inner and outer jacket is filled with high density K-wool insulation material.

6.4 Central Heat Sink

In order to obtain the required sensitivity, the heat sink must be kept at a very precise temperature ($\pm 0.001\text{K}$). Additionally, the heat sink must be sufficiently large that an exotherm (or endotherm) from the calorimeter cell has negligible effect on the heat sink temperature.

The heat sink is a cylindrical aluminium block of length 13.5cm and diameter 14cm. The block is composed of 5 parts including the calorimeter cell as shown in Figure 6.3. The end pieces have dimensions of 6cm length, 14cm diameter with a 7cm diameter / 5.5mm deep hollow machined out in the centre to accommodate the heat flow detecting units (thermopiles of dimensions 40mm x 40mm x 5mm deep), a 7cm diameter / 5mm deep PTFE insert which completely surrounds the thermopiles and a 0.5mm thick copper back plate. The PTFE insert is to isolate the thermopile from the heat sink to ensure that the full temperature change from the calorimeter cell is measured by the thermopiles only, without any heat loss or gain from the heat sink. The thermopiles, PTFE insert and heat sink surface of each end piece must be of the same height to ensure good thermal contact with the calorimeter cell.

The thickness of the middle portion of the calorimeter depends on the thickness of the cell used, typically 1.5cm. The middle and two end pieces of the heat sink are held together by three 85mm long, 10mm diameter socket cap allen bolts countersunk to a depth of 20mm. A rectangular hollow in the centre part of the middle piece (5.5cm x 1.5cm), in line with the cut-outs in the inner and outer jackets, allows the fully assembled calorimeter cell to be push fitted directly into the centre of the heat sink. The aluminium cage of the calorimeter cell is isolated from direct contact with the heat sink, as described later, but in good contact with the aluminium surface of the thermopiles. After the cell is push fitted into the centre of the heat sink, the remaining cylinder hollow is filled with a machined aluminium end-piece which fits tightly into the heat sink. The tufnell axle is connected at each side of the heat sink via a tufnell bracket into which the axle is attached by araldite glue and pinned with an allen screw. The brackets are then attached to the heat sink by 6 evenly spaced screw / washer connections. Drilled

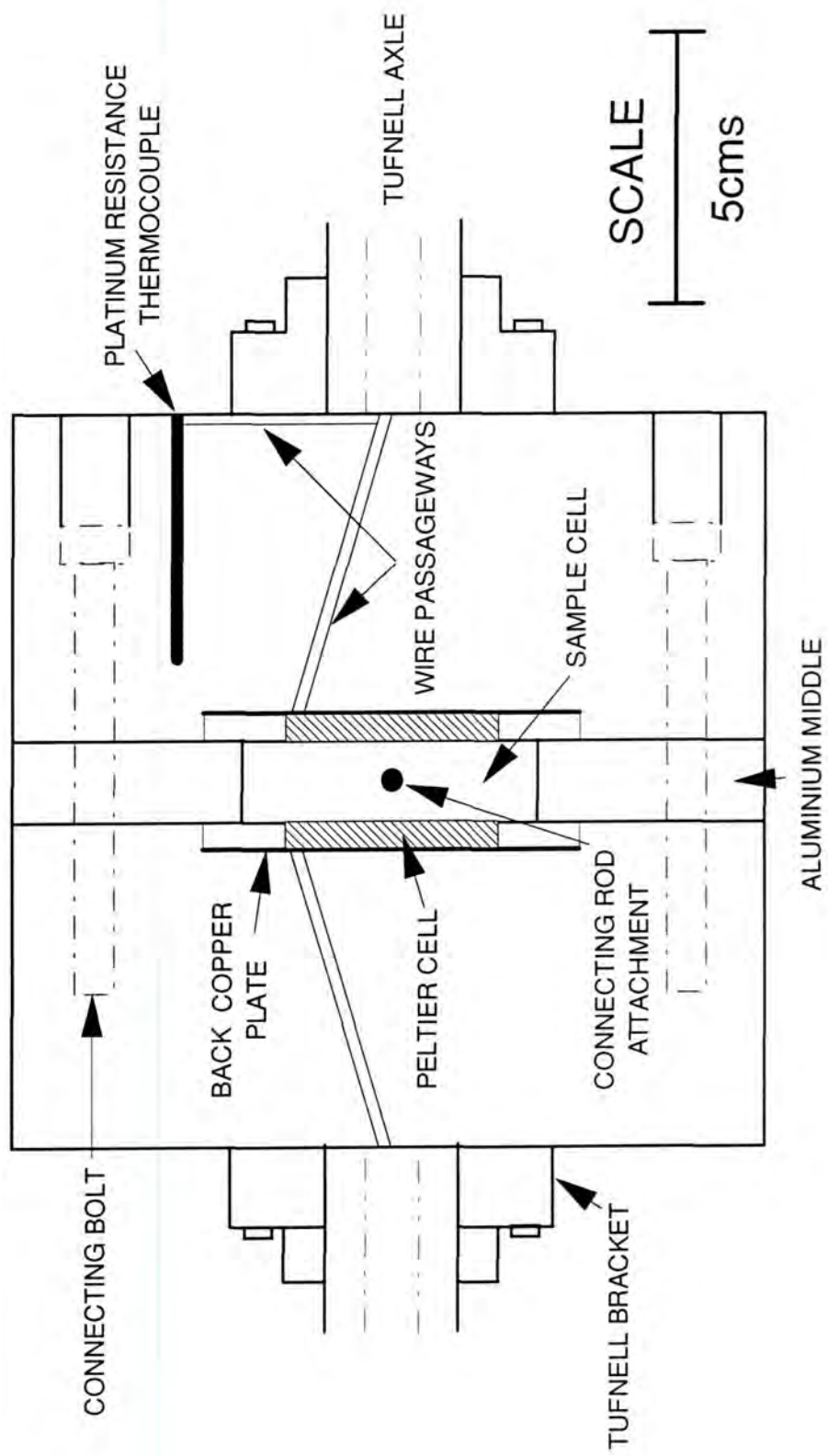


Figure 6.3 : Polymer Blend Calorimeter - Central Heat Sink Section

passageways through the heat sink unit and the centre of the tufnell axle allow the wires from the thermopiles to be led out at both ends. All wire insulation is capable of resisting temperatures in excess of 393K. The temperature of the block is measured by a four terminal 100 Ω platinum resistance thermometer which is placed as near to the calorimeter cell as possible.

6.5 Heat Flow Detecting Units

The central heat sink contains two thermopiles each of dimensions 40mm x 40mm x 5mm deep, joined in series. Each thermopile consists of numerous thermocouple junctions joined in series between two polished, smooth aluminium plates, one of which contains lugs for screw attachment to the heat sink. To ensure good conductivity a copper plate is sandwiched between the thermopile and the heat sink and all surfaces are smeared with heat sink compound.

The total copper plate and thermopile thickness must equal the depth of the hollow to ensure that the surface of the thermopile is exactly in alignment with the surrounding heat sink surface. Holes in the hollow allow wires to be led out to passageways in the heat sink unit and the tufnell axle.

A round PTFE piece of thickness equal to the depth of the hollow is carefully machined to accommodate the thermopiles and exit wires, so as to reduce the air space present. This PTFE piece then fits snugly around the thermopile allowing all heat into or out of the calorimeter cell to be conducted through the thermopile units (to be measured) and not the heat sink. The thermopiles are capable of operating at temperatures up to 393K.

The thermopiles, commonly referred to as Peltier cells represent both exotherms and endotherms as very small voltage changes and can monitor heat changes down to the μ V level. At equilibrium i.e. no heat flow, the voltage output from the thermopiles is zero.

6.6 Calorimeter Cell

The calorimeter cell assembly is shown in Figure 6.4. The cell consists of four PTFE sections which are secured together by steel bolts to produce a hollow where mixing occurs. This hollow contains separate compartments for each polymer, an arched head to encourage mixing when the cell is inverted and is surrounded by a 1mm thick aluminium cage. A 1mm thick, silicon gasket acts as a seal between the aluminium and PTFE to prevent sample leakage. In solvent experiments the silicon gasket swelled badly in contact with aliphatic or aromatic solvents, resulting in leakage. In these experiments, "Viton" (fluorinated carbon sheeting) was successfully used as the gasket seal. The PTFE components act as heat insulators and allow the "heats of mixing" to only flow through the face of the aluminium to the thermopile where it is detected and monitored. The cell measures 5.5cm x 5.5cm after assembly and is secured by steel brackets and bolts on either side.

The cell is inserted into the heat sink through the preheater oven and "tufnell passage" using a long handling rod which is screwed into one of the steel brackets. It is important that the surface of the aluminium is flush with the surrounding PTFE surface and that when inserted the assembled cell fits snugly into the heat sink. This ensures good contact between the cell and the thermopiles with negligible heat loss.

When assembled the calorimeter is enclosed in an aluminium housing 41cm high x 46cm wide which is secured to a tufnell baseboard by screws. All aluminium plates of the housing are fixed to an aluminium bar sub-frame by allen-headed screws and each plate can be readily removed to gain access to the end plates of the heat jackets. The spaces between the outer jacket and the housing are tightly packed with high density K-wool insulation. One plate on the housing has a cut-out in line with the cut-outs from the inner/outer jackets and the heat sink to enable the sample to be loaded through the preheater oven. After inverting the calorimeter cell, the polymers are mixed by a stirring lever mechanism attached to an electric motor at a speed of 5 rpm. This stirring mechanism has been designed to "rock" the calorimeter cell gently from side to side

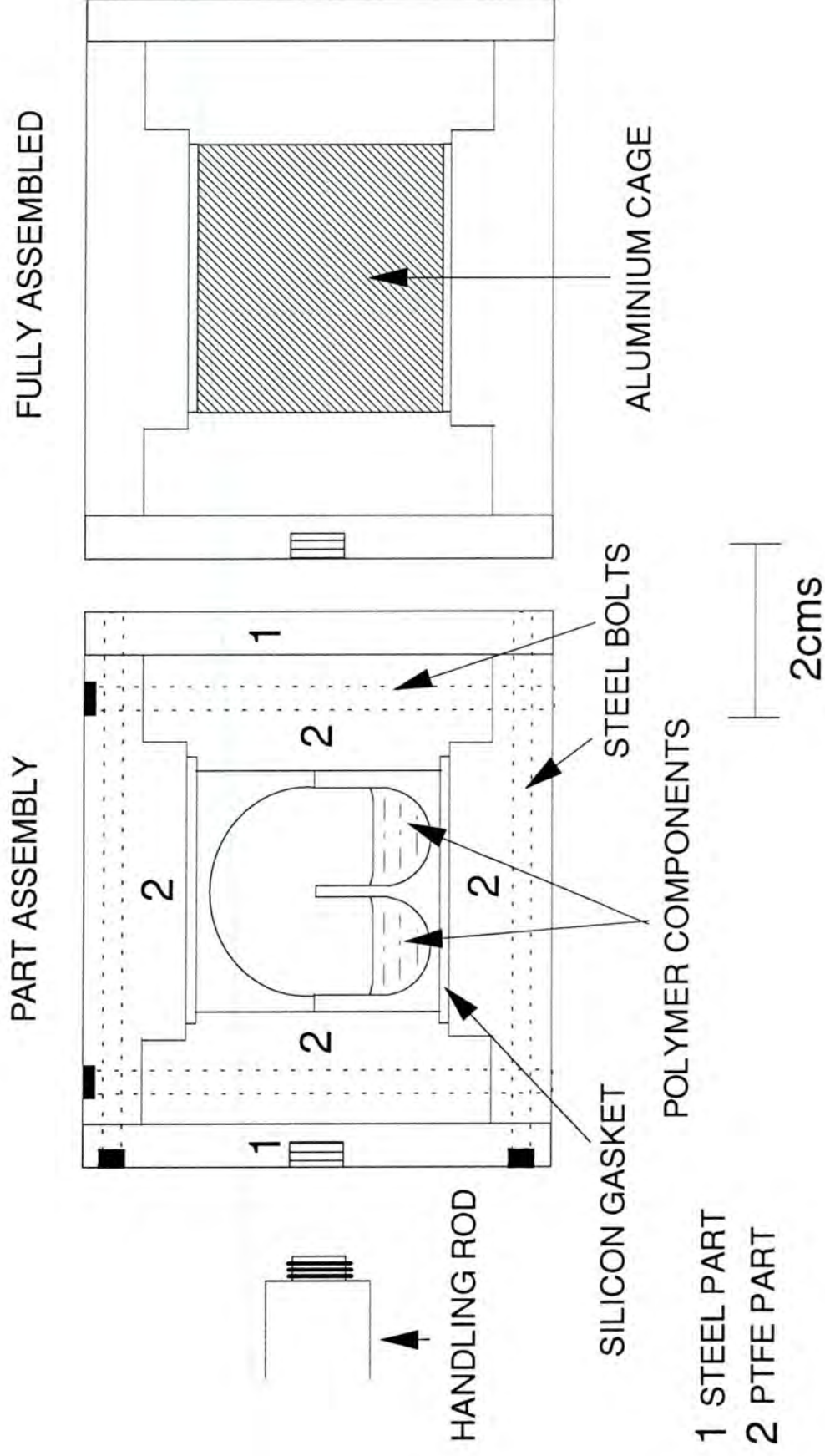


Figure 6.4 : Polymer Blend Calorimeter - Calorimeter Cell Design

rather than a complete rotation. Sockets and connectors from the control and measuring circuits are mounted on the side of the aluminium housing.

6.7 Preheating Oven

A preheating oven was fixed to the outside of the calorimeter at the cell loading cut-out entrance. This consists of 4 x 7mm thick aluminium plates which are screwed together to form a rectangular hollow (7cm x 7cm x 8cm deep) and then mounted on a 1cm thick PTFE sheet (16cm x 16cm). The PTFE acts as a heat insulator between the oven and the calorimeter housing. The oven is heated by 2 x 50W wire wound resistors on each of the four aluminium sides. The complete unit is enclosed in an aluminium housing of dimensions 16cm x 16cm x 11cm deep. The space between the oven and its housing is packed with K-wool insulation. The front of the oven is closed by a sliding tufnell door which is fixed to a tufnell frame (16cm x 16cm x 1cm deep). The oven plus housing and PTFE sheet is mounted onto the calorimeter by allen-type screws. The preheating oven is controlled at the outer jacket temperature and stores the calorimeter cell prior to loading into the heat sink. This ensures that the cell is loaded at approximately the same temperature as the heat sink and thereby reduces the equilibration time.

6.8 Temperature Control

Both the inner and outer jacket heaters are zero voltage switched at mains frequency. The inner jacket is controlled by pulse width modulation using a specialised Precision Thermometer/Controller (Parr Model 1671) : a digital signal is used to switch on a solid state relay which is supplied with normal or boost windings on a transformer. The boost winding i.e. higher voltage, is used for rapid heating of the inner jacket during initial heating or maintaining elevated temperatures. The inner jacket is precisely controlled to $\pm 0.001\text{K}$ by the controller using a specialised 1000Ω Platinum Resistance Thermometer (PRT) - supplied by TC Thermocouples, which is embedded in the wall of the jacket.

The temperature difference between the inner/outer jackets and inner jacket/preheating oven are sensed by a differential pair of 100 Ω PRT's which are embedded in both jackets and the preheating oven. This difference is amplified in an instrumentation amplifier which has a differential input and then passes to a 2-term temperature controller to produce an output DC voltage of the correct polarity and level to enable the outer jacket (and preheating oven) to "track" the inner jacket temperature. Using this purpose built "tracking system", the outer jacket and preheating oven are controlled at 2K below the inner jacket temperature.

An independent PRT indicator using 4 wire 100 Ω PRT's is used to monitor the heat sink, outer jacket and preheating oven temperatures.

Circuit diagrams outlining the temperature control system between the outer jacket, preheating oven and inner jacket are shown in Figures 6.5, 6.6 and 6.7.

6.9 Data Measurement, Analysis and Storage

To assimilate and examine experimental data i.e. the voltage output measurements from the thermopiles and the temperature of the inner jacket, a computer program has been written in Quickbasic for an IBM PC. It performs the following functions:

6.9.1 Instrument Parameters

Important parameters from the inner jacket controller i.e. set points, alarms and data log interval etc. can be set from the PC menu. These settings can be read into a program file together with the respective voltage/temperature data obtained. This ensures that identical settings are used for comparable experiments. Communication between the controller and the computer is by an RS232 link.

6.9.2 Measurement

After the calorimeter has reached temperature equilibrium (usually 48 hours after initial start-up) data accumulation can begin. The required experimental parameters are first downloaded to the controller. As the "heat of mixing" experiment proceeds, the

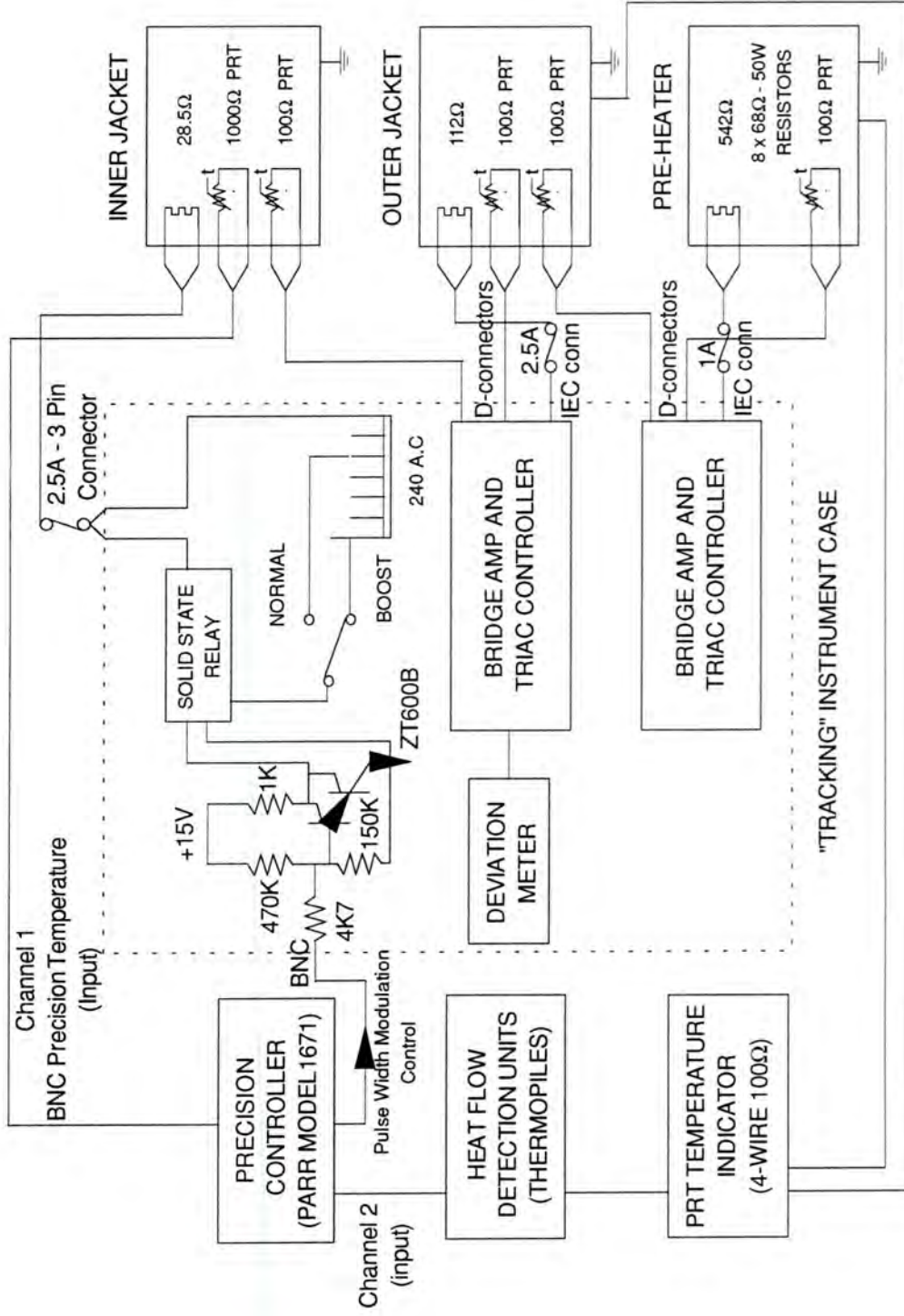


Figure 6.5 : Polymer Blend Calorimeter - Basic System Interconnections

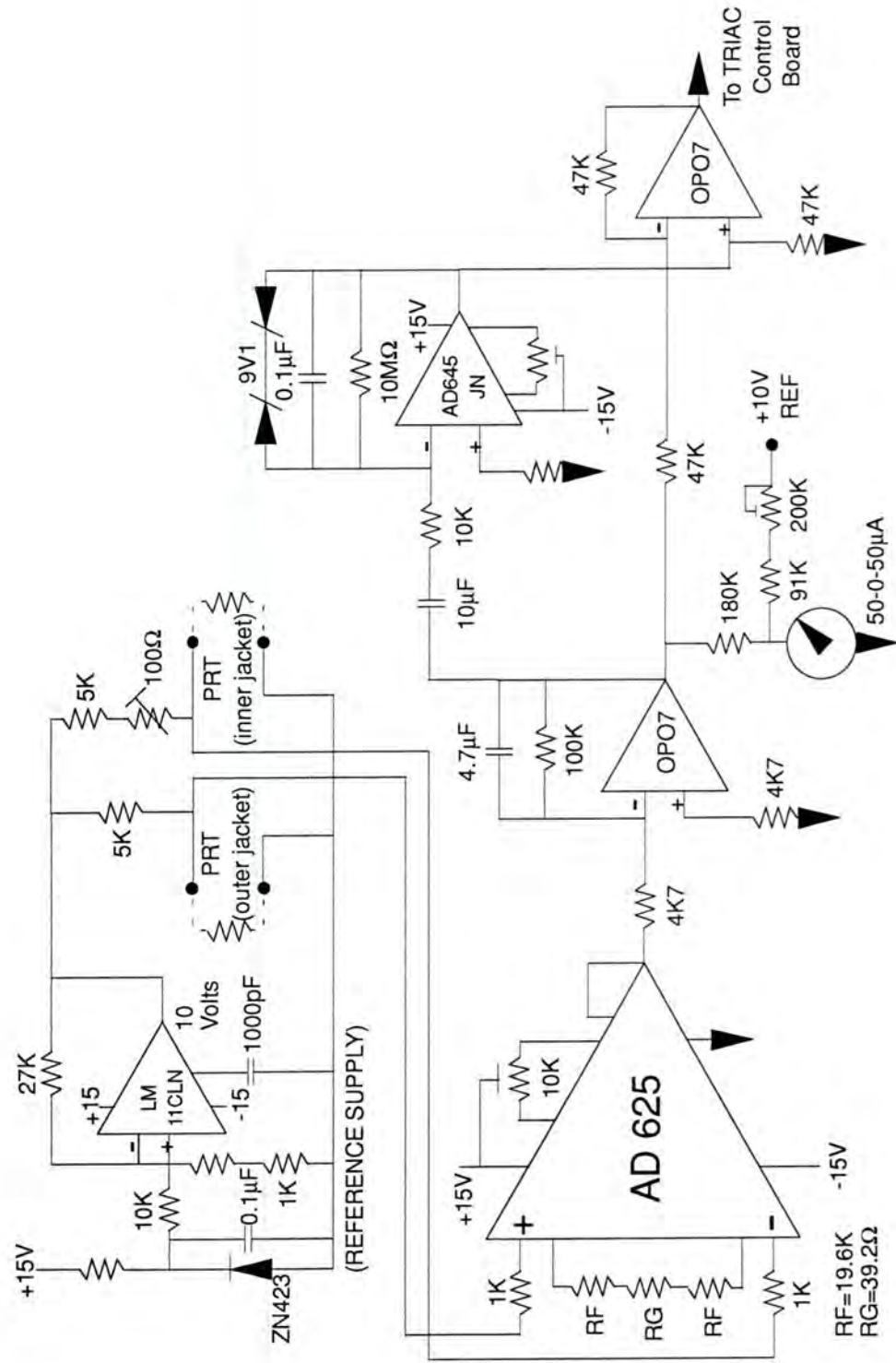


Figure 6.6 : Differential Heater Controllers for Inner:Outer Jacket and Outer Jacket:Pre-heater

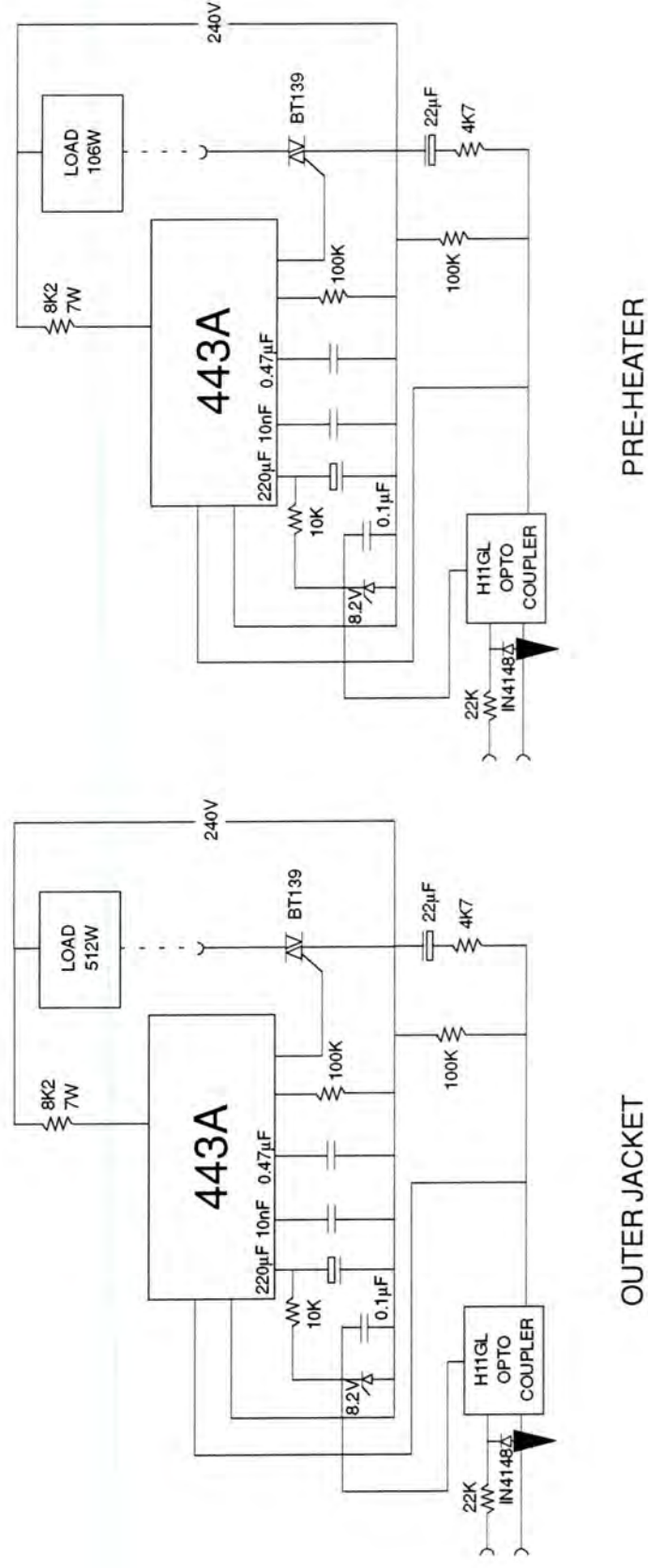


Figure 6.7 : Polymer Blend Calorimeter - TRIAC Modules (Outer Jacket and Pre-heating Oven)

current values of inner jacket temperature and thermopile voltage are read from the controller and transferred at a pre-set time interval to the computer to be displayed graphically. Up to 4000 temperature/voltage data pairs can be accepted at an interval of between 1 and 128 seconds.

6.9.3. Data Analysis

A selected area of the data points can be expanded horizontally for closer examination. The voltage profile can be integrated between two moveable markers and the area of integration displayed.

6.9.4 Data Storage and Retrieval

Acquired data are stored in disc files along with the controller settings.

6.10 Mains Voltage Conditioning

Mains voltage "spikes" severely hinder the accuracy of the data integration, and it is essential that these are removed by a voltage conditioning i.e. filter system, which then supplies the "stabilised" mains voltage to all calorimeter instruments.

A schematic diagram of the calorimeter and its peripheral devices are shown in Figure 6.8.

6.11 References

1. C. Chong, PhD Thesis, Imperial College of Science and Technology (1981).
2. E.J. Prosen and M.V. Kilday, Journal of Research (National Bureau of Standards) - A. Physics and Chemistry, 77A, No.2 (1973).

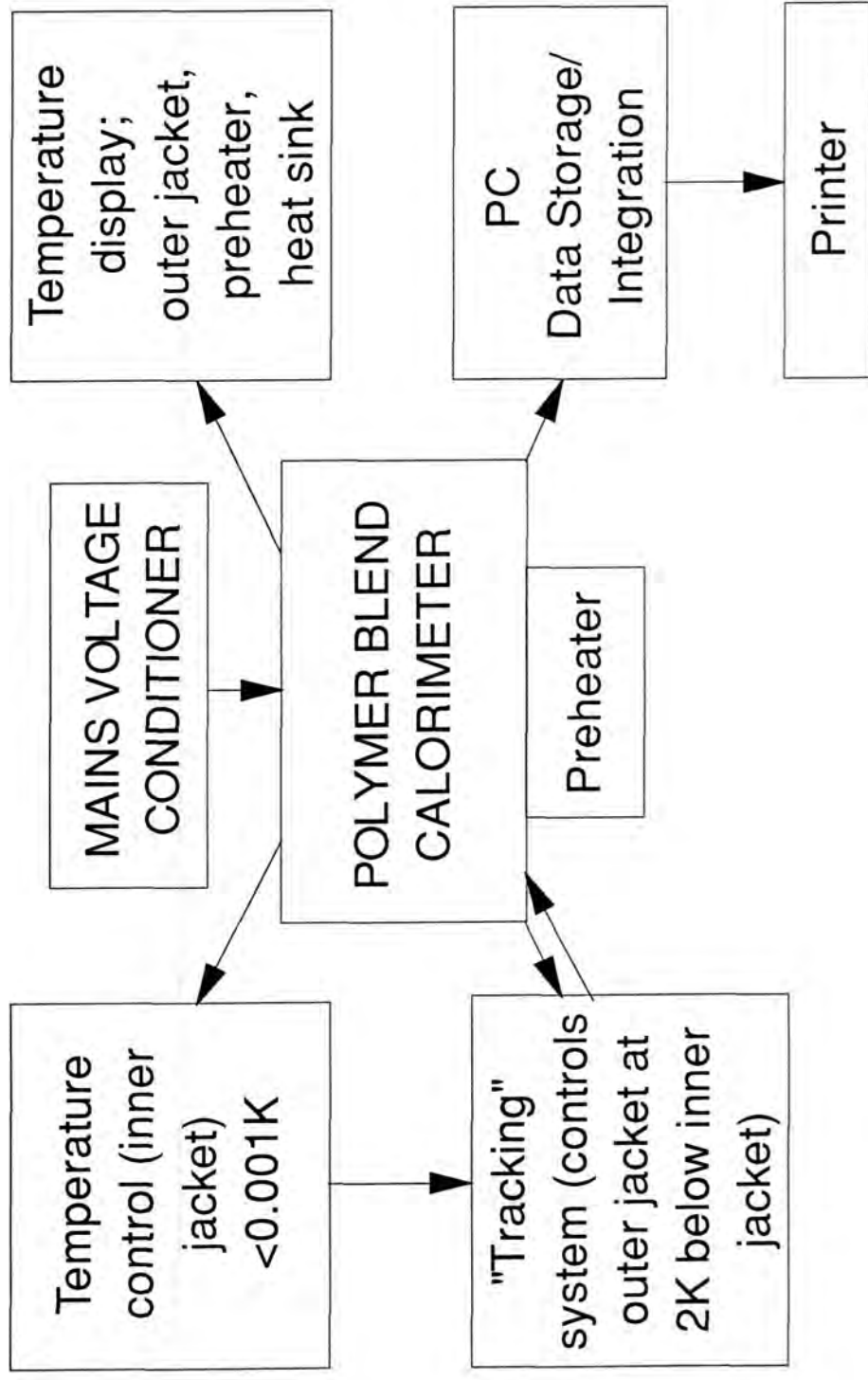


Figure 6.8 : Schematic Diagram of Polymer Blend Calorimeter

CHAPTER 7
"HEAT OF MIXING" CALORIMETRY

7.1 Introduction

The free energy of mixing (ΔG_{mix}) is the fundamental thermodynamic quantity that controls miscibility in polymer blends :

$$\Delta G_{\text{mix}} = \Delta H_{\text{mix}} - T\Delta S_{\text{mix}} \quad (7.1)$$

where ΔH_{mix} = enthalpy (heat) change on mixing, ΔS_{mix} = entropy change on mixing. For a polymer blend to be miscible, two conditions must be fulfilled :

$$\Delta G_{\text{mix}} < 0 \quad (7.2)$$

$$\left(\frac{\partial^2 \Delta G_{\text{mix}}}{\partial \phi_2^2} \right)_{T,P} > 0 \quad (7.3)$$

where ϕ_2 is the volume fraction of component 2. The Flory-Huggins lattice theory assumes that the entropy change, ΔS_{mix} in eqn. 7.1 is due essentially to configurational entropy changes which favour miscibility in blends but are very small for high molecular weight polymers. Consequently, the enthalpic contribution plays a dominant role in determining the sign of ΔG_{mix} . Therefore, in many polymer blends the observed miscibility is a direct result of a negative (exothermic) "heat of mixing" contribution to the overall free energy of the process¹.

For several blend systems, specific interactions such as hydrogen bonding or dipolar coupling result in negative ΔH_{mix} values^{2,3} and thereby a favourable contribution to the free energy of mixing. However, when only weak dispersive or van der Waals forces act between the repeat units of the two polymers, the heat of mixing is positive

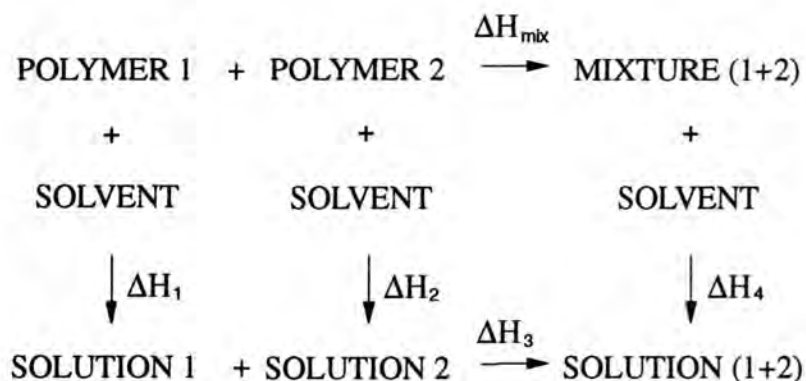
(endothermic)⁴ and if entropic contributions are considered negligible, ΔG_{mix} is positive and consequently, the blend is immiscible.

In contrast, blends containing low molecular weight components have significant configurational entropy contributions which can dominate the enthalpic contribution resulting in a negative ΔG_{mix} value which is favourable to miscibility. In these cases, blends can be miscible despite unfavourable (endothermic) heat of mixing values⁵.

It therefore appears clear that knowledge of the heat of mixing i.e. the enthalpic interaction, is fundamental in understanding polymer-polymer miscibility and "Calorimetry" is the most direct method of determining this thermodynamic parameter. Unfortunately, the heat of mixing in relatively high molecular weight polymer blends cannot generally be measured in the bulk (or melt) state due to their high viscosities, low diffusion coefficients and generally very small heat changes. Crystalline polymers may also have melting temperatures greater than the maximum operating temperature of the calorimeter and consequently, the melt state of the polymers cannot be obtained.

The problems of direct calorimetry measurements in polymer blends can be resolved, in principle, by measuring the heat of mixing of low molecular weight analogues which have molecular structures representative of the polymer chain. The major difficulty in this technique is the importance in choosing the correct polymer analogue as different analogues for the same polymer can give widely different results⁶. Mixing of these analogues occurs readily in the melt form due to their low viscosity. Since the heat of mixing results from energy changes due to close neighbour interactions, this value should approximately be independent of molecular weight unless strong steric restrictions associated with the polymers are present. This technique has been used extensively and good correlations have been found between the miscibility of a polymer blend and the sign of the "heat of mixing" of their analogues^{3,6,7}.

Another indirect method of determining the ΔH_{mix} in cases where direct calorimetry cannot be performed, is to measure the "heat of solution" of a polymer or a mixture of two polymers by a solvent. By appropriate measurements of this type and application of Hess's law, the heat of mixing value can be inferred⁸⁻¹⁰ as shown :



From the above cycle, ΔH_{mix} is calculated from:

$$\Delta H_{\text{mix}} = \Delta H_1 + \Delta H_2 + \Delta H_3 - \Delta H_4 \quad (7.4)$$

This technique requires great accuracy as the final ΔH_{mix} value is computed from small differences between much larger numbers.

In this study, heat of mixing measurements for several EVA-based polymer blends have been determined **directly** in the melt state using the calorimeter previously described in Chapter 6. This has been possible as these polymers are relatively low molecular weight with low melt viscosities and the melting points of the semi-crystalline polymers are below the maximum operating temperature of the calorimeter (393K). The indirect methods (and potential inaccuracies) described above have therefore been avoided.

The heat of mixing has also been determined for each of these polymers on blending with docosane (C22 n-alkane) in the melt phase. Docosane represents a very low molecular weight polyethylene-type component with a very large and favourable configurational entropy contribution towards blend miscibility.

Enthalpic interactions between polymer and docosane solutions (in toluene solvent) have also been studied.

7.2. Flory-Huggins Theory

Flory and Huggins independently related the heat of mixing (ΔH_{mix}) of two components to the interaction parameter (χ) with the following expression¹¹:

$$\Delta H_{\text{mix}} = kT\chi_{1,2}n_1\phi_2 \quad (7.5)$$

where:

- k = Boltzmann Constant ($1.380662 \times 10^{-23} \text{ J K}^{-1}$)
- T = Absolute Temperature (K)
- χ = Flory - Huggins Binary Interaction Parameter (χ)
- n_1 = Number of molecules of solvent
- ϕ_2 = Volume fraction of solute

Although this expression originally was derived for polymer solutions, it can be expressed for polymer blends as :

$$\Delta H_{\text{mix}} = kT\chi_{1,2}m_1n_1\phi_2 \quad (7.6)$$

where:

- m_1 = Number average degree of polymerisation of component A.
- n_1 = Number of molecules of component A.
- ϕ_2 = Volume fraction of component B.

χ values determined from these heat of mixing measurements represent the **enthalpic** interaction between the components.

In eqn. 7.5, m_1 for the solvent is generally accepted as 1 and therefore the m_1 term disappears. In this study, component A in the EVA-polymer and docosane-polymer blends represents the EVA and docosane components respectively.

Using eqn. 7.6, enthalpic χ values for these blends were calculated from each measured value of ΔH_{mix} . The determined χ values are represented both per chain and repeat unit of component A i.e. $\chi_{1,2}m_1$ and $\chi_{1,2}$ respectively.

From the ΔH_{mix} values, the free energy of mixing (ΔG_{mix}) values were also calculated using the classical Flory-Huggins relationship :

$$\Delta G_{\text{mix}} = RT (n_1 \ln \phi_1 + n_2 \ln \phi_2 + m_1 n_1 \phi_2 \chi_{1,2}) \quad (7.7)$$

which is derived (see Chapter 2) from :

$$\Delta G_{\text{mix}} = \Delta H_{\text{mix}} - T\Delta S_{\text{mix}} \quad (7.8)$$

and,
$$\Delta G_{\text{mix}} = \underbrace{m_1 n_1 \phi_2 \chi_{1,2} RT}_{\text{ENTHALPIC}} - \underbrace{(-RT(n_1 \ln \phi_1 + n_2 \ln \phi_2))}_{\text{ENTROPIC}} \quad (7.9)$$

7.3 Materials

All polymers apart from NECPE were supplied by EXXON Chemicals Ltd. and separately dried in a vacuum oven at 373K for 24hrs to remove possible solvent residues. Docosane was of analytical grade and used as supplied by Aldrich. Docosane and polymer solutions were prepared ($\approx 10\% \text{w/w}$) using Analar grade toluene. High purity ($>99\%$), anhydrous samples of diglyme and dodecane were supplied by Aldrich in "sure-seal" bottles under nitrogen.

7.4 Apparatus and Measurement

The heat of mixing for each blend system was determined using the calorimeter described in Chapter 6.

The components are blended in a reaction cell and the heat flow into or out of this cell is measured as an output voltage from the surrounding heat flow devices (thermopiles). The calorimetric experiment involves the measurement of the thermopile output voltage at various fixed sampling intervals (usually 2-5 seconds). Integration of the voltage vs. time profile is representative of the heat flow due to blending i.e. the "heat of mixing".

7.5 Experimental

The temperature of the calorimeter is set from a PC which has an interface with the temperature controller. All major settings i.e. alarms, set points, data storage etc. can be set through the computer and then downloaded to the temperature controller memory. All settings are filed on computer discs together with the relevant voltage vs. time data.

Although the inner and outer jackets reach the set point temperatures very rapidly, the solid aluminium heat sink which ultimately contains the reaction cell, takes approximately 48 hours to reach temperature (by heat diffusion from the inner jacket) and then equilibrate.

Approximately 0.5g of each component (or 0.5cm³ of the polymer and docosane solutions) is weighed to 5 decimal places into separate compartments of the PTFE sample holder. To encourage mixing in the melt blends when the cell is inverted, a single, round glass ball (diameter ~3mm) is placed in one of the compartments. An aluminium cage is then placed around the sample holder and the holder is sealed by another PTFE end piece. The loaded cell is placed for at least one hour in a preheater attached to the front of the calorimeter. This equilibrates the cell at a temperature of 2K below the heat sink temperature which is essential in reducing the stabilisation time when the cell is inserted into the heat sink and also avoids possible cooling of the heat sink.

After insertion, the cell is left for a further hour to ensure an acceptable stability level in the voltage output from the thermopiles cells which is monitored as "baseline noise". When equilibrium has been attained, the axle of the heat sink is rotated through 180 degrees, the cell is subsequently inverted and mixing begins. The axle is then attached to a twin-gearbox electric motor which rotates at 5 rpm to slowly "rock" the heat sink and reaction cell through approximately 70 degrees to mix the components. Periodically, the cell is inverted into its original position to ensure that any component residues in the holder compartments are "washed" with the mixture.

Measurement of the voltage vs. time data continues until the output voltage from the thermopiles returns to its baseline value. The total change in the voltage output due to

heat changes from mixing is integrated using the PC and converted to a "heat of mixing" value from electrical calibration data. Typical experimental times for each blend sample range from 60-90 minutes containing up to 3000 separate voltage and temperature data points.

For each blend system, the determined heat of mixing, free energy of mixing and interaction parameter values are plotted at various compositions. The total composition dependence of these values is then represented either as a linear or polynomial fit which essentially serve as a "guide to the eye".

7.6 Electrical Calibration

The calibration cell was similar to the sample cell described earlier but contained a 150Ω ($\pm 0.01\%$) wire wound resistor (supplied by Vishay-Mann). A variable current was applied to the resistor over a range of time periods and the resulting output voltage change integrated and recorded. The energy input can be calculated as follows:

$$E = I^2Rt \quad (7.10)$$

where:

E = Energy (J)

I = Current (A)

R = Resistance (Ω)

t = Time (seconds)

When the integrated voltage output is plotted against the calculated electrical energy supplied, a very good linear relationship is obtained. From this calibration, the response of the calorimeter can be converted into a measure of the enthalpy (heat change) within the system.

The electrical calibration is very dependent on the contents of the reaction cell and this is due to changes in thermal conductivity and heat capacity. This effect is highlighted by comparing the calibrations of an empty cell (Table 7.1) with that

containing 1cm³, 2cm³ and 3cm³ of distilled water (Table 7.2) as shown in Figure 7.1. The volume of water appeared to have little effect on the calibration (as long as the resistor was **fully** immersed) which suggests that electrical calibration is strongly dependent on the surface area coverage of the resistor. Thus, it is clear that electrical calibration must be carried out with the resistor completely immersed in a mixture of the same compositional ratio to that which is to be measured.

Energy Input (J)	Area (x10 ⁻⁴)
0.972	1249
1.944	2240
3.139	3584
4.050	4788

Table 7.1 : Electrical Calibration at 301.95K - empty reaction cell

Energy Input (J)	Area (1cm ³ Water) (x10 ⁻⁴)	Area (2cm ³ Water) (x10 ⁻⁴)	Area (3cm ³ Water) (x10 ⁻⁴)
0.972	2173	2194	2580
1.944	4636	4305	4754
3.038	7269	7270	7348
4.050	9668	9406	9726

Table 7.2 : Electrical Calibration at 301.95K - cell containing distilled water

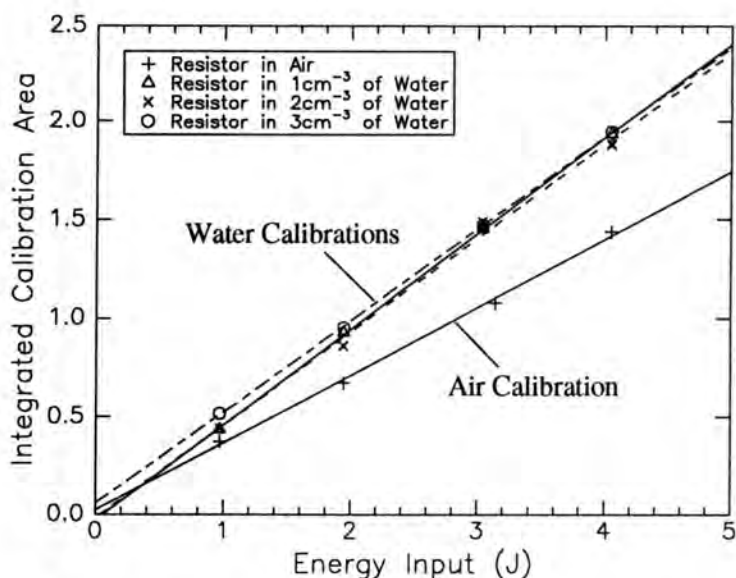


Figure 7.1 : Electrical Calibrations in Water and Air

7.7 Calorimeter Testing

To confirm the accuracy of the calorimeter in determining heat of mixing values, various well-characterised blend systems were measured and compared to reported values. However, determination of the "heat of neutralisation" in a standard acid-base reaction has not been possible as the exothermic heat of mixing values were very inconsistent and up to three times greater than the literature values. The excess exothermic heat was confirmed as being due to the reaction of the acid/base with the aluminium surface. The calorimeter was therefore tested using the endothermic heat of mixing between dodecane and diglyme (diethylene glycol dimethyl ether) which has been comprehensively reported by Booth et. al.¹².

As an additional check of the instrument accuracy, the endothermic heat of mixing vs. composition relationship between oligomeric mixtures of polystyrene and polybutadiene was studied and again compared to reported values¹³. Electrical calibration was again carried out for each blend system.

7.7.1 Diglyme:Dodecane Blend

The endothermic heat of mixing in a diglyme (56%^{w/w}) : dodecane (44%^{w/w}) (Figure 7.2) blend at 301.95K was determined in duplicate using an electrical calibration of the same blend composition ratio (Table 7.3, Figure 7.3). From these results (Table 7.4), the ΔH_{mix} values for the blend were determined at 13.91 ± 0.33 J/g with the error based on the standard deviation of two separate measurements. This value closely agrees with the literature value of 14.35 ± 0.2 J/g (Booth et. al.¹²) and justifies the use of an electrical calibration to determine the heat change.

Energy Input (J)	Area (x10 ⁻⁴)
4.98	110
9.96	219
15.00	333
19.97	444

Table 7.3 : Electrical Calibration - diglyme (55.6 %^{w/w}) : dodecane (44.4 %^{w/w}) at 301.95K (Total Weight of Mixture = 0.90517g)

Diglyme Wt. (g)	Diglyme Wt. (%)	Dodecane Wt. (g)	Dodecane Wt. (%)	Area (x 10 ⁻⁴)	ΔH_{mix} (J/g mixture)
0.50296	56.5	0.38791	43.5	268	13.58
0.50038	55.8	0.39673	44.2	283	14.23

Table 7.4 : Heat of Mixing in diglyme : dodecane mixtures at 301.95K

$$\Delta H_{\text{mix}} (\text{diglyme:dodecane}) = 13.91 \text{ J/g} \pm 0.33$$

$$\text{Literature value (C. Booth et al.}^{12}\text{)} = 14.35 \text{ J/g} \pm 0.2$$

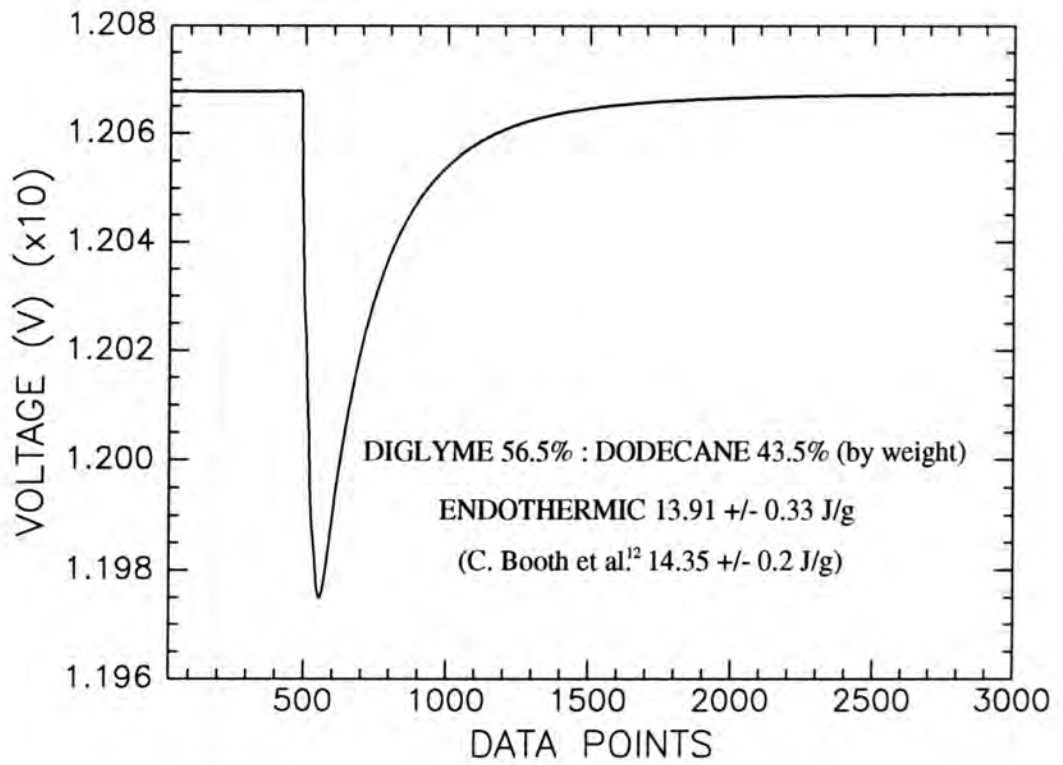


Figure 7.2 : Heat of Mixing in Diglyme:Dodecane blends at 301.95K

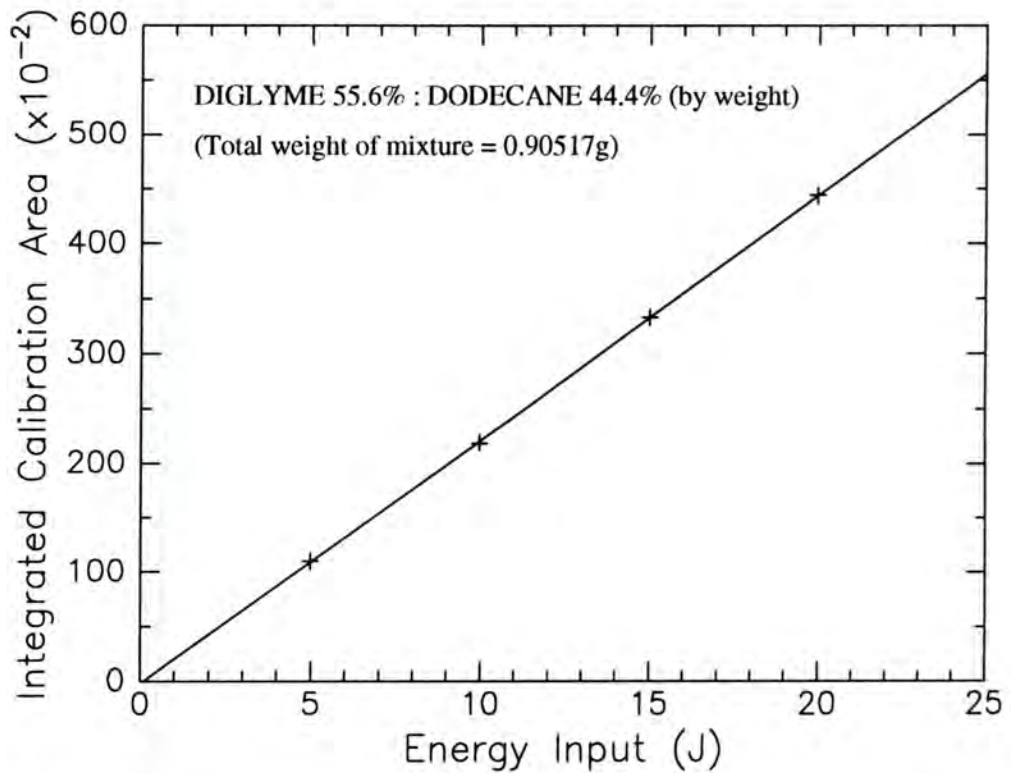


Figure 7.3 : Electrical Calibration in Diglyme:Dodecane blends at 301.95K

7.7.2 Polystyrene : Polybutadiene Blends

Oligomeric samples of polystyrene (PS) and polybutadiene (PBD) of peak average molecular weights 980 and 760 respectively, were supplied by Polymer Laboratories. Each polymer had a quoted polydispersity of 1.09. The heat change on blending these polymers at 341.45K were to be compared with reported literature results on a very similar system (PS1010 and PBD960 blends at 343.25K¹³) to give another indication of the accuracy of the calorimeter.

From ¹³C nmr analysis (Table 7.5), the structure of the PBD760 was very similar to the PBD960 polymer used in the original heat of mixing experiments¹³.

Assigned Structure	PBD 760 Mole %	PBD 960 Mole % (Original Sample)
Trans 1, 4	47	49
Cis 1, 4	37	36
Vinyl 1, 2	16	15

Table 7.5 : ¹³C nmr analysis on poly(butadiene) samples

Initial mixing experiments between the PS980 and PBD760 polymers showed an initial sharp endotherm followed by a large exothermic interaction which appeared to increase in magnitude as the PBD760 concentration increased. As the PBD760 alone produced a large exotherm on gentle agitation in the calorimeter cell, polymer oxidation was suspected at the blend temperature which was accelerated due to the increased aeration from agitation. An antioxidant (2,6-di-tert-butyl-4-methyl phenol) was therefore added to the PBD760 at 0.5%w/w and the blending experiments repeated. Blends containing antioxidant showed, as before, an initial endothermic heat change on mixing but no subsequent exothermic interaction.

Calibration of the blend was carried out as per the literature i.e. in a 50:50 wt.% blend composition ratio (Table 7.6). Figure 7.4 shows the calibration profiles and a typical blend thermogram. From this calibration, heat of mixing values at various compositions were determined (Table 7.7) and compared to the profile of the analogue blend system¹³ (Figure 7.5). Due to a shortage of the PS and PBD samples, multiple measurements to determine error limits have not been possible and only single heat change values are shown. However, the agreement between the two heat of mixing data sets is very good and within the error bars quoted in the literature ($\pm 8\%$).

Energy (J)	Area (x 10 ⁻⁴)
0.5022	2440
0.9984	4780
1.5000	7190
2.0088	9750

Table 7.6 : Electrical Calibration - PS 980 (50.4 %^W/_w):PBD 760 (49.6 %^W/_w) at 341.45K (Total Weight of Mixture = 1.74978g)

PS 980 Wt. (g)	PS 980 (Vol. Fract.*)	PBD 760 Wt. (g)	PBD 760 (Vol. Fract.*)	Area (x10 ⁻⁴)	ΔH_{mix} (J/g mixture)
0.07188	0.0903	0.61257	0.9097	1600	0.4916
0.28098	0.2710	0.63873	0.7290	5040	1.1374
0.30370	0.4592	0.30225	0.5408	4350	1.4914
0.67701	0.6652	0.28797	0.3348	5120	1.1011
0.91209	0.8706	0.11452	0.1294	2040	0.4161

Table 7.7 : Heat of Mixing in PS 980 : PBD 760 blends at 341.45K

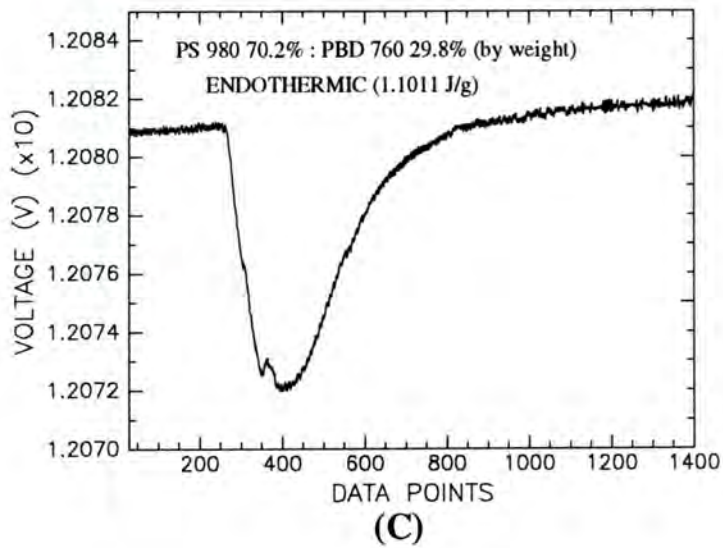
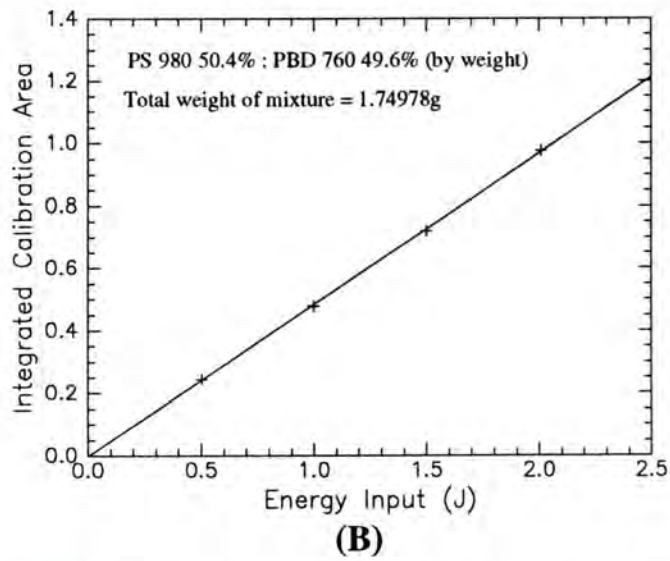
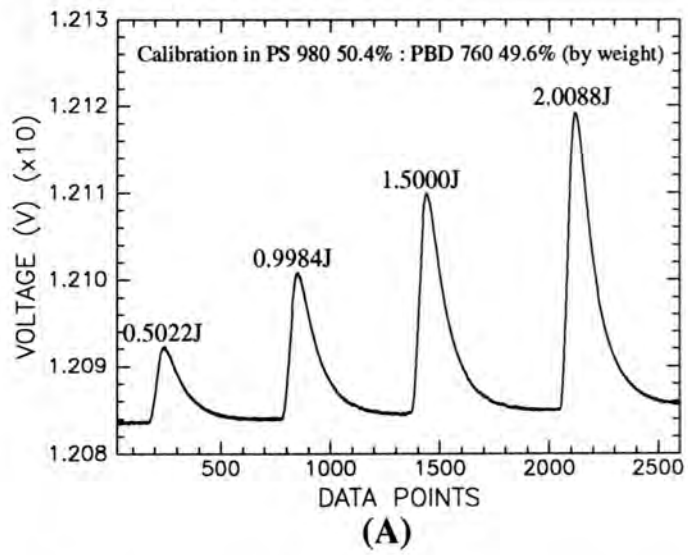


Figure 7.4 : PS980 : PBD760 Blends : Calibration Profiles (A,B) and typical Thermogram (C).

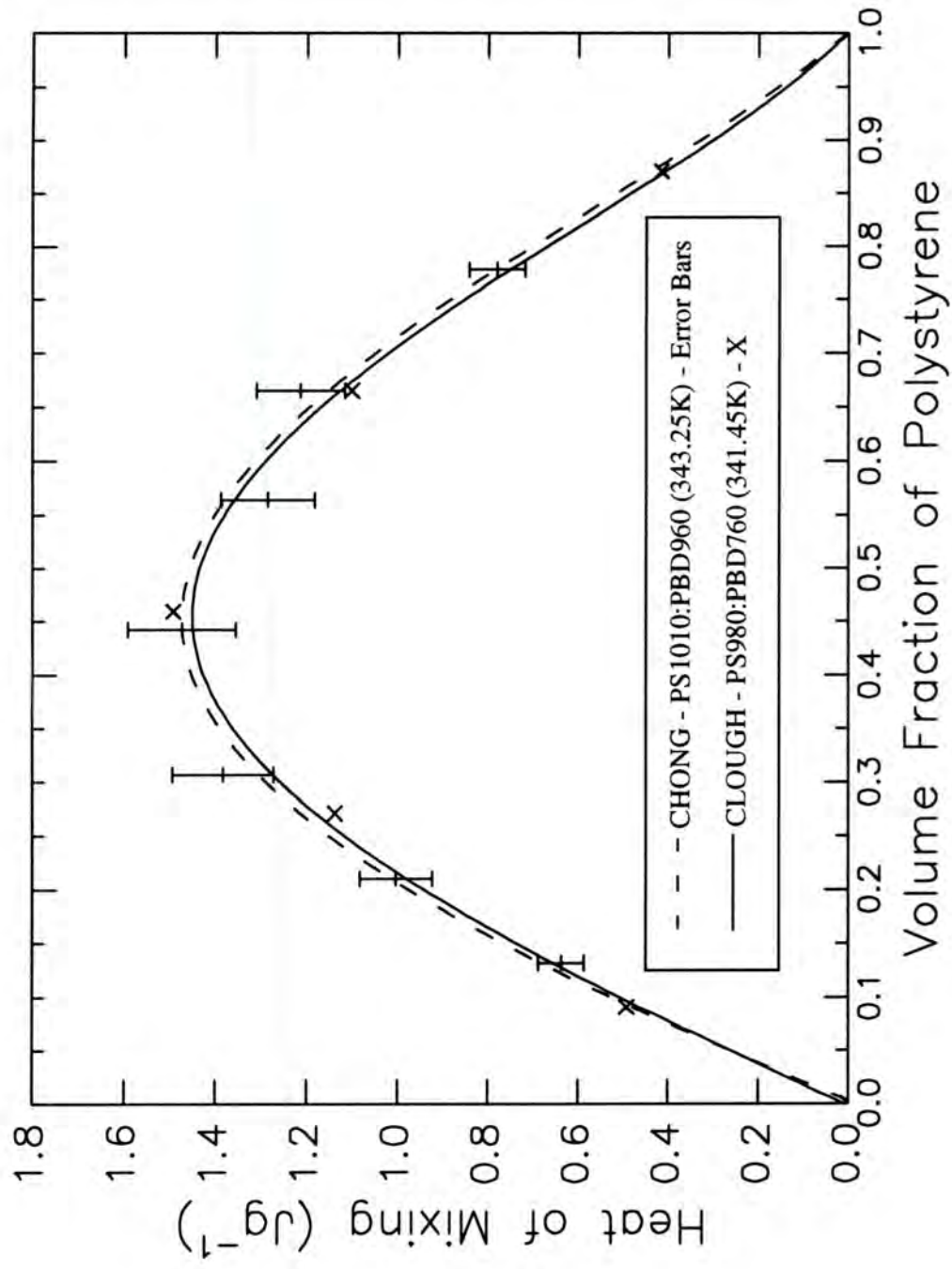


Figure 7.5 : Comparison of Heat of Mixing profiles in PS980:PBD760 and PS1010:PBD960 Blends

* From Polymer Handbook (Brandrup, Immergut) :

PS 980 Density = 1.04 - 1.065 g/cm³ (1.053 Av.)

PBD 760 Density = 0.890 g/cm³ (sec. butyl lithium initiator)

7.8 Heat of Mixing Results

The experimental heat of mixing values for the various blend systems are described in the following sections and have been normalised per unit gram of the total blend mixture. The error bars for these values which represent ± 1 standard deviation have been estimated from multiple measurements on the 50:50 wt.% blends. The enthalpic interaction parameter (χ) and free energy of mixing (ΔG_{mix}) values have been calculated from the Flory-Huggins expressions, eqns. 7.6 and 7.7 respectively.

Subsequent plots show enthalpic χ values per repeat unit of either EVA (in EVA:polymer blends) or docosane (in docosane:polymer blends). The number average degree of polymerisation i.e. repeat units, in EVA (86) is obtained from an average M_n value of 3020 and a vinyl acetate:ethylene molar ratio of 1:7 (see Chapter 3). Consequently, the enthalpic χ values for EVA:PE blends can be compared with χ values determined from small angle neutron scattering measurements (Chapter 9) as both techniques represent χ values per repeat unit or segment.

Heat of mixing results are shown in detail in Appendix B as Tables B.1-B.4 (EVA-polymer blends) and Tables B.5-B.9 (docosane-polymer blends).

7.8.1 Blank Heat Effects

Blank heat effects which are due to mechanical agitation of these polymers in the presence of a glass mixing ball and **not** specific close neighbour interactions were determined by loading both the sample holder compartments with the same component (one of which contained the glass mixing ball !) and carrying out a heat of mixing measurement.

In these experiments, the blank heat effects were all endothermic, due possibly to an increase in the vaporisation rate of solvent residues. The blank heat changes in EVA,

FVA and PI were very small ($< 0.01\text{J/g}$) and almost at the limit of the calorimeter detectability i.e. close to baseline noise. LMPI had a slightly greater blank heat effect of 0.016J/g . The heat effects from these components were considered to be negligible i.e. within experimental error compared to the heat of mixing values reported for the EVA-polymer blends.

However, the EXXON-supplied PE (docosyl diester of poly(ethylene glycol)) component had a significant endothermic blank heat effect of 0.11J/g . This commercial sample was believed to be unsuitable for "heat of mixing" experiments as ^{13}C nmr analysis indicated that it contained significant amounts of unreacted free docosanoic acid (up to 10%). Also, the molecular weight distribution of the poly(ethylene glycol) component was relatively wide due to the use of a range of molecular weights (M_p 200, 400 and 600) in the industrial esterification. This sample could therefore not be classified as a pure, standard component representative of the docosyl diester of poly(ethylene glycol). The ester used in the following calorimetry experiments was therefore prepared by the docosyl diesterification of poly(ethylene glycol) M_p 400 (Code NECPE - see Chapter 3 - experimental) and ^{13}C nmr showed no free acid impurities. The blank heat effect of this component had a smaller endotherm (approximately 0.05J/g) and the weighted fraction contribution of this "blank" was subtracted from the heat of mixing value of the blends.

The blank heat effect for docosane showed a small endothermic peak of heat change approximately 0.02J/g , but as this is within the experimental error of the docosane-polymer heat of mixing measurements (typically $\pm 2\text{-}6\%$ for values ranging $0.60\text{-}3.25\text{J/g}$) this correction was also considered to be negligible.

The blank heat effects of the toluene solvent used in the docosane and polymer solutions was very small and could not be determined from the electrical calibration i.e. $<0.001\text{J/g}$. No "blank heat" correction was therefore required.

7.8.2 EVA Blends with FVA, PI, LMPI and NECPE (Tables B.1-B.4)

Calibration of each blend was carried out at 5 compositions : 0.1, 0.3, 0.5, 0.7 and 0.9 EVA volume fraction. For each blend system apart from EVA:LMPI, heat of mixing values were determined at 9 composition ratios ranging from 0.1-0.9 EVA volume fraction, using a calibration of the most applicable composition. Heat of mixing for the EVA:LMPI blend was determined at 5 composition ratios (0.1-0.9 EVA volume fraction) using again the most suitable calibration graph.

The effect of blend composition changes on the calibration graphs was negligible and considerably less than the errors noted in multiple analysis on the 50:50 wt.% blends (\pm 1 standard deviation based on a small sample population).

In all the EVA based-polymer blends, the heat of mixing was endothermic with a maximum heat change of approximately 0.15J/g (EVA:FVA) and 0.40J/g (EVA:PE, EVA:PI and EVA:LMPI) as shown in Figures 7.6 and 7.7. Examples of the calorimeter thermograms for each blend system are shown in Figure 7.8.

EVA blends with FVA, PE, PI and LMPI had heat of mixing standard deviations of 9%, 7%, 3% and 5% respectively, calculated from at least 3 measurements on the 50:50 wt.% composition ratio. The larger error in the EVA:FVA blend was attributed to the high molecular weight and polydispersity of the FVA polymer resulting in a high melt viscosity and possibly lower thermal conductivity.

The calculated interaction parameters and the free energy of mixing values for each of these blends are shown in Figures 7.9-7.11.

7.8.3 Docosane Blends with EVA, FVA, PI, LMPI and NECPE (Tables B.5-B.9)

Calibration of each blend was carried out at 3 compositions, 0.1, 0.5 and 0.9 EVA volume fraction. For each blend system, heat of mixing values were determined at 5 composition ratios ranging from 0.1-0.9 EVA volume fraction using the most applicable calibration. As in the EVA-polymer blends, changes in the blend composition had negligible effect on the calibration graph.

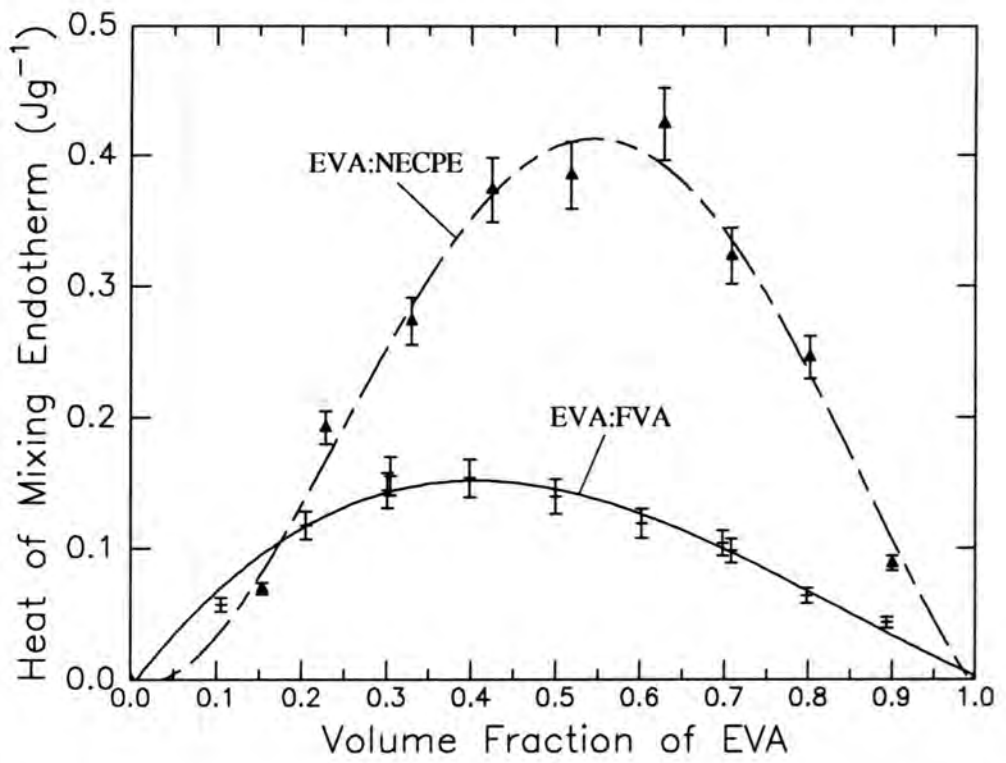


Figure 7.6 : Heat of Mixing measurements in EVA:FVA and EVA:NECPE Blends

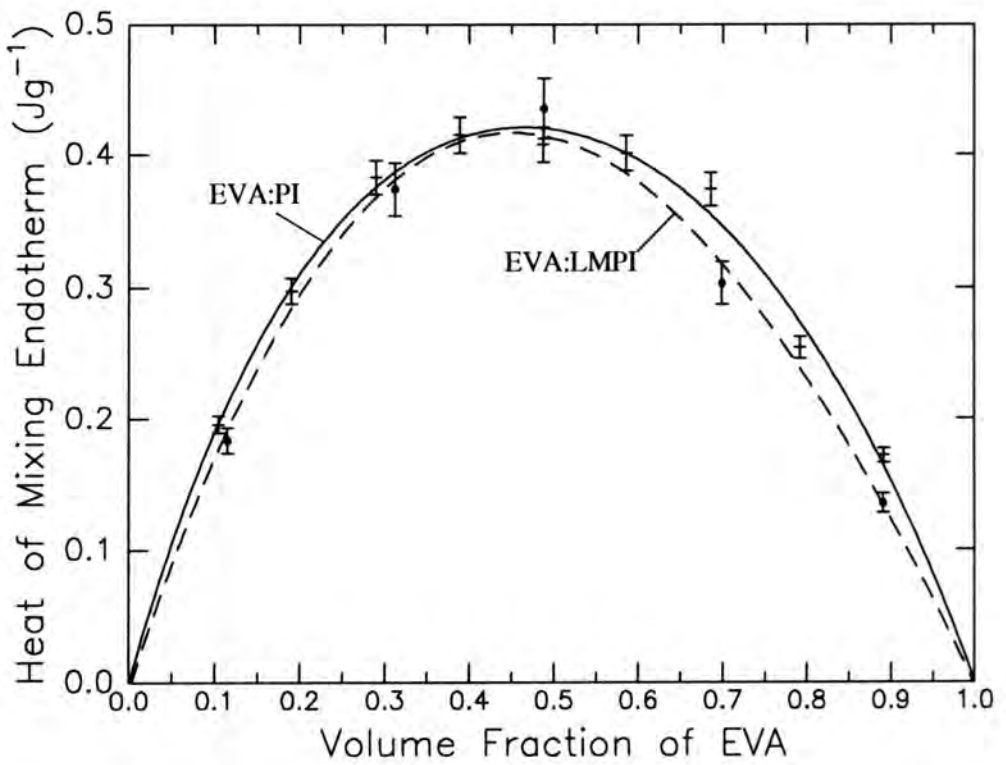


Figure 7.7 : Heat of Mixing measurements in EVA:PI and EVA:LMPI Blends

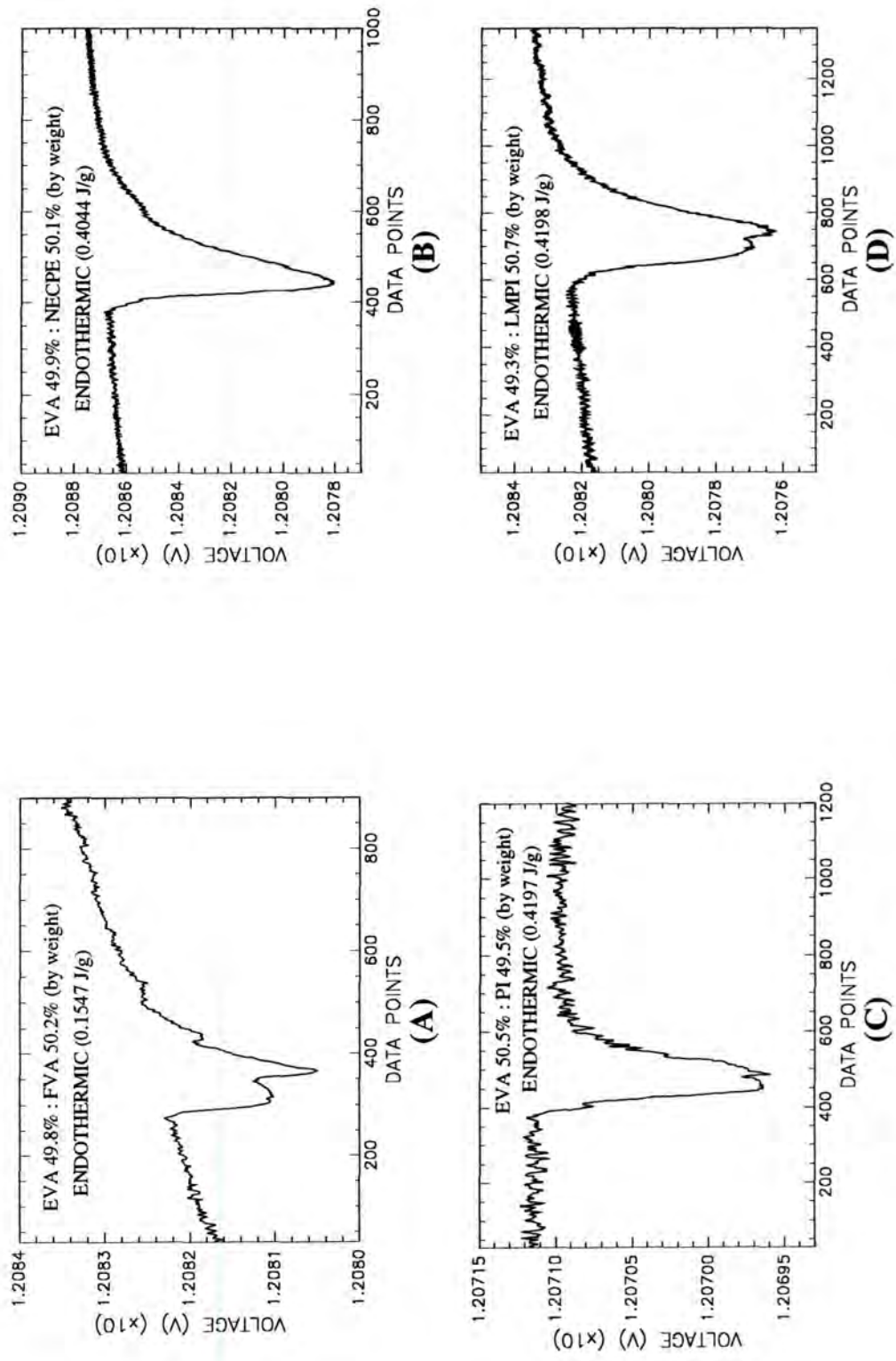


Figure 7.8 : Thermograms of EVA:FVA (A); EVA:NECPE (B); EVA:PI (C) and EVA:LMPI (D) Blends.

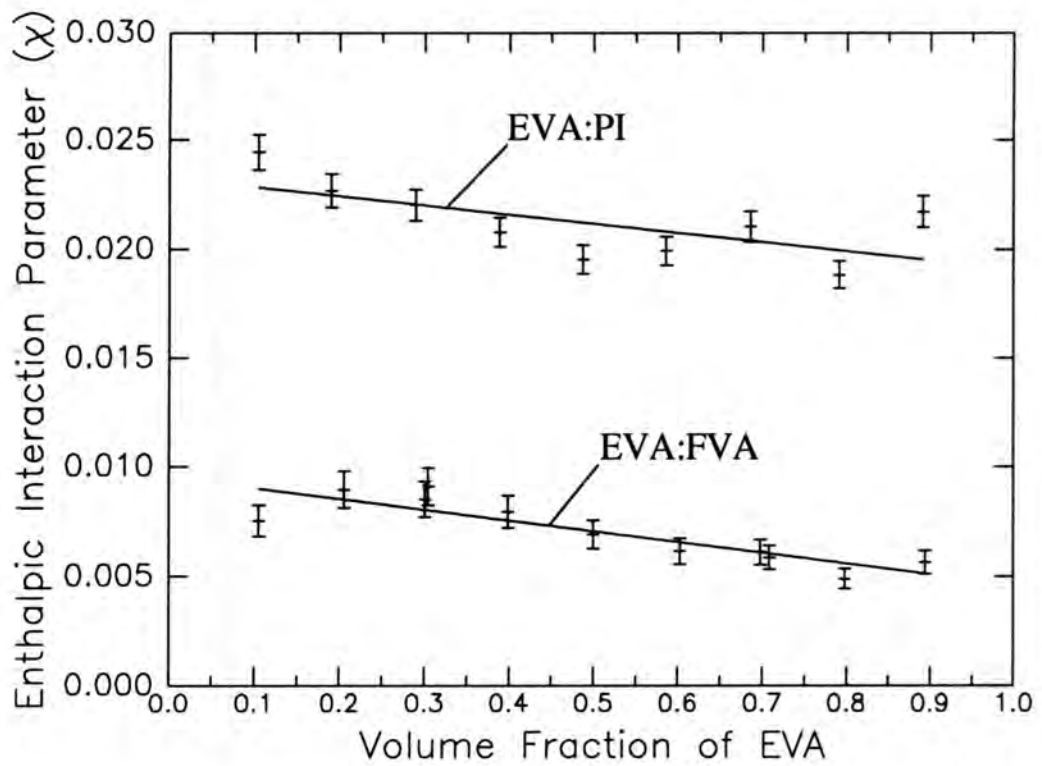


Figure 7.9 : Enthalpic Interaction Parameters (χ) in EVA:FVA and EVA:PI Blends.

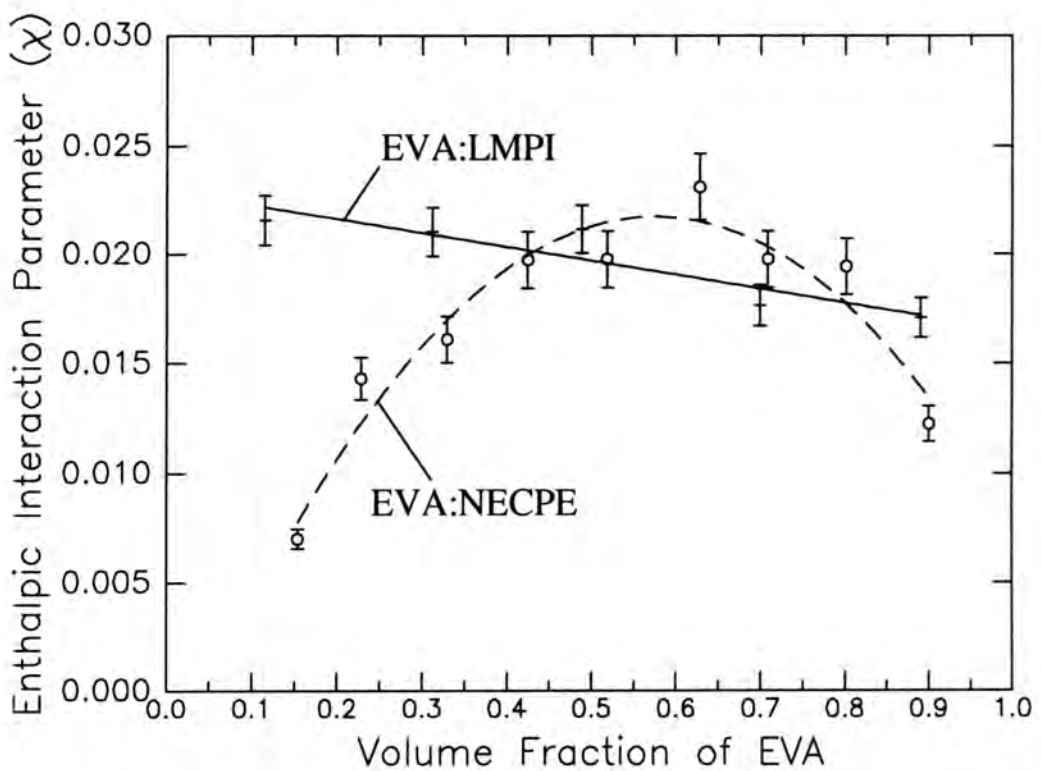


Figure 7.10 : Enthalpic Interaction Parameters (χ) in EVA:NECPE and EVA:LMPI Blends.

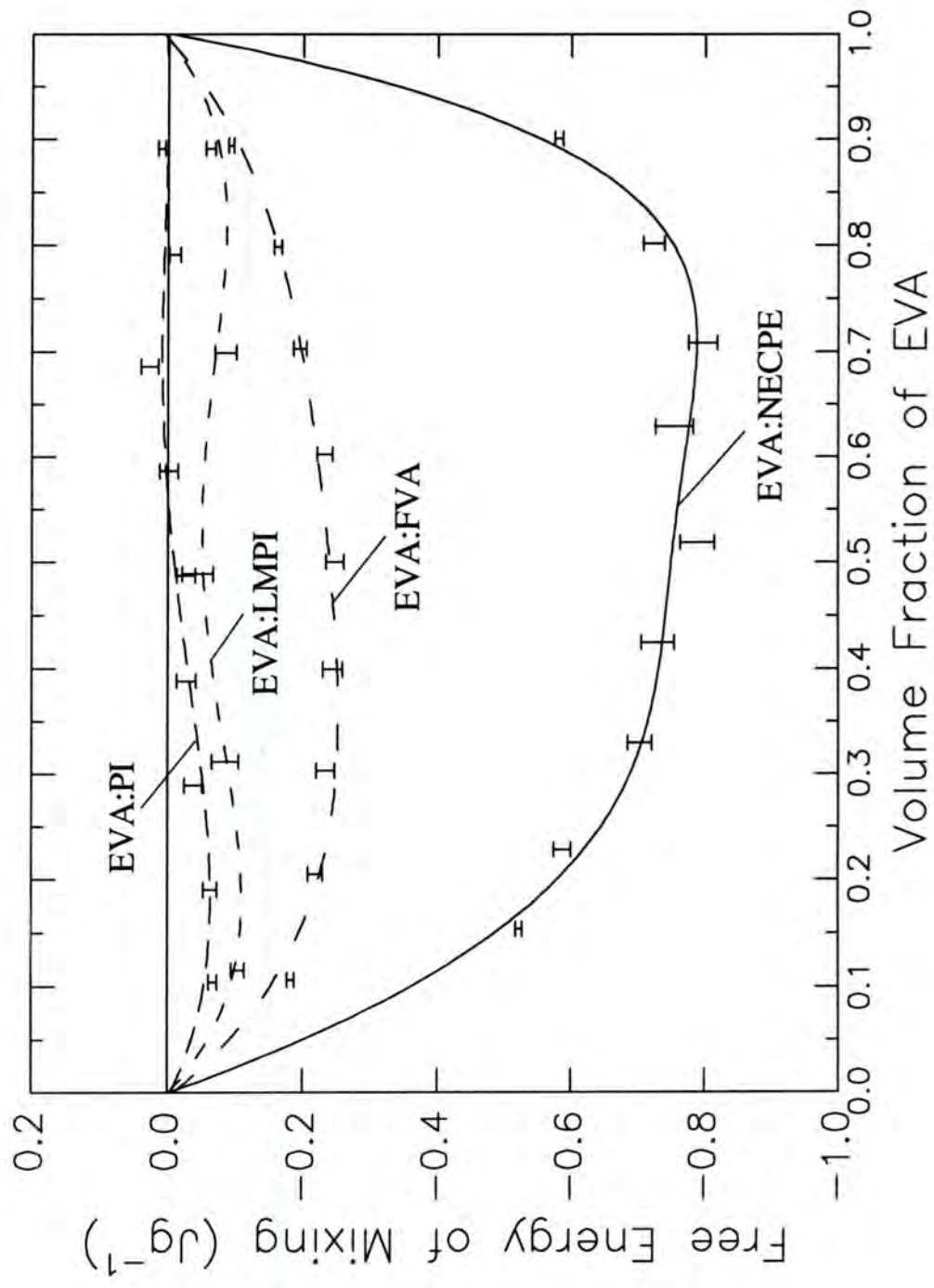


Figure 7.11 : Free Energy of Mixing values in EVA:FVA, EVA:NECPE, EVA:PI and EVA:LMPI Blends.

All blends had endothermic heat of mixing values with large maximum heat changes of approximately 0.60J/g (docosane:PI) to 3.25J/g (docosane:NECPE), as shown in Figure 7.12. From multiple measurements, typical standard deviations ranged from 2-6%. Examples of the calorimeter thermograms for each blend system are shown in Figure 7.13.

The calculated interaction parameters and free energy of mixing values for these blends are shown in Figures 7.14 and 7.15 respectively.

7.8.4 Solution Blending of Docosane with EVA, FVA, PI, LMPI and NECPE (in toluene solvent)

Docosane and polymer solutions were prepared in Analar toluene solvent of concentration $\approx 10\%$ w/w. Electrical calibration was carried out in Analar toluene. Heat of mixing values due to solution blending were determined at the 50:50 wt.% composition ratio.

In all the blends of docosane and polymer solutions, the heat of mixing was small (typically $3-7 \times 10^{-2}$ J/g) and endothermic (Table 7.7).

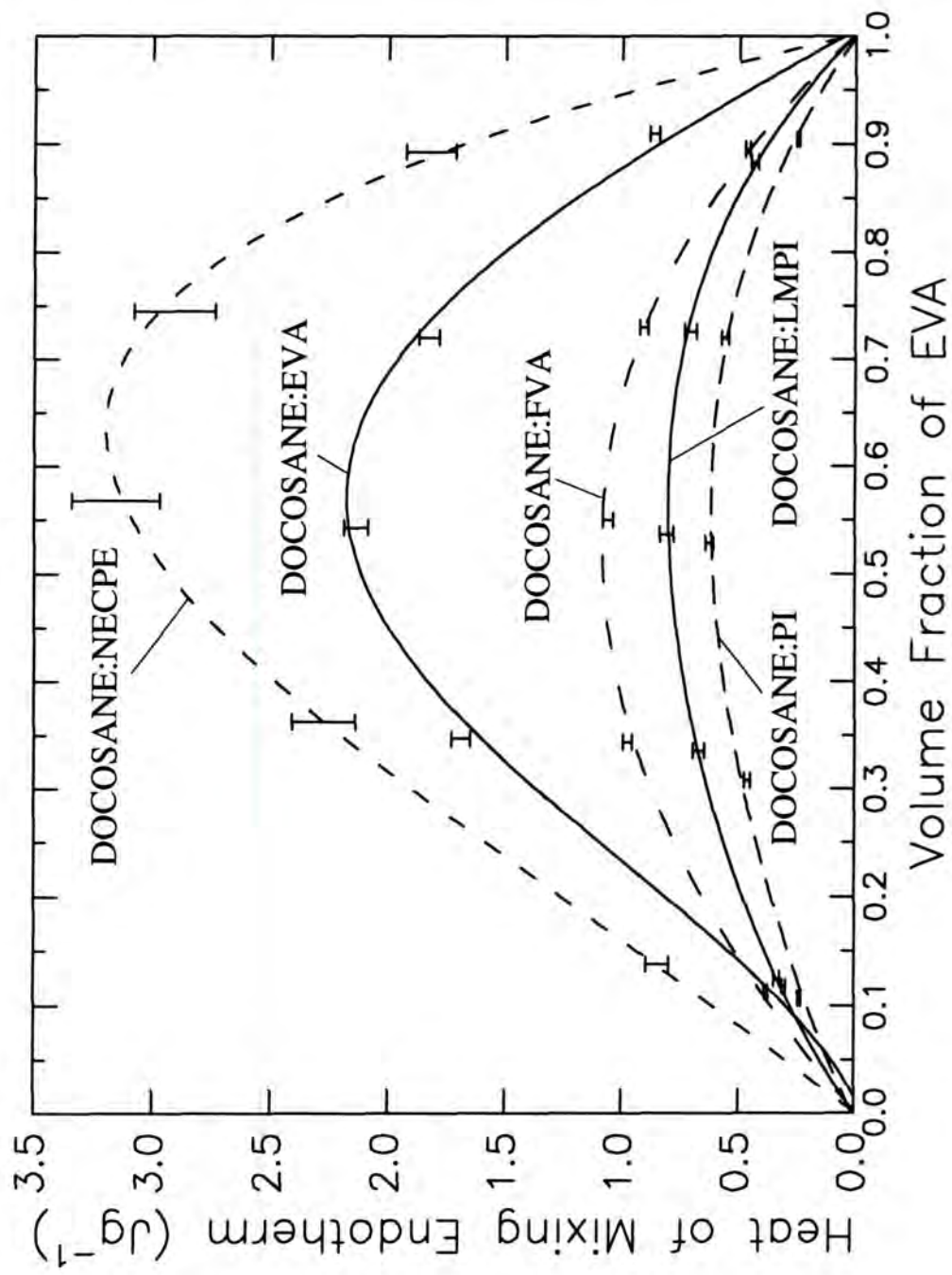
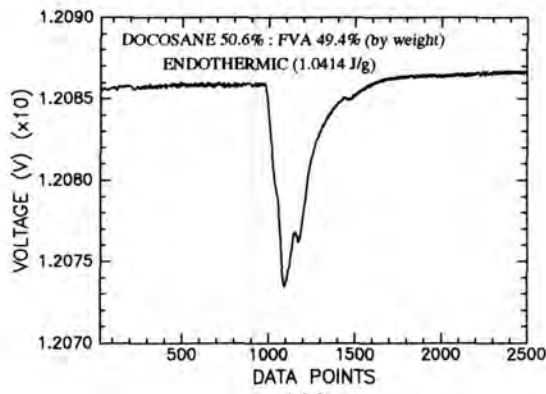
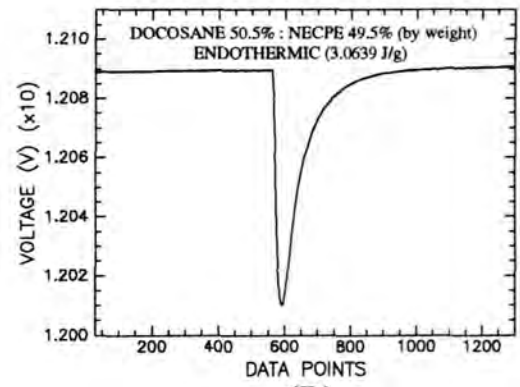


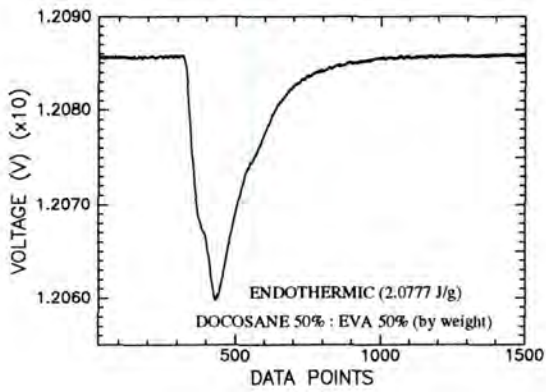
Figure 7.12 : Heat of Mixing measurements in Docosane blends with NECPE, EVA, FVA, LMPI and PI.



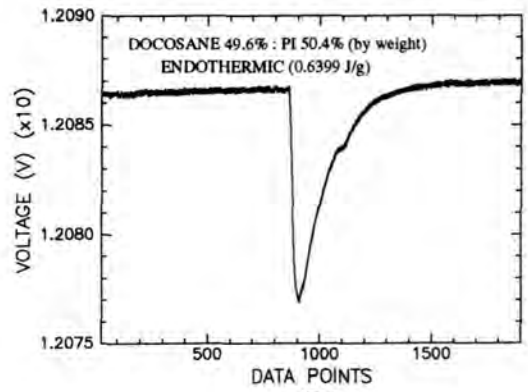
(A)



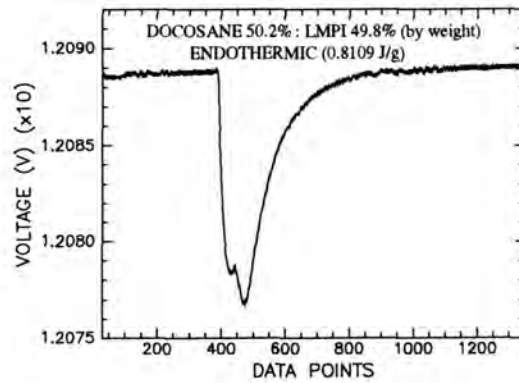
(B)



(C)



(D)



(E)

Figure 7.13 : Thermograms of Docosane Blends with FVA (A); NECPE (B); EVA (C); PI (D) and LMPI (E).

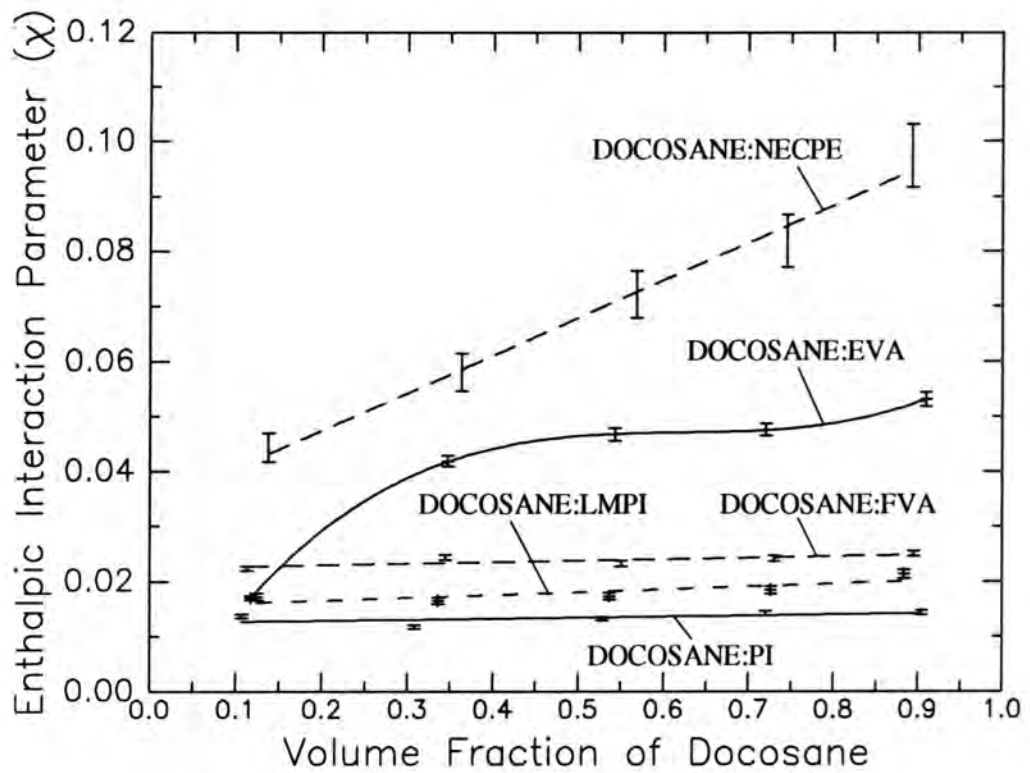


Figure 7.14 : Enthalpic Interaction Parameters (χ) in Docosane blends with NECPE, EVA, FVA, LMPI and PI.

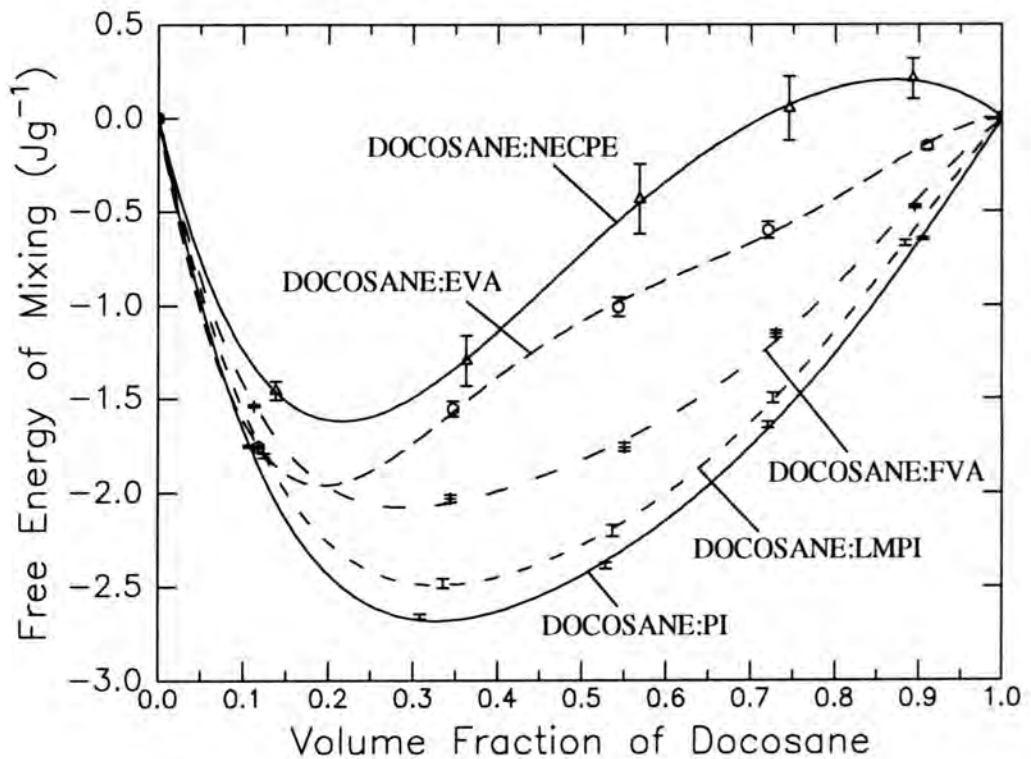


Figure 7.15 : Free Energy of Mixing values in Docosane blends with NECPE, EVA, FVA, LMPI and PI.

Blend Solutions Wt. (g)	Polymer Wt. (g) (Solution Concentration % ^{w/w})	ΔH_{mix} Meas. ($\times 10^{-2}\text{J}$)	ΔH_{mix} ($\times 10^{-2}\text{J/g}$)
EVA 0.43398 C22 0.42590	0.04344 (10.01) 0.04344 (10.20)	4.80	5.58
LMPI 0.43398 C22 0.42573	0.04348 (10.02) 0.04342 (10.20)	2.74	3.19
NECPE 0.43423 C22 0.42649	0.04325 (9.96) 0.04350 (10.20)	6.20	7.20
FVA 0.43694 C22 0.42589	0.04396 (10.06) 0.04344 (10.20)	5.30	6.14
PI 0.43456 C22 0.42657	0.04376 (10.07) 0.04351 (10.20)	4.17	4.84

Table 7.7 : Heat of Mixing in Docosane-polymer solutions

7.9 Discussion

The true miscibility in blends can only be characterised by considering the free energy of mixing (ΔG_{mix}) which incorporates both enthalpic and entropic contributions. The Flory-Huggins lattice theory assumes that the configurational entropy is the only contribution to the entropy change on mixing and equals ΔS_{mix} . For high molecular weight **linear** molecules, this term is small as the number of possible configurations that the chains can adopt on the lattice is small. In this case, the free energy term will be dependent on the enthalpic contribution (ΔH_{mix}) with a negative (exothermic) ΔH_{mix} value resulting in a negative ΔG_{mix} which satisfies one of the two criteria for miscibility to occur (eqns. 7.2, 7.3). However, for low molecular weight mixtures, the entropic contribution becomes more significant and favourable to miscibility. Therefore, in the diglyme:dodecane mixture which is used to establish the accuracy of the calorimeter measurements, the heat of mixing is endothermic which suggests (based on the enthalpic contribution) that the blend favours immiscibility, but due to the small oligomeric-type chain lengths involved, the configurational entropy contribution dominates in this system, resulting in a negative ΔG_{mix} value and blend miscibility¹².

However, branching in polymers which produce in effect low-molecular weight "side-arms", can make a large contribution to the entropy of mixing and this is not accounted for in the lattice theory. A highly branched polymer of high molecular weight may have an entropic contribution closely resembling that of a low molecular weight linear polymer by virtue of a similar concentration of chain (or branch) ends. Thus, it is likely that in the blends containing branched aliphatic polymer chains i.e. FVA, PI and LMPI, the calculated ΔG_{mix} values from the lattice theory maybe inaccurate. Also, the effect of polydispersity is not accounted for in the original lattice theory and this may significantly effect the ΔG_{mix} value, especially in the case of FVA which has a high polydispersity value of approximately 4.

Heats of mixing in all the studied blend systems was endothermic (+ve ΔH_{mix}) and therefore the resulting enthalpic interaction parameter (χ) values are positive. Thus, the blends appear to favour immiscibility taking into account only the enthalpic component.

Positive enthalpic interaction parameters have also been "predicted" for the EVA-polymer blends from the DSC melting point depression analysis (Chapter 4). Additionally, positive enthalpic χ values have been determined for EVA:PE blends from small angle neutron scattering measurements and these values (per polymer segment) agree in magnitude to those obtained from heat of mixing calorimetry (see Chapter 9).

For the EVA-polymer blends, the dependence of χ on composition (Figures 7.9, 7.10) indicates that EVA blends with branched polymers i.e. FVA, PI and LMPI have χ values which appear to show a slight linear decrease on increasing EVA volume fraction. However, in the EVA:NECPE blends, χ has a much greater concentration dependence as shown by the pronounced curvature of the χ values as a function of the EVA volume fraction. It has been suggested^{5,12} that the linear concentration dependence of enthalpic χ values can be understood in terms of the surface area ratio of the interacting segments (from each of the blend components). Therefore, the linear composition dependence of the enthalpic χ values in the EVA:FVA, EVA:PI and EVA:LMPI blends may possibly be due to differences in the size and shape of the separate polymer component segments which are thought to be considerable due to the large degree of branching in the FVA, PI and LMPI components¹⁴. However, surface area effects on free energy χ values still do not account for some of the complex phase diagram shapes¹⁵. In contrast, the "average" segment surface area difference in the EVA:NECPE blends is much smaller¹⁴ and not believed to be significant. Therefore, the curvature of the enthalpic heat of mixing χ values versus composition profile of the EVA:NECPE blend cannot be described by the Flory-Huggins lattice theory (based on random mixing of polymer chains) or surface area differences alone. In similar systems it has been speculated^{5,12} that this curvature is attributed to non-random mixing of the polymer chains due to the quasi-chemical interaction of polymer segments which from large, positive interchange energies result in volume changes.

There is some justification for believing that the theory of non-random mixing may be applicable to the EVA:NECPE blends. EVA and NECPE are regarded as copolymers with EVA having ethylene (84 mole %) and vinyl acetate (16 mole %) segments whilst

NECPE has docosane and poly(ethylene glycol) "block" segments. Therefore, as both components have polar and non-polar segments **along** the polymer chain, they are likely to have unfavourable interactions between segments of the same polymer. Consequently, on blending the EVA and NECPE components, a "driving force" towards reducing the number of these interactions may result in a degree of "order" during mixing i.e. non-randomness. Several authors^{16,17} have reported that these copolymer-type blends are likely to be miscible due to *intramolecular* rather than *intermolecular* interactions. This effect is displayed by some EVA copolymers which are miscible with poly(vinyl chloride) whereas polyethylene and poly(vinyl acetate) homopolymers are immiscible with poly(vinyl chloride)¹⁸. Therefore, it is suggested that the curvature of the enthalpic χ values with composition as observed in the EVA:NECPE blends may possibly be due to non-random mixing between the components due to unfavourable polar and non-polar interactions along the polymer chain of both components. In contrast, EVA blends with the branched polymers, FVA, PI and LMPI appear to indicate random mixing i.e. reasonably constant χ values with no pronounced curvature which maybe due to the difference in polarity type between these polymers and NECPE i.e. PI and LMPI are homopolymers with each repeat segment having branched octadecyl ester links to a poly(itaconic acid) backbone and the polarity of this segment is constant along the polymer chain rather than the distinct polar and non-polar "blocks" as in NECPE (and EVA). Similarly, the polarity of FVA which is a strictly alternating copolymer of tetradecylfumarate and vinyl acetate, is also thought to be constant along the polymer chain. Therefore, these results suggest that when blended with EVA, changes in polarity type between the essentially linear (NECPE) and branched (FVA, PI and LMPI) polymers may determine the type of mixing at a molecular level. The composition dependence of χ values is discussed further in Chapter 9 - using small angle neutron scattering data.

The calculated ΔG_{mix} values for these EVA-polymer blends (Figure 7.11) taking into account the configurational entropy contribution, suggests that the EVA:NECPE blend is miscible with large, negative ΔG_{mix} values (satisfying one of the miscibility criteria,

eqn. 7.2). In contrast, the EVA:PI blend appears to have ΔG_{mix} values bordering on the immiscibility boundary i.e. $\Delta G_{\text{mix}}=0$. EVA:FVA and EVA:LMPI blends have larger, negative ΔG_{mix} values than the EVA:PI and would be expected to have greater miscibility. However, although the ΔG_{mix} versus composition profile for the EVA:LMPI blend is negative at all points, the shape of the profile is such that within a certain composition range at 341.45K, there is a possibility that eqn. 7.3 may not be satisfied and immiscibility may occur within this range. However, in the EVA:LMPI blend, only 5 free energy values are available and ideally, further compositions should be evaluated to confirm this free energy profile.

DSC melting point depression analysis (Chapter 4) and Optical Microscopy (Chapter 5) also agree with these predictions i.e. at the melt temperature, the EVA:NECPE blend is very miscible, the EVA:PI blend has little or no miscibility and that the miscibility of the EVA:FVA, EVA:LMPI blends lies between these two extremes.

As all the EVA-polymer blends have positive (endothermic) heat of mixing values which favour immiscibility, it is clear that to achieve miscibility, the entropic contribution must be favourable and dominate. This suggests that the miscibility of the EVA:NECPE blend is due to the very low molecular weight of the NECPE component which subsequently results in a large configurational entropy contribution, favourable to miscibility.

The effect of molecular weight on the final miscibility can clearly be seen by comparing EVA blends with polyitaconate samples of slightly different molecular weight i.e. PI (M_n 9900) and LMPI (M_n 6600). As expected, the heat of mixing values of both blends is essentially identical (Figure 7.7) but due to the larger configurational entropy contribution from the lower molecular weight LMPI, the resulting larger, negative ΔG_{mix} values for the EVA:LMPI blend indicate greater miscibility than the EVA:PI blend. The increase in miscibility due to a slight decrease in the molecular weight of the polyitaconate from M_n 9900 to M_n 6600 has also been shown by Optical Microscopy (Chapter 5) and DSC melting point depression analysis (Chapter 4).

Docosane-polymer blends have much larger endothermic heat of mixing values than the EVA-polymer blends (Figure 7.12) but due to the very large configurational entropy contribution from the low molecular weight docosane component, these blends all show larger, negative ΔG_{mix} values than the EVA-polymer blends (Figure 7.15). Therefore, it can be predicted that these docosane-polymer blends are all highly miscible, although the docosane:NECPE blend at high docosane volume fractions may become immiscible if the ΔG_{mix} value becomes positive. Docosane blends with NECPE and EVA have the largest heat of mixing values of the docosane based polymer blends and the resulting enthalpic interaction parameters decrease as the volume fraction of docosane decreases. In contrast, the highly branched polymers i.e. FVA, PI and LMPI have relatively small heat of mixing values and the resulting enthalpic interaction parameters appear (as in the EVA-based blends) to be essentially independent of concentration (Figure 7.14) as predicted by the Flory-Huggins theory. It is interesting to note that again the large composition dependence of enthalpic χ values in docosane-polymer blends is associated with the EVA and NECPE polymers which have both polar and non-polar segments **along** the chain.

For all the blends studied in the melt state, the heat of mixing is endothermic and enthalpically, these blends favour immiscibility. Miscibility can therefore only be achieved by a large, dominant and favourable entropic contribution presumably from a low molecular weight component as in the case of the EVA:NECPE and docosane-based blends.

Blending of docosane and polymer solutions in toluene result in very small heat of mixing endotherms, close to the detectability limit of the calorimeter. At these solution concentrations ($\approx 10\% \text{w/w}$) these interactions are sufficiently small that significant measurement errors are expected. Therefore, the solution blending technique of monitoring interactions in a common solvent system appears to be practical only in blend systems which either show a significantly large interaction or for components which have sufficiently high melt viscosities and/or melting point that direct melt blending is not possible.

7.10 **References**

1. K.Solc, Ed., "Polymer Compatibility and Incompatibility - Principles and Practices", Harwood Academic, New York (1982).
2. Y.Jinghua, G.C.Alfonso, A.Turturro and E.Pedemonte, *Polymer*, 34, 1465 (1993).
3. C.J.T.Landry and D.M.Teegarden, *Macromolecules*, 24, 4310 (1991).
4. G.Allen, Z.Chai, C.L.Chong, J.S.Higgins and J.Tripathi, *Polymer*, 25, 239 (1984).
5. J.K.H.Al-Kafaji, Z.Ariffin, J.Cope and C.Booth, *J. Chem. Soc., Faraday Trans. 1*, 81, 223 (1985).
6. C.A.Cruz, J.W.Barlow and D.R.Paul, *Macromolecules*, 12, 726 (1979).
7. C.Zhikuan, S.Ruona, D.J.Walsh, and J.S.Higgins, *Polymer*, 24, 263 (1983).
8. P.N.Aukett and C.S. Brown, *Journal of Thermal Analysis*, 33, 1079 (1988).
9. F.E.Karasz and W.J.Macknight, *Pure Appl. Chem.*, 52, 409 (1980).
10. A.Brunacci, J.Yin, E.Pedemonte and A.Turturro, *Thermochimica Acta*, 227, 117 (1993).
11. P.J.Flory, "Principles of Polymer Chemistry", Cornell University Press (1953).
12. J.K.H.Al-Kafaji and C.Booth, *J. Chem. Soc., Faraday Trans. 1*, 79, 2695 (1983).
13. C.Chong, PhD Thesis, Imperial College of Science and Technology (1981).
14. D.W.Van Krevelen, "Properties of Polymers", Elsevier (1972).
15. G.Allen and J.C.Bevington, Vol 7, "Comprehensive Polymer Science", Pergamon Press, (1989).
16. D.R.Paul and J.W.Barlow, *Polymer*, 25, 487 (1984).
17. G.ten Brinke, F.E.Karasz and W.J.MacKnight, *Macromolecules*, 16, 1827 (1983).
18. C.F.Hammer, *Macromolecules*, 4, 69 (1971).

CHAPTER 8

WIDE ANGLE X-RAY SCATTERING (WAXS)

8.1 Introduction

X-ray scattering is a widely used technique in the study of polymer structures^{1,2,3}. Scattering occurs as a result of interaction with electrons in the material which produce diffraction patterns that vary with the scattering angle. Consequently, the terms "scattering" and "diffraction" are both commonly applied to describe X-ray techniques. X-ray scattering (or diffraction) techniques are generally categorised into wide angle X-ray scattering (WAXS) and small angle X-ray scattering (SAXS), with polymer structure information obtained at large and small scattering angles respectively. WAXS is generally used to characterise structures on a scale of 10Å or smaller whereas SAXS has a much wider scale of 10-10⁴Å. The instrumentation and data analysis of these two techniques are very different although the basic X-ray scattering principles are the same.

In this study, WAXS has been used primarily to determine the degree of crystallinity in FVA, PE and PI polymers. From these crystallinity values and the enthalpies of fusion (from DSC measurements), the enthalpy of fusion for a theoretical 100% crystalline polymer (ΔH_f) can be predicted. Values of ΔH_f for each semi-crystalline polymer have subsequently been incorporated into the Nishi-Wang expression for determining the Flory-Huggins blend interaction parameter, χ , using melting point values (Chapter 4).

WAXS analysis has also been used to indicate possible crystallisation effects on blending "amorphous" EVA with these crystalline polymers and to relate and identify the two separate crystalline phases in PE (noted in DSC measurements - Chapter 4) to their corresponding diffraction profiles.

8.2 Theory

When X-rays of a given wavelength interact with electrons in an atom, the incident X-rays are scattered coherently and incoherently. Coherent scattering occurs when the electrons are so tightly bound to the atomic nuclei that no energy exchange occurs. Consequently, the coherent scattering shows no change in the incident X-ray wavelength and can be utilised for structural studies. In contrast, incoherent scattering involves a loss in energy of the photon to the electron i.e. absorption, which results in a change in the wavelength of the scattered beam. In diffraction studies, incoherent scattering is present as a continuous background which needs to be subtracted during measurements to obtain accurate information about crystallinity.

The basic WAXS principle is based on a procedure devised by Bragg⁴, in which crystals were used as diffraction gratings for monochromatic X-rays. Bragg related the path length difference between two X-ray beams which are in phase after diffraction ($2d(\sin\theta)$) to a whole number of wavelengths ($n\lambda$) giving the classical Bragg equation :

$$n\lambda = 2d(\sin\theta) \text{ (at maximum diffraction)} \quad (8.1a)$$

where n is an integer, λ is the X-ray wavelength, d represents the distance between successive crystalline lattice planes (generally known as the d -spacing) and θ is the glancing angle at which diffraction occurs. The scattering angle i.e. the direction of the scattered beam in relation to the incident beam is customarily denoted by 2θ .

The validity of eqn. 8.1a is demonstrated using Figure 8.1 which shows X-rays of wavelength λ impinging at an angle θ on two adjacent crystallographic planes (1 and 2) separated by an interplanar distance, d . The path length difference between the X-rays diffracted by planes 1 and 2 is $2b$. From this geometry, it is clear that the diffracted waves from the two planes will be in phase when :

$$n\lambda = 2b = 2d(\sin\theta) \quad (8.1b)$$

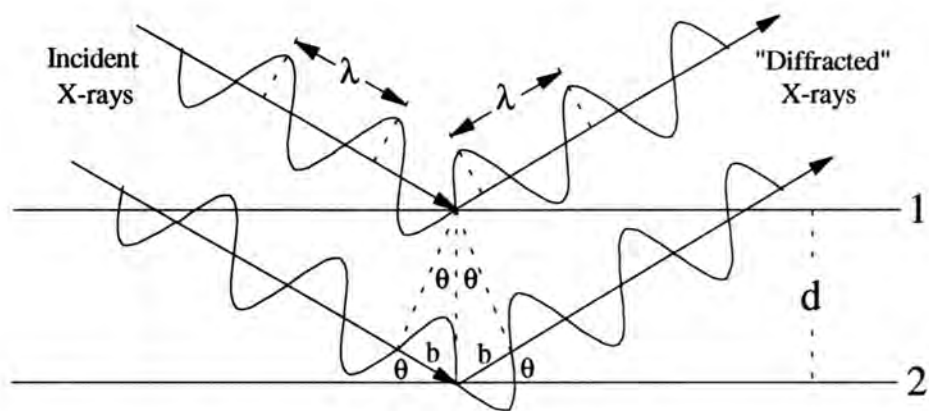


Figure 8.1 : Geometry of the Bragg Equation

Figure 8.1 shows the case where $n=1$, i.e. first order diffraction from the given planes. At particular, larger values of θ , n will equal 2, 3, 4... giving second, third, fourth orders etc. from the same set of crystallographic planes.

From this relationship, WAXS using various scattering angles (2θ) and known X-ray wavelength produces "diffraction patterns" of the various crystalline phases present. From suitable background subtraction of these patterns, the d -spacings can be measured and the level of crystallinity calculated to give information on the crystal structure and size.

X-rays used in structure characterisation generally have wavelengths in the range 0.5-2.5Å. In this study (as for most polymeric samples) a CuK_α emission line is used with an average wavelength of 1.54Å.

8.3 Determining Crystallinity in Polymers

Although various methods are available for determining the degree of crystallinity in semi-crystalline polymers³, wide angle X-ray scattering is the most fundamental and absolute method². This is because the basic concept of crystallinity i.e. a two-phase model consisting of crystalline and amorphous regions can clearly be shown by X-ray scattering patterns. The amorphous phase is identified by a broad diffuse scattering pattern - the "amorphous halo" whereas the crystalline phases produce scattering only at well defined 2θ angles.

In contrast to low molecular weight materials, the crystalline diffraction profiles of polymers generally show peak broadening due to crystal imperfections. Nevertheless, scattering patterns can generally distinguish between the crystalline and amorphous phases. However, the major problem in using WAXS to determine accurate crystallinity values is associated with separation of these crystalline and amorphous phases.

Various X-ray methods are available for determining the crystallinity of a polymer from the diffraction intensities of the separate amorphous and crystalline phases⁵⁻⁸ which are generally based on two techniques, external or internal comparison. In determining the degree of crystallinity from X-ray diffraction patterns, it is generally assumed that the interface regions between the crystalline and amorphous phases are negligible and that the scattering capability (integrated intensity) of these two phases in the same polymer are similar.

8.3.1 External Comparison

The determination of crystallinity was first treated using external comparison methods over 40 years ago^{9,10} and the basic principles are still in use today. These methods essentially use the intensity of one of the components in a sample i.e. usually the amorphous phase and compare it with the intensity of that component in a 100% concentration i.e. a "reference" pattern. These methods are generally used in cases where 100% amorphous "reference" samples can be obtained either by rapid quenching of the sample from the melt e.g. poly(ethylene terephthalate)⁸ or by controlling the sample temperature above the melting point^{1,2}. Although the 100% amorphous reference may differ in some details from the amorphous halo in the crystalline sample, it is expected that the integrated intensities of these phases will be very similar. Therefore, after suitable background subtractions, the integrated intensity due to crystalline scattering (I_C) can be calculated from the integrated intensities of the sample (amorphous and crystalline) (I_T) and the 100% amorphous reference (I_A), as shown :

$$I_C = I_T - I_A \quad (8.2)$$

Consequently, the degree of crystallinity (X_c) can be determined from :

$$X_c = \frac{I_c}{I_T} \quad (8.3)$$

8.3.2 Internal Comparison

These methods, of which that proposed by Ruland¹¹ is the most universally used, compare the ratio of the integrated intensity under the characteristic sharp crystalline peaks to the total intensity, assuming that the total intensity is independent of the crystallinity of the sample¹. The degree of crystallinity is then defined again by eqn. 8.3 where I_c is now obtained by integrating the intensity contribution of the crystalline phases and I_T is the total scattering intensity. This method tends to be used when standard "reference" samples are not available and therefore, separation of the crystalline, amorphous and background intensities is carried out in an arbitrary manner. The crystalline and amorphous phases are distinguished by drawing a tangent to the diffraction curve between the crystalline peak intensity troughs. However, this method is likely to underestimate the true crystallinity due to a certain crystalline fraction which is "lost" in the amorphous halo and therefore not accounted for. Background scattering is usually accounted for by a simple straight line connection between the intensity minima. Discrepancies can also occur due to a tendency to overestimate the background scattering, thereby underestimating the integrated amorphous scattering, resulting in larger crystallinity values. Due to difficulties in obtaining 100% amorphous or 100% crystalline "reference" samples, internal comparison methods are generally more widely used.

A relatively recent development of the internal comparison method is the use of "curve fitting" computer software which use reiterative mathematical analysis to differentiate between the crystalline and amorphous phases.

8.4 Experimental

WAXS data at room temperature were obtained using a Siemens D-5000 Diffractometer operated at 40kV voltage and 40mA current with a 2mm entrance slit and a 0.6mm detector slit. The range of 2θ angle scanned was $4 - 90^\circ$ with a step size of 0.02° and a dwell time at each step of 3 seconds. A monochromator before the detector removes any contribution from K_β radiation of the Cu anode X-ray tube. Sample temperatures were controlled using a TTK2-HC Programmer, a Heat Controller (supplied by Anton-Paar K.G., A-8054 Graz, Austria) and a TTK-LNC Liquid Nitrogen Controller (Anton-Parr). The standard heating and cooling rates for all samples was 10Kmin^{-1} . The d-spacing alignment of the instrument was checked regularly with a quartz crystal reference. Due to changes in the sample holder, experiments at room temperature have a d-spacing accuracy of $\pm 0.004\text{\AA}$ whereas sub-ambient and elevated temperatures have a d-spacing accuracy of $\pm 0.02\text{\AA}$.

The samples were spread evenly in the sample holder and irradiated with a collimated beam of X-rays (CuK_α). The intensity of the scattered X-rays was measured as a function of the 2θ scattering angle. Diffraction profiles were analysed by a Siemens Diffrac-AT software program which included integrating the intensities of each profile over the complete 2θ range. The Siemens Diffrac-AT FIT V.3.0 "curve-fitting" program was available to help in determining the separate crystalline and amorphous phases.

8.5 Determination of Crystallinity in FVA, PE and PI polymers

In this work, diffraction profiles on the crystalline FVA, PE and PI polymers do not show distinct amorphous and crystalline phases i.e. the crystalline phase is sufficiently broad due to crystal imperfections that it "overlaps" the amorphous halo as shown for PI in Figure 8.2. Therefore, in these polymers it is very difficult to assign an amorphous halo unambiguously. Consequently, as reported in other crystallinity studies on polymers^{5,8} the separate crystalline and amorphous integrated intensities of these polymers cannot be determined directly in the crystalline state without the use of curve fitting programs.

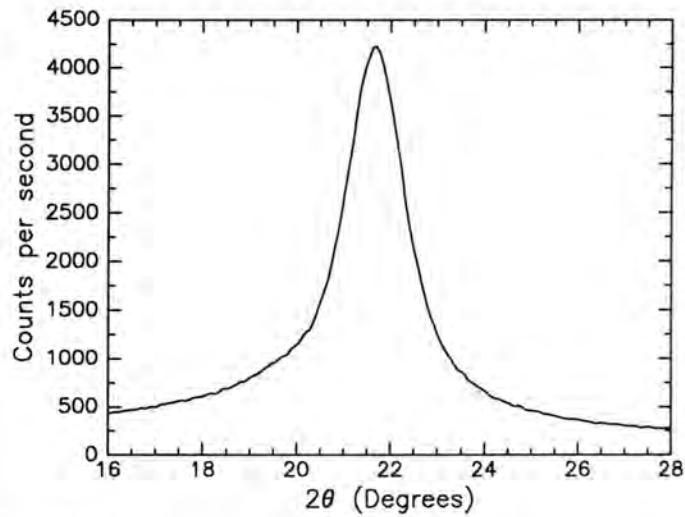


Figure 8.2 : Diffraction profile of PI at room temperature

Crystallinity values for these polymers have therefore been obtained using several methods :

1. Using an external comparison method the crystallinity of the polymers have been determined by comparing the X-ray diffraction profile of the crystalline solid with that of a 100% amorphous "reference" obtained at a sample temperature greater than the crystalline melting point.
2. Internal comparison methods (with and without curve fitting) have been used to determine the degree of crystallinity in various blends of EVA with the PE and PI crystalline polymers (see Chapter 3 for blend preparation details). From the EVA composition dependence of these crystallinity values, the crystallinity of the PE and PI polymers was determined by extrapolation.
3. From the heat of fusion ratio of the semi-crystalline polymers (DSC measurements) to the known literature value for 100% crystalline linear polyethylene, the degree of crystallinity has been predicted assuming polyethylene-type crystallisation.

8.5.1 External Comparison Method

In this method, the diffraction profiles of the solid, crystalline FVA, PI and PE polymers are compared to that of the corresponding 100% amorphous component and the degree of crystallinity calculated from eqn. 8.3.

The 100% amorphous profile is achieved with the polymers in the molten melt state. In the PE and PI components this melt temperature is at 353K and 343K respectively whereas due to the sub-ambient melting point of FVA, the pure amorphous pattern can be obtained at 298K, with subsequent cooling to 263K required in order to obtain the diffraction profile of the solid, crystallised polymer.

Diffraction profiles of the amorphous and crystalline phases in FVA, PE and PI polymers are shown in Figure 8.3. In all cases, scattering from the empty sample holder is subtracted from the sample profiles. However, in contrast to the standard sample holder used only at room temperatures (for internal comparison methods), the use of a stainless steel sample holder in these temperature controlled experiments results in several additional diffraction peaks at 2θ values of $43-45^\circ$ which are subsequently noted in the diffraction profile of the samples. The integrated intensity of these "metallic diffraction" peaks is therefore subtracted from the total integrated intensity of the sample profile. After subtraction of the holder, the integrated intensity of the 100% amorphous component (I_A) is regarded as representative of the amorphous component in the diffraction profiles of the crystalline solid sample (I_T). The degree of crystallinity values for the FVA, PE and PI polymers calculated using eqn. 8.3 are shown in Table 8.1.

Polymer	% Crystallinity
FVA	18.0
PE	29.3
PI	27.1

Table 8.1 : Crystallinity in FVA, PE and PI polymers (External Comparison Method)

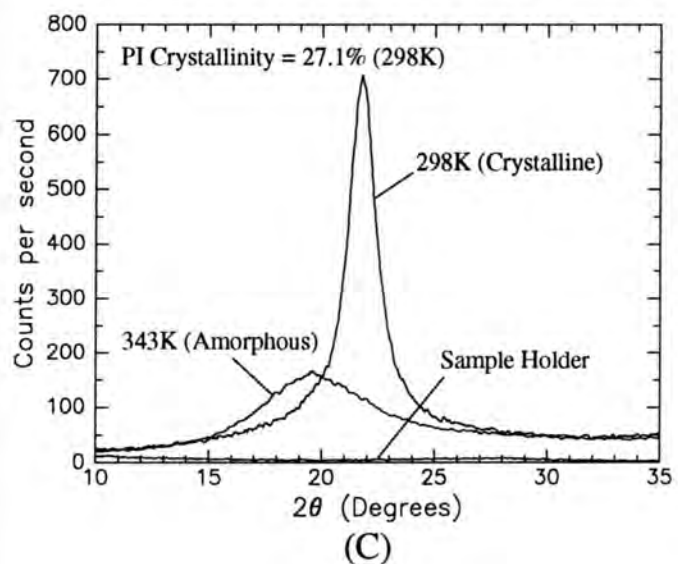
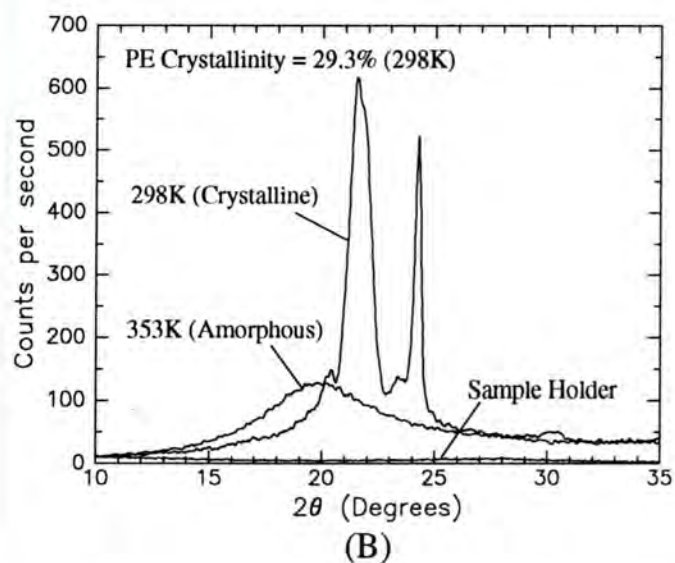
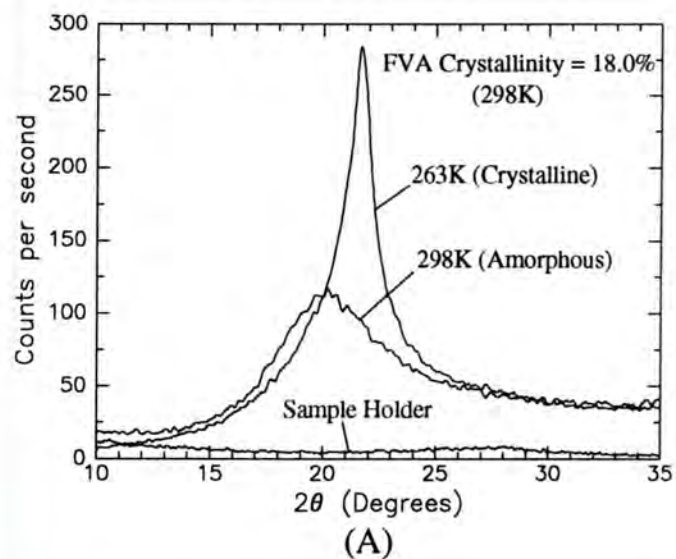


Figure 8.3 : Amorphous and Crystalline diffraction profiles of FVA (A); PE (B); PI (C)
(External Comparison Method)

8.5.2 Internal Comparison Method 1

This basic internal comparison method has been used to estimate the degree of crystallinity in the PE and PI polymers at room temperature (approximately 298K) using various EVA:PE and EVA:PI blend samples respectively. Determining crystallinity in FVA was not possible at this temperature due to its sub-ambient melting point.

Examples outlining this particular method of determining crystallinity in these blends are shown in Figures 8.4 and 8.5. The background intensity is arbitrarily drawn as a straight line between the intensity minima and this is then subtracted from the total sample intensity. The resulting intensity then represents sample scattering due to amorphous and crystalline phases only (I_T). The amorphous ($I_T - I_C$) and crystalline (I_C) phases are distinguished by a straight line connecting the crystalline peak intensity minima. As the amorphous (EVA) content of the EVA:PE and EVA:PI blends increases, the separate crystalline and amorphous phases can be clearly identified and integrated. Crystallinity at each blend composition was determined (after background subtraction) as the ratio of the integrated crystalline area to the total sample (amorphous and crystalline) scattering according to eqn. 8.3 (Tables 8.2 and 8.3). In the pure PE and PI components, no direct crystallinity measurements are possible due to severe peak broadening which "overlaps" the amorphous halo.

Blend (W/w)	% Crystallinity
EVA 75% : PE 25%	4.8
EVA 60% : PE 40%	16.7
EVA 50% : PE 50%	13.8
EVA 40% : PE 60%	17.8
EVA 33% : PE 67%	22.8
EVA 20% : PE 80%	23.1
EVA 17% : PE 83%	25.6

Table 8.2 : Crystallinity in EVA:PE blends (Internal Comparison Method 1)

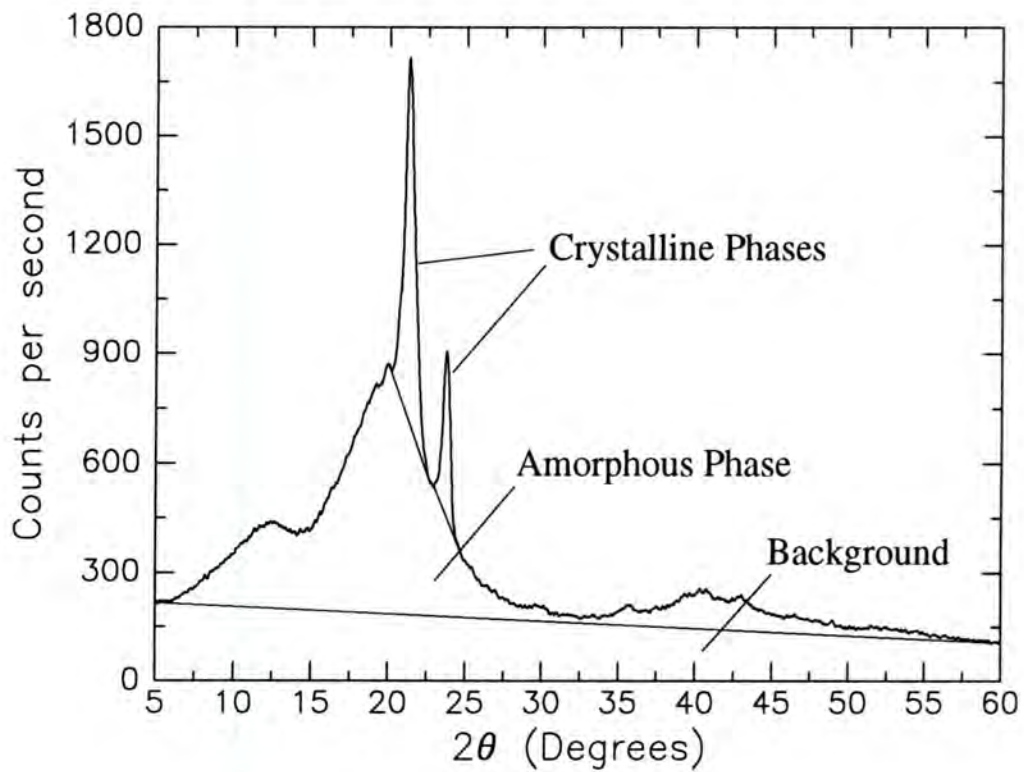


Figure 8.4 : Crystallinity in 60%EVA:40%PE blend at room temperature (Internal Comparison Method 1)

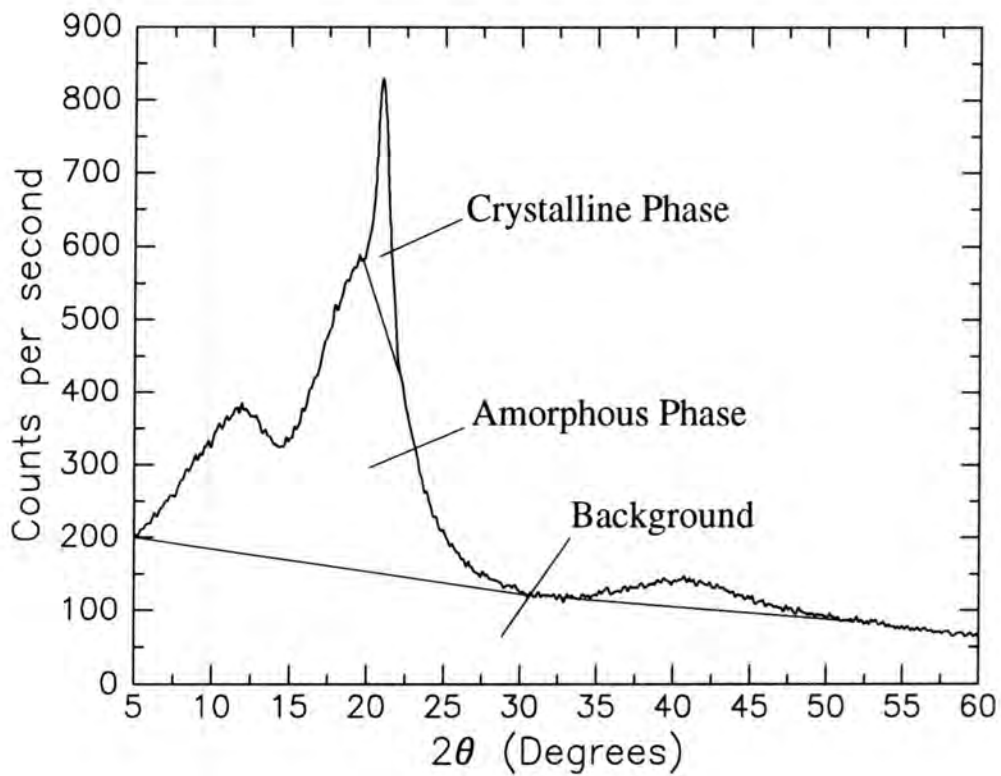


Figure 8.5 : Crystallinity in 73%EVA:27%PI blend at room temperature (Internal Comparison Method 1)

Blend (W/w)	% Crystallinity
EVA 73% : PI 27%	6.5
EVA 55% : PI 45%	16.1
EVA 39% : PI 61%	21.2
EVA 30% : PI 70%	23.6
EVA 15% : PI 85%	29.7

Table 8.3 : Crystallinity in EVA:PI blends (Internal Comparison Method 1)

From the EVA composition dependence of these blend crystallinity values which is assumed to be linear (Figures 8.6 and 8.7), the crystallinity of PE and PI were determined (by extrapolation) to be 31.0% and 35.7% respectively.

Although FVA is amorphous at room temperature due to its sub-ambient melting point, various EVA:FVA blends were cooled and held at 263K in order to crystallise the FVA component. At all EVA:FVA blend compositions, no separate crystalline and amorphous phases could be identified and consequently, no crystalline measurements were possible using this basic internal comparison method.

Although the resulting % crystallinity against EVA weight fraction plots are reasonably linear, it should be noted that the accuracy of this method (as mentioned previously) suffers from possible discrepancies due to "lost" crystallinity present in the "amorphous halo", incorrect background estimation and possible differences in the scattering capabilities of PI and PE to EVA.

8.5.3 Internal Comparison Method 2 (Profile Fitting)

This method is an elaborate development of the basic internal comparison method outlined in section 8.5.2. Rather than assigning the background as straight line connections between the intensity minima, the diffraction profile of the empty sample holder alone (under identical scattering conditions) is regarded as a better representation of the background signal. As an example of this method, Figure 8.8 shows the

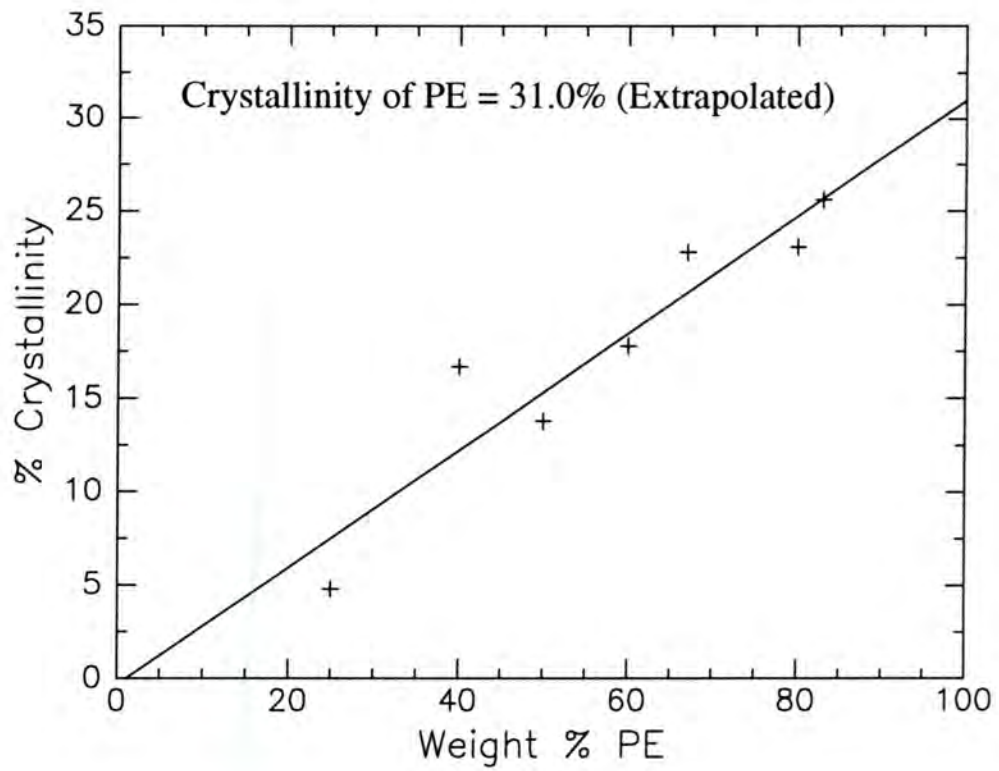


Figure 8.6 : Crystallinity values in EVA:PE blends at room temperature (Internal Comparison Method 1)

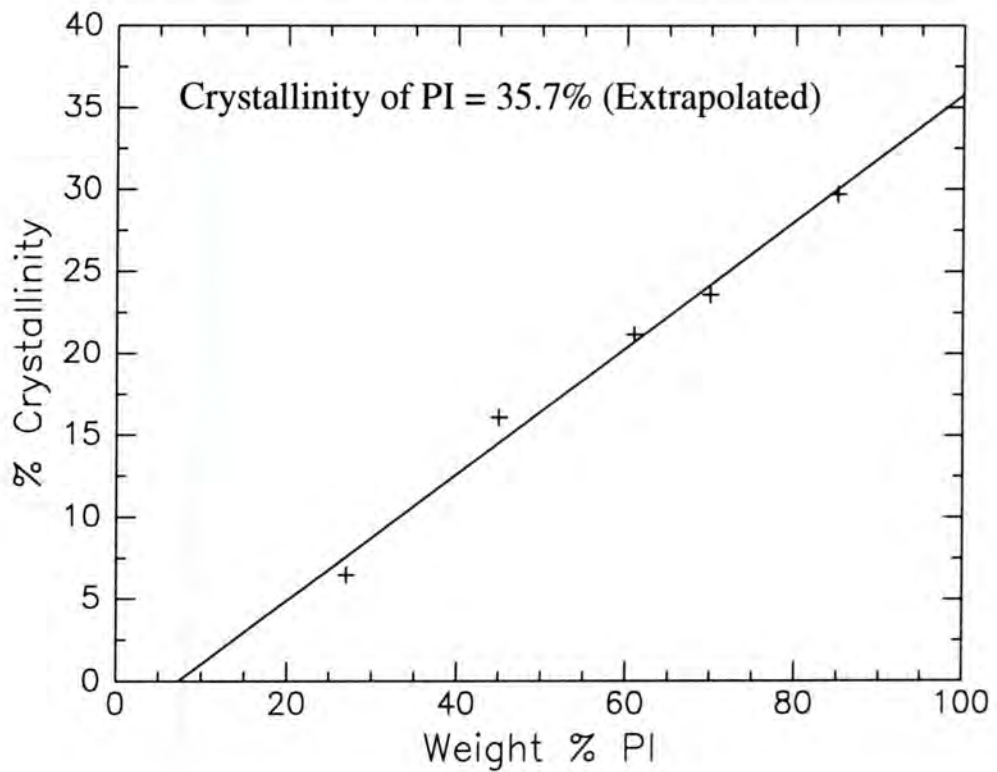


Figure 8.7 : Crystallinity values in EVA:PI blends at room temperature (Internal Comparison Method 1)

diffraction profiles of a 60%EVA:40%PE blend in comparison with an empty sample holder. After background subtraction, the resulting profile (Figure 8.9) is representative of amorphous and crystalline phases only and is analysed by the Diffrac-AT V.3.0 curve fitting program to determine the separate amorphous and crystalline phases. The fitting program has various mathematical fit options to estimate these separate scatter components which include the type (Lorentz, Voight and Gaussian¹²) and number (1-10) of fitting curves to be used in the fit analysis. The quality of the fit is indicated by a reliability factor and overlaid onto the original sample profile. The profile fit for each blend can be optimised using the various number and type of fitted curve options. For both EVA:PE and EVA:PI blends, the most suitable fitted curve option was Gaussian with a fitting reliability of typically 95-97%. In the EVA:PI blends the crystalline phase was a single diffraction peak and consequently, the number of fitted curves was two i.e. the separate amorphous and crystalline phases. As the diffraction profile of PE shows two separate crystalline diffraction phases, the number of fitted curves in the EVA:PE blends was generally three (including the amorphous halo). The degree of crystallinity in these blends was again determined using eqn. 8.3 (Tables 8.4 and 8.5). The EVA composition dependence of these values is shown in Figures 8.10 and 8.11.

Blend (w/w)	% Crystallinity
EVA 60% : PE 40%	9.9
EVA 50% : PE 50%	11.1
EVA 40% : PE 60%	12.0
EVA 33% : PE 67%	18.9
EVA 20% : PE 80%	16.5
EVA 17% : PE 83%	20.1

Table 8.4 : Crystallinity in EVA:PE blends (Internal Comparison Method 2)

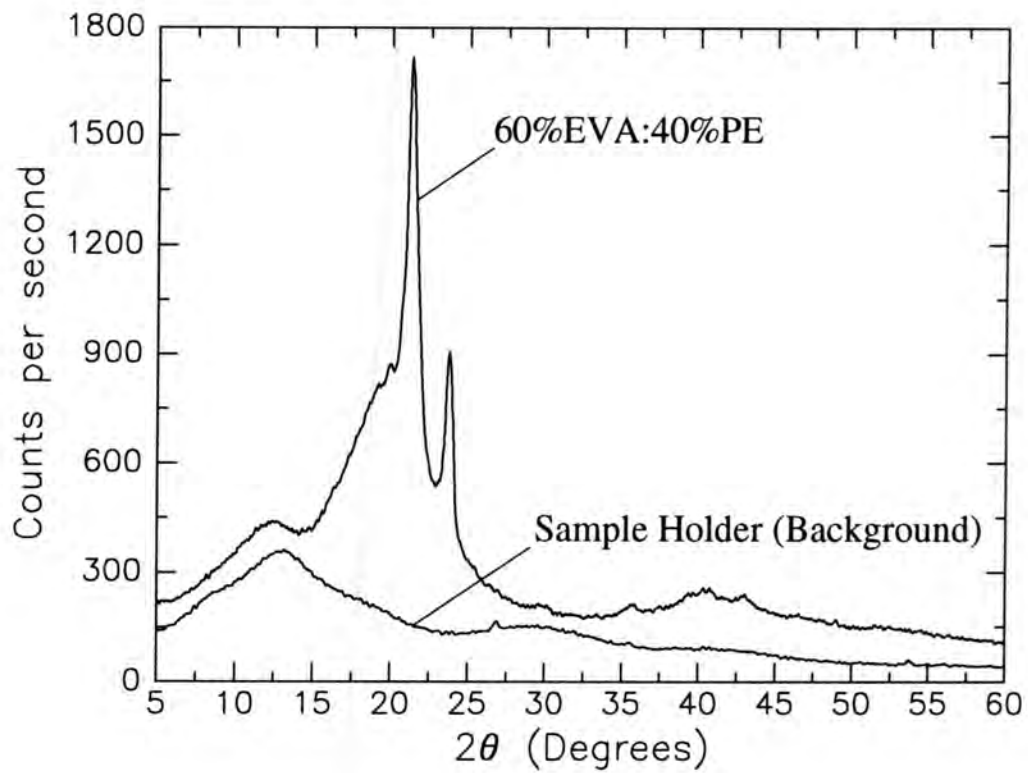


Figure 8.8 : Crystallinity in 60%EVA:40%PE blend at room temperature (Internal Comparison Method 2)

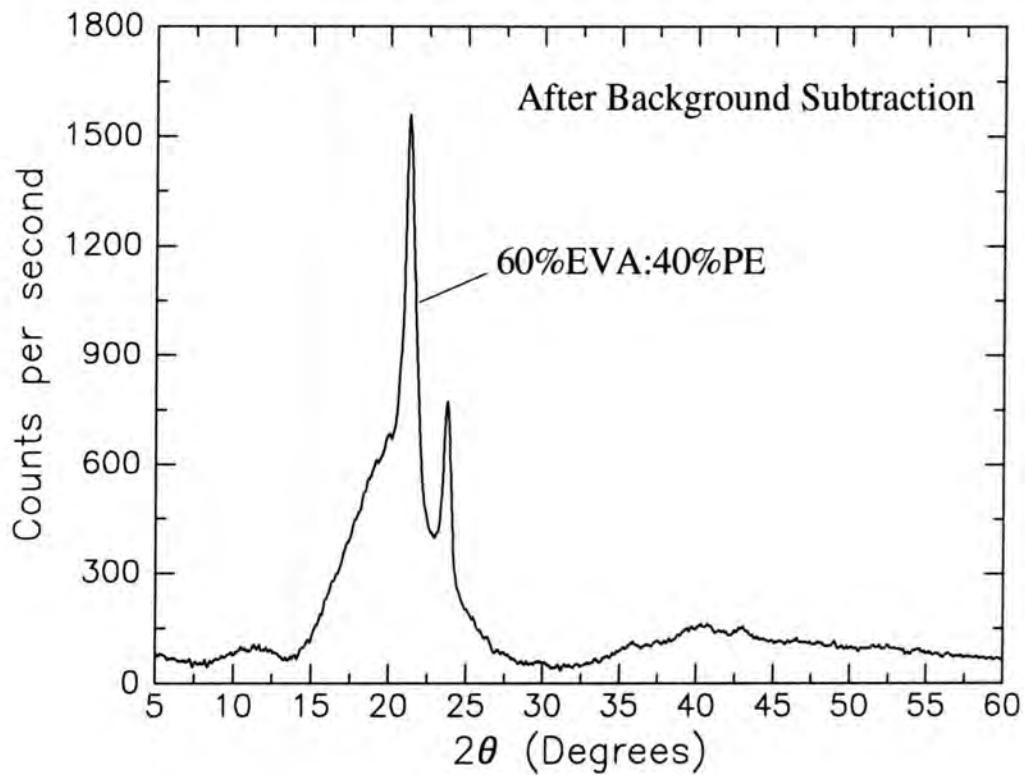


Figure 8.9 : Crystallinity in 60%EVA:40%PE blend at room temperature - after background subtraction (Internal Comparison Method 2)

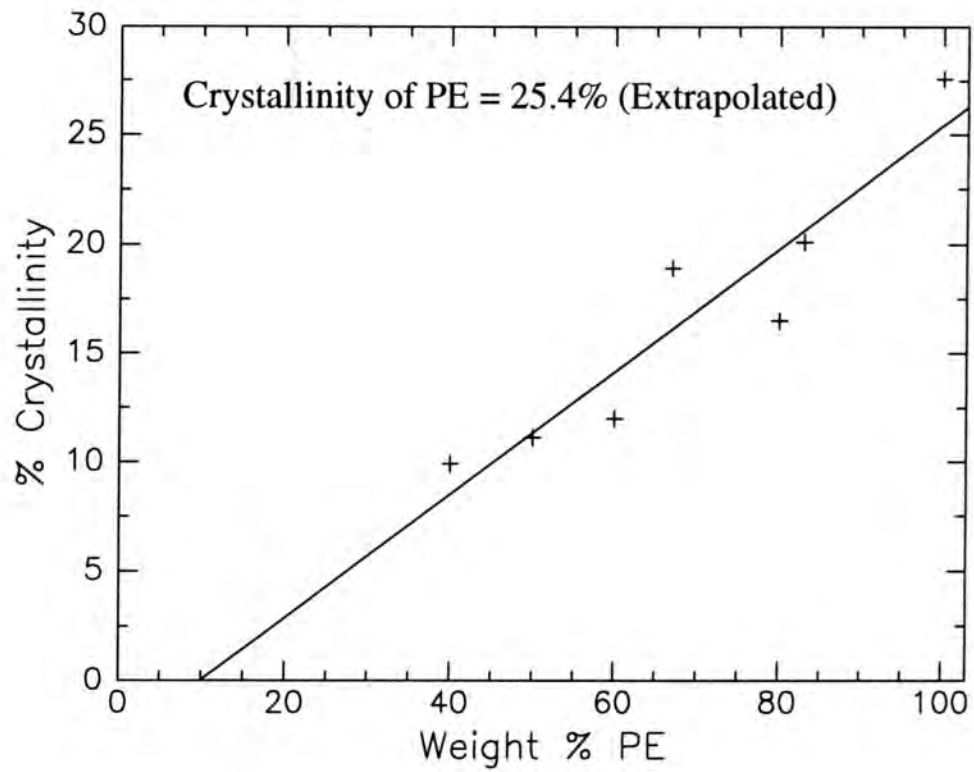


Figure 8.10 : Crystallinity values in EVA:PE blends at room temperature (Internal Comparison Method 2)

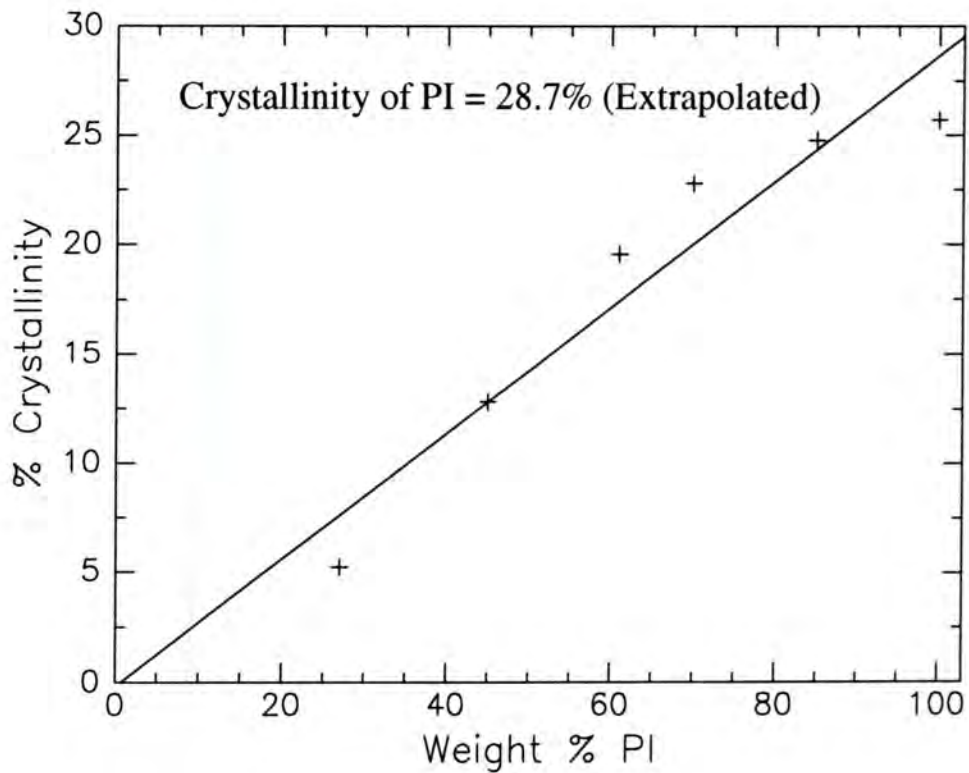


Figure 8.11 : Crystallinity values in EVA:PI blends at room temperature (Internal Comparison Method 2)

Blend (W/w)	% Crystallinity
EVA 73% : PI 27%	5.2
EVA 55% : PI 45%	12.8
EVA 39% : PI 61%	19.6
EVA 30% : PI 70%	22.8
EVA 15% : PI 85%	24.8

Table 8.5 : Crystallinity in EVA:PI blends (Internal Comparison Method 2)

In contrast to the basic method outlined in section 8.5.2, the degree of crystallinity in the pure PE and PI components can also be determined directly using identical curve fitting options to that applied to the blends, in order to distinguish between the separate crystalline and amorphous components. Consequently, **direct** crystallinity values of the pure PE and PI components were determined to be 27.6% and 25.7% respectively. These values show reasonable agreement with extrapolated PE and PI crystallinity values of 25.4% and 28.7% respectively which have been determined (using the curve fitting program) from crystallinity values at various compositions, as shown in Figures 8.10 and 8.11.

As in section 8.5.2, the degree of crystallinity in the EVA:FVA blends or the pure FVA component has not been determined as the curve fit is unreliable i.e. the fit does not accurately represent the sample diffraction profile. This may be an effect of the very broad diffraction peak in these blends (covering a 2θ range of approximately 25°) from which the separate crystalline and amorphous contributions cannot be distinguished at any composition (unlike the EVA:PE and EVA:PI blends).

8.5.4 Crystallinity from Heat of Fusion values

An estimate of crystallinity can also be obtained from the ratio of the polymer "heat of fusion" value to that of 100% crystalline linear polyethylene (288.70J/g - literature value¹³) assuming that the sample crystallisation is of a polyethylene type. This method

of estimating crystallinity has been used successfully for various polyitaconates¹⁴ in which ordering of the long chain aliphatic branches appears to be the main crystalline phase i.e. the polymer backbone is essentially amorphous, hence the justified comparison with polyethylene crystallisation.

Therefore, this method is particularly suitable for the polyitaconate sample (PI), in which crystallisation is assumed to be due to ordering of the octadecyl branches. From comparison with similar structures¹⁵, FVA can also be viewed as an amorphous backbone with crystallisable tetradecyl aliphatic branches and the degree of crystallinity can similarly be estimated from heat of fusion values.

From X-ray diffraction profiles and DSC measurements (Chapter 4) it is clear that PE contains two separate crystalline phases. It is thought that these phases represent the poly(ethylene glycol) and docosyl crystalline segments with the higher melting phase assumed to be docosyl crystallisation¹⁶. As this high melting crystalline phase accounts for approximately 86% of the total heat of fusion value, crystallisation in PE can be assumed to be due essentially to polyethylene type ordering of the docosyl ends. Consequently a reasonable estimate of crystallinity in the PE sample can also be obtained from the ratio of the docosyl heat of fusion value to that of 100% crystalline linear polyethylene. The estimated crystallinity values for the FVA, PE and PI polymers using this method are shown in Table 8.6.

Polymer	ΔH_f (DSC) J/g	% Crystallinity
FVA	44.87	15.5
PE	104.56	36.2
PI	94.63	32.8

Figure 8.6 : Crystallinity in FVA, PE and PI polymers (from Heat of Fusion values)

This method for estimating crystallinity based on polyethylene is clearly suited to polymers capable of very fast crystallisation rates which consequently tend to result in

reproducible heat of fusion values (as in polyethylene). The FVA, PE and PI polymers show this very fast crystallisation characteristic with quenching experiments showing little effect on the heat of fusion values compared to that obtained using slower cooling rates (see Chapter 4).

The % crystallinity values for these polymers, obtained from the various methods outlined in sections 8.5.1-8.5.4 are compared in Table 8.7.

Polymer	Internal Comp. (Method 1)	Internal Comp. (Method 2)	External Comp.	Heat of Fusion
FVA	—	—	18.0	15.5
PE	31.0	25.4 (27.6 ^A)	29.3	36.2
PI	35.7	28.7 (25.7 ^A)	27.1	32.8

^AInternal Comparison Method 2 (curve fitting) **directly** on FVA, PE and PI polymers.

Table 8.7

8.6 Crystallisation in EVA:FVA, EVA:PE and EVA:PI Blends

The powder diffraction profiles for various EVA:PE and EVA:PI blends are shown in Figures 8.12 and 8.13 respectively, with the corresponding lattice plane d-spacings noted in Tables 8.8 and 8.9. As expected, in all blends the intensity of the crystalline peak decreases as the amorphous (EVA) content increases. However in the EVA:PE blends there is a marked shift in the crystalline peaks to lower 2θ values on increasing EVA concentration, which results in a significant increase in the d-spacing values of the two crystalline phases (+0.16Å (Peak A), +0.12Å (Peak B)). In the EVA:PI blends the increase in the crystalline (PI) d-spacing due to EVA blending is smaller (+0.05Å).

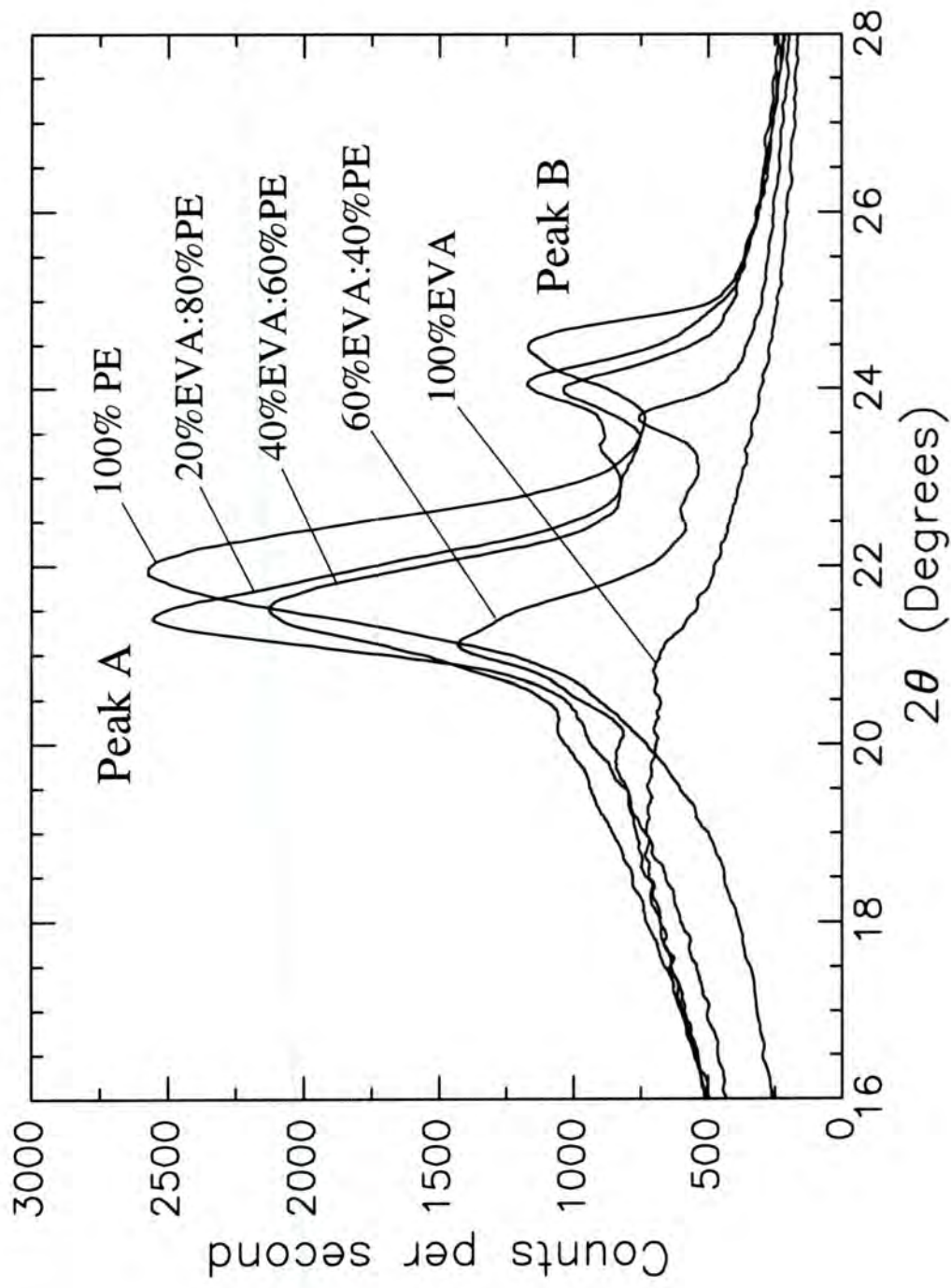


Figure 8.12 : Diffraction profiles of EVA:PE blends at room temperature

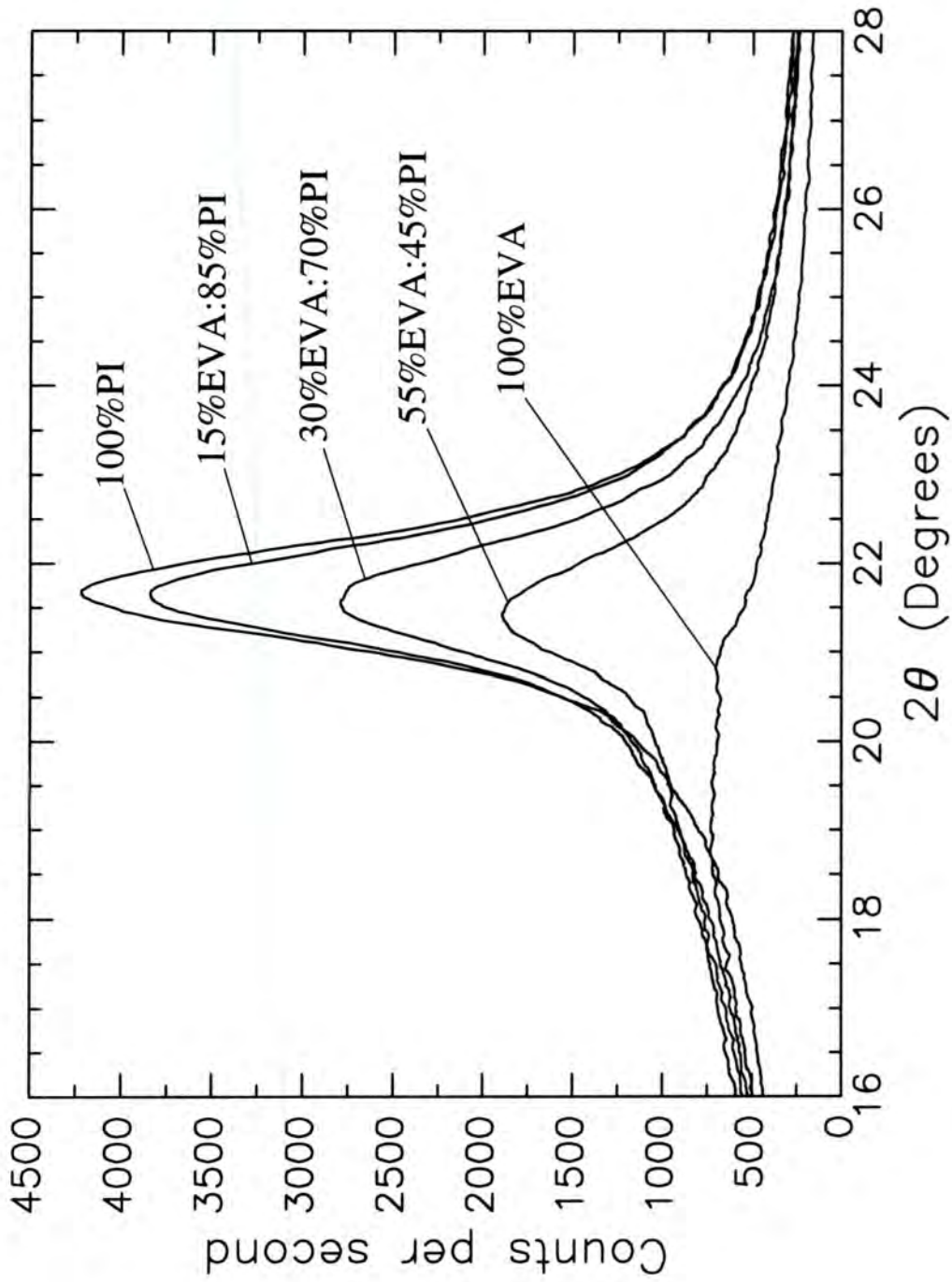


Figure 8.13 : Diffraction profiles of EVA:PI blends at room temperature

Sample (w/w)	Lattice plane d-spacings (Å)	
	Peak A	Peak B
100% PE	4.045	3.633
20% EVA : 80% PE	4.145	3.697
40% EVA : 60% PE	4.123	3.708
60% EVA : 40% PE	4.202	3.756

Table 8.8 : Lattice plane d-spacings for EVA:PE blends.

Sample (w/w)	Lattice plane d-spacings (Å)
100% PI	4.098
15% EVA : 85% PI	4.101
30% EVA : 70% PI	4.118
55% EVA: 45% PI	4.145

Table 8.9 : Lattice plane d-spacings for EVA:PI blends.

For the FVA and EVA:FVA blends, diffraction profiles were carried out at 263K in order to crystallise the FVA component. A change in the sample holder was required for these low temperature measurements and consequently the d-spacing accuracy is only $\pm 0.02\text{Å}$ compared to $\pm 0.004\text{Å}$ for the EVA:PE and EVA:PI blends at room temperature (using the standard sample holder). The d-spacing values of the crystalline phase in the EVA:FVA blends (Table 8.10) can therefore, at best only "indicate" a slight increase in the d-spacing value on increasing EVA content.

Sample (W/w)	Lattice plane d-spacings (Å)
100% FVA	4.09
15% EVA : 85% FVA	4.05
30% EVA : 70% FVA	4.08
46% EVA : 54% FVA	4.10
60% EVA : 40% FVA	4.10
83% EVA : 17% FVA	4.15

Table 8.10 : Lattice plane d-spacings for EVA:FVA blends.

8.7 Crystallinity in "Amorphous" EVA

DSC measurements on EVA show no distinct crystalline melting phase and is assumed to be amorphous (Chapter 4). However, the EVA diffraction profile at 298K suggests a possible small crystalline peak at a d-spacing of 4.10Å which appears to increase slightly in intensity as the temperature is lowered to 263K and finally 223K (Figure 8.14). Consequently, a small degree of crystallisation may be occurring within this temperature range. The degree of crystallisation in EVA at 298K appears to be very small (1-2%).

8.8 Identification of crystalline phases in PE

For these measurements, a pure sample of PE was prepared (code NECPE - see Chapter 3) from the docosyl diesterification of poly(ethylene glycol) M_p 400. From the powder diffraction profile of NECPE at 263K (Figure 8.15) the two crystalline phases are well defined, narrow peaks at 4.11Å and 3.69Å. In the industrial PE sample, these crystalline phases were broader and slightly overlapped which is possibly due to impurities disrupting crystallinity e.g. unesterified docosanoic acid or the use of a poly(ethylene glycol) sample with a wide molecular weight range i.e. a mixture of M_p 200, 400 and 600 samples.

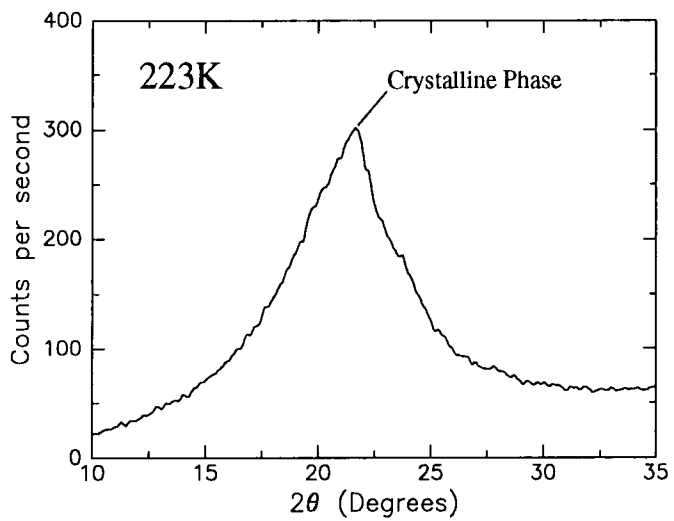
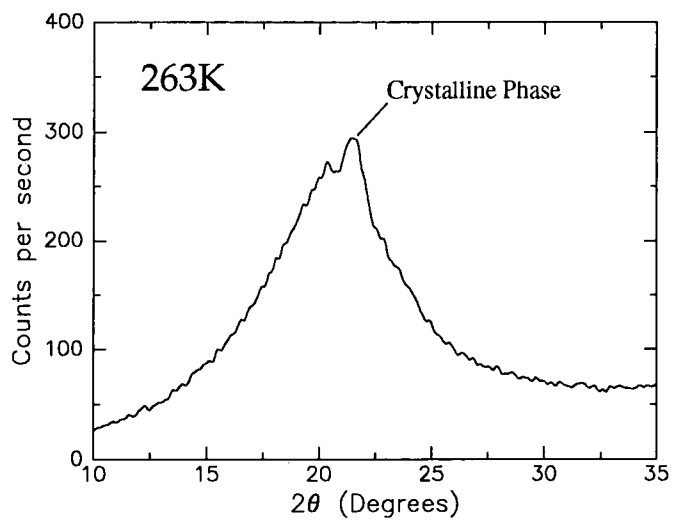
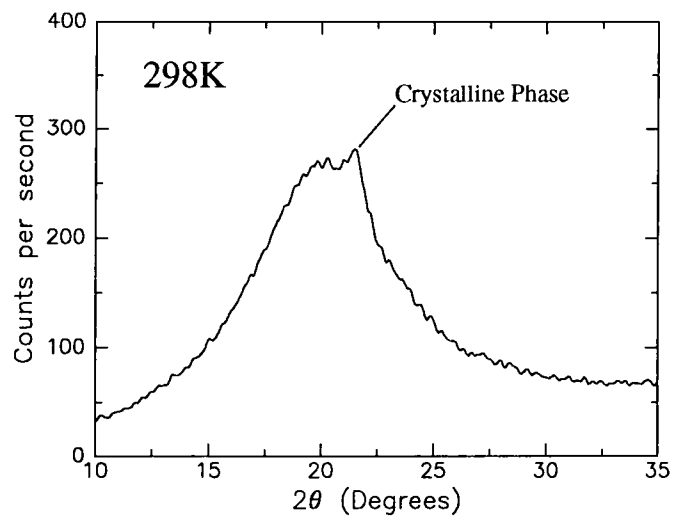


Figure 8.14 : Diffraction profiles for EVA at 298K, 263K and 223K.

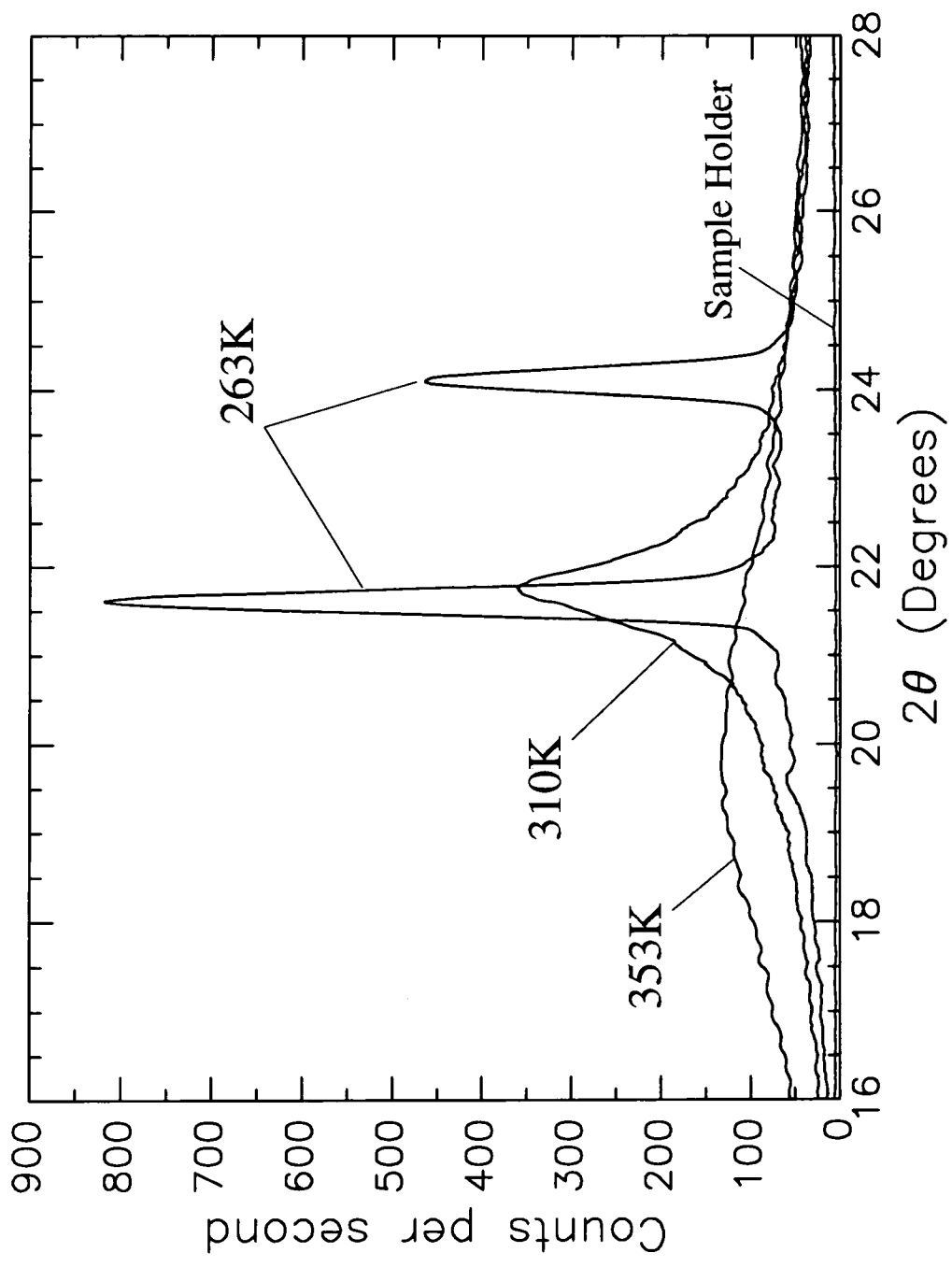


Figure 8.15 : Diffraction profiles of NECPE at 263K, 310K and 353K

At a temperature of 310K, the diffraction pattern of NECPE now shows a single broad crystalline phase at 4.08Å. The temperature of 310K corresponds to the temperature at which the lower melting phase of NECPE is molten i.e. amorphous, whereas the higher melting phase continues to be crystalline. This strongly suggests that the crystalline scatter peaks at 3.69Å and 4.11Å correspond to the lower and higher melting crystal phases in the DSC thermogram of NECPE respectively. To confirm this, the melt temperature is increased further to 353K i.e. at which the higher melting crystal phase is also amorphous and as expected the diffraction profile shows no crystal phase, only an amorphous halo. It can be speculated that the crystalline diffraction peak at 310K is very broad due to relaxation effects of melting the lower melt phase.

As mentioned previously in section 8.5.4, the crystalline phases noted in the X-ray scattering and the DSC measurements are thought to be due to separate poly(ethylene glycol) and docosane crystallisation. Comparison of the diffraction profiles of NECPE and poly(ethylene glycol) M_p 400 samples at 263K (Figure 8.16) appear to indicate that the crystal phase at 3.69Å in the NECPE sample i.e. the lower melting phase, closely coincides with one of the two crystal phases noted in the poly(ethylene glycol) sample suggesting that the phase at 3.69Å may also be due to poly(ethylene glycol) type crystallisation. Consequently, it appears likely that the crystal phase at 4.11Å i.e. the higher melting phase in NECPE is due to docosyl crystallisation. Further evidence to support this view is that the assigned docosyl d-spacing value (4.11Å) is very similar to that noted in the PI sample which has also been attributed to aliphatic (octadecyl) crystallisation. The higher melting phase in the NECPE sample also has a very similar melting point to that of docosanoic acid.

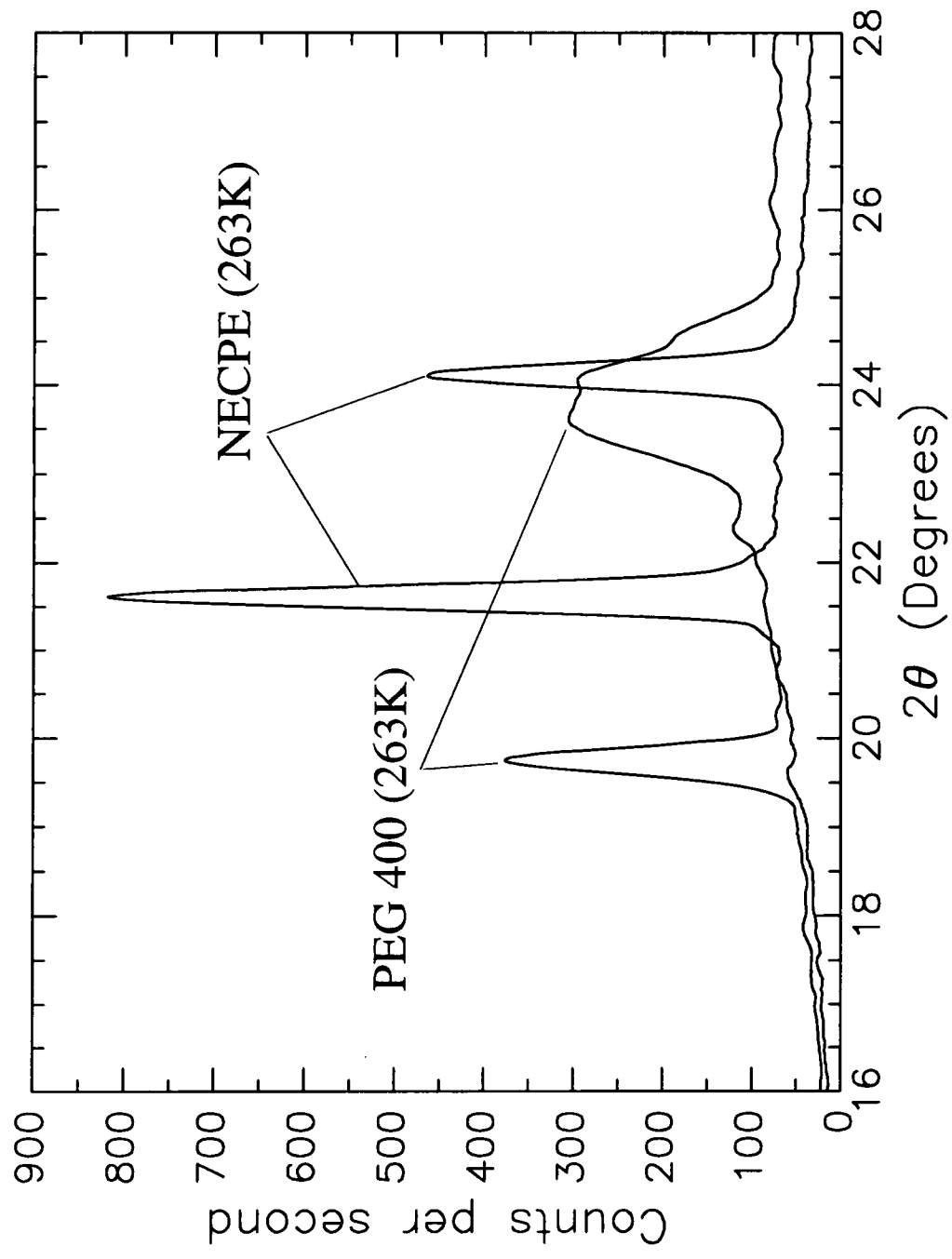


Figure 8.16 : Comparison of NECPE and PEG 400 diffraction profiles at 263K

8.9 Discussion

The determination of crystallinities in this study using both internal and external comparison methods has been based on a rather simplified expression (eqn. 8.3). Although many complex variations of these experimental methods have been proposed^{1,2} for specific polymer types, the objective of this work was merely to provide reasonable crystallinity estimates for each polymer using established methods.

The crystallinity values for PE and PI polymers determined using internal (with and without curve fitting) and external comparison methods show reasonable agreement with each other and that predicted by heat of fusion values. Crystallinities determined from the internal comparison methods may suffer from the assumption that the EVA composition dependence of the determined blend crystallinities is linear i.e. the scattering capabilities of the two blend components are similar and blending does not effect the crystallisation characteristics of the polymers. The main inadequacy of the external comparison method, is that scattering from the molten (amorphous) polymer may not provide an appropriate "reference template" as interchain distances may increase due to thermal expansion and consequently, the amorphous halo in the melt and solid, crystalline samples may be different.

The crystallinity values of 31.0% and 35.7% for the PE and PI polymers respectively, (obtained from an internal comparison method) were used in the Nishi-Wang expression to determine the Flory-Huggins interaction parameter (χ) from melting point analysis (see Chapter 4). For this analysis, the FVA crystallinity was taken as 15.5% obtained from heat of fusion values which compares closely with a value of 18.0% from the external comparison method. Crystallinity values for similar type structures i.e. LMPI, DPE, NECPE and NECME were estimated by comparison with these values as outlined in Appendix A.1.

The separate crystalline phases in NECPE (and PE), the identification of which had only been speculated¹⁶, has been assigned and related to the two melting endotherms observed in DSC measurements (Chapter 4). Clearly, the poly(ethylene glycol) and

docosyl crystalline phases correspond to the low and high melting endotherms which have lattice plane d-spacing values (in NECPE) of 3.69Å and 4.11Å respectively.

Starkweather has discussed the influence of a second polymer on the crystallisation of a semi-crystalline component in a miscible blend¹⁹. There appears to be no general rule by which one can predict the influence of the observed miscibility on crystallisation. The tendency to crystallise can either increase or decrease depending on the effect of blend composition on the relationship between the glass transition temperature (T_g) and the crystallisation temperature (T_c) i.e. crystallisation is reduced when the T_g approaches T_c . When a blend is miscible, the blend has a single T_g value which varies smoothly with composition between the values of the individual components. Determination of the T_g values for the polymers in this study has not been possible (see Chapter 4) and therefore the relationship of T_g and T_c values on blend composition has not been determined.

From the diffraction profiles of the EVA:PE blends which are known to be miscible (DSC, SANS, Optical Microscopy), the lattice plane d-spacing of the previously assigned docosyl crystallisation appears to expand (increase) as the EVA content of the blend increases. This may be due to cocrystallisation between the long ethylene sequences in EVA and the docosyl ends of the PE polymer indicating that these polymers are miscible in the crystalline and amorphous regions. Similar systems involving ethylene copolymers²⁰ also show this cocrystallisation effect with a corresponding expansion in the d-spacings. The DSC heat of fusion values also indicate possible cocrystallisation effects with heat of fusion values for the docosyl phase in these blends greater than predicted based on simple dilution of EVA and PE. Since the EVA copolymer used in this study is not thought to be miscible with the poly(ethylene glycol) segment of the PE sample^{17,18}, it is surprising that the d-spacing associated with this segment also expands on increasing EVA content which suggests cocrystallisation and consequently, miscibility between the crystalline phases. However, heat of fusion values for this crystalline phase in the EVA:PE blends suggest a possible tendency for crystallisation to be hindered. It can only be speculated that the PE molecule, due to the

low molecular weight of the docosyl and poly(ethylene glycol) segments, maybe viewed hypothetically as a miscible blend which may consequently result in a single T_g value for the PE sample. Clearly, this view of miscibility is achieved from the covalent bonding between the inner poly(ethylene glycol) and the outer docosyl units. As discussed previously, the dependence of such a single T_g value on the EVA content and its relationship with the T_c value of the blend will determine the crystallisation tendency. Consequently, this relationship maybe such that crystallisation in **both** phases i.e. docosyl and poly(ethylene glycol), is enhanced resulting in an expansion of their d-spacing values.

In contrast, the EVA:PI and EVA:FVA blends show a much smaller expansion in the d-spacing values and in addition, the heat of fusion values are smaller than predicted based on the simple dilution by the EVA component. This suggests that crystallisation of the aliphatic side chains may possibly be hindered due to blending. As crystallisation in the FVA and PI polymers is due essentially to the aliphatic side chain (branches), frustration of crystallisation on blending with EVA may indicate an inability to assimilate the long ethylene sequences (in EVA) with these side chain crystalline regions. This maybe due to the higher molecular weight of the PI and FVA polymers (compared to PE) which reduces mobility. The high packing density of these aliphatic side chains may also resist incorporation from the EVA sequences. Therefore, the presence of EVA may actually hinder rather than enhance this side chain crystallisation.

Additionally, as suggested elsewhere¹⁹, the tendency towards cocrystallisation is considerably enhanced when the polymer components have similar repeat unit lengths. In the EVA:PE blends, the average repeat unit lengths are similar by virtue of both polymer components having essentially polyethylene-type repeat units. In the case of the branched polymers, FVA and PI, although the main (amorphous) polymer backbone has a similar repeat unit length to that of EVA, each repeat unit is a highly branched structure and consequently, the dimensions are somewhat different to that of the average EVA repeat unit.

Although EVA in this diffraction study (and from DSC measurements) is assumed to be amorphous, the diffraction profile of the sample appears to indicate a small degree of crystallinity at 298K which crystallises further on cooling to 223K. This maybe due to crystallising ethylene segments in the copolymer and may explain, in part the speculated cocrystallisation between EVA and PE which results in an expansion of the d-spacing values in PE and larger than predicted heat of fusion values for these blends. This small degree of crystallisation in EVA accounts for the observed opaqueness of the sample at room temperature which disappears on heating.

8.10 References

1. F.J.Balta-Calleja and C.G.Vonk, "X-ray Scattering of Synthetic Polymers", Vol. 8, Elsevier (1989).
2. L.E.Alexander, "X-ray Diffraction Methods in Polymer Science", Wiley-Interscience, New York (1969).
3. Encyclopedia of Polymer Science and Engineering, Second Edition, Vol. 17, Wiley-Interscience (1987).
4. W.L.Bragg. Proc. Cambridge Phil. Soc., 17, 43 (1913).
5. N.S.Murthy and H.Minor, Polymer, 31, 996 (1990).
6. N.Yao, Polymer, 33, 1802 (1992).
7. S.J.Guerrero, H.Veloso and E.Randon, Polymer, 31, 1615 (1990).
8. S.Polizzi, G.Fagherazzi, A.Benedetti, M.Battagliarin and T.Asano, Eur. Poly. J., 27, 85 (1991).
9. J.M.Goppel, Appl. Sci. Res. A1, 3 (1947).
10. J.J.Arlman, Appl. Sci. Res. A1, 347 (1949).
11. W.Ruland, Acta Cryst., 14, 1180 (1961).
12. Siemens Diffrac-AT V.3.0 Fit Guide.
13. F.A.Quinn and L.J.Mandelkern, J. Am. Chem. Soc., 80, 3178 (1958).
14. R.Diaz-Calleja, A.Ribes-Greus, L.Gargallo and D.Radic, Polymer International, 25, 51 (1991).
15. Z. Huiyang, Z. Weibang and L. Zhuomei, J. App. Poly. Sci., 43, 919 (1991).
16. R.D. Tack, EXXON Communication (1992).
17. S.Cimmino, E.Martuscelli, M.Saviano and C.Silvestre, Polymer, 32, 1461 (1991).
18. C.D.Han, H.S.Chung and J.K.Kim, Polymer, 33, 546 (1992).
19. H.W.Starkweather Jr., "Polymer Compatibility and Incompatibility - Principles and Practices" (Ed. K.Solc), Harwood Academic, New York (1982).
20. H.W.Starkweather Jr., J. App. Poly. Sci., 25, 139 (1980).

CHAPTER 9

SMALL ANGLE NEUTRON SCATTERING

9.1 Introduction

Small angle neutron scattering (SANS) is a powerful technique for studying the miscibility of polymer blends and predicting their phase equilibria^{1,2,3} and represents a significant experimental development in polymer science. From SANS measurements on a polymer blend in the miscible region, in which one of the components is deuterium labelled, the intense scattering due to concentration fluctuations enables the effective binary interaction parameter, χ_{eff} , to be determined. The advantage of the SANS technique in comparison with the melting point depression analysis (see Chapter 4), is that the interaction parameters can be determined in the miscible melt region at various compositions and temperatures. The use of melting point (and glass transition) temperature effects in polymer blends to ascertain miscibility are macroscopic techniques. Consequently, these techniques cannot measure the "concentration fluctuations" within a polymer blend which are large enough to be classed as "domains". However, SANS can monitor these domain-type structure effects (which represent the degree of random molecular mixing within a miscible blend) in order to determine the temperature dependence of the χ_{eff} values at various compositions. Consequently, from this dependence, the type of phase diagram and the spinodal temperatures can be predicted.

The determination of χ_{eff} values from SANS measurements is based on de Gennes⁴ "random phase approximation" (RPA) calculation for miscible blends near to their critical (phase separation) point. Using this approach, several miscible blends have shown χ_{eff} values which are composition and molecular weight dependent^{5,6,7}. This contradicts the original definition of the Flory-Huggins interaction parameter, χ_{FH} which was assumed to be purely enthalpic in origin and consequently, independent of molecular weight and composition^{8,9}. Clearly, only when there is no dependence of χ_{FH} on molecular weight or composition does $\chi_{\text{eff}} = \chi_{\text{FH}}$.

In this study, χ_{eff} values over a range of temperature and compositions have been determined for a blend of deuterated poly(ethylene glycol) docosyl diester (DPE) and hydrogenous poly(ethylene-co-vinyl acetate) (EVA). From the temperature dependence of these χ_{eff} values, spinodal temperatures at various blend compositions have been predicted. Radius of gyration values for each component at various temperatures and compositions have also been determined.

Applying both the classical Flory¹⁰ and recent Koningsveld¹¹ thermodynamic theories, the separate entropic and enthalpic contributions to these χ_{eff} values can be assessed. Consequently, "heat of mixing" values for the EVA:DPE blend system have been predicted and compared to values determined by calorimetry for the fully hydrogenous blend i.e. NECPE and EVA (see Chapter 7).

9.2 Theory

9.2.1 Thermodynamics

Applying the Flory-Huggins lattice theory to a binary polymer mixture results in the following expression for the Gibbs free energy of mixing, ΔG_{mix} :

$$\frac{\Delta G_{\text{mix}}}{RT} = \frac{\phi_1}{m_1} \text{Ln}\phi_1 + \frac{\phi_2}{m_2} \text{Ln}\phi_2 + \phi_1\phi_2\chi_{\text{FH}} \quad (9.1)$$

where subscripts 1 and 2 refer to the two blend components (1-EVA, 2-DPE) which are assumed to have equal segment volumes. ϕ_i is the volume fraction, m_i is the number average degree of polymerisation, R is the gas constant (8.314 JK⁻¹mol⁻¹), T is the absolute temperature and χ_{FH} is the Flory-Huggins interaction parameter. The second differential of eqn. 9.1 is expressed as :

$$\frac{\partial^2}{\partial\phi_2^2} \left(\frac{\Delta G_{\text{mix}}}{RT} \right) = \frac{1}{m_1\phi_1} + \frac{1}{m_2\phi_2} - 2\chi_{\text{FH}} \quad (9.2)$$

At the spinodal phase boundary :

$$\frac{\partial^2}{\partial \phi_2^2} \left(\frac{\Delta G_{\text{mix}}}{RT} \right) = 0 \quad (9.3)$$

Therefore at the spinodal, eqn. 9.2 becomes :

$$\chi_s = \frac{1}{2m_1\phi_1} + \frac{1}{2m_2\phi_2} \quad (9.4)$$

where χ_s is the value of the interaction parameter for the polymer mixture at the spinodal. The original Flory-Huggins lattice theory assumes that χ_{FH} values are purely enthalpic and consequently are not dependent on molecular weight or composition. However, small angle neutron scattering on polymer mixtures provides **effective** χ values (χ_{eff}) which contain both molecular weight and composition dependence. Only when there is no dependence of χ_{FH} on molecular weight or composition do χ_{FH} values correspond to χ_{eff} values from SANS measurements. There have been many discussions on the dependence of χ_{FH} on composition which have recently resulted in several reviews^{12,13,14}. Clearly, the original Flory-Huggins model improves if the interaction parameter is allowed to be concentration dependent. Koningsveld¹¹ defined a concentration and temperature dependent interaction parameter as $g_{12}(\phi, T)$ which replaced the original χ_{FH} term in eqn. 9.2 by the following expression :

$$\chi_{\text{FH}} = -\frac{1}{2} \left(\frac{\partial^2 g_{12} \phi_1 \phi_2}{\partial \phi_2^2} \right) \quad (9.5)$$

Koningsveld et. al.^{11,15} expressed g_{12} as :

$$g_{12} = \alpha + \frac{\beta_s + (\beta_H / T)}{1 - \gamma\phi_2} \quad (9.6)$$

where α and β_s are empirical entropy correction terms, β_H is an enthalpic term related to the internal energy per contact of occupied lattice sites. γ is given by :

$$\gamma = 1 - \frac{\sigma_2}{\sigma_1} \quad (9.7)$$

where σ_2/σ_1 is the ratio of surface areas of polymer segments 2 and 1 respectively. From neutron scattering measurements, the determined χ_{eff} values can be expressed as :

$$\chi_{\text{eff}} = -\frac{1}{2} \left(\frac{\partial^2 g_{12} \phi_1 \phi_2}{\partial \phi_2^2} \right) = a + \frac{b}{T} \quad (9.8)$$

where \underline{a} and \underline{b} represent respectively, the entropic and enthalpic contributions to the second derivative of the excess free energy of mixing, with respect to concentration. From eqn. 9.6, Koningsveld^{15,16} defined the \underline{a} and \underline{b} terms by :

$$a \text{ (Entropic)} = \alpha + \frac{\beta_s(1-\gamma)}{(1-\gamma\phi_2)^3} \quad (9.9)$$

$$b \text{ (Enthalpic)} = \frac{\beta_H(1-\gamma)}{(1-\gamma\phi_2)^3} \quad (9.10)$$

From eqns. 9.1, 9.5 and 9.6, an expression for the enthalpy or "heat of mixing" was defined as¹⁷ :

$$\frac{\Delta H_{\text{mix}}}{R} = \phi_1 \phi_2 \frac{\beta_H}{(1 - \gamma \phi_2)} \quad (9.11)$$

γ and β_H values can generally be determined from both "heat of mixing" and small angle neutron scattering measurements. The α and β_S values are determined solely from neutron scattering measurements.

It should be noted that if the surface area of both polymer segments are very similar, $\gamma=0$. Consequently, eqns. 9.9 and 9.10 can be simplified to $\underline{a}=\alpha+\beta_S$ and $\underline{b}=\beta_H$ respectively.

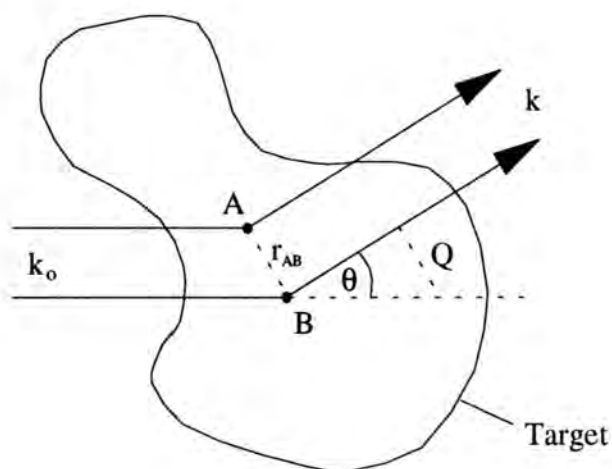
9.2.2 Small Angle Neutron Scattering (SANS)

From Bragg's law, for a molecule to scatter radiation, the wavelength of that radiation must be comparable to the distance between the atoms in the molecule. In neutron scattering, the range of neutron wavelengths can be sufficiently low as to be comparable with electromagnetic radiation used in X-ray crystallography i.e. 1.54Å which corresponds approximately with the length of a C-C single bond. Therefore, by increasing the neutron wavelength, structures can be identified which range from atoms, molecular segments to complete molecules.

Neutron scattering measurements are carried out on a very similar fashion to that of X-ray and light scattering experiments i.e. collimated radiation is scattered by the sample and recorded on a detector. However, in neutron scattering, isotopes of the same element can have very different scattering capabilities. This difference is clearly noted in the isotopes of hydrogen i.e. ^1H has a neutron scattering cross-section of $1.75 \times 10^{-24} \text{ cm}^2$ whereas ^2H has a value of $5.6 \times 10^{-24} \text{ cm}^2$. Therefore, neutrons unlike X-rays or light can differentiate between these hydrogen isotopes. Consequently, the principal use of neutron scattering is to distinguish one molecule from its neighbour using generally the highly atypical scattering properties of the hydrogen isotopes. In using this technique, it is clear that one of the components must be selectively deuterated. In addition it should be noted that only the coherently scattered neutrons i.e. in which phase is conserved,

can produce structural information about the sample. Incoherent scattering generally contributes to the background signal and is subsequently subtracted from the total sample signal.

In the case of polymers in the solid state, the coherent scattering from neighbouring nuclei gives interference effects from which structural information can be obtained. As shown in Figure 9.1, there is a phase difference of $(k - k_0)r_{AB}$ for the scattering between two nuclei separated in space by r_{AB} where k_0 and k are vectors parallel to the incident and scattered neutron directions respectively. For elastic scattering, k_0 and k are equal in magnitude.



$$Q \text{ (Scattering Vector)} = k - k_0$$

Figure 9.1

However, for polymer blends in the one phase (miscible) region near to the critical point of phase separation, the local concentration (ϕ) has large fluctuations. In neutron scattering (as in light and X-ray scattering), the essential parameter is the scattering wave vector, Q . Q is the resultant between the vectors for the incident radiation, k_0 and the scattered radiation, k and is expressed as:

$$Q = k - k_0 = 4\pi \sin(\theta / 2) / \lambda \quad (9.12)$$

As: $\lambda = 2d \sin(\theta / 2) \quad \text{(Bragg's Law)} \quad (9.13)$

where λ is the neutron wavelength, d is the distance between the scattering bodies and θ is the scattering angle. Combining eqns. 9.12 and 9.13 :

$$d = 2\pi / Q \text{ (in nm)} \quad (9.14)$$

Eqn. 9.14 is a very useful expression and allows the instrument to be configured to ensure that the selected Q range is sufficient to "identify" the systems to be studied. A typical SANS instrument will have a Q range between $0.005 \rightarrow 0.2 \text{ \AA}^{-1}$, allowing the study of scattering bodies, $30 \rightarrow 1250 \text{ \AA}$ in diameter which is ideal for the study of many colloidal-type systems including polymer blends.

What is actually measured in neutron scattering is a correlation function between the concentration at two points i.e. r_A and r_B :

$$S_{12}(r_A - r_B) = \langle \phi_1(r_A) \phi_2(r_B) \rangle - \langle \phi_1 \rangle \langle \phi_2 \rangle \quad (9.15)$$

where 1 and 2 are the species present ($\phi_1 + \phi_2 = 1$), $\langle \rangle$ denotes a thermal average and S_{12} is the scattering power.

Scattering can be expressed in terms of a differential coherent scattering cross-section - $d\Sigma/d\Omega$ i.e. $Nd\sigma/d\Omega$ where σ is the coherent neutron scattering cross-section, Ω is the range or "spread" of the scattering angle and N is the number density of scattering bodies in the sample. The differential coherent scattering cross-section, $d\Sigma/d\Omega$, obtained from the intensity of scattered neutrons from a mixture of deuterated and hydrogenous polymers is related to the complete correlation functions at a range of Q values i.e. the structure factor $S(Q)$, as follows:

$$\frac{d\Sigma}{d\Omega}(Q) = K \frac{(b_H - b_D)^2}{V} S(Q) \quad (9.16)$$

$S(Q)$ can be expressed as the scattering power at a given value of Q . K is a factor containing instrument parameters (incident intensity neutrons, cross-sectional area of beam and sample thickness etc.). V is the molar volume of an arbitrary repeat unit based on the volume fraction weighted sum of the individual molar volumes of the hydrogenated and deuterated polymer repeat units and is expressed as :

$$V = \frac{\text{Volume of repeat unit}}{\text{Avogadro No.}}$$

The term b_i in eqn. 9.16 is the sum of all the neutron scattering lengths of atoms in a repeat unit of the deuterated (subscript D) and hydrogenous (subscript H) polymers which can be related to the coherent neutron scattering cross-section of the repeat unit, σ , by the expression, $\sigma=4\pi b^2$. The quantity $(b_H-b_D)^2/V$ is representative of the difference between the neutron scattering density of the deuterated and hydrogenated polymers. If (b_H-b_D) is zero, there will be no coherent scattering.

$d\Sigma/d\Omega$ can be regarded as the intensity, $I(Q)$ which is converted to absolute units (cm^{-1}) by suitable calibration of the instrument. Therefore, eqn. 9.16 can be expressed as:

$$I(Q) = K \frac{(b_H - b_D)^2}{V} S(Q) \quad (9.17)$$

de Gennes⁴ using a "Random Phase Approximation" (RPA) has expressed the calculation of the correlation functions at a given Q value in terms of the Debye function¹⁸, $g_D(R_{gi}, Q)$ for the scattering by a Gaussian polymer chain with radius of gyration (R_{gi}) :

$$\frac{1}{S(Q)} = \frac{1}{m_1 \phi_1 g_D(R_{g1}, Q)} + \frac{1}{m_2 \phi_2 g_D(R_{g2}, Q)} - 2\chi \quad (9.18)$$

where,
$$g_D(R_{gi}, Q) = (2/u^2)(\exp(-u) + u - 1) \quad (9.19)$$

and
$$u = Q^2 R_{gi}^2 \quad (9.20)$$

from eqn. 9.12,
$$Q = 4\pi \sin(\theta/2) / \lambda$$

If $Q=0$, then the Debye function $g_D(R_{gi}, Q=0)$ is equal to 1 and eqn. 9.18 becomes :

$$\frac{1}{S(0)} = \frac{1}{m_1 \phi_1} + \frac{1}{m_2 \phi_2} - 2\chi = 0 \quad (9.21)$$

which on rearrangement, corresponds to the χ_s spinodal expression in eqn. 9.4. Therefore at the spinodal, $S(Q)^{-1}=0$ and consequently, $S(Q)$ and the intensity $I(Q)$ are infinite (see eqn. 9.17).

In the region where Q is small i.e. $QR_g < 1$, the inverse intensity may be written in a simple form which is obtained by expansion of the Debye function at small Q , as shown by Guinier¹⁹ :

$$g_D(R_{gi}, Q) = 1 - \frac{Q^2 R_{gi}^2}{3} \quad (9.22)$$

$$R_{gi}^2 = \frac{m_i a_i^2}{6} \quad (9.23)$$

where a_i is the statistical step length of the polymer molecule. From inserting eqn. 9.22 into eqn. 9.18, we obtain the Ornstein-Zernike expression⁴ :

$$S(Q) = \frac{1}{2(\chi_s - \chi)(1 + Q^2 \xi^2)} \quad (9.24)$$

where χ_s is the value of χ at the spinodal, as defined in eqn. 9.4. ξ is the average concentration fluctuation length in the miscible state and is defined by :

$$\xi = \frac{a_i}{6} [\phi_1 \phi_2 (\chi_s - \chi)]^{-1/2} \quad (9.25)$$

In the miscible region, the value of ξ will be small but will tend towards infinity as the spinodal temperature is reached i.e. as χ approaches χ_s . For polymer blends this is a good approximation while $\xi \leq R_g$. Therefore, the concentration fluctuation distance, ξ must not be larger than the interaction range which could be similar in magnitude to that of the R_g values.

Where $QR_g > 1$, the Debye functions are reduced and g_D^{-1} increases. Consequently the last term in eqn. 9.18 (-2χ) becomes negligible and can be expressed as :

$$S(Q) = (\phi_1 \phi_2 12) / (Q^2 a_i^2) \quad (9.26)$$

Therefore the use of eqns. 9.18, 9.24 and 9.26 essentially depends on the range of Q used in the small angle diffractometer i.e. $QR_g < 1$ or $QR_g > 1$. If the Guinier condition i.e. $QR_g < 1$ is fulfilled then combining eqns. 9.17 and 9.24 results in the following expression:

$$\frac{1}{I(Q)} = \left[\frac{2V(\chi_s - \chi)}{(b_H - b_D)^2} \right] + \left[\frac{2V(\chi_s - \chi)Q^2 \xi^2}{(b_H - b_D)^2} \right] \quad (9.27)$$

Therefore, from the Ornstein-Zernike plots ($I(Q)^{-1}$ vs. Q^2) of eqn. 9.27 :

$$\text{Slope} = \left[\frac{2V(\chi_s - \chi)\xi^2}{(b_H - b_D)^2} \right] \quad (9.28)$$

$$\text{Intercept } (I(Q)^{-1} \text{ at } Q = 0) = \left[\frac{2V(\chi_s - \chi)}{(b_H - b_D)^2} \right] \quad (9.29)$$

$$\xi^{-2} = \left[\frac{\text{Intercept}}{\text{Slope}} \right] \quad (9.30)$$

Eqns. 9.28, 9.29 and 9.30 can be used to determine values of ξ and χ_{eff} , using slope and intercept values from the $I(Q)^{-1}$ vs. Q^2 plots. χ_{eff} (and radius of gyration) values can also be obtained by fitting scattering intensity data to eqns. 9.17 and 9.18.

As previously shown, both the scattering law, $S(Q)$ and the scattering intensity, $I(Q)$, are infinite at the spinodal point when $Q=0$. Therefore, $I(Q)^{-1}$ at $Q=0$ i.e. the intercept value of the $I(Q)^{-1}$ vs. Q^2 plots, is 0 at the spinodal. The spinodal temperature at each composition can therefore be determined by extrapolating these intercept values against reciprocal temperature to $I(Q)^{-1}=0$. As $\chi_{\text{eff}}=\chi_S$ at the spinodal, a similar extrapolation of the χ_{eff} values against reciprocal temperature to the value of χ_S (determined by eqn. 9.4) also enables the spinodal temperature to be determined. The concentration fluctuation length, ξ , can also be used to determine blend spinodal temperatures. From eqn. 9.25, ξ approaches infinity as χ_{eff} approaches χ_S . Consequently, ξ^{-2} (defined by eqn. 9.30) is zero at $\chi_{\text{eff}}=\chi_S$ and therefore, extrapolation of ξ^{-2} values against reciprocal temperature to $\xi^{-2}=0$ provides another means of determining the spinodal temperature.

Additionally, from the dependence of χ_{eff} values on temperature, the relative χ (enthalpic) and χ (entropic) contributions can be predicted using the Flory derived relationships¹⁰ :

$$\chi \text{ (enthalpic)} = -T[d\chi/dT] \quad (9.31)$$

$$\chi \text{ (entropic)} = d(\chi T)/dT \quad (9.32)$$

9.3 Experimental

Hydrogenous poly(ethylene-co-vinyl acetate) - EVA, supplied by Exxon Chemicals Limited was heated at 373K (24 hours) under vacuum to remove solvent residues. The fully deuterated docosyl diester of poly(ethylene glycol) (DPE) was prepared in two major stages, polymerisation of deuterated polyethylene glycol (Mol. Wt. 400) and subsequent esterification with deuterated docosanoic acid. See Chapter 3 for experimental details.

9.3.1 Blend Preparation

The EVA:DPE blends were prepared by solvent casting from chloroform (HPLC Grade) stock solutions with a total polymer concentration of 5% w/v. The five blends contained DPE volume fractions of 0.09, 0.19, 0.28, 0.48 and 0.73. The solvent was allowed to evaporate at room temperature and the blends finally dried in a vacuum oven at 323K for 48 hours.

9.3.2 Small Angle Neutron Scattering Experiments

Sufficient samples of the blends and pure EVA, DPE samples were used to completely fill a PTFE washer (1.3cm internal diameter, 1mm thick), sandwiched between two quartz windows. To avoid air bubbles in the sample, the top quartz window seal was placed on the sample after melting and then compressed. The samples were then mounted in a cylindrical brass cell and held tightly (to avoid leakage) by a brass ring retainer.

The brass cells were placed in a heated cell holder, mounted in the beam line of the small angle diffractometer (LOQ) on the ISIS pulsed neutron source at the Rutherford Appleton Laboratory. This type of neutron source initially uses a particle accelerator and synchrotron to raise protons to high energy states which are then subsequently directed at a non-fissile Uranium-238 target which releases approximately 25 neutrons for every incident proton. The incident neutron beam, collimated using various devices, is directed at the sample and the scattered radiation is recorded on a two-dimensional electronic detector. The neutron sensitive area on LOQ is 64cms x 64cms. Using the pulsed neutron source, the sample geometry is fixed i.e. θ is constant and the range of Q values is provided by the wavelength distribution of the incident neutron beam.

Scattered neutron intensities were collected at three temperatures, 353K, 368K and 383K. In this temperature range, thermogravimetric analysis on EVA and DPE samples showed no weight loss indicating thermal stability. Due to time constraints, the blend containing 0.09 volume fraction DPE was analysed only at 353K. To enable the background to be subtracted, scattering intensities were recorded for pure hydrogenous

EVA and deuterated DPE samples. The range of neutron wavelengths used was $0.5 \leq \lambda \text{\AA} \leq 12$ and the scattering vector range accessible was approximately $0.01 \leq Q/\text{\AA}^{-1} \leq 0.2$. All the scattered intensities recorded were radially isotropic about the incident beam direction and were corrected for transmission and thickness before subtraction of background using the appropriate volume fraction weighted sum of the scattering from the pure EVA and DPE components. The scattering intensities were corrected to an absolute scale by calibrating the instrument using a blend of deuterated and hydrogenated polystyrene of equal molecular weight. The molecular weights and blend composition were known accurately. The background scattering for this calibrant mixture was obtained using a random copolymer of hydrogenated and deuterated styrene of the same composition and molecular weight as the calibrant mixture.

9.4 Results

The quantity, $(b_H - b_D)^2/V$ which represents the difference between the neutron scattering density of DPE and EVA, is highly dependent on correctly defining the type of repeat unit in each polymer. Additionally, the value of χ_s is based on the degree of polymerisation i.e. the number of repeat units (m) in the polymer chain. Therefore, the accuracy of the χ_{eff} values is dependent on an accurate definition of the polymer repeat unit. In homopolymers, this is not a problem as the repeat unit can be clearly defined. In this study, the hydrogenous EVA is a random copolymer of vinyl acetate and ethylene in the molar ratio of 1:7 respectively (see Chapter 3 - nmr analysis) and the repeat unit can be defined on a molar basis i.e. ($1/8$ vinyl acetate repeat unit) plus ($7/8$ ethylene repeat unit). However, the deuterated material, DPE is a low molecular weight poly(ethylene glycol) segment which has been diesterified with docosanoic acid. An accurate definition of the repeat unit in this type of component can be difficult as it depends on the classification of the aliphatic docosyl ends as either a single docosyl repeat unit or a poly(ethylene) - type component consisting of multiple ethylene repeat units. For consistency in defining the repeat units of both EVA and DPE polymers, the DPE component was treated as an ABA - type block copolymer in which the docosyl ends

(A) were treated as a poly(ethylene) type component (as in the EVA polymer) with multiple ethylene repeat units. The ester groups attaching these separate polymer "blocks" were also accounted for in defining the repeat unit of DPE which (as in EVA) was based on the molar fraction contributions i.e. from ethylene, ethylene glycol and ester repeat units. From this DPE repeat unit, the scattering length (b_D), molar volume of the repeat unit (V) and the number of repeat units (m) can be determined. The volume of the repeat units in both EVA and DPE were determined from Van Krevelen²⁰ at $36.5 \text{ cm}^3\text{mol}^{-1}$ and $33.2 \text{ cm}^3\text{mol}^{-1}$ respectively, using group contribution increments. The similarity of these values to the volume of the poly(ethylene) repeat unit, $32.2 \text{ cm}^3\text{mol}^{-1}$ indicates the large contribution from the poly(ethylene) type component in both these polymers. As the value of the DPE repeat unit volume was based on hydrogenous rather than deuterated group contributions, the actual segment volume of the deuterated component may differ slightly from the calculated value. Therefore, clearly the segment volumes of both EVA and DPE polymers are very similar and effectively occupy the same unit cell volume, as required by the Flory-Huggins lattice theory. It is interesting to note that if the aliphatic docosyl ends in DPE are regarded as **single** repeat units, the values of m , V , b_D and χ_S are significantly altered which result in a large increase in the χ_{eff} values. However, these large χ_{eff} values show a similar dependence on composition and temperature as the previously determined χ_{eff} values (in which the docosyl group is classified as a series of ethylene repeat units). Consequently, the determined spinodal temperatures using both mathematical treatments are identical with only the absolute χ_{eff} values effected.

Figure 9.2 shows Ornstein-Zernike plots ($I(Q)^{-1}$ vs Q^2) for each blend composition at 353K, 368K and 383K respectively, in the Q range $0.001 \leq Q^2/\text{\AA}^{-2} \leq 0.008$, which represented the best linear fit to the scattering data. The error bars for the $I(Q)^{-1}$ data are derived from neutron counting statistics. All plots show that $I(Q)^{-1}$ increases with Q^2 and that the intercept value i.e. $I(Q)^{-1}$ at $Q=0$, increases with a decrease in the DPE volume fraction. Data below 0.001\AA^{-2} have been omitted as this region contained large scattering deviations, as noted in other blend systems^{3,5}. The concentration fluctuation

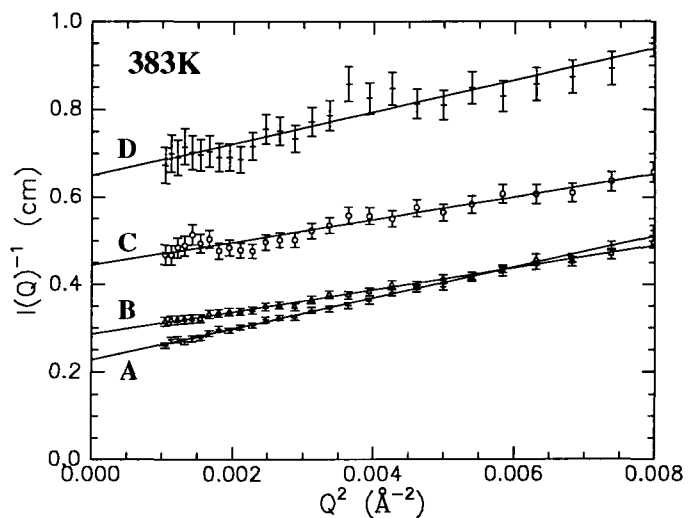
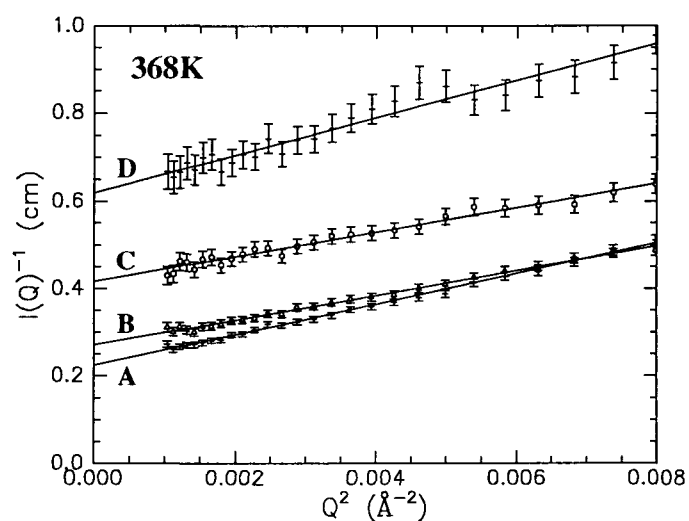
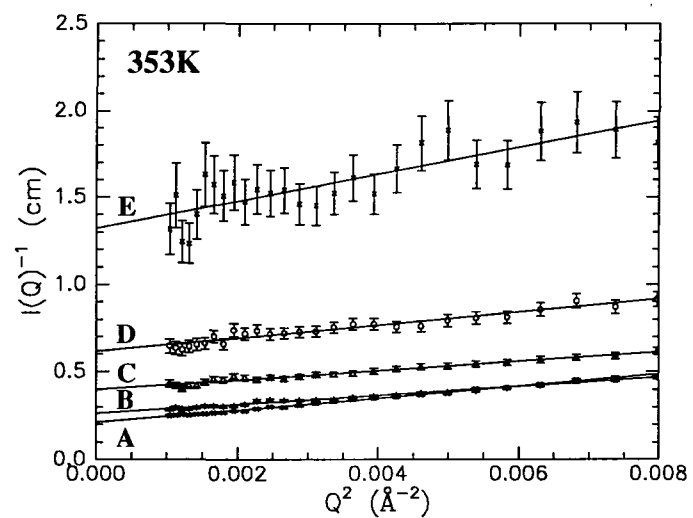


Figure 9.2 : Ornstein-Zerniche plots at 353K, 368K and 383K for :
 0.73DPE (A); 0.48DPE (B); 0.28DPE (C); 0.19DPE (D); 0.09DPE (E).

length, ξ , and χ_{eff} values of each blend at 353K, 368K and 383K were obtained from the slope and intercept values of these plots using eqns. 9.29 and 9.30. χ_s values were calculated from eqn. 9.4 using degree of polymerisation (m) values and volume fractions. The intercept value of these plots represented $I(Q)^{-1}$ at $Q=0$. Relevant values from analysis of this data are shown in Table 9.1.

Figures 9.3 and 9.4 show χ_{eff} and $[I(Q)^{-1}$ at $Q=0]$ values plotted against reciprocal temperature (T^{-1}) for each blend composition. The data points of χ_{eff} and $[I(Q)^{-1}$ at $Q=0]$ were determined within a narrow temperature range to avoid thermal degradation of the DPE component and all appeared to exhibit reasonably linear relationships with T^{-1} . From a long extrapolation of these data, the spinodal temperatures can be estimated i.e. χ_{eff} is extrapolated until it intersects a line indicating the value of χ_s and the $[I(Q)^{-1}$ at $Q=0]$ values are extrapolated to a value of zero. From both these extrapolations the predicted spinodal temperatures closely agree. In the case of ξ^{-2} , due to the values being very similar and close to the extrapolated point of intersection i.e. zero, the long extrapolation of these values to the spinodal temperature has the greatest potential inaccuracy and therefore this extrapolation has been discounted. The spinodal temperatures for each of the blend compositions are shown in Table 9.2 and the predicted phase boundary is shown in Figure 9.5.

Blend Code	EVA Vol. Fraction (ϕ_1)	Temp. (K)	1/Temp. (K^{-1}) ($\times 10^{-3}$)	Segment Volume (V) ($\times 10^{-23}$ cm ³)	Intercept ($(I(Q)^{-1}$ at $Q=0$)	Slope ($(I(Q)^{-1}/Q)$)	χ_s	χ_{eff} ($\times 10^{-3}$)	χ_{eff} Temp	ξ^{-2} (Intercept/Slope) $\times 10^{-2}$
0.09DPE	0.907	353	2.833	6.010	1.322 (0.004)	77.30 (9.90)	0.164	-23.14 (5.62)	-8.167 (1.982)	1.711 (0.310)
0.19DPE	0.812	353	2.833	5.958	0.614 (0.008)	37.42 (2.08)	0.085	-2.643 (1.19)	-0.933 (0.420)	1.641 (0.120)
0.28DPE	0.715	353	2.833	5.905	0.398 (0.004)	26.82 (0.93)	0.060	2.248 (0.54)	0.794 (0.190)	1.485 (0.068)
0.48DPE	0.520	353	2.833	5.798	0.262 (0.002)	25.61 (0.58)	0.042	3.147 (0.34)	1.111 (0.121)	1.025 (0.033)
0.73DPE	0.271	353	2.833	5.661	0.212 (0.002)	34.23 (0.46)	0.041	9.395 (0.28)	3.316 (0.098)	0.620 (0.014)
0.19DPE	0.812	368	2.717	5.958	0.620 (0.008)	42.46 (2.00)	0.085	-3.492 (1.14)	-1.285 (0.420)	1.460 (0.092)
0.28DPE	0.715	368	2.717	5.905	0.415 (0.004)	28.33 (0.93)	0.060	-0.215 (0.54)	-0.079 (0.198)	1.466 (0.063)
0.48DPE	0.520	368	2.717	5.798	0.271 (0.002)	28.03 (0.49)	0.042	1.815 (0.29)	0.668 (0.106)	0.968 (0.024)
0.73DPE	0.271	368	2.717	5.662	0.224 (0.002)	34.87 (0.44)	0.041	7.641 (0.27)	2.812 (0.098)	0.643 (0.013)
0.19DPE	0.812	383	2.611	5.958	0.649 (0.010)	36.22 (2.48)	0.085	-7.592 (1.42)	-2.908 (0.544)	1.791 (0.161)
0.28DPE	0.715	383	2.611	5.905	0.443 (0.005)	26.00 (1.29)	0.060	-4.257 (0.74)	-1.630 (0.285)	1.705 (0.110)
0.48DPE	0.520	383	2.611	5.798	0.286 (0.002)	25.22 (0.45)	0.042	-0.329 (0.26)	-0.126 (0.101)	1.134 (0.028)
0.73DPE	0.271	383	2.611	5.662	0.227 (0.002)	35.23 (0.50)	0.041	7.175 (0.30)	2.748 (0.116)	0.645 (0.015)

Segment Volume (V) values obtained from the volume fractions of EVA ($V = 6.061 \times 10^{-23}$ cm³) and DPE ($V = 5.513 \times 10^{-23}$ cm³). χ_s determined from eqn. 9.4 using repeat units (m) of 87 (EVA) and 34 (DPE). χ_{eff} values obtained using $(b_H - b_D)^2$ value of 1.704×10^{-23} cm². b_H (EVA) = 0.052×10^{-12} cm, b_D (DPE) = 4.180×10^{-12} cm.

Table 9.1 : SANS measurements on EVA:DPE blends

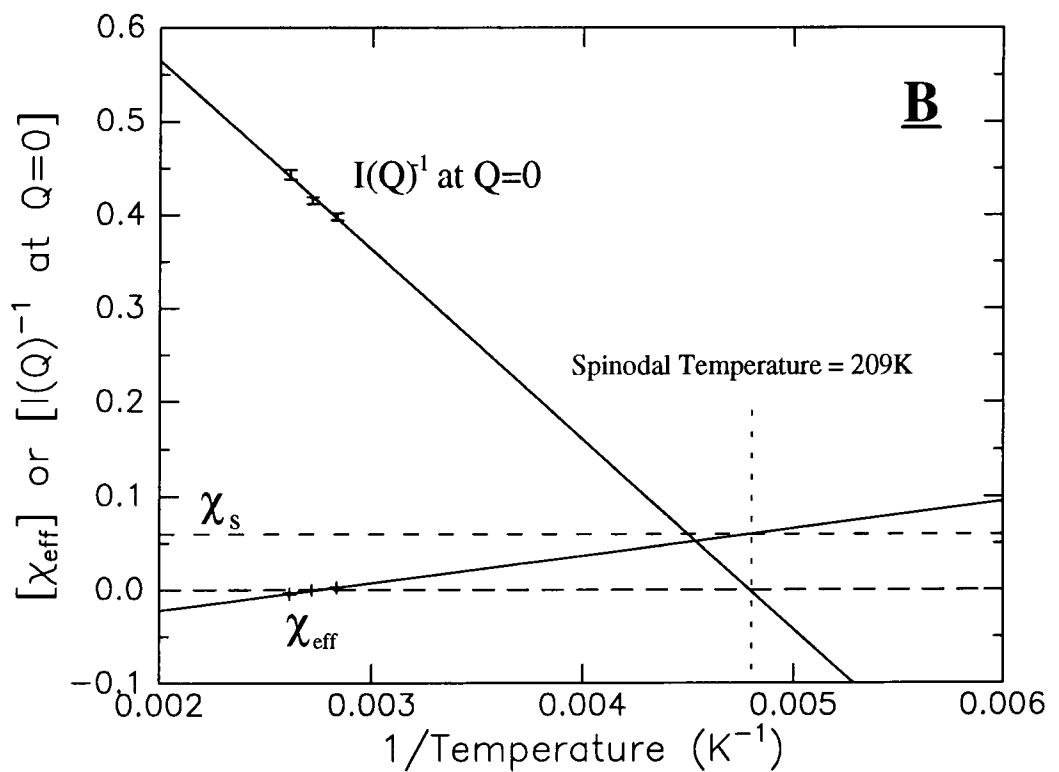
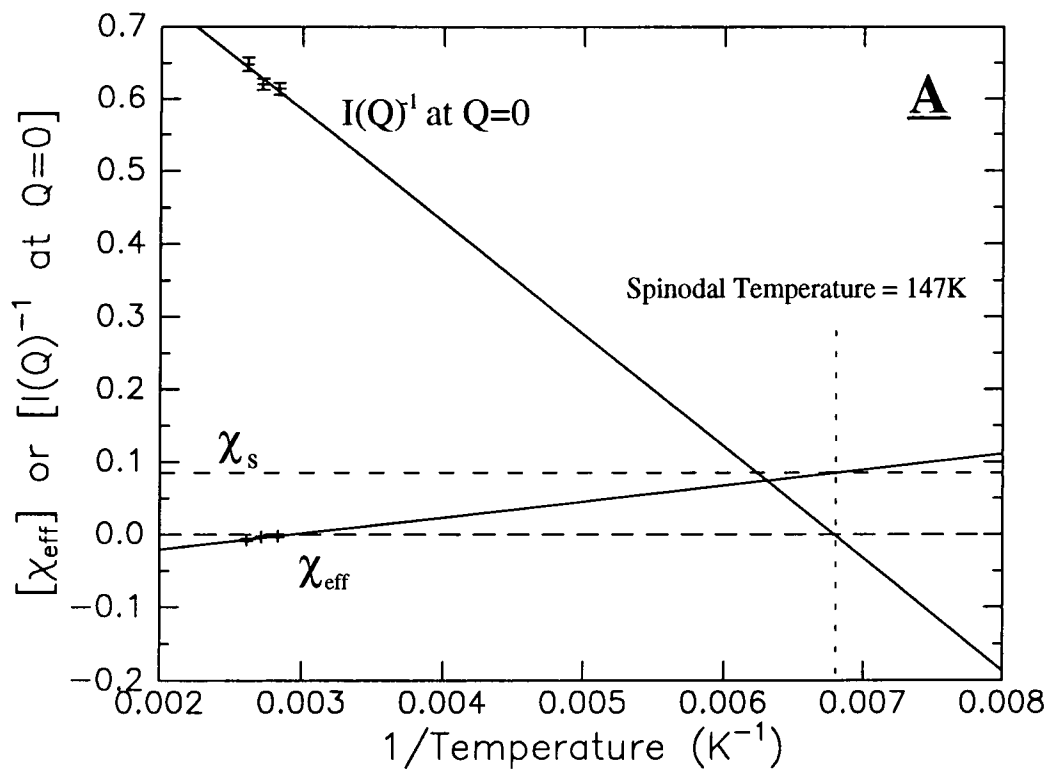


Figure 9.3 : Predicted Spinodal Temperatures in : 0.19DPE (A); 0.28DPE (B).

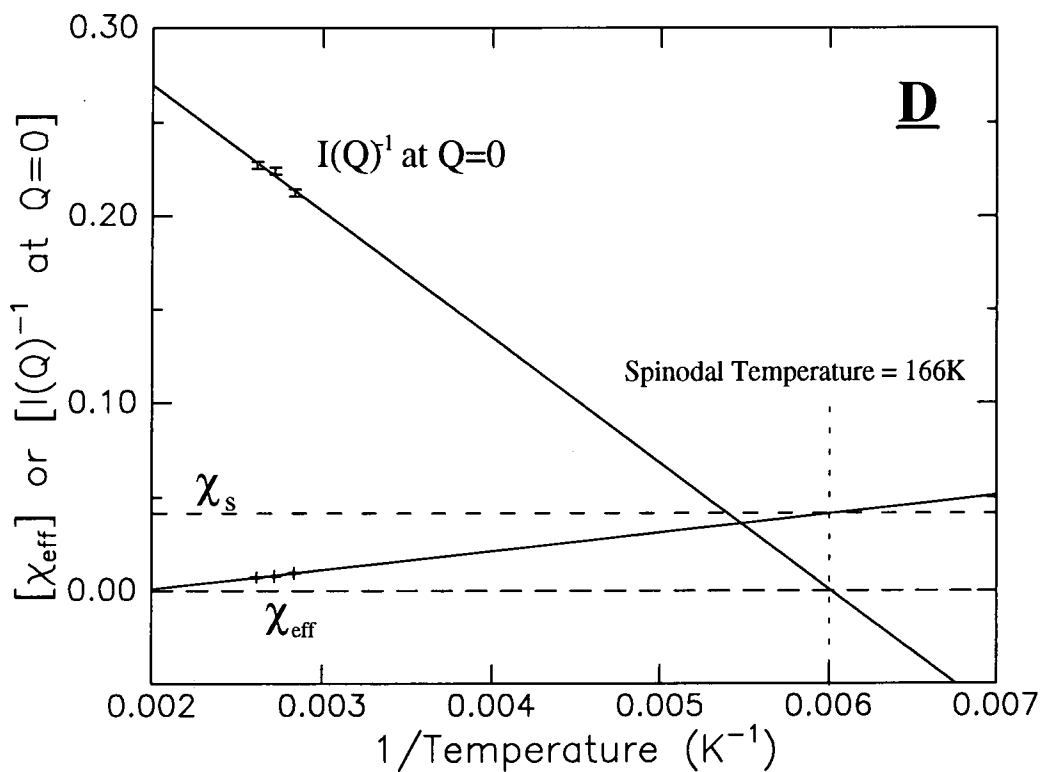
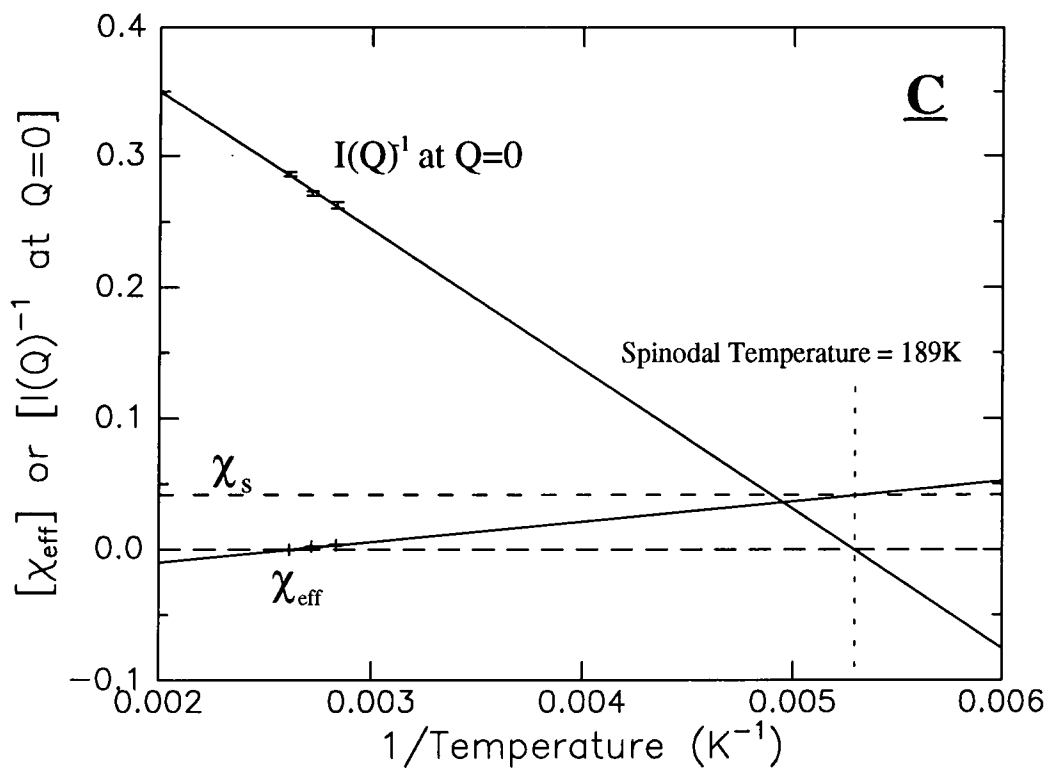


Figure 9.4 : Predicted Spinodal Temperatures in : 0.48DPE (C); 0.73DPE (D).

Blend	Spinodal Temperature (K)
0.19DPE	147
0.28DPE	209
0.48DPE	189
0.73DPE	166

Table 9.2

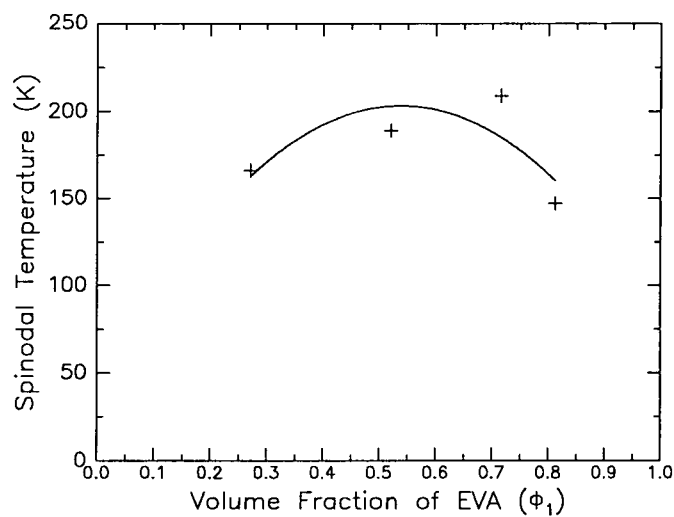


Figure 9.5 : Predicted Spinodal phase boundary in EVA:DPE blends

Figure 9.6 shows the variation of the determined χ_{eff} values as a function of the EVA volume fraction (ϕ_1) at 353K, 368K and 383K. In the EVA volume fraction range of 0.27-0.81, this relationship appears to be reasonably linear. However, at 353K an additional blend composition (0.91 EVA volume fraction) was measured and the resulting χ_{eff} values show a rather pronounced curvature with composition. The observed composition dependence of χ_{eff} values at these melt temperatures contradicts the original definition of χ_{FH} from the Flory-Huggins lattice theory. Figure 9.7 also compares these χ_{eff} values with the spinodal curve calculated using eqn. 9.4. Clearly, at these temperatures and compositions, $\chi_{\text{eff}} < \chi_{\text{S}}$ and the EVA:DPE blends are predicted to be miscible from these data.

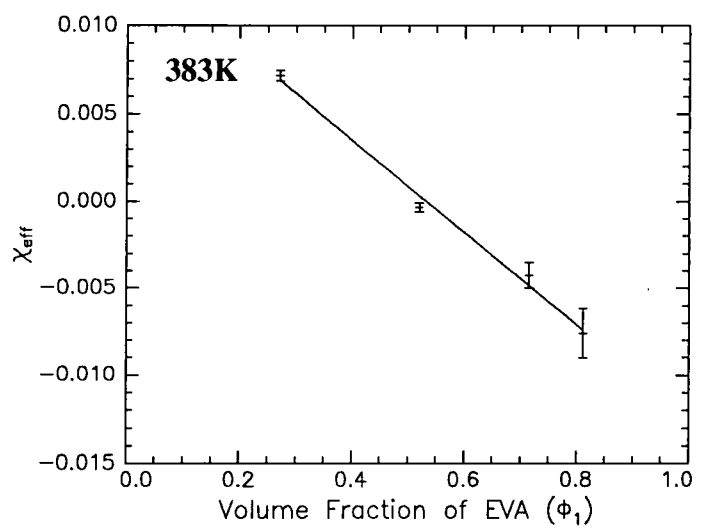
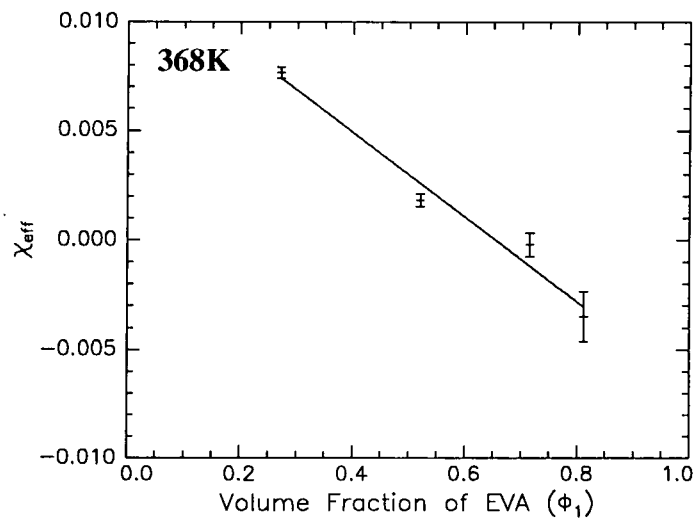
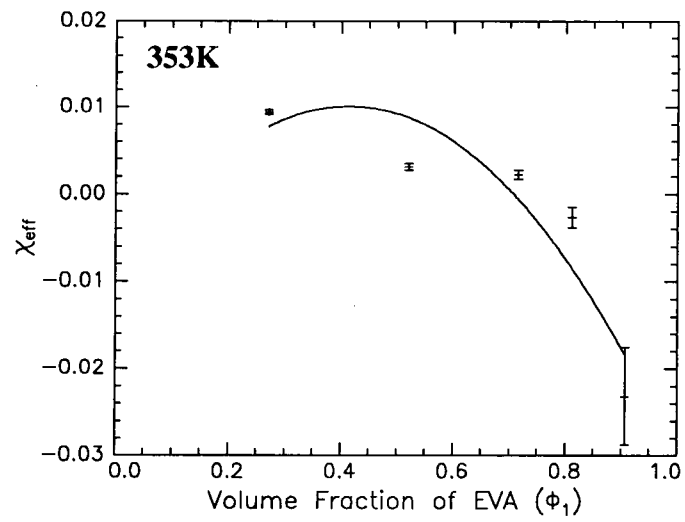


Figure 9.6 : Dependence of χ_{eff} on EVA volume fraction at 353K, 368K and 383K.

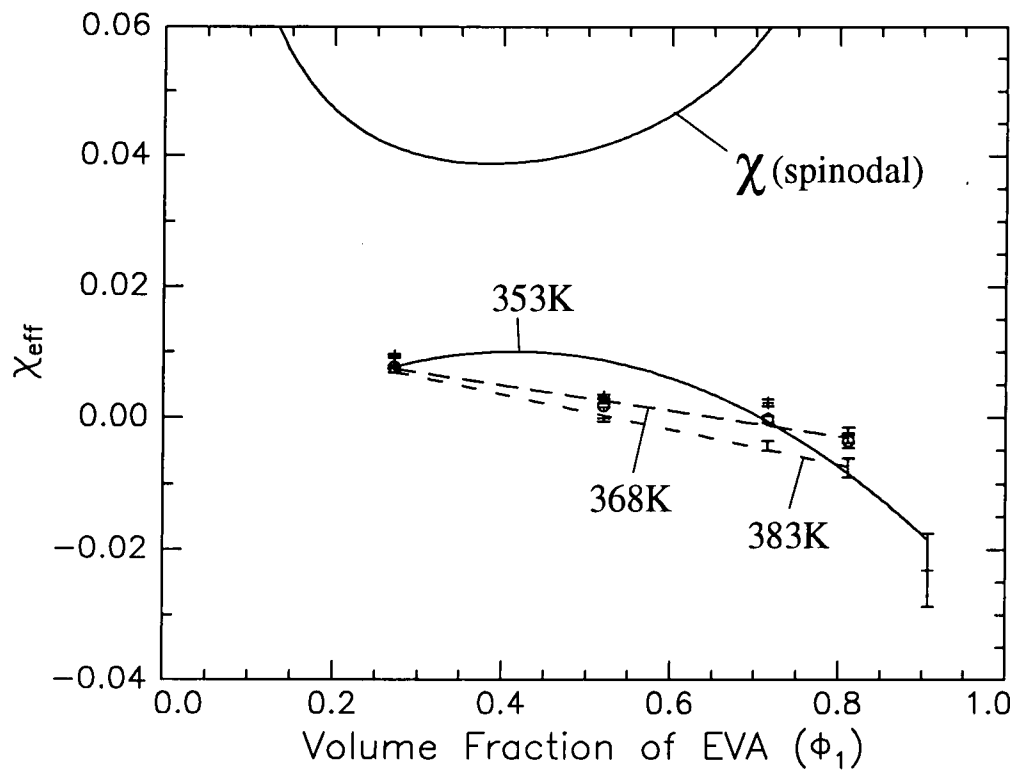


Figure 9.7 : Comparison of χ_{eff} values with the χ (spinodal) curve.

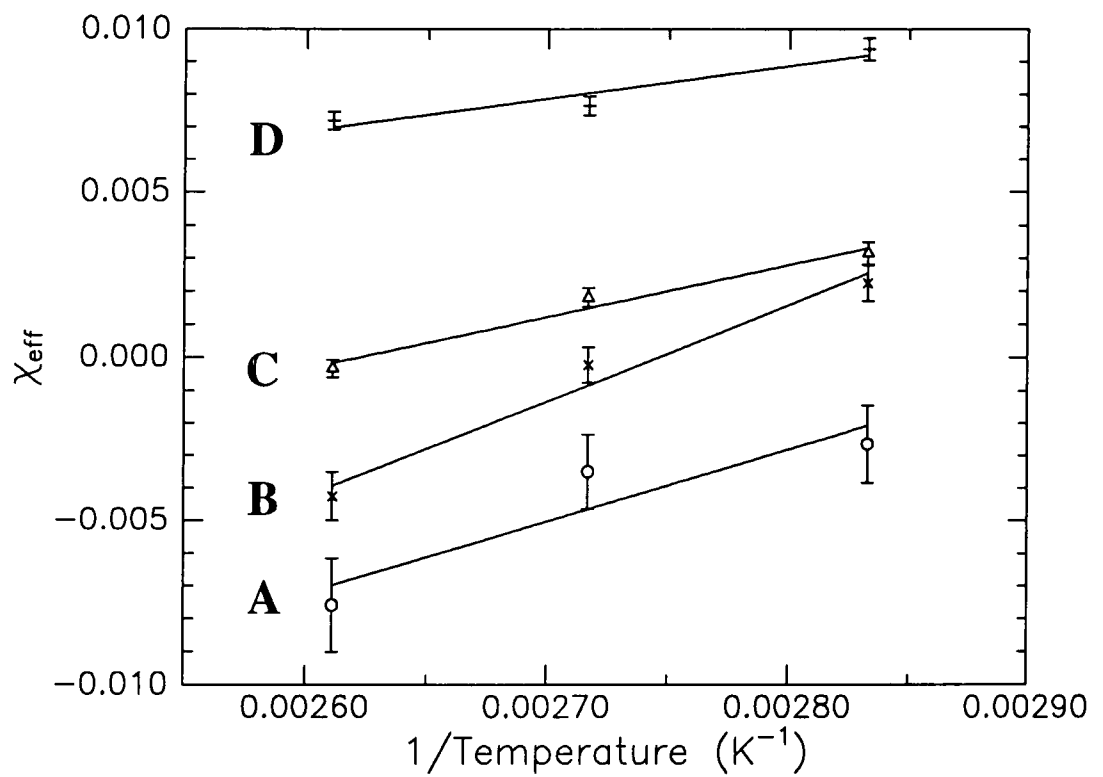


Figure 9.8 : Temperature dependence of χ_{eff} values in :
0.19DPE (A); 0.28DPE (B); 0.48DPE (C); 0.73DPE(D).

Figure 9.8 shows the temperature dependence (T^{-1}) of the determined χ_{eff} values. Although only three data points are available for each composition, the variation appears to indicate linearity over this temperature range. Using eqn. 9.8, analysis of these data results in values of \underline{a} (eqn. 9.9) and \underline{b} (eqn. 9.10) from the intercept and slope respectively and are listed in Table 9.3.

Blend	\underline{a} (Intercept) ($\times 10^{-2}$)	\underline{b} (Slope)	$\beta_{\text{H}} (\gamma=0.06)$	$\beta_{\text{S}} (\gamma=0.06)$ ($\times 10^{-1}$)	$\alpha (\gamma=0.06)$ ($\times 10^{-1}$)
0.19 DPE	-6.46 (2.46)	22.06 (9.03)	22.68 (9.28)	5.45 (1.60) (fitted a values)	-6.05 (1.62) (fitted a values)
0.28 DPE	-8.01 (1.32)	29.18 (4.87)	29.48 (4.91)		
0.48 DPE	-4.09 (0.69)	15.59 (2.52)	15.20 (2.45)		
0.73 DPE	-1.94 (0.84)	10.08 (3.09)	9.38 (2.87)		
			Average =19.18 (8.76)		

Table 9.3 : Enthalpic and Entropic contributions to χ_{eff} values

Terms \underline{a} and \underline{b} represent respectively the separate entropic and enthalpic contributions to these χ_{eff} values. At all blend compositions, the \underline{a} and \underline{b} values are negative and positive respectively i.e. the χ_{eff} values decrease with increasing temperature (eqn. 9.8) which again indicates that these blends have an upper critical solution temperature (UCST) at which phase separation occurs. Table 9.3 also includes values of β_{H} , β_{S} and α . The values of β_{H} were calculated from the \underline{b} values using eqn. 9.10 and a γ value of 0.06 which was obtained using Bondi group contributions²¹ to determine the surface area of the polymer segment ($\sigma_{\text{DPE}} = 2.96 \times 10^9 \text{ cm}^2 \text{ mol}^{-1}$, $\sigma_{\text{EVA}} = 3.14 \times 10^9 \text{ cm}^2 \text{ mol}^{-1}$). β_{S} and α were obtained from the \underline{a} values using a non-linear least squares fit to eqn. 9.9 with $\gamma=0.06$ (see Figure 9.9).

It should be noted that due to the limited number of data points, all these values suffer from relatively large error bars. Indeed as γ is very close to zero i.e. the segment

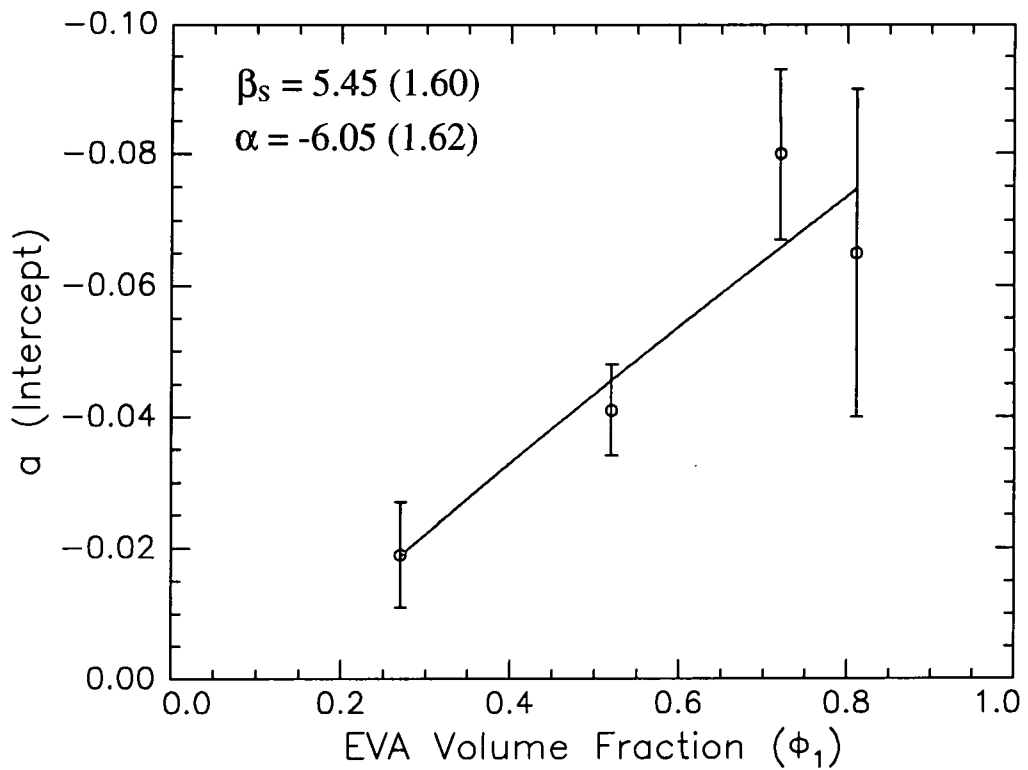


Figure 9.9 : Non-linear least squares fit of eqn. 9.9 ($\gamma=0.06$) to determine β_s and α values.

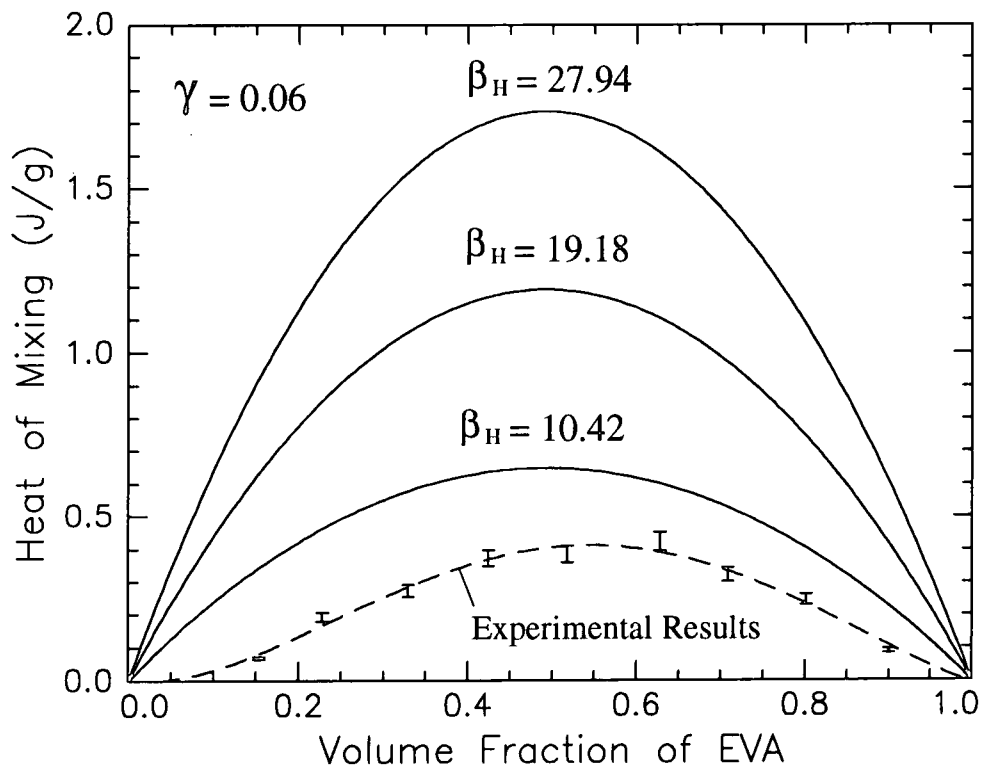


Figure 9.10 : Comparison of experimental and predicted (from eqn. 9.11, $\beta_H=19.18 \pm 8.76$, $\gamma=0.06$) "heat of mixing" values.

volumes of both components are very similar, then according to eqn. 9.10, $\underline{h}=\beta_H$ with both values independent of composition. However, clearly this composition independence is not shown in Table 9.3. Therefore, from these original β_H values, an average β_H value (and error) was obtained i.e. 19.18 ± 8.76 and this range was subsequently used in eqn. 9.11 to predict heat of mixing values on blending the EVA and DPE components. The subsequent heat of mixing values have been converted from J repeat unit⁻¹ to Jg⁻¹ by dividing throughout by 34.5 i.e. the average repeat unit weight of EVA (34.86g) and DPE (34.16g). Figure 9.10 shows this predicted range with EVA volume fraction in comparison with experimental results on the hydrogenous EVA:NECPE blend system (see Chapter 7). Both predicted and experimental heat of mixing values are endothermic resulting in a positive χ (enthalpic) value. However, clearly the calorimetric results are outside the predicted heat of mixing range and suggest a possible difference between the enthalpic interactions in the EVA:DPE and EVA:NECPE blends.

To appreciate the relative importance of variations in both β_H and γ values in predicting heat of mixing values (eqn. 9.11), heat of mixing values were determined using a fixed β_H or γ value with error variations only encompassed within the corresponding γ and β_H values respectively. The range of β_H values previously determined (19.18 ± 8.76) was assumed to contain the "true" value of β_H . Therefore, using the average β_H value of 19.18 and the determined \underline{h} values in Table 9.3, a non-linear least squares fit was applied to eqn. 9.10 which results in a γ value of -0.487 ± 0.414 , as shown in Figure 9.11. This large range of possible γ values was applied to eqn. 9.11 using the fixed β_H value of 19.18 and a heat of mixing range was predicted, as shown in Figure 9.12. To note the effect of variations in the β_H value, γ was fixed at the average fitted value of -0.487 and the variable β_H values (19.18 ± 8.76) were applied to eqn. 9.11 to again give a heat of mixing range (Figure 9.13). Clearly, the predicted heat of mixing ranges are considerably more dependent on variations in the β_H value than that of the γ value. As the variation in the determined β_H values from neutron scattering

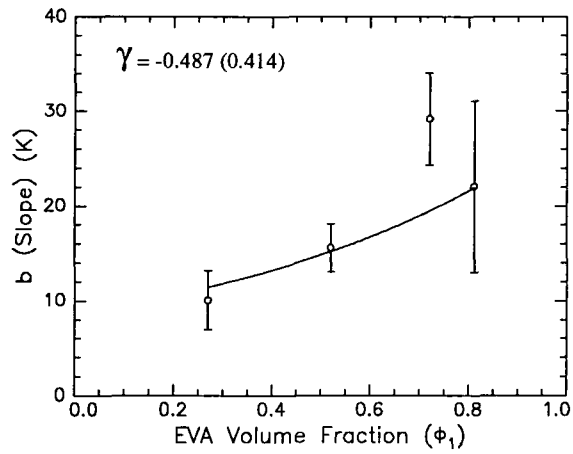


Figure 9.11 : Non-linear least squares fit of eqn. 9.10 ($\beta_H = 19.18$) to determine range of γ values.

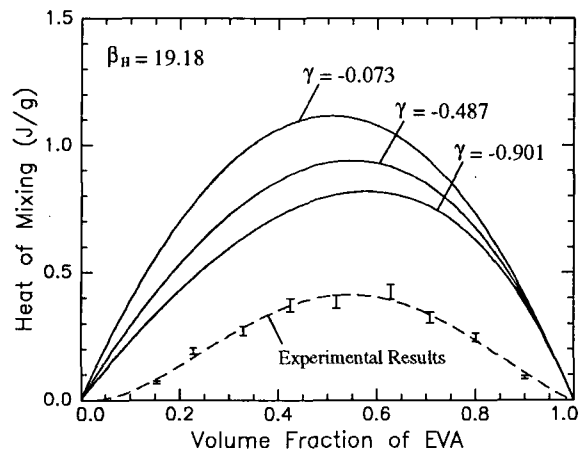


Figure 9.12 : Comparison of experimental and predicted (from eqn. 9.11, $\beta_H=19.18$, $\gamma= -0.487 \pm 0.414$) "heat of mixing" values.

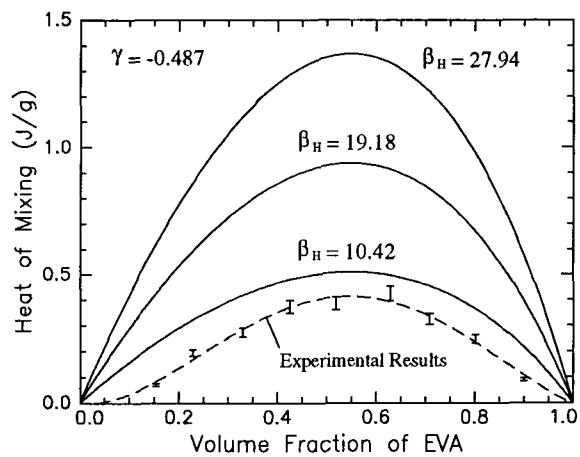


Figure 9.13 : Comparison of experimental and predicted (from eqn. 9.11, $\beta_H=19.18 \pm 8.76$, $\gamma= -0.487$) "heat of mixing" values.

measurements is large (with $\gamma=0.06$) this may account to some extent for differences between experimental and predicted results.

From the Flory derived expressions (eqns. 9.31 and 9.32) and the slopes of χ_{eff}/T and $(\chi_{\text{eff}}T)/T$ (Figure 9.14), the separate χ (enthalpic) and χ (entropic) contributions to χ_{eff} have been determined for each composition at 353K, 368K and 383K (Table 9.4).

Blend	χ_{eff}/T (slope) ($\times 10^{-4}$)	$(\chi_{\text{eff}}T)/T$ = χ (entropic) (slope) ($\times 10^{-2}$)	χ (enthalpic) (353K) ($\times 10^{-2}$)	χ (enthalpic) (368K) ($\times 10^{-2}$)	χ (enthalpic) (383K) ($\times 10^{-2}$)
0.19DPE	-1.65 (0.63)	-6.58 (2.45)	5.82 (2.21)	6.07 (2.30)	6.32 (2.40)
0.28DPE	-2.17 (0.30)	-8.08 (1.31)	7.65 (1.07)	7.98 (1.12)	8.30 (1.16)
0.48DPE	-1.16 (0.16)	-4.12 (0.68)	4.09 (0.55)	4.26 (0.58)	4.44 (0.60)
0.73DPE	-0.74 (0.25)	-1.89 (0.85)	2.61 (0.88)	2.72 (0.91)	2.83 (0.95)

Table 9.4 : χ (enthalpic) and χ (entropic) contributions to χ_{eff} values

Figure 9.15, showing the dependence of χ (enthalpic) and χ (entropic) values on composition at 353K in comparison with the calculated values of χ at the spinodal, χ_s (as determined by eqn. 9.4) is typical of these blends. From these separate contributions, the miscibility of the blend appears to be due to a very dominant and favourable χ (entropic) contribution i.e. χ (entropic) $<\chi_s$ with the χ (enthalpic) contribution actually appearing to favour immiscibility i.e. χ (enthalpic) $\approx\chi_s$.

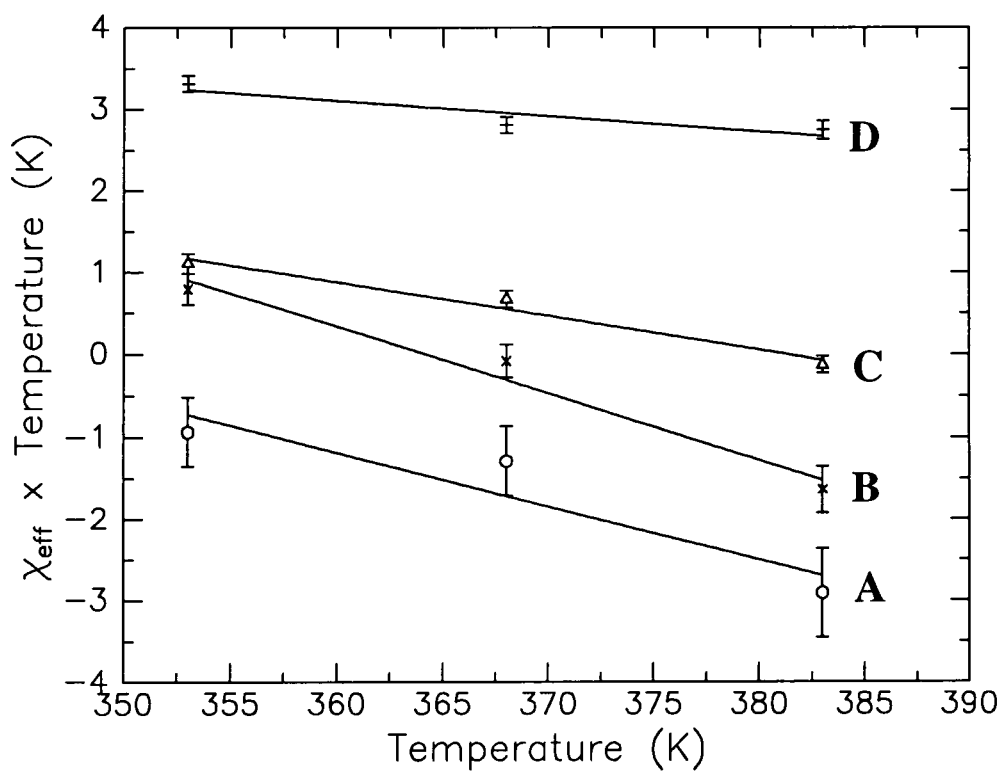
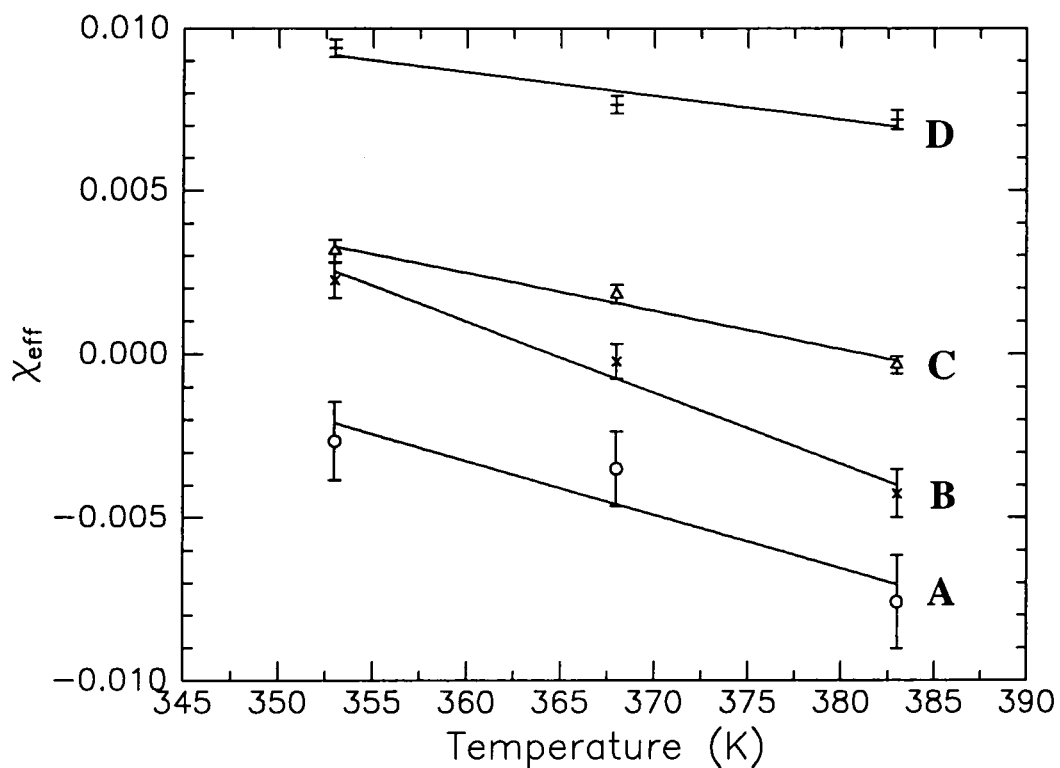


Figure 9.14 : Dependence of temperature on χ_{eff} and $(\chi_{\text{eff}}T)$ values for : 0.19DPE (A); 0.28DPE (B); 0.48DPE (C); 0.73DPE (D).

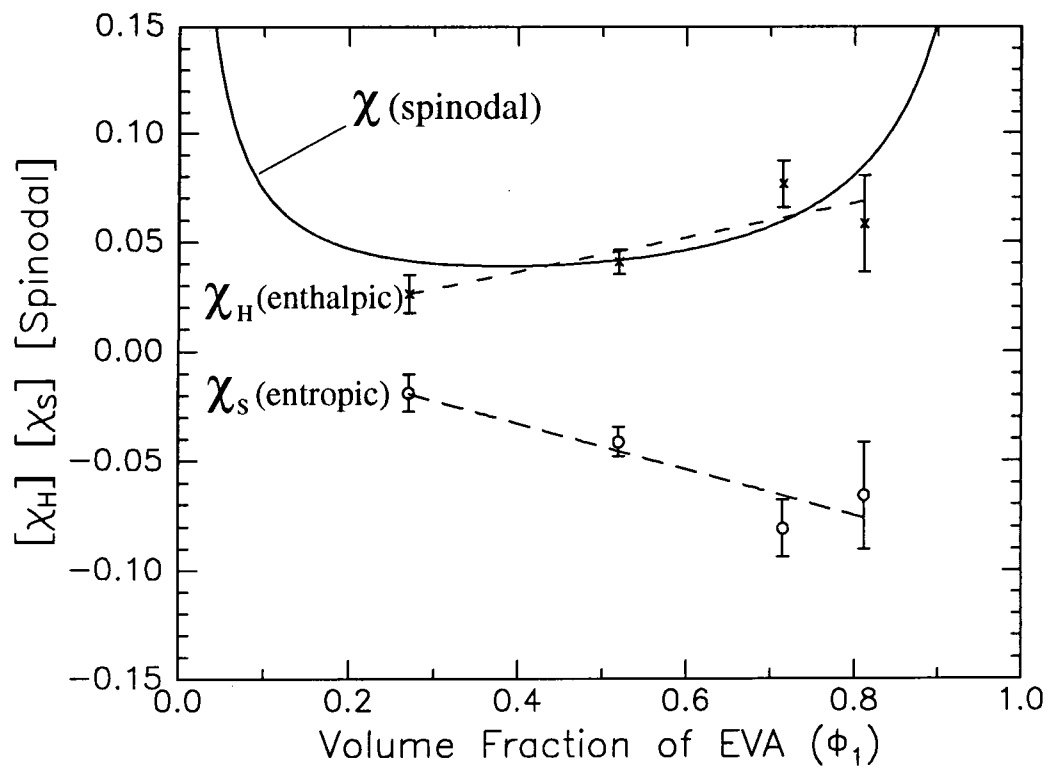


Figure 9.15 : χ (enthalpic) and χ (entropic) contributions to χ_{eff} values at 353K.

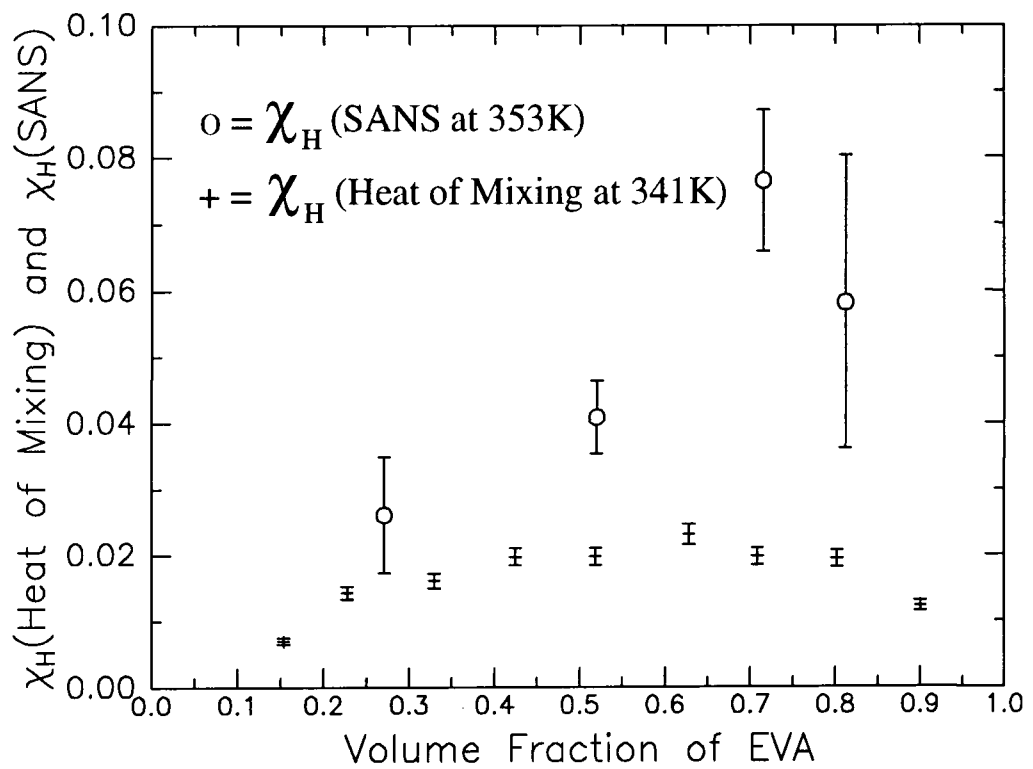


Figure 9.16 : χ_H (enthalpic) values from SANS and Heat of Mixing measurements

9.5 Comparison of χ (enthalpic) values from SANS and Heats of Mixing

Figure 9.16 compares χ (enthalpic) values determined from SANS (at 353K) and heat of mixing (at 341K) measurements (Chapter 7).

χ (enthalpic) values from these techniques are of a similar magnitude and appear to indicate a composition dependence. Due to the limited number of χ (enthalpic) values from SANS and their relatively large error bars, the true composition dependence is not clear. In contrast, χ (enthalpic) values from heats of mixing show a clear parabolic composition dependence.

9.6 Determination of Radii of Gyration (and χ_{eff}) values

Radii of gyration (R_{gi}) values were determined by the non-linear least squares fitting of eqn. 9.17 to the neutron scattering data using the reciprocal of eqn. 9.18 as the expression for $S(Q)$. The only adjustable parameters of the fit were radii of gyration values for the hydrogenous and deuterated components, R_{gH} and R_{gD} respectively and the equation was fitted over the Q range $0.01\text{-}0.2\text{\AA}^{-1}$. χ_{eff} values used in the fit were as determined from the Ornstein-Zernike plots and are shown (with the remaining fit parameters) in Table 9.1.

The resulting fitted values of R_{gH} and R_{gD} at various compositions and temperatures are shown in Table 9.5. The average R_{gH} (EVA) and R_{gD} (DPE) values were determined at $21.77\pm 3.97\text{\AA}$ and $12.97\pm 2.01\text{\AA}$ respectively, over the temperature and composition ranges.

Using these R_{gH} and R_{gD} values as fixed fitting parameters, the least squares fitting of eqn. 9.17 was also used to determine χ_{eff} values. These values are also shown in Table 9.5 and are compared to χ_{eff} values (determined from Ornstein-Zernike plots) in Figure 9.17.

Blend Code	EVA Vol. Fraction (ϕ_1)	Temp. (K)	R_{gH} (EVA) Å	R_{gD} (DPE) Å	χ_{eff} (eqn. 9.17)
0.09DPE	0.907	353	27.27	13.51	-0.6387e-01
0.19DPE	0.812	353	19.31	13.55	-0.1525e-01
0.28DPE	0.715	353	29.67	8.87	-0.1371e-02
0.48DPE	0.520	353	17.87	15.08	-0.2250e-02
0.73DPE	0.271	353	20.09	15.66	0.4106e-02
0.19DPE	0.812	368	27.33	12.22	-0.1775e-01
0.28DPE	0.715	368	20.60	12.43	-0.3509e-02
0.48DPE	0.520	368	17.64	15.59	-0.5691e-02
0.73DPE	0.271	368	22.94	11.41	0.1417e-02
0.19DPE	0.812	383	20.36	13.21	-0.1863e-01
0.28DPE	0.715	383	17.06	13.15	-0.7165e-02
0.48DPE	0.520	383	18.91	14.30	-0.5366e-02
0.73DPE	0.271	383	23.98	9.59	0.1773e-03

Table 9.5 : Determination of Radii of Gyration ($R_{g,i}$) and χ_{eff} values in EVA:DPE blends

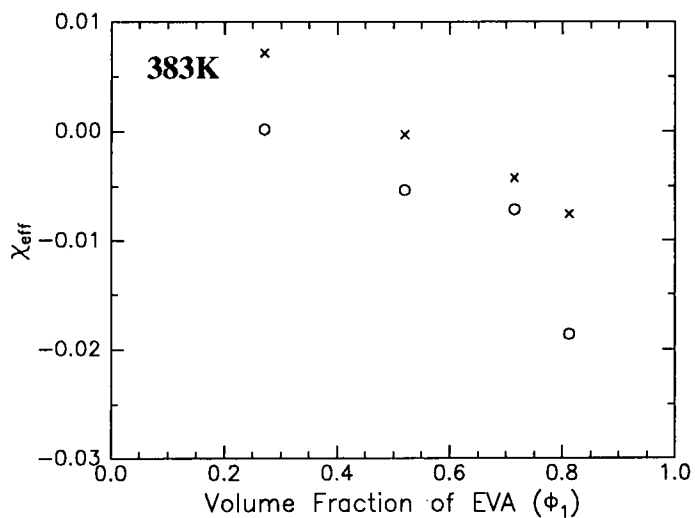
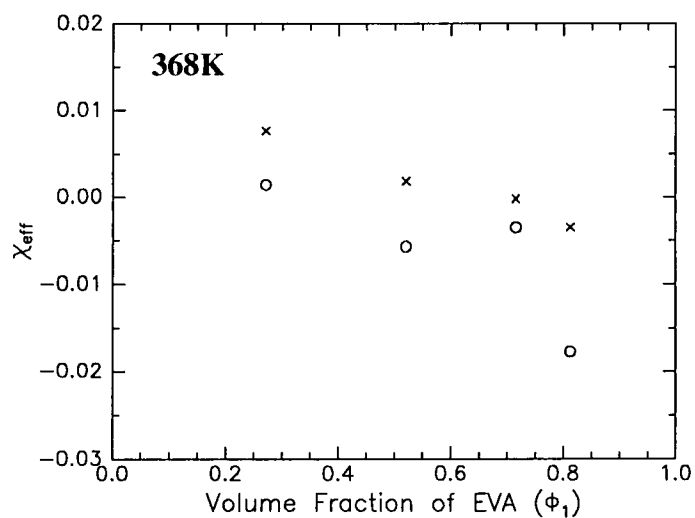
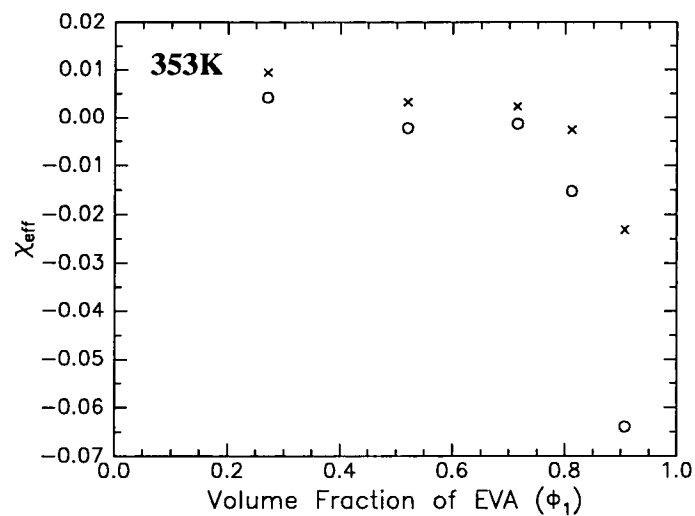


Figure 9.17
 Comparison of χ_{eff} values from Ornstein Zernike plots (X) and Radius of Gyration measurements (O) at 353K, 368K and 383K.

9.7 Discussion

From SANS measurements, the determined χ_{eff} values clearly indicate that blends of hydrogenous poly(ethylene-co-vinyl acetate) - EVA and deuterated poly(ethylene glycol) docosyl diester - DPE, are miscible at melt temperatures of 353K-383K for DPE volume fractions of 0.19, 0.28, 0.48 and 0.73. χ_{eff} values also appear to decrease reasonably linearly with increasing EVA volume fraction, except at high EVA volume fractions (0.09DPE) and such a dependence has been observed in other polymer blends⁶.

Spinodal temperatures for each blend composition, predicted from the extrapolation of χ_{eff} and $[I(Q)^{-1} \text{ at } Q=0]$ data points with reciprocal temperature, characterise the phase boundary of the blend as an upper critical solution temperature (UCST) at approximately 200K. However, a long extrapolation of these data is required to determine these spinodal temperatures which considerably magnifies any small error deviation in the observed linear relationship between 353K and 383K. Consequently, the accuracy of the spinodal temperature determination inevitably suffers. As the presence of the UCST is below the crystallisation temperature of the DPE component, this prediction is somewhat hypothetical, as the phase boundary cannot be observed on cooling to <200K due to prior crystallisation of DPE.

From the dependence of the χ_{eff} values with reciprocal temperature, the separate entropic (\underline{a}) and enthalpic (\underline{b}) contributions to χ_{eff} (eqn. 9.8) have been determined from the intercept and slope respectively. The entropy of mixing factor, \underline{a} is negative in all blends and favourable to miscibility which consequently results in negative α and positive β_S values (from a non-linear least squares fit to eqn. 9.9). In contrast, the enthalpic term, \underline{b} (and β_H) is positive at each composition, unfavourable to miscibility and would be expected to show endothermic (positive) heat of mixing values when the DPE and EVA components are blended. The negative and positive signs of the \underline{a} and \underline{b} terms respectively are consistent with other blends known to exhibit UCST behaviour²². In contrast, a well-known blend exhibiting LCST behaviour i.e. polystyrene and poly(vinyl methyl ether) blends have positive \underline{a} and negative \underline{b} values⁶. The \underline{b} terms have been used in eqn. 9.10 (using $\gamma=0.06$ as calculated from Bondi contributions²¹) to

determine β_H values for each blend composition. As the calculated value of γ is very small i.e. the cross sectional area of both component repeat units are similar, this should result (from eqn. 9.10) in values of \underline{h} and β_H which are essentially independent of composition with $\underline{h} \approx \beta_H$. However, both the \underline{h} and β_H values in Table 9.3 appear to display a possible parabolic dependence on composition although due to the large variations in both \underline{h} and β_H values, this cannot be confirmed. The β_H values were therefore averaged and the standard deviation calculated to give the variation in β_H . From the variation in these β_H values and using a γ value of 0.06, a maximum and minimum "heat of mixing" range was predicted from eqn. 9.11 and compared to experimental results on the hydrogenous blend, EVA and NECPE (see "Heat of Mixing" - Chapter 7). Clearly there is a discrepancy between predicted and experimental values which possibly suggests a difference in the enthalpic interaction between the EVA blend systems containing hydrogenous (NECPE) and deuterated (DPE) components. Deuteration undoubtedly accounts for some alteration in the value of χ_{eff} and consequently, the "heat of mixing" value. However, another contribution towards this difference maybe the wide variation in the \underline{h} (and β_H) values due to only three (χ_{eff} versus T^{-1}) data points being available in which to determine the \underline{h} value. The predicted heat of mixing ranges are clearly more dependent on variations in the β_H rather than the γ value, as shown in Figures 9.12 and 9.13. Therefore, the variation about the mean β_H value in Table 9.3 which is based on only four data points may not represent the true β_H variation and consequently, the minimum and maximum heat of mixing range may be significantly changed, possibly encompassing the experimental results.

An additional analysis of these data has been the determination of the relative χ (enthalpic) and χ (entropic) contributions, as derived by Flory¹⁰, to the χ_{eff} values. From these contributions (Figure 9.15), the χ (enthalpic) values are positive (indicating an endothermic heat of mixing) and are similar to χ_S , appearing to favour immiscibility. However, due to a very dominant and favourable χ (entropic) contribution, $\chi_{\text{eff}} < \chi_S$, indicating that the blend is miscible in this temperature range. This clearly agrees with

the conclusions from the determined entropic (a) and enthalpic (b) terms and the endothermic heat of mixing values (predicted and experimental).

χ (enthalpic) values from SANS and heat of mixing measurements (Figure 9.16) are of a similar magnitude and appear to indicate some composition dependence. Differences between the absolute values obtained from these techniques may again be attributed to possible differences in the enthalpic interaction with EVA due to deuteration of the poly(ethylene glycol) ester.

The R_{gH} and R_{gD} values, determined from a non-linear least squares fit of eqn. 9.17 are as expected, relatively small due to the low molecular weight of both components. The radii of gyration for each component appear to show no apparent dependence on temperature or blend composition. From these R_{gi} values and the Q range sampled during these experiments i.e. $0.001 \leq Q^2/\text{\AA}^{-2} \leq 0.008$, the Guinier condition ($QR_{gi} < 1$) is essentially fulfilled justifying the use of the Ornstein-Zernike expression (eqn. 2.24) to determine χ_{eff} values.

χ_{eff} values determined from these R_{gi} values and a non-linear least squares fit of eqn. 9.17 closely agree with χ_{eff} values from the Ornstein-Zernike plots and again indicate that the EVA:DPE blend is miscible at these melt temperatures.

Deuterating one of the polymer components in neutron scattering measurements is generally based on the assumption that this results in no significant change in the chemical or physical characteristics of the component i.e. χ between deuterated and hydrogenous isomers of the same polymer is effectively 0. However, the effects of changing the hydrogen mass are not completely negligible e.g. the melting point of ice is increased by 4K on deuteration²³. In polymer blends, this thermodynamic difference has also been highlighted, the lower critical solution temperature of polystyrene and poly(vinyl methyl ether) blends is increased by up to 40K on deuterating the polystyrene component²⁴. Also, blends of hydrogenous and deuterated homopolymers i.e. polybutadiene²² and polystyrene²⁵ have shown phase separation and have been characterised by an upper critical solution temperature. Therefore, clearly $\chi \neq 0$ between deuterated and hydrogenous isomers of the same polymer and the change in properties

due to deuteration is dependent on the magnitude of this χ value. Buckingham and Hentschel²⁶ discussed theoretically the contribution to χ of specific volume differences between the deuterated and hydrogenous polymers and predicted, several years before it was confirmed experimentally, that high molecular weight mixtures of homopolymer isomers should exhibit phase segregation. Polarizability differences in isotopic polymer mixtures has also been suggested as a possible contribution to χ ⁵. Therefore, clearly thermodynamic differences exist between deuterated and hydrogenous components and consequently the isotope labelling technique must be employed with caution.

The interaction between DPE and EVA is assumed to be comparable with that of the fully hydrogenous blend system i.e. NECPE and EVA, which has been characterised using various techniques, outlined in other chapters. In view of the small amount of deuterated blend material available, the most suitable method of determining possible thermodynamic differences between the interactions of EVA:DPE and EVA:NECPE blend systems was by melting point depression analysis (see Chapter 4). Consequently, blending the semi-crystalline DPE and NECPE polymers with amorphous EVA results in very similar melting point depression values with the determined interaction parameters indicating miscibility in both blends at the melting point. Therefore, it appears therefore that deuteration in these blends does not significantly alter the "thermodynamics of mixing" and SANS analysis results can be related to the characterisation of the hydrogenous blend. However, it should be noted that the isotopic effect is not negligible as shown by the DPE component having a melting point 8K below that of the hydrogenous NECPE.

The SANS-determined χ_{eff} values in this study appear to show a composition dependence which contradicts the original assumptions of the Flory-Huggins lattice theory. Several theories have been proposed to explain this dependence which has been noted from SANS measurements on numerous polymer blends. Muthukumar¹² has suggested that monomer concentration fluctuations result in deviations from the lattice theory. Sanchez et. al.^{6,27} have suggested that the volume changes on mixing which arise in experimental systems²⁸ result in composition dependent χ_{eff} values. Such volume

changes (or free volume effects) are not accounted for in either the lattice theory or the RPA approach which assumes that polymer blends are incompressible in deriving the structure factor (S). The compositional dependence of χ_{eff} values have also been attributed to departures in the initial Flory-Huggins assumption that χ is a local parameter, only defined through nearest neighbour interactions²⁹. Freed³⁰ and recently Kumar¹³ have attempted to account for the effects of free volume on the scattering from a polymer blend i.e. developing a compressible form of the RPA. From Monte Carlo simulations, Kumar suggested that the unusual composition dependence of χ_{eff} is due, at least in part, to excess volume changes on mixing which are not incorporated into the "incompressible" RPA approach.

The general implication of all these theories is that the concentration dependence of SANS determined χ values is a direct manifestation of the general inadequacies e.g. assuming incompressibility of polymer blends, of both the original Flory-Huggins lattice theory and the RPA.

9.8 **References**

1. M.Shibayama, H.Yang and R.S.Stein, C.C.Han, *Macromolecules*, 18, 2187 (1985).
2. H.Hasegawa, S.Sakurai, M.Takenaka, T.Hashimoto and C.C.Han, *Macromolecules*, 24, 1813 (1991).
3. I.Hopkinson, F.T.Kiff, R.W.Richards, S.M.King and H.Munro, *Polymer*, 35, 1722 (1994).
4. P.G.de Gennes, "Scaling Concepts in Polymer Physics", Cornell University Press (1979).
5. F.S.Bates, M.Muthukumar, G.D.Wignall and L.J.Fetters, *J. Chem. Phys.*, 89, 535 (1988).
6. C.C.Han, B.J.Bauer, J.C.Clark, Y.Muroga, Y.Matsushita, M.Okada, Q.Tran-cong, T.Chang and I.C.Sanchez, *Polymer*, 29, 2002 (1988).
7. N.P.Balsara, L.J.Fetters, N.Hadjichristidis, D.J.Lohse, C.C.Han, W.W.Graessley and R.Krishnamoorti, *Macromolecules*, 25, 6137 (1992).
8. P.J.Flory, *J. Chem. Phys.*, 9, 660 (1941).
9. M.L.Huggins, *J. Chem. Phys.*, 9, 440 (1941).
10. P.J.Flory, "Principles of Polymer Chemistry", Cornell University Press (1953).
11. R.Koningsveld, in "Integration of Fundamental Polymer Science and Technology", L.A.Kleintjens, P.J.Lemstra, Eds., Elsevier Applied Science, Amsterdam (1986).
12. M.Muthukumar, *J. Chem. Phys.*, 85, 4722 (1986).
13. S.K.Kumar, *Macromolecules*, 27, 260 (1994).
14. R.Krishnamoorti, W.W.Graessley, N.P.Balsara and D.J.Lohse, *J. Chem. Phys.*, 100, 3894 (1994).
15. I.G.Voight-Martin, K.H.Leister, R.Rosenau and R.Koningsveld, *J. Polym. Sci., Polym. Phys. Ed.*, 24, 723 (1986).
16. R.Koningsveld and L.A.Kleintjens, *J. Polym. Sci., PS* 61, 221 (1977).
17. P.E.Tomlins and J.S.Higgins, *Macromolecules*, 21, 425 (1988).

18. P.Debye, *J. Phys. Colloid Chem.*, 51, 18 (1947).
19. A.Guinier and G.Fournet, "Small Angle Scattering of X-rays", John Wiley and Sons, New York (1955).
20. D.W.Van Krevelen, "Properties of Polymers", Elsevier (1990).
21. A.Bondi, *J. Phys. Chem.*, 68, 441 (1964).
22. F.S.Bates, S.B.Dierker and G.D.Wignall, *Macromolecules*, 19, 1938 (1986).
23. *Handbook of Chemistry and Physics*, 68th Edition, CRC Press, Boca Raton, FL (1988).
24. H.Yang, G.Hadziioannou and R.S.Stein, *J. Polym. Sci., Polym. Phys. Ed.*, 21, 159 (1983).
25. F.S.Bates and G.D.Wignall, *Macromolecules*, 19, 932 (1986).
26. A.D.Buckingham and H.G.E.Hentschel, *J. Polym. Sci. Polym. Phys. Ed.*, 18, 853 (1980).
27. I.C.Sanchez, *Annual Rev. Mater. Sci.*, 13, 387 (1983).
28. J.K.H.Al-Kafaji, Z.Ariffin, J.Cope and C.Booth, *J. Chem. Soc., Faraday Trans. 1*, 81, 223 (1985).
29. J.G.Curro and K.S.Schweizer, *Macromolecules*, 24, 6736 (1991).
30. H.Tang, K.F.Freed, *Macromolecules*, 24, 958 (1991).

CHAPTER 10

CONCLUSIONS

(and suggestions for Future Work)

The objective of this work was to characterise the thermodynamics and miscibility of several poly(ethylene-co-vinyl acetate), EVA, based polymer blends. This characterisation was to include assessing the relative enthalpic and entropic thermodynamic contributions to the interaction parameter (χ) of these blends, determined from the classical Flory-Huggins lattice theory.

To determine the enthalpic component of the blend interaction parameter (χ_H), a specialised blend calorimeter was designed and constructed to measure the "heat of mixing" on blending these polymers in the melt state (Chapter 6). Additionally, "heats of mixing" have been determined for each of these polymers on blending with docosane (C22 alkane). Docosane was selected to represent a polyethylene-type component with a large configurational entropy contribution, favourable to miscibility. Combining these enthalpy values with configurational entropy of mixing values (calculated from the Flory-Huggins lattice theory) has enabled the free energy change on mixing to be estimated for each blend. However, the original lattice theory is unable to estimate configurational entropy contributions from either the aliphatic/ester branching in these polymers (which produce in effect low molecular weight side-arms) or the high polydispersity of the FVA component. Consequently, due to these inadequacies, the resulting free energy changes may not be accurately determined. Comparing the predicted miscibilities from these free energy values and other techniques in this study, will indicate the suitability of the lattice theory approach in characterising miscibility from heat of mixing measurements in these highly branched and polydispersed (FVA) components.

In all the blends studied, the heat of mixing was endothermic and consequently, the enthalpic interaction parameter values were positive i.e. unfavourable to miscibility. The EVA and docosane based blends with the highly branched polymers, FVA, PI and LMPI

have enthalpic interaction parameters which are reasonably independent of composition (as defined in the original lattice theory). These blends show a slight linear decrease in χ_H values with increasing EVA content which may possibly be attributed to surface area (and hence contact area) differences between the polymer repeat units. In contrast, blends involving the essentially "linear" polymers, NECPE and EVA show a large composition dependence in the χ_H values which cannot be described by the lattice theory (based on random mixing) or surface area differences alone. It is suggested that this dependence may be attributed to non-random mixing of the polymer components due to quasi-chemical interactions in polymers containing distinct polar and non-polar segments. The estimated free energy of mixing values for the EVA:NECPE blend were found to be negative over the composition range, satisfying one of the two criteria for miscibility to occur. In contrast, the free energy change in the EVA:PI blend suggests possible immiscibility i.e. $\Delta G_{\text{mix}} \approx 0$. The remaining polymer-polymer blends, EVA:FVA and EVA:LMPI have negative free energy change values between these two extremes which suggest some degree of miscibility. The docosane-polymer blends show much larger, negative free energy changes than the polymer-polymer blends and suggest that these blends are miscible.

It should be noted that if the free energy vs. composition profiles show two peak minima rather than a smooth concave dependence, certain blend compositions will show immiscible phase behaviour despite a negative free energy change i.e. the second miscibility criteria, $\delta^2 \Delta G_{\text{mix}} / \delta \phi^2 > 0$, is not fulfilled. In this study, the number of calculated free energy change values for each blend is limited and the composition profile is unable to identify if this phase behaviour occurs. Possible phase boundaries for these blends within this melt temperature range were characterised using optical microscopy techniques (Chapter 5).

It is clear from the endothermic heat change on blending, that miscibility in these blends can only be achieved by a large, dominant entropic contribution. The Flory-Huggins lattice theory assumes that configurational entropy (which increasingly favours miscibility as the molecular weight of the components decrease) is the only contribution

to the total entropy of mixing, ignoring possible excess entropy contributions from volume changes and non-random mixing etc.. Consequently, it is suggested that miscibility in these blends especially the EVA:NECPE and the docosane-polymer systems is due to the relatively low molecular weight of these components.

The effect of configurational entropy changes due to molecular weight on predicted blend miscibilities has clearly been shown by comparing EVA blends with the polyitaconate samples of slightly different molecular weight values i.e. PI (M_n 9900) and LMPI (M_n 6600). As expected, the heat of mixing profiles and the composition dependence of the χ_H values are essentially identical. However, the larger, more favourable configurational entropy contribution from the lower molecular weight LMPI component results in a free energy value which suggests that the EVA:LMPI blend has the greater miscibility.

Blends involving "amorphous" EVA and semi-crystalline polymers were ideally suited to a straightforward and widely used method of determining χ from the melting point depression of the semi-crystalline polymer when blended with the EVA component. Using DSC, the melting point of various blend compositions were determined and using the classical Nishi-Wang expression, the free energy χ interaction parameter was determined at the melt temperature. Melting point depression values across the composition range varied from 2-17K, representing the various degrees of miscibility between the amorphous phases of EVA and the semi-crystalline polymers. The various poly(ethylene glycol) ester samples in this study, all show two melting phases which have been assigned (wide angle X-ray scattering - Chapter 8) to separate poly(ethylene glycol) and docosyl crystallisation. EVA blends with these esters all show large negative interaction parameters, determined from the melting point of the high melting (docosyl) endotherm which strongly suggests miscibility in the observed melting point range, as predicted from heat of mixing measurements at a similar temperature. In contrast, the lower melting (poly(ethylene glycol)) endotherm was unaffected by EVA composition, suggesting that the amorphous phase of poly(ethylene glycol) is immiscible with EVA, as previously reported in similar systems. In contrast, the EVA:PI and EVA:FVA blends

have small, negative interaction parameters which indicate only "borderline miscibility". The larger melting point depression and negative χ value for the EVA:LMPI blend suggests greater miscibility than either the EVA:PI or EVA:FVA blends. The increase in the observed melting point depression value and miscibility of the EVA:LMPI blend compared to that of EVA:PI can again be attributed to the greater configurational entropy contribution of the LMPI component due to its lower molecular weight (as suggested in heat of mixing measurements).

With the exception of FVA, predicted blend miscibilities from both the heat of mixing measurements and the free energy χ values from melting point depression agree suggesting that although the PI and LMPI components are highly branched, the Flory-Huggins expression for calculating configurational entropy contributions still appears to be applicable in determining free energy of mixing values. Although melting point analysis suggests that both the EVA:FVA and EVA:PI blends have little or no miscibility, free energy values determined using the heat of mixing measurements indicate that the EVA:FVA blends have the greater miscibility. The discrepancy between these predicted miscibilities is likely to be due to the high polydispersity value of FVA (approximately 4). The use of M_n rather than M_w values for FVA overestimates the favourable configurational entropy component, suggesting greater miscibility than would be the case if the higher molecular weight fractions of FVA were accounted for. EVA blends with the hydrogenated poly(n-alkyl norbornenes) samples - 9210 and 9233, showed no observable melting point depression and were assumed to be immiscible at the melt temperature which was confirmed by optical microscopy (Chapter 5). Due to the high molecular weight and polydispersity of the 9210 and 9233 samples it is assumed that favourable configurational entropy contributions were very small when blended with EVA. Consequently, in the absence of specific intermolecular interactions i.e. an exothermic heat of mixing value, this results in blend immiscibility.

The full Nishi-Wang expression is generally not applied to polymer blends as configurational contributions are usually assumed to be negligible. However, in this study, the full expression was used in an attempt to quantify the configurational entropy

contribution to the observed melting point depression and consequently, to "predict" enthalpic interaction parameters. This again assumes that configurational entropy is the main entropic contribution. For all blends with an observed melting point depression, the enthalpic interaction parameter was positive indicating that enthalpically, the blends favour immiscibility. Consequently, these blends are predicted to have endothermic heat of mixing values as confirmed by heat of mixing measurements (Chapter 7) and again suggests that miscibility in these blends must be due to a dominant and favourable entropy contribution. In contrast, applying the full expression to the original Nishi-Wang melting point measurements on a PVF₂:PMMA blend results in free energy and enthalpic interaction parameters which are both negative. Consequently, this suggests exothermic heat of mixing values, as speculated by several authors, arising from the polar interaction between the components.

Blends showing melting point depression values which suggest miscibility i.e. EVA:LMPI and the higher melting phase in the EVA:poly(ethylene glycol) ester blends, also have heat of fusion values greater than predicted. This may indicate miscibility in the crystalline as well as amorphous phases resulting in cocrystallisation between the ethylene sequences in EVA and the aliphatic docosyl ends (in the esters) or octadecyl branches (in LMPI). In contrast, the EVA:FVA, EVA:PI blends and the lower melting crystalline phase in the EVA:poly(ethylene glycol) ester blends have small melting point depressions and heat of fusion values which are smaller than predicted, suggesting that crystallisation in these blends is hindered due to the presence of the EVA component. This difference in the crystallisation effects in EVA:PE and EVA:PI blends was also shown by wide angle X-ray scattering (Chapter 8) in which the EVA:PE blends showed a significant expansion in the lattice plane d-spacings on increasing EVA content whereas the expansion in the EVA:PI (and possibly EVA:FVA) blends was smaller.

Morphologies of EVA blends with FVA, PI, PE and LMPI, observed using phase contrast optical microscopy (Chapter 5) show agreement with the predicted miscibility of these blends from both melting point and heat of mixing measurements. The EVA:LMPI and EVA:PE blends form homogenous (miscible) morphologies on cooling

from the melt with no separate polymer phases noted. In contrast, EVA:FVA and EVA:PI blends show phase separation to varying degrees. However, the EVA:FVA blend forms a miscible blend at high EVA concentrations and from morphologies obtained at various melt temperatures, this is shown as a "miscibility window" from 323-473K. The EVA:PI morphologies at various melt temperatures suggest upper critical solution temperature behaviour with all blend compositions miscible at $\approx 450\text{K}$. The observed large miscibility difference between EVA:PI and EVA:LMPI blends clearly supports the miscibility predictions from both heat of mixing and melting point measurements.

The degree of crystallinity in the PI, PE and FVA polymers was determined by wide angle X-ray scattering using both internal and external comparison methods (Chapter 8). These values show good agreement with those obtained by comparing the heat of fusion values of each polymer (Chapter 4) with the literature value for 100% crystalline polyethylene. Melting point measurements suggest that EVA is amorphous i.e. no clearly defined melting endotherm. However, diffraction profiles indicate that a small degree of crystallinity is present in EVA at room temperature which crystallises further on cooling.

Small angle neutron scattering (Chapter 9) was used to determine χ_{eff} values for blends of hydrogenous poly(ethylene-co-vinyl acetate) and deuterated poly(ethylene glycol) docosyl diester at melt temperatures of 353-383K. At all compositions, the blends were miscible within this temperature range. Spinodal temperatures for each blend composition were predicted from the long extrapolation of χ_{eff} values as a function of reciprocal temperature to the χ value at the spinodal phase boundary. From these values the phase boundary of the blend was characterised as an upper critical solution temperature, at approximately 200K. From the dependence of χ_{eff} values with reciprocal temperature, the separate entropic and enthalpic components to blend miscibility were estimated from the intercept and slope values respectively. From the variation in the enthalpic component, minimum and maximum heat of mixing values between these components were predicted and compared to experimental results on the fully

hydrogenous blend, EVA:NECPE (Chapter 7). Both predicted and experimental values show endothermic heat changes but the observed discrepancy between the values suggests a possible difference in the enthalpic interaction between blends which are totally hydrogenous and those which have deuterated components. This isotopic effect has been reported extensively in other blend systems. In addition, the relative χ (enthalpic) and χ (entropic) contributions to χ_{eff} values have been derived and clearly indicate that miscibility in this blend is again due to a very dominant and favourable entropic contribution.

χ (enthalpic) values from SANS and heat of mixing measurements are of a similar magnitude and appear to indicate a composition dependence. In contrast, χ (free energy, enthalpic) values from the melting point depression technique are much greater in magnitude than those obtained from SANS and heat of mixing measurements, although all three techniques conclude that the blend is miscible. It becomes apparent from the numerous determinations of χ from melting point values, that this technique traditionally gives much larger χ values to that obtained from SANS and calorimetry techniques. In truth, the melting point technique is probably subject to the greater inaccuracies which have been highlighted by several authors. From these limitations, it is clear that this technique should be viewed, at best, as a relatively quick method of determining blend miscibility before recourse is made to other more demanding methods including SANS and heat of mixing calorimetry.

The various thermodynamic approaches to characterising miscibility in these blends (using melting point depression, heats of mixing and small angle neutron scattering techniques) are derived from the original Flory-Huggins lattice theory. These techniques show good agreement in their predictions of blend miscibility (including relative enthalpic and entropic contributions) and that experimentally observed with optical microscopy. The polymers in this study have relatively low molecular weight and polydispersity values (with the exception of FVA). Therefore, configurational entropy contributions on blending these components are believed to be large and the lattice theory assumption that configurational entropy is the only entropic contribution may be

justified. However, the lattice theory is unable to estimate the entropic components due to branching in these polymers which are also thought to contribute to the configurational entropy.

Therefore, in conclusion, the Flory-Huggins lattice theory (despite its many well documented limitations and subsequent refinements) appears to be particularly suited to the thermodynamic characterisation of miscibility in these polymer blends containing low molecular weight, branched components.

Suggestions for Future Work

The successful construction of a polymer blend calorimeter has provided a unique method of determining the absolute enthalpic interaction parameter in these blends. This value is fundamental to understanding blend miscibility. Furthermore, heat of mixing calorimetry is ideally suited to the characterisation of the enthalpic interaction between these low melt viscosity/low melting point polymer components. In this study, enthalpic interaction parameters have been determined at one melt temperature and limited blend compositions. Clearly, further work is required to determine the temperature dependence of these values at a greater number of compositions. This will enable the true shape of the free energy of mixing curves to be defined, from which phase behaviour (UCST, LCST) may be identified.

This study has indicated the dependence of blend miscibility on the molecular weight i.e. configurational entropy, of the polymer components. The EVA component was relatively low molecular weight with a molecular weight distribution i.e. polydispersity of ≈ 2 . It is suggested that further work may involve the fractionation of this polymer into a range of well defined molecular weight/low polydispersity samples. Consequently, the use of these EVA polymer fractions in blends will establish, in greater detail, the molecular weight dependence on blend miscibility. This will be of particular interest for blends in which immiscible phase behaviour has been observed i.e. EVA:FVA and EVA:PI.

Configurational entropy in these polymer blends is clearly a major entropic contribution. However, volume changes on mixing, as reported by many authors, may contribute significantly to an excess entropy term which ultimately may determine phase behaviour. The Flory-Huggins lattice theory cannot estimate this excess entropy term due to the initial assumption that no volume change occurs on mixing. Therefore, further work may concentrate on the use of an "equation of state" approach, in order to consider these excess entropy volume changes (as a function of temperature, pressure and composition) and their contribution to blend miscibility.

APPENDIX A

Melting Point Analysis Results

PARAMETER	EVA	PI	LMPI	FVA	PE	NECPE	NECME	DPE
\bar{V}_u (Volume of repeat unit) (cm ³)	36.972	709.570	689.538	309.851	93.611	93.611 ^a	71.589 ^a	104.455 ^a
Molecular Weight of repeat unit (g)	35.308	635.065	635.065	297.457	96.326	96.326	73.665	107.485
% Crystallinity (WAXS)	-	35.7	35.7 ^b	15.5 ^c	31.0	31.0 ^d	25.9 ^e	24.3 ^e
ΔH_f (DSC) (J/g)	-	94.63	95.17	44.87	104.56 ^f	106.57 ^f	88.99 ^f	83.67 ^f
ΔH_f (100% Crystalline) (J/g)	-	265.07	266.58	288.70	337.29	343.77	343.77	343.77
ΔH_u (100% Crystalline repeat unit) (J/g)	-	168337	169297	85876	32490	33114	25324	36950

a - Determined from the density of PE (1.029 g/cm³ at 288K).

b - Crystallinity predicted to be the same as PI (35.7% determined by WAXS - Chapter 6) due to very similar ΔH_f values.

c - Predicted value based on the ratio of ΔH_f (DSC) to theoretical ΔH_f (288.7J/g for 100% crystalline polyethylene).

d - Crystallinity predicted to be the same as PE (31.0% determined by WAXS - Chapter 6) due to very similar ΔH_f values.

e - Crystallinities predicted by comparing ΔH_f values to NECPE ΔH_f (DSC) of crystallinity 31.0%.

f - Higher melting endotherm (Peak 2).

Appendix A.1 : Parameters in Melting Point Depression Analysis

Blend (%w/w)	ϕ_1	ϕ_1^2 ($\times 10^{-3}$)	T_m (Onset) K	Average T_m (Onset) K	ΔH_f (J/g)	Average ΔH_f (J/g)	$\left[\frac{1}{T_{mb}^{\circ}} - \frac{1}{T_m^{\circ}} \right]$ (K^{-1})($\times 10^{-6}$)
PI	-	-	323.82, 323.83, 323.39	323.68 (0.251) (T_m°)	94.34, 95.56, 94.00	94.63 (0.82)	-
EVA 9.61 PI 90.39	0.0906	8.210	323.33, 323.25, 323.01	323.20 (0.167)	82.57, 82.51, 82.54	82.54 (0.03)	4.588 (1.60)
EVA 14.55 PI 85.45	0.1376	18.939	323.05, 323.19, 323.38	323.21 (0.166)	75.85, 76.30, 76.76	76.30 (0.46)	4.493 (1.59)
EVA 17 PI 83	0.1610	25.934	323.13, 323.14, 323.28	323.18 (0.084)	75.55, 75.49, 75.42	75.49 (0.07)	4.780 (0.80)
EVA 21.02 PI 78.98	0.1996	39.851	323.22, 322.93, 322.69	322.95 (0.265)	75.38, 69.86, 74.43	73.22 (2.95)	6.983 (2.54)
EVA 24.96 PI 75.04	0.2376	56.474	323.06, 323.65, 322.83	323.18 (0.423)	67.19, 67.75, 66.69	67.21 (0.53)	4.780 (4.06)
EVA 30.07 PI 69.93	0.2872	82.504	322.64, 323.11, 322.88	322.88 (0.235)	61.61, 62.99, 60.39	61.66 (1.30)	7.655 (2.26)
EVA 39 PI 61	0.3747	140.39	322.76, 322.65, 322.59	322.67 (0.086)	53.44, 55.44, 53.53	54.14 (1.13)	9.670 (0.83)
EVA 55 PI 45	0.5339	285.05	322.05, 322.09, 322.57	322.24 (0.289)	36.50, 38.32, 38.39	37.74 (1.07)	13.806 (2.79)
EVA 73 PI 27	0.7170	514.12	321.79, 321.74, 321.28	321.60 (0.281)	20.23, 20.48, 20.27	20.33 (0.13)	19.982 (2.72)

Table A.2 : Melting Point Depression in EVA:PI Blends

Blend (%w/w)	$\left[\frac{1}{T_{mb}^{\circ}} - \frac{1}{T_m^{\circ}} \right]$ (K ⁻¹) (x10 ⁻⁶)	$\frac{\Delta H_{2u}}{R\bar{V}_{2u}}$ (K mol cm ⁻³)	$\frac{\Delta H_{2u}}{R\bar{V}_{2u}} \left[\frac{1}{T_{mb}^{\circ}} - \frac{1}{T_m^{\circ}} \right]$ (mol cm ⁻³) (x10 ⁻⁴)	$\frac{\ln(1-\phi_1)}{m_2}$ (x10 ⁻⁴)	$\phi_1 \left(\frac{1}{m_2} - \frac{1}{m_1} \right)$ (x10 ⁻⁴)	Y (mol cm ⁻³) (x10 ⁻⁴)	$\frac{\phi_1^2}{T_{mb}^{\circ}}$ (K ⁻¹) (x10 ⁻⁴)
EVA 9.61 PI 90.39	4.588 (1.600)	28.5334	1.309 (0.456)	-59.363	46.095	-11.959 (0.456)	0.254
EVA 14.55 PI 85.45	4.493 (1.590)	28.5334	1.282 (0.454)	-92.535	70.008	-21.244 (0.454)	0.586
EVA 17.00 PI 83.00	4.780 (0.804)	28.5334	1.364 (0.230)	-109.745	81.924	-26.457 (0.230)	0.802
EVA 21.02 PI 78.98	6.983 (2.543)	28.5334	1.993 (0.726)	-139.176	101.556	-35.627 (0.726)	1.234
EVA 24.96 PI 75.04	4.780 (4.055)	28.5334	1.364 (1.157)	-169.589	120.895	-47.331 (1.157)	1.747
EVA 30.07 PI 69.93	7.655 (2.256)	28.5334	2.184 (0.644)	-211.627	146.122	-63.320 (0.644)	2.555
EVA 39.00 PI 61.00	9.670 (0.826)	28.5334	2.759 (0.236)	-293.430	190.607	-100.064 (0.236)	4.351
EVA 55.00 PI 45.00	13.806 (2.786)	28.5334	3.939 (0.795)	-477.088	271.603	-201.546 (0.795)	8.846
EVA 73.00 PI 27.00	19.982 (2.719)	28.5334	5.701 (0.776)	-788.990	364.764	-418.525 (0.776)	15.986

m_2 = Degree of polymerisation in PI (16), m_1 = Degree of polymerisation in EVA (86).

Table A.3 : Determination of the Blend Interaction Parameter (χ) in EVA:PI Blends

Blend (%w/w)	ϕ_1	ϕ_1^2 ($\times 10^{-3}$)	T_m (Onset) K	Average T_m (Onset) K	ΔH_f (J/g)	Average ΔH_f (J/g)	$\left[\frac{1}{T_{mb}^{\circ}} - \frac{1}{T_m^{\circ}} \right]$ (K^{-1})($\times 10^{-6}$)
LMPI	-	-	318.84 318.59	318.72 (0.18)	95.25 95.09	95.17 (0.11)	-
EVA 9.58 LMPI 90.42	0.093	8.594	317.85 317.98	317.92 (0.09)	85.84 85.87	85.86 (0.02)	7.895 (2.66)
EVA 30.09 LMPI 69.91	0.293	86.042	316.49 316.42	316.46 (0.05)	69.41 68.71	69.06 (0.49)	22.407 (2.27)
EVA 50.28 LMPI 49.72	0.494	243.777	315.66 315.41	315.54 (0.18)	54.18 52.84	53.51 (0.95)	31.620 (3.58)
EVA 70.18 LMPI 29.82	0.694	481.856	313.37 313.48	313.43 (0.08)	34.35 33.68	34.02 (0.47)	52.955 (2.59)

A 12% LMPI : 88% EVA blend was prepared but the crystalline melting peak was very broad and no onset value was determined.

Table A.4 : Melting Point Depression in EVA:LMPI Blends

Blend (%w/w)	$\left[\frac{1}{T_{mb}^{\circ}} - \frac{1}{T_m^{\circ}} \right]$ (K ⁻¹) (x10 ⁻⁶)	$\frac{\Delta H_{2u}}{RV_{2u}}$ (K mol cm ⁻³)	$\frac{\Delta H_{2u}}{RV_{2u}} \left[\frac{1}{T_{mb}^{\circ}} - \frac{1}{T_m^{\circ}} \right]$ (mol cm ⁻³) (x10 ⁻⁴)	$\frac{\ln(1-\phi_1)}{m_2}$ (x10 ⁻⁴)	$\phi_1 \left(\frac{1}{m_2} - \frac{1}{m_1} \right)$ (x10 ⁻⁴)	Y (mol cm ⁻³) (x10 ⁻⁴)	$\frac{\phi_1^2}{T_{mb}^{\circ}}$ (K ⁻¹) (x10 ⁻⁴)
EVA 9.58 LMPI 90.42	7.895 (2.66)	29.5297	2.331 (0.786)	-97.288	81.926	-13.031 (0.786)	0.270
EVA 30.09 LMPI 69.91	22.407 (2.27)	29.5297	6.617 (0.670)	-347.191	259.222	-81.353 (0.670)	2.719
EVA 50.28 LMPI 49.72	31.620 (3.58)	29.5297	9.337 (1.057)	-680.700	436.326	-235.037 (1.057)	7.726
EVA 70.18 LMPI 29.82	52.955 (2.59)	29.5297	15.637 (0.763)	-1184.688	613.442	-555.608 (0.763)	15.374

m_1 = Degree of polymerisation in EVA (86), m_2 = Degree of polymerisation in LMPI (10).

Table A.5 : Determination of the Blend Interaction Parameter (χ) in EVA:LMPI Blends

Blend (%w/w)	ϕ_1	ϕ_1^2 ($\times 10^{-3}$)	T_m (Onset) K	Average T_m (Onset) K	ΔH_f (J/g)	Average ΔH_f (J/g)	$\left[\frac{1}{T_{mb}^{\circ}} - \frac{1}{T_m^{\circ}} \right]$ (K^{-1}) ($\times 10^{-6}$)
FVA	-	-	286.41 286.18	286.30	44.54 45.19	44.87 (0.46)	-
EVA 4.60 FVA 95.40	0.046	2.116	286.41 285.71	286.06	42.83 43.02	42.93 (0.13)	2.93 (3.80)
EVA 10.18 FVA 89.82	0.102	10.404	285.65 285.55	285.60	39.73 39.09	39.41 (0.45)	8.56 (3.80)
EVA 14.82 FVA 85.18	0.149	22.201	285.80 285.51	285.66	36.37 36.24	36.31 (0.09)	7.83 (3.80)
EVA 20.13 FVA 79.87	0.202	40.804	285.37 285.40	285.39	34.53 33.10	33.82 (1.01)	11.14 (3.80)
EVA 24.49 FVA 75.51	0.246	60.516	285.03 284.63	284.83	29.68 31.24	30.46 (1.10)	18.03 (3.80)
EVA 29.81 FVA 70.18	0.299	89.401	283.91 284.47	284.19	27.10 24.51	25.81 (1.83)	25.93 (3.80)
EVA 46 FVA 54	0.461	212.521	284.18 284.38	284.28	22.34 20.46	21.40 (1.33)	24.82 (3.80)
EVA 60 FVA 40	0.601	361.201	283.33 283.73	283.53	14.64 15.35	15.00 (0.50)	34.12 (3.80)
EVA 83 FVA 17	0.831	690.561	283.09 282.75	282.92	9.41 8.92	9.17 (0.35)	41.73 (3.80)

Variation in $\left[\frac{1}{T_{mb}^{\circ}} - \frac{1}{T_m^{\circ}} \right]$ values is based on the standard deviation of T_m (Onset) - 0.155K.

Table A.6 : Melting Point Depression in EVA:FVA Blends

Blend (%w/w)	$\left[\frac{1}{T_{mb}^{\circ}} - \frac{1}{T_m^{\circ}} \right]$ (K ⁻¹) (x10 ⁻⁵)	$\frac{\Delta H_{2u}}{R V_{2u}}$ (K mol cm ⁻³)	$\frac{\Delta H_{2u}}{R V_{2u}}$ (mol cm ⁻³) (x10 ⁻⁴)	$\frac{\ln(1-\phi_1)}{m_2}$ (x10 ⁻⁴)	$\phi_1 \left(\frac{1}{m_2} - \frac{1}{m_1} \right)$ (x10 ⁻⁴)	Y (mol cm ⁻³) (x10 ⁻⁴)	$\frac{\phi_1^2}{T_{mb}^{\circ}}$ (K ⁻¹) (x10 ⁻⁴)
EVA 4.60 FVA 95.40	0.293 (0.379)	33.3340	0.977 (1.262)	-8.765	3.186	-4.603 (1.262)	0.075
EVA 10.18 FVA 89.82	0.856 (0.379)	33.3340	2.854 (1.264)	-19.981	7.048	-10.079 (1.264)	0.366
EVA 14.82 FVA 85.18	0.783 (0.379)	33.3340	2.609 (1.264)	-29.848	10.257	-16.982 (1.264)	0.776
EVA 20.13 FVA 79.87	1.114 (0.379)	33.3340	3.713 (1.265)	-41.819	13.929	-24.178 (1.265)	1.432
EVA 24.49 FVA 75.51	1.803 (0.380)	33.3340	6.009 (1.267)	-52.257	16.942	-29.306 (1.267)	2.122
EVA 29.82 FVA 70.18	2.593 (0.381)	33.3340	8.645 (1.270)	-65.864	20.623	-36.597 (1.270)	3.152
EVA 46.00 FVA 54.00	2.482 (0.381)	33.3340	8.273 (1.270)	-114.554	31.786	-74.495 (1.270)	7.485
EVA 60.00 FVA 40.00	3.412 (0.382)	33.3340	11.375 (1.273)	-170.264	41.430	-117.459 (1.273)	12.750
EVA 83.00 FVA 17.00	4.173 (0.383)	33.3340	13.910 (1.276)	-328.943	57.243	-257.791 (1.276)	24.393

m_1 = Degree of polymerisation in EVA (86), m_2 = Degree of polymerisation in FVA (54).

Table A.7 : Determination of the Blend Interaction Parameter (χ) in EVA:FVA Blends

Blend (%w/w)	ϕ_1	ϕ_1^2 ($\times 10^{-3}$)	Peak 1 T_m (Onset) K	Peak 1 ΔH_f (J/g)	Peak 2 T_m (Onset) K	Peak 2 ΔH_f (J/g)	Peak 2 $\left[\frac{1}{T_{mb}^\circ} - \frac{1}{T_m^\circ} \right]$ (K^{-1}) ($\times 10^{-5}$)
PE	-	-	298.16 298.18 298.02 Av = 298.12	16.50 17.44 16.58 Av = 16.84	323.47 324.74 323.48 $T_m^\circ = 323.90$	104.76 105.83 103.09 Av = 104.56	-
EVA 9.98 PE 90.02	0.107	11.45	298.81	15.21	323.83	97.19	0.064 (0.72)
EVA 20.27 PE 79.73	0.215	46.23	298.35	13.09	322.21	86.66	1.616 (0.72)
EVA 29.70 PE 70.30	0.313	97.97	298.97	11.12	320.45	79.53	3.321 (0.72)
EVA 39.88 PE 60.12	0.417	173.89	298.79 299.46 Av = 299.13	8.91 8.92 Av = 8.92	318.75 319.45 Av = 319.10	69.89 70.10 Av = 70.00	4.641 (0.72)
EVA 50.03 PE 49.97	0.519	269.36	298.89	6.78	317.35	58.20	6.369 (0.72)
EVA 60.06 PE 39.94	0.618	381.92	298.83 299.09 Av = 298.96	4.69 5.23 Av = 4.96	312.55 313.15 Av = 312.85	49.78 50.76 Av = 50.27	10.902 (0.72)
EVA 75 PE 25	0.764	583.70	298.89	2.44	307.15	35.30	16.833 (0.72)

Variation in $\left[\frac{1}{T_{mb}^\circ} - \frac{1}{T_m^\circ} \right]$ values is based on the standard deviation of the Peak 2 T_m (Onset) - 0.371K.

Table A.8 : Melting Point Depression in EVA:PE Blends

Blend (%w/w)	Peak 2 $\left[\frac{1}{T_{mb}^{\circ}} - \frac{1}{T_m^{\circ}} \right]$ (K ⁻¹) (x10 ⁻⁵)	$\frac{\Delta H_{2u}}{R \bar{V}_{2u}}$ (K mol cm ⁻³)	$\frac{\Delta H_{2u}}{R \bar{V}_{2u}} \left[\frac{1}{T_{mb}^{\circ}} - \frac{1}{T_m^{\circ}} \right]$ (mol cm ⁻³) (x10 ⁻⁴)	$\frac{\ln(1-\phi_1)}{m_2}$ (x10 ⁻⁴)	$\phi_1 \left(\frac{1}{m_2} - \frac{1}{m_1} \right)$ (x10 ⁻⁴)	Y (mol cm ⁻³) (x10 ⁻⁴)	$\frac{\phi_1^2}{T_{mb}^{\circ}}$ (K ⁻¹) (x10 ⁻⁴)
EVA 9.98 PE 90.02	0.067 (0.707)	41.7437	0.279 (2.953)	-94.035	76.515	-17.241 (2.953)	0.352
EVA 20.27 PE 79.73	1.619 (0.711)	41.7437	6.760 (2.968)	-201.757	154.188	-40.810 (2.968)	1.435
EVA 29.70 PE 70.30	3.324 (0.715)	41.7437	13.875 (2.984)	-312.626	224.305	-74.446 (2.984)	3.054
EVA 39.88 PE 60.12	4.644 (0.718)	41.7437	19.386 (2.997)	-449.385	298.883	-131.115 (2.997)	5.445
EVA 50.03 PE 49.97	6.372 (0.722)	41.7437	26.600 (3.014)	-609.818	372.114	-211.103 (3.014)	8.486
EVA 60.06 PE 39.94	10.905 (0.733)	41.7437	45.520 (3.058)	-802.733	443.398	-313.815 (3.058)	12.222
EVA 75.00 PE 25.00	16.837 (0.747)	41.7437	70.282 (3.117)	-1202.320	547.636	-584.401 (3.117)	18.990

m_1 = Degree of polymerisation in EVA (86), m_2 = Degree of polymerisation in PE (12).

Table A.9 : Determination of the Blend Interaction Parameter (χ) in EVA:PE Blends

Blend (%w/w)	ϕ_1	ϕ_1^2 ($\times 10^{-3}$)	Peak 1 T_m (Onset) K	Peak 1 Average T_m (Onset) K	Peak 1 ΔH_f (J/g)	Peak 1 Average ΔH_f (J/g)	Peak 2 T_m (Onset) K	Peak 2 Average T_m (Onset) K	Peak 2 ΔH_f (J/g)	Peak 2 Average ΔH_f (J/g)	Peak 2 $\left[\frac{1}{T_{mb}^0} - \frac{1}{T_m^0} \right]$ (K^{-1}) ($\times 10^{-5}$)
NECPE	0	0	301.85 302.14 301.80 301.72 302.26	301.95 (0.23)	18.50 19.00 19.31 19.32 18.34	18.89 (0.45)	328.57 328.65 328.11 328.06 328.17	328.31 (0.28)	106.73 104.62 107.93 107.50 106.05	106.57 (1.31)	0
10.01% EVA 89.99% NECPE	0.107	11.45	302.17 301.85	302.01 (0.23)	16.44 16.90	16.67 (0.33)	326.83 326.65	326.74 (0.13)	97.32 98.11	97.72 (0.56)	1.464 (0.382)
30.58% EVA 69.42% NECPE	0.322	103.60	302.17 302.12 302.03 302.16	302.12 (0.06)	13.43 13.19 12.97 12.81	13.10 (0.27)	324.83 324.82 324.62 324.60	324.72 (0.12)	79.60 80.19 82.11 79.60	80.38 (1.19)	3.368 (0.374)
50.32% EVA 49.68% NECPE	0.522	272.32	301.35 301.25 301.68 301.41	301.42 (0.18)	8.45 8.43 8.40 8.01	8.32 (0.21)	320.75 320.75 320.95 320.55	320.75 (0.16)	59.91 61.13 60.37 60.08	60.37 (0.54)	7.179 (0.415)
70.40 % EVA 29.60% NECPE	0.719	517.41	300.90 300.88 300.71	300.83 (0.10)	3.89 4.17 4.32	4.13 (0.22)	315.25 315.65 315.65	315.52 (0.23)	37.60 37.94 38.97	38.17 (0.71)	12.347 (0.491)
89.44% EVA 10.56% NECPE	0.901	812.24	*	*	1.62 1.17 1.36	1.38 (0.23)	*	*	17.44 18.93 16.52	17.63 (1.22)	*

In the 89.44% EVA blend, the Peak 1 and Peak 2 melting endotherms had merged to form a broad melting phase. Accurate melting points are therefore not available for this composition.

Table A.10 : Melting Point Depression in EVA:NECPE Blends

Blend (%w/w)	Peak 2 $\left[\frac{1}{T_{mb}^{\circ}} - \frac{1}{T_m^{\circ}} \right]$ (K ⁻¹) (x10 ⁻⁵)	$\frac{\Delta H_{2u}}{RV_{2u}}$ (K mol cm ⁻³)	$\frac{\Delta H_{2u}}{RV_{2u}} \left[\frac{1}{T_{mb}^{\circ}} - \frac{1}{T_m^{\circ}} \right]$ (mol cm ⁻³) (x10 ⁻⁴)	$\frac{\ln(1-\phi_1)}{m_2}$ (x10 ⁻⁴)	$\phi_1 \left(\frac{1}{m_2} - \frac{1}{m_1} \right)$ (x10 ⁻⁴)	Y (mol cm ⁻³) (x10 ⁻⁴)	$\frac{\phi_1^2}{T_{mb}^{\circ}}$ (K ⁻¹) (x10 ⁻⁴)
EVA 10.01 NECPE 89.99	1.464 (0.382)	42.5455	6.227 (1.624)	-80.856	64.002	-10.627 (1.624)	0.351
EVA 30.58 NECPE 69.42	3.368 (0.374)	42.5455	14.327 (1.590)	-277.439	192.480	-70.632 (1.590)	3.190
EVA 50.32 NECPE 49.68	7.179 (0.415)	42.5455	30.544 (1.767)	-527.013	312.066	-184.403 (1.767)	8.490
EVA 70.40 NECPE 29.60	12.347 (0.491)	42.5455	52.531 (2.088)	-907.508	430.153	-424.824 (2.088)	16.399

m_1 = Degree of polymerisation in EVA (86), m_2 = Degree of polymerisation in NECPE (14).

Table A.11 : Determination of the Blend Interaction Parameter (χ) in EVA:NECPE Blends

Blend (%w/w)	ϕ_1	ϕ_1^2 (x10 ⁻³)	Peak 1 T_m (Onset) K	Peak 1 Average T_m (Onset) K	Peak 1 ΔH_f (J/g)	Peak 1 Average ΔH_f (J/g)	Peak 2 T_m (Onset) K	Peak 2 Average T_m (Onset) K	Peak 2 ΔH_f (J/g)	Peak 2 Average ΔH_f (J/g)	Peak 2 $\left[\frac{1}{T_{mb}^0} - \frac{1}{T_m^0} \right]$ (K ⁻¹) (x10 ⁻⁵)
NECME	0	0	299.72 300.03 299.87	299.87 (0.16)	16.10 16.04 15.05	15.73 (0.59)	315.65 315.64 315.09	315.46 (0.32)	91.06 88.31 87.60	88.99 (1.83)	
EVA 10.08 NECME 89.92	0.108	11.61	299.44 299.48 299.48	299.47 (0.02)	13.39 13.65 13.75	13.60 (0.19)	313.55 313.75 313.55	313.62 (0.12)	79.77 81.63 81.55	80.98 (1.05)	1.860 (0.444)
EVA 30.17 NECME 69.83	0.318	100.90	299.44 299.60 299.44	299.49 (0.09)	9.96 9.38 9.78	9.71 (0.30)	310.75 310.75 311.55	311.02 (0.46)	67.15 63.83 65.84	65.61 (1.67)	4.525 (0.797)
EVA 50.02 NECME 49.98	0.519	269.83	299.66 300.17 299.67	299.83 (0.29)	6.24 6.33 6.71	6.43 (0.25)	307.25 308.25 308.25	307.92 (0.58)	51.12 52.30 52.91	52.11 (0.91)	7.762 (0.932)
EVA 70.43 NECME 29.57	0.720	517.83	300.03 300.35 300.46 299.71	300.14 (0.34)	2.85 2.53 3.13 3.54	3.01 (0.43)	*	*	33.58 31.90 36.05 37.05	34.65 (2.34)	*

In the 70.43% EVA blend (and also an 88.55% EVA blend), Peak 1 and 2 melting endotherms overlapped to form a single, broad, crystalline melting phase. Accurate melting points are therefore not available for these compositions.

Table A.12 : Melting Point Depression in EVA:NECME Blends

Blend (%w/w)	Peak 2 $\left[\frac{1}{T_{mb}^o} - \frac{1}{T_m^o} \right]$ (K ⁻¹) (x10 ⁻⁵)	$\frac{\Delta H_{2u}}{R\bar{V}_{2u}}$ (K mol cm ⁻³)	$\frac{\Delta H_{2u}}{R\bar{V}_{2u}} \left[\frac{1}{T_{mb}^o} - \frac{1}{T_m^o} \right]$ (mol cm ⁻³) (x10 ⁻⁴)	$\frac{\ln(1-\phi_1)}{m_2}$ (x10 ⁻⁴)	$\phi_1 \left(\frac{1}{m_2} - \frac{1}{m_1} \right)$ (x10 ⁻⁴)	Y (mol cm ⁻³) (x10 ⁻⁴)	$\frac{\phi_1^2}{T_{mb}^o}$ (K ⁻¹) (x10 ⁻⁴)
EVA 10.08 NECME 89.92	1.860 (0.444)	42.5456	7.913 (1.888)	-103.664	85.441	-10.311 (1.888)	0.370
EVA 30.17 NECME 69.83	4.525 (0.797)	42.5456	19.253 (3.390)	-347.468	251.838	-76.377 (3.390)	3.244
EVA 50.02 NECME 49.98	7.762 (0.932)	42.5456	33.025 (3.967)	-665.067	411.350	-220.693 (3.967)	8.743

m_1 = Degree of polymerisation in EVA (86), m_2 = Degree of polymerisation in NECME (11).

Table A.13 : Determination of the Blend Interaction Parameter (χ) in EVA:NECME Blends

Blend (%w/w)	ϕ_1	ϕ_1^2 ($\times 10^{-3}$)	Peak 1 T_m (Onset) K	Peak 1 Average T_m (Onset) K	Peak 1 ΔH_f (J/g)	Peak 1 Average ΔH_f (J/g)	Peak 2 T_m (Onset) K	Peak 2 Average T_m (Onset) K	Peak 2 ΔH_f (J/g)	Peak 2 Average ΔH_f (J/g)	Peak 2 $\left[\frac{1}{T_{mb}^0} - \frac{1}{T_m^0} \right]$ (K^{-1}) ($\times 10^{-5}$)
DPE	0	0	296.04 295.96 295.57 295.65	295.81 (0.23)	15.46 14.50 15.57 15.21	15.19 (0.48)	320.81 320.23 320.41 320.43	320.47 (0.24)	83.97 81.83 85.15 83.74	83.67 (1.37)	
EVA 25.69 DPE 74.31	0.271	73.66	294.62 294.38 294.85	294.62 (0.24)	10.64 10.58 10.58	10.60 (0.03)	318.25 317.85 317.89	318.00 (0.22)	67.86 68.41 67.96	68.08 (0.29)	2.424 (0.451)
EVA 50.17 DPE 49.83	0.520	270.76	295.36 295.88	295.62 (0.37)	6.29 6.03	6.16 (0.18)	312.25 312.55	312.40 (0.21)	50.54 49.65	50.10 (0.63)	8.061 (0.449)
EVA 70.00 DPE 30.00	0.715	511.85	295.77 295.57	295.67 (0.14)	2.99 3.11	3.05 (0.08)	306.75 307.15	306.95 (0.28)	34.39 34.29	34.34 (0.07)	13.744 (0.531)
EVA 80.00 DPE 20.00	0.812	658.82	295.83 295.53	295.68 (0.21)	1.69 1.34	1.52 (0.25)	302.35 303.75	303.05 (0.99)	25.00 24.70	24.85 (0.21)	17.937 (1.308)

A 10% DPE : 90% EVA Blend was prepared, but Peak 1 and Peak 2 melting endotherms merged into single, broad melting phase. Melting points are therefore not available for this composition.

Table A.14 : Melting Point Depression in EVA:DPE Blends

Blend (%w/w)	Peak 2 $\left[\frac{1}{T_{mb}^{\circ}} - \frac{1}{T_m^{\circ}} \right]$ (K ⁻¹) (x10 ⁻⁵)	$\frac{\Delta H_{2u}}{RV_{2u}}$ (K mol cm ⁻³)	$\frac{\Delta H_{2u}}{RV_{2u}} \left[\frac{1}{T_{mb}^{\circ}} - \frac{1}{T_m^{\circ}} \right]$ (mol cm ⁻³) (x10 ⁻⁴)	$\frac{\ln(1-\phi_1)}{m_2}$ (x10 ⁻⁴)	$\phi_1 \left(\frac{1}{m_2} - \frac{1}{m_1} \right)$ (x10 ⁻⁴)	Y (mol cm ⁻³) (x10 ⁻⁴)	$\frac{\phi_1^2}{T_{mb}^{\circ}}$ (K ⁻¹) (x10 ⁻⁴)
EVA 25.69 DPE 74.31	2.424 (0.451)	42.5455	10.312 (1.920)	-287.851	215.172	-62.367 (1.920)	2.316
EVA 50.17 DPE 49.83	8.061 (0.449)	42.5455	34.295 (1.910)	-667.901	412.537	-221.070 (1.910)	8.667
EVA 70.00 DPE 30.00	13.744 (0.531)	42.5455	58.476 (2.258)	-1142.540	567.205	-516.859 (2.258)	16.675
EVA 80.00 DPE 20.00	17.937 (1.308)	42.5455	76.313 (5.566)	-1517.802	643.505	-797.984 (5.566)	21.739

m_1 = Degree of polymerisation in EVA (86), m_2 = Degree of polymerisation in DPE (11).

Table A.15 : Determination of the Blend Interaction Parameter (χ) in EVA:DPE Blends

Blend (%w/w)	T _m (Onset) K	Average T _m (Onset) K	T _m (Peak) K	Average T _m (Peak) K	ΔH _f (J/g)	Average ΔH _f (J/g)
9210	300.60	300.40 (0.19)	302.73	302.51 (0.35)	45.63	45.85 (0.36)
	300.27		302.35		45.91	
	300.22		302.10		46.32	
	300.52		302.85		45.52	
EVA 10.01 9210 89.99	300.27	300.12 (0.11)	302.35	302.26 (0.13)	45.89	43.14 (1.95)
	300.02		302.35		43.13	
	300.13		302.25		41.56	
	300.04		302.08		41.98	
EVA 30.07 9210 69.93	299.76	300.05 (0.27)	301.86	302.53 (0.62)	39.62	39.15 (0.73)
	300.27		303.03		39.43	
	300.28		303.09		39.47	
	299.88		302.14		38.06	
EVA 49.85 9210 50.15	299.74	299.59 (0.21)	302.02	301.83 (0.17)	21.04	22.13 (3.65)
	299.67		301.71		19.14	
	299.35		301.75		26.20	
	299.92		301.31		6.09	
EVA 70.05 9210 29.95	299.91	299.95 (0.06)	301.40	301.35 (0.05)	7.10	6.27 (0.76)
	300.02		301.33		5.62	
	299.93		301.25		2.55	
EVA 89.88 9210 10.12	300.01	300.19 (0.38)	301.31	301.52 (0.42)	3.03	2.94 (0.36)
	300.62		302.01		3.25	

Table A.16 : Melting Point Depression in EVA:9210 Blends

Blend (%w/w)	T _m (Onset) K	Average T _m (Onset) K	T _m (Peak) K	Average T _m (Peak) K	ΔH _f (J/g)	Average ΔH _f (J/g)
9233	281.46	281.39 (0.06)	286.78	286.87 (0.15)	33.47	33.60 (0.29)
	281.36		287.04		33.40	
	281.35		286.78		33.94	
EVA 10.16 9233 89.84	281.45	281.42 (0.06)	286.91	286.82 (0.15)	32.00	30.95 (0.92)
	281.35		286.65		30.52	
	281.47		286.91		30.32	
EVA 30.07 9233 69.93	281.43	281.27 (0.14)	286.78	286.56 (0.22)	25.53	24.23 (1.48)
	281.21		286.35		24.55	
	281.16		286.55		22.62	
EVA 50.22 9233 49.78	281.80	281.81 (0.19)	286.71	286.60 (0.21)	16.44	15.58 (2.01)
	281.57		286.58		16.87	
	282.04		286.31		12.58	
EVA 69.97 9233 30.03	281.84	*	286.78	286.36 (0.48)	16.41	2.96 (0.54)
	*		287.06		2.87	
			286.06		3.70	
EVA 87.94 9233 12.06		*	286.06	286.21 (0.45)	2.88	1.62 (0.72)
			286.26		2.40	
			285.86		1.33	
	*		286.11	2.69		
	*		285.99	1.10		
			286.86	1.37		

* T_m (Onset) values not determined due to low crystallinity and broad crystalline phase.

Table A.17 : Melting Point Depression in EVA:9233 Blends

APPENDIX B

"Heat of Mixing" Calorimetry Results

Wt. EVA (g)	n ₁ EVA (x10 ⁻⁴)	φ ₁ EVA	Wt. FVA (g)	n ₂ FVA (x10 ⁻⁵)	φ ₂ FVA	ΔH _{mix} (x10 ⁻² J) meas.	ΔH _{mix} (x10 ⁻² J/g)	ΔG _{mix} (x10 ⁻² J/g) calc.	Chain Unit χ _{1,2}	Repeat Unit χ _{1,2} (x10 ⁻³)
0.89987	2.97970	0.89365	0.10765	0.67344	0.10635	4.37	4.34 (0.41)	-9.36 (0.41)	0.486 (0.046)	5.65 (0.53)
0.82631	2.73613	0.79805	0.21020	1.31498	0.20195	6.63	6.39 (0.60)	-16.27 (0.60)	0.423 (0.040)	4.91 (0.46)
0.84332	2.79245	0.69793	0.36690	2.29528	0.30207	12.60	10.41 (0.98)	-19.59 (0.98)	0.526 (0.049)	6.12 (0.57)
0.84346	2.79291	0.70848	0.34888	2.18255	0.29152	11.70	9.82 (0.92)	-19.51 (0.92)	0.506 (0.048)	5.88 (0.55)
0.71568	2.36980	0.60235	0.47493	2.97110	0.39765	14.18	11.91 (1.12)	-23.27 (1.12)	0.530 (0.050)	6.16 (0.58)
0.56672	1.87656	0.49842	0.57330	3.58649	0.50158	15.26	13.39 (1.26)	-25.32 (1.26)	0.571 (0.054)	6.64 (0.62)
0.68029	2.25262	0.49922	0.68600	4.29152	0.50078	21.13	15.47 (1.45)	-23.22 (1.45)	0.660 (0.062)	7.67 (0.72)
0.57305	1.89752	0.50220	0.57100	3.57210	0.49780	14.93	13.05 (1.23)	-25.57 (1.23)	0.557 (0.052)	6.47 (0.61)
0.48624	1.61007	0.39872	0.73709	4.61114	0.60128	18.79	15.36 (1.44)	-24.44 (1.44)	0.684 (0.064)	7.95 (0.74)
0.36287	1.20156	0.30104	0.84695	5.29840	0.69896	17.46	14.43 (1.35)	-23.87 (1.35)	0.732 (0.069)	8.52 (0.80)
0.37158	1.23040	0.30468	0.85245	5.33281	0.69532	19.00	15.52 (1.46)	-22.89 (1.46)	0.782 (0.074)	9.10 (0.85)
0.24430	0.80894	0.20525	0.95093	5.94889	0.79475	14.06	11.76 (1.10)	-21.91 (1.10)	0.770 (0.072)	8.96 (0.84)
0.10654	0.35278	0.10558	0.90727	5.67576	0.89442	5.80	5.72 (0.54)	-18.27 (0.54)	0.648 (0.061)	7.53 (0.71)

Data : EVA : Density 0.955g/cm³, Mol Wt. (Mn) 3020. FVA : Density 0.960g/cm³, Mol Wt. (Mn) 15985.

ΔH_{mix} values have an error of ± 9.4% (± 1 S.D) from 3 measurements on 50:50 weight fraction blends.

χ repeat unit value based on 86 EVA repeat units.

Table B.1 : Heat of Mixing in EVA:FVA Blends at 341.45K.

Wt. EVA (g)	n_1 EVA ($\times 10^{-4}$)	ϕ_1 EVA	Wt. PI (g)	n_2 PI ($\times 10^{-5}$)	ϕ_2 PI	ΔH_{mix} ($\times 10^{-2}$ J) meas.	ΔH_{mix} ($\times 10^{-2}$ J/g)	ΔG_{mix} ($\times 10^{-2}$ J/g) calc.	Chain Unit $\chi_{1,2}$	Repeat Unit $\chi_{1,2}$ ($\times 10^{-3}$)
0.90654	3.00179	0.89113	0.10379	1.04849	0.10887	17.34	17.16 (0.57)	0.92 (0.57)	1.869 (0.062)	21.73 (0.72)
0.80935	2.67997	0.79123	0.20014	2.02182	0.20877	25.73	25.49 (0.84)	-1.07 (0.84)	1.620 (0.053)	18.84 (0.63)
0.84820	2.80861	0.68553	0.36465	3.68371	0.31447	45.38	37.41 (1.24)	2.62 (1.24)	1.810 (0.060)	21.04 (0.70)
0.72341	2.39540	0.58576	0.47945	4.84342	0.41424	48.28	40.14 (1.33)	-0.17 (1.33)	1.714 (0.057)	19.93 (0.66)
0.50624	1.67629	0.48430	0.50520	5.10355	0.51570	41.52	41.05 (1.35)	-2.55 (1.35)	1.692 (0.056)	19.67 (0.65)
0.50873	1.68454	0.48923	0.49775	5.02829	0.51077	39.56	39.31 (1.30)	-4.19 (1.30)	1.620 (0.053)	18.83 (0.65)
0.51212	1.69576	0.48846	0.50261	5.07738	0.51154	42.59	41.97 (1.39)	-1.55 (1.39)	1.729 (0.057)	20.11 (0.67)
0.44439	1.47149	0.38840	0.65581	6.62501	0.61160	45.67	41.51 (1.38)	-2.80 (1.38)	1.788 (0.059)	20.79 (0.69)
0.31113	1.03023	0.28926	0.71645	7.23760	0.71074	39.38	38.32 (1.27)	-3.81 (1.27)	1.894 (0.063)	22.03 (0.73)
0.17728	0.58702	0.19020	0.70737	7.14587	0.80980	26.33	29.76 (0.99)	-6.34 (0.99)	1.951 (0.064)	22.69 (0.75)
0.11468	0.37974	0.10444	0.92160	9.31003	0.89556	20.29	19.58 (0.65)	-6.74 (0.65)	2.102 (0.069)	24.44 (0.81)

Data : EVA : Density 0.955g/cm³, Mol Wt. (Mn) 3020. PI : Density 0.895g/cm³, Mol Wt. (Mn) 9899.

ΔH_{mix} values have an error of $\pm 3.3\%$ (± 1 S.D.) from 3 measurements on 50:50 weight fraction blends.

χ repeat unit value based on 86 EVA repeat units.

Table B.2 : Heat of Mixing in EVA:PI Blends at 341.45K.

Wt. EVA (g)	n_1 EVA ($\times 10^{-4}$)	ϕ_1 EVA	Wt. LMPI (g)	n_2 LMPI ($\times 10^{-4}$)	ϕ_2 LMPI	ΔH_{mix} ($\times 10^{-2}$ J) meas.	ΔH_{mix} ($\times 10^{-2}$ J/g)	ΔG_{mix} ($\times 10^{-2}$ J/g) calc.	Chain Unit $\chi_{1,2}$	Repeat Unit $\chi_{1,2}$ ($\times 10^{-2}$)
0.10279	0.34036	0.11514	0.76185	1.15414	0.88486	15.87	18.35 (0.97)	-10.44 (0.97)	1.856 (0.098)	2.158 (0.114)
0.33481	1.10864	0.31178	0.71276	1.07978	0.68822	39.19	37.41 (1.98)	-8.54 (1.98)	1.809 (0.096)	2.104 (0.112)
0.54002	1.78815	0.48439	0.55436	0.83981	0.51561	45.94	41.98 (2.22)	-6.08 (2.22)	1.755 (0.093)	2.041 (0.108)
0.62342	2.06430	0.48851	0.62950	0.95364	0.51149	57.89	46.21 (2.45)	-1.79 (2.45)	1.931 (0.102)	2.246 (0.119)
0.53750	1.77980	0.49242	0.53432	0.80945	0.50758	45.55	42.50 (2.25)	-5.44 (2.25)	1.776 (0.094)	2.065 (0.110)
0.77890	2.57914	0.69905	0.32339	0.48991	0.30095	33.44	30.34 (1.61)	-8.60 (1.61)	1.518 (0.080)	1.765 (0.094)
0.88101	2.91725	0.89065	0.10432	0.15804	0.10935	13.31	13.50 (0.72)	-6.30 (0.72)	1.470 (0.078)	1.709 (0.091)

Data : EVA : Density 0.955g/cm³, Mol Wt. (Mn) 3020. LMPI : Density 0.921g/cm³, Mol Wt. (Mn) 6601.

ΔH_{mix} values have an error of $\pm 5.3\%$ (± 1 S.D) from 3 measurements on 50:50 weight fraction blends.

χ repeat unit value based on 86 EVA repeat units.

Table B.3 : Heat of Mixing in EVA:LMPI Blends at 341.45K.

Wt. EVA (g)	n_1 EVA ($\times 10^{-4}$)	ϕ_1 EVA	Wt. NECPE (g)	n_2 NECPE ($\times 10^{-4}$)	ϕ_2 NECPE	ΔH_{mix} ($\times 10^{-2}$ J) meas.	ΔH_{mix} ($\times 10^{-2}$ J/g)	ΔG_{mix} ($\times 10^{-2}$ J/g) calc.	Chain Unit $\chi_{1,2}$	Repeat Unit $\chi_{1,2}$ ($\times 10^{-2}$)
0.13229	0.43805	0.15352	0.78597	6.54975	0.84648	6.36	6.93 (0.46)	-52.20 (0.46)	0.604 (0.040)	0.703 (0.046)
0.20378	0.67477	0.22788	0.74396	6.19967	0.77212	18.23	19.24 (1.27)	-58.69 (1.27)	1.233 (0.081)	1.433 (0.095)
0.31762	1.05172	0.32932	0.69699	5.80825	0.67068	27.73	27.33 (1.80)	-70.28 (1.80)	1.385 (0.091)	1.610 (0.106)
0.41305	1.36772	0.42459	0.60314	5.02617	0.57541	37.95	37.35 (2.47)	-72.99 (2.46)	1.699 (0.112)	1.975 (0.130)
0.52025	1.72268	0.52191	0.51350	4.27917	0.47809	40.56	39.24 (2.59)	-78.25 (2.59)	1.735 (0.114)	2.017 (0.133)
0.43704	1.44715	0.51748	0.43910	3.65917	0.48252	30.45	34.75 (2.29)	-82.54 (2.29)	1.536 (0.101)	1.786 (0.118)
0.45400	1.50331	0.51729	0.45648	3.80400	0.48271	36.82	40.44 (2.67)	-76.85 (2.67)	1.787 (0.118)	2.078 (0.137)
0.57447	1.90222	0.51717	0.57789	4.81575	0.48283	45.52	39.50 (2.61)	-77.78 (2.61)	1.746 (0.115)	2.030 (0.134)
0.64890	2.14868	0.62821	0.41380	3.44833	0.37179	45.08	42.42 (2.80)	-75.41 (2.80)	1.988 (0.131)	2.311 (0.153)
0.74853	2.47858	0.70840	0.33200	2.76667	0.29160	34.90	32.30 (2.13)	-79.73 (2.13)	1.701 (0.112)	1.978 (0.131)
0.79668	2.63801	0.80176	0.21225	1.76875	0.19824	24.82	24.60 (1.62)	-72.34 (1.62)	1.672 (0.110)	1.944 (0.128)
0.92798	3.07278	0.90026	0.11078	0.92317	0.09974	9.19	8.85 (0.58)	-58.14 (0.58)	1.056 (0.070)	1.228 (0.081)

Data : EVA : Density 0.955g/cm³, Mol Wt. (Mn) 3020. NECPE : Density 1.029g/cm³, Mol Wt. (Mn) 1200.
 ΔH_{mix} values have an error of $\pm 6.6\%$ (± 1 S.D) from 4 measurements on 50:50 weight fraction blends.
 χ repeat unit value based on 86 EVA repeat units.

Table B.4 : Heat of Mixing in EVA:NECPE Blends at 341.45K.

Wt. C22 (g)	n_1 C22 ($\times 10^{-3}$)	ϕ_1 C22	Wt. EVA (g)	n_2 EVA ($\times 10^{-4}$)	ϕ_2 EVA	ΔH_{mix} ($\times 10^{-2}$ J) meas.	ΔH_{mix} ($\times 10^{-2}$ J/g)	ΔG_{mix} ($\times 10^{-2}$ J/g) calc.	Chain Unit $\chi_{1,2}$	Repeat Unit $\chi_{1,2}$ ($\times 10^{-2}$)
0.09237	0.29738	0.11762	0.83301	2.75831	0.88238	27.91	30.16 (0.72)	-175.69 (0.72)	0.375 (0.009)	1.703 (0.041)
0.31477	1.01339	0.34720	0.71148	2.35589	0.65280	173.30	168.86 (4.05)	-155.49 (4.05)	0.923 (0.022)	4.194 (0.101)
0.50463	1.62464	0.54550	0.50544	1.67364	0.45450	209.86	207.77 (4.99)	-106.07 (4.99)	1.001 (0.024)	4.551 (0.109)
0.60510	1.94810	0.54315	0.61186	2.02603	0.45685	264.90	217.67 (5.22)	-96.74 (5.22)	1.048 (0.025)	4.766 (0.114)
0.50370	1.62165	0.53999	0.51585	1.70811	0.46001	219.69	215.47 (5.17)	-99.71 (5.17)	1.037 (0.025)	4.715 (0.113)
0.69787	2.24677	0.72042	0.32558	1.07808	0.27958	186.86	182.58 (4.38)	-59.91 (4.38)	1.048 (0.025)	4.763 (0.114)
0.80060	2.57751	0.90967	0.09557	0.31645	0.09033	77.35	86.31 (2.07)	-15.09 (2.07)	1.170 (0.028)	5.319 (0.128)

Data : EVA : Density 0.955g/cm³, Mol Wt. (Mn) 3020. C22 : Density 0.7944 g/cm³, Mol Wt. 310.61g.

ΔH_{mix} values have an error of $\pm 2.4\%$ (± 1 S.D) from 3 measurements on the 50:50 weight fraction blends.

χ repeat unit value is based on 22 Docosane repeat units.

Table B.5 : Heat of Mixing in Docosane:EVA Blends at 341.45K.

Wt. C22 (g)	n_1 C22 ($\times 10^{-3}$)	ϕ_1 C22	Wt. FVA (g)	n_2 FVA ($\times 10^{-5}$)	ϕ_2 FVA	ΔH_{mix} ($\times 10^{-2}$ J) meas.	ΔH_{mix} ($\times 10^{-2}$ J/g)	ΔG_{mix} ($\times 10^{-2}$ J/g) calc.	Chain Unit $\chi_{1,2}$	Repeat Unit $\chi_{1,2}$ ($\times 10^{-2}$)
0.09490	0.30553	0.11278	0.90220	5.64404	0.88722	37.83	37.94 (0.76)	-153.82 (0.76)	0.492 (0.010)	2.234 (0.045)
0.30603	0.98526	0.34411	0.70490	4.40976	0.65589	98.54	97.48 (1.95)	-202.91 (1.95)	0.537 (0.011)	2.441 (0.049)
0.52861	1.70184	0.55277	0.51684	3.23328	0.44723	108.88	104.14 (2.08)	-176.88 (2.08)	0.504 (0.010)	2.290 (0.046)
0.56961	1.83384	0.54961	0.56408	3.52881	0.45039	122.72	108.25 (2.17)	-173.67 (2.17)	0.523 (0.010)	2.379 (0.048)
0.51287	1.65117	0.54859	0.50999	3.19043	0.45141	107.51	105.11 (2.10)	-177.09 (2.10)	0.508 (0.010)	2.309 (0.046)
0.63482	2.04378	0.72981	0.28402	1.77679	0.27019	83.39	90.75 (1.82)	-115.33 (1.82)	0.532 (0.011)	2.418 (0.048)
0.87030	2.80191	0.89516	0.12317	0.77054	0.10484	46.02	46.32 (0.93)	-47.32 (0.93)	0.552 (0.011)	2.508 (0.050)

Data : FVA : Density 0.960g/cm³, Mol Wt. (Mn) 15985. C22 : Density 0.7944 g/cm³, Mol Wt. 310.61g.

ΔH_{mix} values have an error of $\pm 2\%$ (± 1 S.D) from 3 measurements on the 50:50 weight fraction blends.

χ repeat unit value is based on 22 Docosane repeat units.

Table B.6 : Heat of Mixing in Docosane:FVA Blends at 341.45K.

Wt. PI (g)	n ₁ PI (x10 ⁻⁵)	φ ₁ PI	Wt. C22 (g)	n ₂ C22 (x10 ⁻³)	φ ₂ C22	ΔH _{mix} (x10 ⁻² J) meas.	ΔH _{mix} (x10 ⁻² J/g)	ΔG _{mix} (x10 ⁻² J/g) calc.	Chain Unit χ _{1,2}	Repeat Unit χ _{1,2} (x10 ⁻²)
0.88650	8.95545	0.89333	0.09396	0.30250	0.10667	23.09	23.55 (0.66)	-175.40 (0.66)	0.301 (0.008)	1.368 (0.038)
0.73493	7.42429	0.69212	0.29018	0.93423	0.30788	47.32	46.16 (1.29)	-266.19 (1.29)	0.258 (0.007)	1.172 (0.033)
0.52738	5.32761	0.47463	0.51815	1.66817	0.52537	66.90	63.99 (1.79)	-238.34 (1.79)	0.298 (0.008)	1.353 (0.038)
0.53341	5.38852	0.47078	0.53222	1.71347	0.52922	67.31	63.16 (1.77)	-238.14 (1.77)	0.294 (0.008)	1.336 (0.037)
0.50122	5.06334	0.46909	0.50352	1.62107	0.53091	60.97	60.68 (1.70)	-240.16 (1.70)	0.282 (0.008)	1.284 (0.036)
0.31575	3.18972	0.27999	0.72070	2.32027	0.72001	57.90	55.86 (1.56)	-164.03 (1.56)	0.314 (0.009)	1.427 (0.040)
0.10538	1.06455	0.09545	0.88640	2.85374	0.90455	24.42	24.63 (0.69)	-64.48 (0.69)	0.316 (0.009)	1.435 (0.040)

Data : PI : Density 0.895g/cm³, Mol Wt. (Mn) 9899. C22 : Density 0.7944 g/cm³, Mol Wt. 310.61g.
ΔH_{mix} values have an error of ± 2.4% (± 1 S.D) from 3 measurements on the 50:50 weight fraction blends.
χ repeat unit value is based on 22 Docosane repeat units.

Table B.7 : Heat of Mixing in Docosane:PI Blends at 341.45K.

Wt. LMPI (g)	n_1 LMPI ($\times 10^{-4}$)	ϕ_1 LMPI	Wt. C22 (g)	n_2 C22 ($\times 10^{-3}$)	ϕ_2 C22	ΔH_{mix} ($\times 10^{-2}$ J) meas.	ΔH_{mix} ($\times 10^{-2}$ J/g)	ΔG_{mix} ($\times 10^{-2}$ J/g) calc.	Chain Unit $\chi_{1,2}$	Repeat Unit $\chi_{1,2}$ ($\times 10^{-2}$)
0.82056	1.24308	0.87530	0.10083	0.32462	0.12470	30.57	33.18 (1.23)	-180.15 (1.23)	0.379 (0.014)	1.722 (0.064)
0.70173	1.06307	0.65916	0.31297	1.00760	0.34084	67.29	66.32 (2.45)	-249.51 (2.45)	0.357 (0.013)	1.622 (0.060)
0.71251	1.07940	0.66932	0.30363	0.97753	0.33068	68.49	67.41 (2.49)	-246.93 (2.49)	0.369 (0.014)	1.676 (0.062)
0.51306	0.77725	0.46556	0.50800	1.63549	0.53444	85.30	83.54 (3.09)	-217.89 (3.09)	0.395 (0.015)	1.794 (0.066)
0.49090	0.74368	0.46136	0.49434	1.59151	0.53864	79.89	81.09 (3.00)	-219.23 (3.00)	0.383 (0.014)	1.742 (0.064)
0.49835	0.75496	0.46250	0.49955	1.60829	0.53750	77.49	77.66 (2.87)	-222.97 (2.87)	0.367 (0.014)	1.668 (0.062)
0.31747	0.48094	0.28090	0.70099	2.25682	0.71910	71.57	70.27 (2.60)	-154.20 (2.60)	0.398 (0.015)	1.808 (0.067)
0.30550	0.46281	0.26706	0.72320	2.32832	0.73294	73.34	71.29 (2.64)	-145.20 (2.64)	0.415 (0.015)	1.888 (0.070)
0.10961	0.16605	0.11614	0.71950	2.31641	0.88386	35.89	43.28 (1.60)	-66.88 (1.60)	0.470 (0.017)	2.136 (0.079)

Data : LMPI : Density 0.921g/cm³, Mol Wt. (Mn) 6601. C22 : Density 0.7944 g/cm³, Mol Wt. 310.61g.

ΔH_{mix} values have an error of $\pm 3.7\%$ (± 1 S.D) from 3 measurements on the 50:50 weight fraction blends.

χ repeat unit value is based on 22 Docosane repeat units.

Table B.8 : Heat of Mixing in Docosane:LMPI Blends at 341.45K.

Wt. NECPE (g)	n_1 NECPE ($\times 10^{-4}$)	ϕ_1 NECPE	Wt. C22 (g)	n_2 C22 ($\times 10^{-3}$)	ϕ_2 C22	ΔH_{mix} ($\times 10^{-2}$ J) meas.	ΔH_{mix} ($\times 10^{-2}$ J/g)	ΔG_{mix} ($\times 10^{-2}$ J/g) calc.	$\chi_{1,2}$ Chain Unit	$\chi_{1,2}$ Repeat Unit ($\times 10^{-2}$)
0.87308	7.27567	0.86212	0.10780	0.34706	0.13788	82.86	84.47 (4.98)	-145.79 (4.98)	0.975 (0.058)	4.434 (0.262)
0.68860	5.73833	0.63696	0.30299	0.97547	0.36304	225.50	227.41 (13.42)	-129.67 (13.42)	1.278 (0.075)	5.811 (0.343)
0.48029	4.00242	0.43084	0.48983	1.57699	0.56916	297.23	306.39 (18.08)	-52.33 (18.08)	1.541 (0.091)	7.004 (0.413)
0.47531	3.96092	0.42781	0.49079	1.58008	0.57219	293.15	303.44 (17.90)	-54.61 (17.90)	1.528 (0.090)	6.944 (0.410)
0.47603	3.96692	0.43696	0.47353	1.52452	0.56304	319.95	336.94 (19.88)	-23.06 (19.88)	1.692 (0.100)	7.690 (0.454)
0.27642	2.30350	0.25493	0.62369	2.00795	0.74507	261.74	290.78 (17.16)	5.12 (17.16)	1.801 (0.106)	8.187 (0.483)
0.12520	1.04333	0.10739	0.80343	2.58662	0.89261	168.95	181.94 (10.73)	20.93 (10.73)	2.143 (0.126)	9.739 (0.575)

Data : NECPE : Density 1.029g/cm³ i.e. PE density, Mol Wt. (Mn) 1200. C22 : Density 0.7944 g/cm³, Mol Wt. 310.61g.

ΔH_{mix} values have an error of $\pm 5.9\%$ (± 1 S.D) from 3 measurements on the 50:50 weight fraction blends.

χ repeat unit value is based on 22 Docosane repeat units.

Table B.9 : Heat of Mixing in Docosane:NECPE Blends at 341.45K.

APPENDIX C

Lectures, Conferences, Courses Attended and Publications

UNIVERSITY OF DURHAM
Board of Studies in Chemistry
Colloquia, Lectures and Seminars given by Invited Speakers

1991

- October 17 Dr. J.A.Salthouse, (University of Manchester).
Son et Lumiere-A Demonstration Lecture.
- October 31 Dr. R.Keeley, (Metropolitan Police Forensic Science).
Modern Forensic Science.
- November 6 Prof. B.F.G.Johnson, (Edinburgh University).
Cluster-surface Analogies.
- November 7 Dr. A.R.Butler, (St.Andrews University).
Traditional Chinese Herbal Drugs: A Different Way of Treating
Disease.
- November 13 Prof. D.Gani, (St.Andrews University).
The Chemistry of PLP Dependent Enzymes.
- November 20 Dr. R.More O'Ferrall, (University College, Dublin).
Some Acid-Catalysed Rearrangements in Organic Chemistry.
- November 28 Prof. I.M.Ward, (IRC in Polymer Science, Leeds University).
SCI Lecture The Science and Technology of Orientated Polymers.
- December 4 Prof. R.Grigg, (Leeds University).
Palladium-Catalysed Cyclisation and Ion-Capture Processes.
- December 5 Prof. A.L.Smith, (Ex. Unilever).
Soap, Detergents and Black Puddings.
- December 11 Dr. W.D.Cooper, (Shell Research).
Colloid Science: Theory and Practice.

1992

- January 22 Dr. K.D.M.Harris, (St.Andrews University).
Understanding the Properties of Solid Inclusion Compounds.
- January 29 Dr. A.Holmes, (Cambridge University).
Cycloaddition Reactions in the Service of the Synthesis of
Piperidine and Indolizidine Natural Products.
- January 30 Dr. M.Anderson, (Sittingbourne, Shell Research).
Recent Advances in the Safe and Selective Chemical
Control of Insect Pests.
- February 12 Prof. D.E.Fenton, (Sheffield University).
Polynuclear Complexes of Molecular Clefts as Models for Copper
Biosites.
- February 13 Dr. J.Saunders, (Glaxo Group Research Limited).
Molecular Modeling in Drug Discovery.

February 19	Prof. E.J.Thomas, (University of Manchester). Applications of Organostannanes to Organic Synthesis.
February 20 Musgrave Lecture	Prof. E.Vogel, (University of Cologne). Porphyrins: Molecules of Interdisciplinary Interest.
February 25 Tilden Lecture:	Prof. J.F.Nixon, (University of Sussex). Phosphaalkynes: New Building Blocks in Inorganic and Organometallic Chemistry.
February 26	Prof. M.L.Hitchman, (Strathclyde University). Chemical Vapour Deposition.
March 5	Dr. N.C.Billingham, (University of Sussex). Degradable Plastics-Myth or Magic?.
March 11	Dr. S.E.Thomas, (Imperial College). Recent Advances in Organoiron Chemistry.
March 12	Dr. R.A.Hann, (ICI Imagedata). Electronic Photography-An Image of the Future.
March 18	Dr. H.Maskill, (Newcastle University). Concerted or Stepwise Fragmentation in a Deamination-type Reaction.
April 7	Prof. D.M.Knight, (University of Durham). Interpreting Experiments: The Beginning of Electrochemistry.
May 13	Dr. J-C.Gehret, (Ciba Geigy, Basel). Some Aspects of Industrial Agrochemical Research.
October 15	Dr. M.Glazer and Dr.S.Tarling, (Oxford University and Birbeck College). It Pays to be British!- The Chemist's Role as an Expert Witness in Patent Litigation.
October 20	Dr. H.E.Bryndza, (Du Pont Central Research). Synthesis, Reactions and Thermochemistry of Metal(alkyl)cyanide Complexes and Their Impact on Olefin Hydrocyanation Catalysis.
October 22 Ingold-Albert Lecture	Prof. A.G.Davies, (University College, London). The Behaviour of Hydrogen as a Pseudometal.
October 28	Dr. J.K.Cockroft, (Durham University). Recent Developments in Powder Diffraction.
October 29	Dr. J.Emsley, (Imperial College, London). The Shocking History of Phosphorus.
November 4	Dr. T.Kee, (University of Leeds). Synthesis and Coordination Chemistry of Silylated Phosphites.
November 5	Dr. C.J.Ludman, (University of Durham). Explosions, A Demonstration Lecture.

- November 11 Prof. D.Robins, (Glasgow University).
Pyrrolizidine Alkaloids: Biological Activity, Biosynthesis and Benefits.
- November 12 Prof. M.R.Truter, (University College, London).
Luck and Logic in Host-Guest Chemistry.
- November 18 Dr. R.Nix, (Queen Mary College, London).
Characterisation of Heterogeneous Catalysts.
- November 25 Prof. Y.Vallee, (University of Caen).
Reactive Thiocarbonyl Compounds.
- November 25 Prof. L.D.Quin, (University of Massachusetts, Amherst)
Fragmentation of Phosphorus Heterocycles as a Route to Phosphoryl Species with Uncommon Bonding.
- November 26 Dr. D.Humber, (Glaxo, Greenford).
AIDS - The Development of a Novel Series of Inhibitors of HIV.
- December 2 Prof. A.F.Hegarty, (University College, Dublin).
Highly Reactive Enols Stabilised by Steric Protection.
- December 2 Dr. R.A.Aitkin, (University of St.Andrews).
The Versatile Cycloaddition Chemistry of $\text{Bu}_3\text{P}\cdot\text{CS}_2$.
- December 3 Prof. P.Edwards, (Birmingham University).
SCI Lecture
What is a Metal?
- December 9 Dr. A.N.Burgess, (ICI Runcorn).
The Structure of Perfluorinated Ionomer Membranes.

1993

- January 20 Dr. D.C.Clary, (University of Cambridge).
Energy Flow in Chemical Reactions
- January 21 Prof. L.Hall, (University of Cambridge).
NMR - A Window to the Human Body.
- January 27 Dr. W.Kerr, (University of Strathclyde).
Development of the Pauson-Khand Annulation Reaction :
Organocobalt Mediated Synthesis of Natural and Unnatural Products.
- February 3 Prof. S.M.Roberts, (University of Exeter).
Enzymes in Organic Synthesis.
- February 10 Dr. D.Gillies, (University of Surrey).
NMR and Molecular Motion in Solution.
- February 11 Prof. S.Knox, (Bristol University).
Tilden Lecture
Organic Chemistry at Polynuclear Metal Centres.
- February 17 Dr. R.W.Kemmitt, (University of Leicester).
Oxatrimethylenemethane Metal Complexes.

February 18	Dr. I.Fraser, (ICI, Wilton). Reactive Processing of Composite Materials.
February 22	Prof. D.M.Grant, (University of Utah). Single Crystals, Molecular Structure and Chemical-Shift Anisotropy
February 24	Prof. C.J.M.Stirling, (University of Sheffield). Chemistry on the Flat-Reactivity of Ordered Systems.
March 3	Dr. K.J.P.Williams, (BP). Raman Spectroscopy for Industrial Analysis.
March 10	Dr. P.K.Baker, (University College of North Wales, Bangor). An Investigation of the Chemistry of the Highly Versatile 7-Coordinate Complexes $[M_2(CO)_3(NCMe)_2]$ (M=Mo,W).
March 11	Dr. R.A.Jones, (University of East Anglia). The Chemistry of Wine Making
March 17	Dr. R.J.K.Taylor, (University of East Anglia).] Adventures in Natural Product Synthesis.
March 24	Prof. I.O.Sutherland, (University of Liverpool). Chromogenic Reagents for Chiral Amine Sensors.
May 13 Boys-Rahman Lecture	Prof. J.A.Pople, (Carnegie-Mellon University Pittsburgh). Applications of Molecular Orbital Theory.
May 21	Prof. L.Weber, (University of Bielefeld). Metallo-phospha Alkenes as Synthons in Organometallic Chemistry
June 1	Prof. J.P.Konopelski, (University of California, Santa Cruz). Synthetic Adventures with Enantiomerically Pure Acetals.
June 7	Prof. R.S.Stein, (University of Massachusetts). Scattering Studies of Crystalline and Liquid Crystalline Polymers.
June 16	Prof. A.K.Covington, (University of Newcastle). Use of Ion Selective Electrodes as Detectors in Ion Chromatography.
June 17	Prof. O.F.Nielsen, (H.C.Ørsted Institute, University of Copenhagen). Low-Frequency IR - and Raman Studies of Hydrogen Bonded Liquids.
October 4	Prof. F.J.Fehler, (University of California at Irvine). Bridging the Gap Between Surfaces and Solution with Sessilquioxanes.
October 20	Dr. P.Quayle, (University of Manchester). Aspects of aqueous ROMP Chemistry.
October 23	Prof. R.Adams, (University of S.Carolina) The Chemistry of Metal Carbonyl Cluster Complexes Containing Platinum and Iron, Ruthenium or Osmium and the Development of a Cluster Based Alkyne Hydrogenation Catalyst
October 27	Dr. R.A.L.Jones, (Cavendish Laboratory) Perambulating Polymers

- November 10 Prof. M.N.R.Ashfold, (University of Bristol)
High Resolution Photofragment Translational Spectroscopy:
A New way to Watch Photodissociation
- November 17 Dr. A.Parker, (Laser Support Facility)
Applications of Time Resolved Resonance Raman Spectroscopy
to Chemical and Biochemical Problems
- November 24 Dr. P.G.Bruce, (University of St. Andrews)
Synthesis and Applications of Inorganic Materials
- December 1 Prof. M.A.McKervy, (Queens University, Belfast)
Functionalised Calixerenes
- January 19 Prof. O.Meth-Cohen, (Sunderland University)
Friedel's Folly Revisited
- January 26 Prof. J.Evans, (University of Southampton)
Shining Light on Catalysts
- February 2 Dr. A.Masters, (University of Manchester)
Modelling Water without Using Pair Potentials
- February 9 Prof. D.Young, (University of Sussex)
Chemical and Biological Studies on the Coenzyme Tetrahydrofolic
Acid
- February 16 Dr. R.E.Mulvey, (University of Strathclyde)
Structural Patterns in Alkali Metal Chemistry
- February 23 Prof. P.M.Maitlis FRS, (University of Sheffield)
Why Rhodium in Homogeneous Catalysis?
- March 2 Dr. C.Hunter, (University of Sheffield)
Non Covalent Interactions between Aromatic Molecules
- April 20 Prof. P.Parsons, (University of Reading)
New Methods and Strategies in Natural Product Synthesis

The author has also attended the following lectures in the IRC in Polymer Science and Technology International Seminar Series.

1992

- March 17 Prof. Sir S.Edwards, (Cavendish Laboratory, University of Cambridge),
at Leeds University.
Phase Dynamics and Phase Changes in Polymer Liquid Crystals
- March 25 Prof. H.Chedron, (Hoechst AG, Frankfurt am Main),
at Durham University.
Structural Concepts and Synthetic Methods in Industrial Polymer Science.
- May 11 Prof. W.Burchard, (University of Freiburg),
at Durham University.
Recent Developments in the Understanding of Reversible and Irreversible Network Formation.
- September 21 Prof. E.L.Thomas, (MIT, Cambridge, Massachusetts),
at Leeds University.
Interface Structures in Copolymer-Homopolymer Blends.

1993

- March 16 Prof. J.M.G.Cowie, (Heriot-Watt University)
at Bradford University
High Technology in Chains : The Role of Polymers in Electronic Applications and Data Processing
- April 1 Prof. H.W.Speiss, (Max-Planck Institut for Polymerforschung, Mainz),
at Durham University.
Multidimensional NMR Studies of Structure and Dynamics of Polymers.
- June 2 Prof. F.Ciardelli, (University of Pisa), at Durham University.
Chiral Discrimination in the Stereospecific Polymerisation of α -olefins.
- June 8 Prof. B.E.Eichinger, (BIOSYM Technologies Inc. San Diego),
at Leeds University.
Recent Polymer Modeling Results and a Look into the Future.
- July 6 Prof. C.W.Macosko, (University of Minnesota, Minneapolis),
at Bradford University.
Morphology Development in Immiscible Polymer-Polymer Blending.

Conferences and Courses attended by the author

March 1992

Macro Group (UK) Family Meeting, Durham University.

September 1992

IRC Club Meeting, Leeds University.

January 1993

IRC Polymer Engineering Course, Bradford University.

March 1993

IRC Polymer Physics Course, Leeds University.

April 1993

Macro Group (UK) Family Meeting, Lancaster University.

July 1993

"The Polymer Conference", Cambridge University.

September 1993

IRC Club Meeting, Durham University.

April 1994

Macro Group (UK) Family Meeting, Birmingham University.

July 1994

MacroAkron '94 IUPAC Meeting, University of Akron, Ohio, USA.

Publications

"Melting point depression in ethylene-vinyl acetate copolymer mixtures"
Polymer, 35, 1045 (1994), N.E.Clough, R.W.Richards and T.Ibrahim.

